AD-A266 406

NASA
Contractor Report 191079

Army Research Laboratory
Contractor Report ARL-CR-49

Sikorsky Aircraft Advanced Rotorcraft Transmission (ART) Program— Final Report

Jules G. Kish
United Technologies Corporation
Stratford, Connecticut

DTIC
ELECTE
JUL 0 1 1993
S B D

March 1993

Prepared for
Lewis Research Center
Under Contract NAS3-25423

DISTRIBUTION STATEMENT A
Approved for public release;
Distribution Unlimited

National Aeronautics and
Space Administration

U.S. ARMY
RESEARCH LABORATORY

93 6 30 052

93-14986

FORWARD

The Advanced Rotorcraft Transmission (ART) program was an Army funded program to advance the state-of-the-art in helicopter transmissions. The program was directed and managed by the Army Aviation Systems Command Propulsion Directorate and the NASA Mechanical Systems Technology Branch, both of the Lewis Research Center in Cleveland, Ohio. The ART program consisted of four research contracts. This report documents the Sikorsky contract. Technical direction for all of the ART contractors was provided by Mr. R. Bill and the technical project managers of the Sikorsky project were Mr. W. Hady (retired) and Mr. T. Krantz, all of the NASA Lewis Research Center.

The Sikorsky technical effort, under contract NAS3-25423, was begun in July, 1988 and ended in April, 1992, and was managed by Mr J. Kish of Sikorsky Aircraft. This report was written by Mr Kish with assistance from Mr. G. Ambrose who prepared the test sections.

Appreciation is extended to all personnel who participated in the design, manufacture and testing conducted during the ART program. Recognition is given to Mr C. Isabelle who directed the design effort conducted by Messrs N. Baldino, D. Donahue, H. Frint, B. Hansen, M. Hayduk, S. Joyce, C. Keller, M. Mullen, D. Ray, and G. Webb. The testing of thin dense chrome Pyrowear 53 was conducted by Mr. M. Lutian of the Sikorsky Structural Technologies Section. Assistance in the composites design area was provided by Mr. D. Nguyen. Manufacturing engineering support was provided by Messrs M. Francis, J. Mucci, and K. Martell. The ART 1/2 size test components were fabricated at Sikorsky in the Development Center under the direction of Mr L. Hoag, in the Production Gear Shop under the direction of Mr. P. FitzGerald, and in the Production Machine Center under the direction of Mr. J. Plunkett. Appreciation is extended to Mr. G. Ambrose, A. Parker, and Mr. D. Ryan for the conduct of the test program, to Mr. L. Zunsky of the Development Center, and to Mr. G. Kollinson, A. Lohr, W. Davidson and R. Warner of the Sikorsky Instrumentation Lab.

Several efforts under the ART contact were provided by sub-contractors. Special thanks is extended to the McGill Manufacturing Co., Valparaiso, Indiana for the design, development, and test of angular contact spherical roller bearings with ceramic rollers. This effort was led by Mr D. Michaels, with assistance from Mr. A. Aggarwal, and supervision by Mr. J. Porter of McGill Manufacturing Co. Appreciation is also extended to Ohio State University and Prof. D. Houser for the conduct of transmission error dynamic analysis.

Accession For
NTIS GRA&I ☑
DTIC TAB ☐
Unannounced ☐
Justification
By
Distribution/
Availability Codes
Avail and/or
Dist Special
A-1

TABLE OF CONTENTS - FINAL REPORT
ADVANCED ROTORCRAFT TRANSMISSION (ART)

	PAGE
Foreword	i
Contents	iii
Summary	1
Introduction	2
Selection of Evaluation Procedures	4
Baseline Aircraft	4
Baseline Transmission	9
Transmission Design Data	10
Methodology	11
Baseline Weight, Noise, MTBR	15
Preliminary Design	17
Split Torque	17
Split Path	20
Trade Off Studies	22
Load Sharing Devices	23
Spring Clutch on Input	27
High Contact Ratio/Buttress/Herringbone Gears	31
Bearingless Bull Gear Design	36
High Hot Hardness Gear Steels	41
Angular Contact Spherical Roller Bearings	41
Composite Main Rotor Shaft/Quill/Standpipe	44
Composite Housings	47
Candidate Transmission Selection	48
Revised Aircraft Power Train Arrangement	48
System Performance Evaluation	51
Approach and Methodology	51
Aircraft Size, Weight, and Performance	52
Life Cycle Cost	54
Detail Design	57
Full Size Aircraft Gearbox	57
Gearing	60
Bearings	61
Lubrication	62
Composite Housings	65
Composite Main Rotor Shaft/Quill/Standpipe	67
Spring Clutch	71
Engine Drive Shaft	71
Accessories	73
Rotor Brake	77
Tail-Take-Off	77
Diagnostics	77

TABLE OF CONTENTS (Cont'd)

	PAGE
Weight, Noise, MTBR	80
1/2 Size Test Gearbox	81
Scaling Attributes	85
Gearing	86
Bearings	87
Internal Shafting	88
Elastomeric Isolator	88
Lubrication	91
Topological Gear Grinding	94
Fabrication	99
Angular Contact Spherical Roller Bearing	99
1/2 Size Test Gearbox	100
1/2 Size Gearbox Test Configuration	110
Test	114
Test Facilities/Instrumentation	114
Material Test Facilities/Instrumentation	114
1/2 Size Gearbox Test Facility/Instrumentation	117
Bearing Test Facility/Instrumentation	123
Test Procedure	125
Material Test Procedure	125
1/2 Size Gearbox Test Procedure, No Load Lube	126
1/2 Size Gearbox Test Procedure, Gear Pattern Dev	127
1/2 Size Gearbox Test Procedure, Dynamic Surveys	128
1/2 Size Gearbox Test Procedure, 200 hr Endurance	132
1/2 Size Gearbox Test Procedure, 200 hr Overtorque	134
Bearing Test Procedure	135
Test Results	137
Material Test Results	137
1/2 Size Gearbox Test Results, No Load Lube	139
1/2 Size Gearbox Test Results, Gear Pattern Dev	141
1/2 Size Gearbox Test Results, Dynamic Surveys	143
1/2 Size Gearbox Test Results, 200 hr Endurance	162
1/2 Size Gearbox Test Results, 200 hr Overtorque	171
Bearing Test Results	179
Conclusions	184
Appendix A, Results of Related IR&D Efforts	188
Composite Housing	188
Inductive Debris Monitor (IDM)	194
Acoustic Emission (AE) Accelerometers	197
Report Documentation Page	199

LIST OF FIGURES - FINAL REPORT
ADVANCED ROTORCRAFT TRANSMISSION (ART)

FIGURE		PAGE
1	ACA Gross Weight, Payload, and Performance	4
2	Power Required for Climb and OEI, 2 vs 3 Engines	6
3	ACA Baseline, Power Required vs Airspeed at Sea Level	7
4	ACA Baseline, Power Required vs Airspeed at 4000 Feet	7
5	ACA Baseline, Payload vs Radius	7
6	ACA Baseline Aircraft	8
7	ACA Baseline Transmission Installation	12
8	ACA Baseline Transmission	13
9	Schematic of Split Torque Main Transmission	17
10	11:1 Split Torque Cross Section	19
11	Schematic of Split Path Main Transmission	20
12	11:1 Split Path Cross Section	21
13	11:1 Split Path Top View	22
14	Tooth Geometry Relationships for Torque Splitting Drive	23
15	Quill Shaft Load Sharing Device	24
16	Helical Gear Load Sharing Scheme	24
17	Composite Block Load Sharing Device	25
18	Elastomeric Torsional Load Sharing Device	26
19	Inverted Elastomeric Torsional Load Sharing Device	27
20	Comparison of ART and Conventional Load Sharing Devices	28
21	Principle of Spring Clutch Actuation	29
22	Spring Design Features	30
23	ART Input Bevel Pinion With Spring Clutch	31
24	Variation of Bending and Contact Stress With Helix Angle	32
25	Herringbone Gear Mesh Design Parameters	33
26	ART/ACA Weight Savings vs Reduction Ratio	34
27	Bull Pinion Bearing Configuration Comparison	35
28	Bull Gear Reaction, All Engines Operative	36
29	Bull Gear Reaction, One Engine Inoperative	37
30	Bull Gear Reaction, Two Engines Inoperative	37
31	Bull Gear Reactions as a Function of Tangential Tooth Load	38
32	Bearingless Bull Gear Design	39
33	Bearingless Bull Gear With Full Recess Action Pinions	40
34	Single Bearing Configurations Which Replace Ball/Roller	42
35	Bearing Life for Steel and Ceramic Rollers	43
36	Mounting of Angular Contact Spherical Roller Bearing	43
37	Standpipe Structure ART/ACA	44
38	Schematic of Standpipe Structure Separate Parts	44
39	ART/ACA Main Rotor/Quill Shaft	45
40	ART/ACA Main Rotor/Quill Shaft, Alternate Arrangement	46
41	Schematic of ART/ACA Composite Housing Assembly	47
42	ACA Aircraft Installation of Split Path Gearbox	49
43	ACA Aircraft Installation of Split Torque Gearbox	49
44	ART/ACA Engine Installation	50
45	Helicopter Design Model	52
46	Correlation of Parametric and Actual Drive System Weight	52
47	Time Phased Elements of Life Cycle Cost	54

LIST OF FIGURES (Cont'd)

FIGURE		PAGE
48	ART Main Gearbox Cross Section	58
49	ART Main Gearbox Top View	59
50	Composite Housing Finite Element Model	65
51	Composite Housing Deformed Shape Plot	66
52	Upper Cover Total Deflection	66
53	Input Housing Major Principal Strain	67
54	Composite Quill, Main Rotor Shaft, Truss Cross Section	68
55	Composite Standpipe/Truss FEA Model	69
56	Composite Standpipe/Truss Total Deflection	70
57	Composite Standpipe/Truss Strain in the Y Direction	70
58	Composite Integral Shaft/Coupling Basic Dimensions	72
59	Composite Integral Shaft/Coupling Angular Misalignment	73
60	ART Engine Input Dynamic Analysis	74
61	ART/ACA Planetary Accessory Drive	75
62	ART/ACA Accessory Drive Using Additional Gear	76
63	ART/ACA Accessory Drive Using Existing Gear	76
64	Generalized Diagnostic System	78
65	Cross Section of 1/2 Size Test Gearbox	82
66	Finite Element Model of Test Gearbox in Test Fixture	83
67	Test Fixture Total Deflection	83
68	Test Fixture Maximum Principal Stress	84
69	Test Gearbox Lower Plate Total Deflection	84
70	Test Gearbox Lower Plate Maximum Principal Stress	85
71	Finite Element Model of Elastomeric Isolator Side Plate	89
72	Elastomeric Isolator Side Plate Deflections	89
73	Elastomeric Isolator Side Plate Hoop Stress	89
74	Elastomeric Isolator Rubber Shear Strain in R-Ø	90
75	Elastomeric Isolator Rubber Shear Strain in Ø-Z	90
76	Elastomeric Isolator Rubber Shear Strain in R-Z	90
77	Maximum Principal Shear Strain vs Angular Position	91
78	1/2 Size Gearbox Location of Jets	92
79	1/2 Size Gearbox Lubrication System Schematic	94
80	FEA Model of Input Spur Pinion	96
81	FEA Model of Input Spur Gear	96
82	FEA Model of Double Helical Pinion	97
83	FEA Model of Double Helical Gear	97
84	Angular Contact Spherical Roller Bearing	99
85	High Contact Ratio Spur Pinion	101
86	Phauter Kapp Grinding Machine	101
87	Cubic Boron Nitride (CBN) Form Grinding Wheel	102
88	Bearing Outer Race/Double Helical Gear Assembly	102
89	Spur Gear Hobbing Prior to Carburization	103
90	Elastomeric Load Sharing Device Side Plate Pocket Milling	104
91	Elastomeric Load Sharing Device Side Plate	104
92	Spur Gear and Elastomeric Load Sharing Device	105
93	Double Helical Pinion in Horizontal Boring Machine	105
94	Completed Double Helical Pinion	106
95	Components of Double Helical Pinion/Spur Gear Assembly	107

LIST OF FIGURES (Cont'd)

FIGURE		PAGE
96	Assembly Fixture, Double Helical Pinion/Spur Gear	107
97	Zeiss Coordinate Measuring Machine	108
98	1/2 Size Gearbox Housing Assembly	109
99	Output Double Helical Bull Gear in Housing	109
100	Test Gearbox Components, 1/2 Size Test Gearbox	110
101	Test Coupon Configuration	114
102	Fretting Contact Pin Configuration	115
103	Fatigue Test Machine	116
104	Slip Amplitude Measurement Apparatus	117
105	Shaft/Coupling Test Facility	117
106	Operators Console	118
107	ART Test and Dummy Gearbox Installation	119
108	ART Gearbox Installation	119
109	Slip Ring Installation, Double Helical Gear	120
110	Slip Ring Installation, ART Gearbox	121
111	ART Instrumentation Console	122
112	Transmission Error Encoder Installation	122
113	Schematic of Bearing Test Facility	123
114	Bearing Test Facility Spindle	124
115	Transmission Error, Method A	131
116	Fretting Fatigue S-N Curve for Polished and TDC Pyrowear	138
117	Typical Vibration Signatures, No Load	141
118	Load Sharing, Initial Pattern Development Survey	141
119	Typical Vibration Signatures, Pattern Development	142
120	Load Sharing, Final Pattern Development Survey	143
121	Stress vs Time, Spur Pinion, Gage #3	144
122	Stress vs Time, Upper Spur Gear, Gage #10	144
123	Stress vs Time, Lower Spur Gear, Gage #15	145
124	Stress vs Time, Upper Double Helical Pinion, Gage #19	145
125	Stress vs Time, Lower Double Helical Pinion, Gage #32	146
126	Stress vs Time, Double Helical Gear, Gage #38	146
127	Vibratory Stress, Spur Pinion Meshing w/Upper Spur Gear	147
128	Vibratory Stress, Spur Pinion Meshing w/Lower Spur Gear	147
129	Vibratory Stress, Upper Spur Gear	148
130	Vibratory Stress, Lower Spur Gear	148
131	Vibratory Stress, Upper Double Helical Pinion	149
132	Vibratory Stress, Lower Double Helical Pinion	149
133	Vibratory Stress, DH Gear Meshing w/Upper DH Pinion	150
134	Vibratory Stress, DH Gear Meshing w/Lower DH Pinion	150
135	Load Sharing, 1st Half of Dynamic Surveys	151
136	Load Sharing, 2nd Half of Dynamic Surveys	152
137	Load Sharing, Steel Survey	153
138	Idler Shaft Torque vs Time, Steel Survey	153
139	Typical Vibration Signatures, Steel Surveys	154
140	Upper Spur TE vs Upper Lat Vib, Elastomer @ 100% Torque	155
141	Lower Spur TE vs Upper Lat Vib, Elastomer @ 100% Torque	155
142	Upper D Hel TE vs Upper Lat Vib, Elastomer @ 100% Torque	156
143	Lower D Hel TE vs Upper Lat Vib, Elastomer @ 100% Torque	156

LIST OF FIGURES (Cont'd)

FIGURE		PAGE
144	Lower Spur TE vs Upper Lat Vib, Steel @ 100% Torque	157
145	Lower D Hel TE vs Upper Lat Vib, Steel @ 100% Torque	157
146	Lower Spur TE, Elastomer vs Steel @ 50% Torque	158
147	Lower Spur TE, Elastomer vs Steel @ 100% Torque	159
148	Lower D Hel TE, Elastomer vs Steel @ 25% Torque	159
149	Lower D Hel TE, Elastomer vs Steel @ 90% Torque	160
150	Axial Motion vs Time @ No Load	161
151	Axial Motion vs Time @ 100% Load	161
152	Torque Sprit History @ 100% Torque	163
153	Thermal Cycling of Elastomer Load Sharing Device	164
154	Test Gearbox, Initial Spalled Tooth, Double Helical	165
155	Test Gearbox, Spalled tooth, Double Helical Pinion	166
156	EHD Film/Surface Roughness vs Temperature	167
157	Upper Cover Vibration Frequency Analysis, Test Gearbox	169
158	Upper Cover Vibration Frequency Analysis, Dummy Gearbox	170
159	Scuffing on -041 DH Pinion, Overtorque Test	173
160	Scuffing on -042 DH Pinion, Overtorque Test	173
161	Scuffing on Bull Gear, Overtorque Test	174
162	Illustration of Shaft Misalignment	175
163	Gear Blank Temperature vs Idler Shaft Load	176
164	Fling-off Oil Temperature vs Idler Shaft Load	177
165	Comparison of Typical Vibration Levels	178
166	Measured and Predicted Induced Thrust, Steel Bearing	180
167	Measured and Predicted Induced Thrust, Ceramic Bearing	180
168	No Oil Survivability Test Results	182
169	1/2 Size Gearbox With Composite Housing	189
170	Unassembled Composite Housing Matched Set	190
171	Composite Housing Gage Location, Upper Plate	190
172	Composite Housing Gage Location, Lower Housing	191
173	Rectangular Strain Gage Rosette	192
174	IDM Sensor Body	195
175	IDM Installed on Composite Housing	195
176	Long Term Trend of Particles Accumulated	196
177	IDM Demo on Aircraft Gearbox With Chip Lights	196

LIST OF TABLES - FINAL REPORT
ADVANCED ROTORCRAFT TRANSMISSION (ART)

TABLE		PAGE
1	Potential ACA Engines	5
2	Aircraft and Engine Parameters for Various Engines	6
3	Baseline Aircraft, Aircraft Design Attributes	9
4	Baseline Aircraft, Summary Weight Statement	10
5	Baseline Aircraft, Mission Analysis	11
6	Summary of Transmission Design Parameters	11
7	Accessory Units Required for ART	14
8	Baseline Transmission System Component Weights	15
9	Baseline Transmission, CH53E MGB Removals	15
10	Baseline Transmission, Cabin and Cockpit Noise Estimates	16
11	Matrix of Bull Gear Designs	32
12	Bull Gear Support Trade Off Study	36
13	Preliminary Design Weight, MTBR, and Noise	48
14	Weight Savings by Downsizing Aircraft for Same Payload	51
15	Downsized Aircraft and Transmission	53
16	Aircraft Weight Savings w/Downsized ART	53
17	Performance at 4,000 ft, 95°F Day	53
18	Transmission Parameters Affecting Life Cycle Cost	55
19	Transmission Operating Cost Per Flight Hour	55
20	Aircraft Operating Cost Per Flight Hour	56
21	Aircraft Fleet Life Cycle Cost	56
22	ART Technology Advances	59
23	Full Sized ART, Basic Gear Data	60
24	Bending and Contact Stress, and Scoring Temperature Rise	60
25	Full Sized ART, Basic Bearing Data	61
26	Full Sized ART, Heat Generation Summary	63
27	Full Sized ART, Required and Actual Lubrication Flow	64
28	Composite Quill, Main Rotor Shaft, Truss Load Conditions	69
29	Diagnostic Strategies	79
30	Diagnostic System Processor Workload	80
31	Weight Comparison	81
32	Relationship of Design Parameters	86
33	One Half Sized ART, Basic Gear Data	87
34	Bending and Contact Stresses, and Scoring Index	87
35	One Half Sized ART, Basic Bearing Summary	87
36	Spring Rates and Strain Summary for Elastomeric Isolator	88
37	One Half Sized ART, Heat Generation Summary	91
38	One Half Sized ART, Actual and Theoretical Flow	93
39	Factors Affecting Gear Tooth Deflections	98
40	1/2 Size Gearbox Configuration Serial Numbers	111
41	1/2 Size Gearbox Configuration Backlash and Preload	112
42	Elastomeric Load Sharing Device Spring Rates	113
43	1/2 Size Gearbox Instrumentation	121
44	Facility and Test Bearing Instrumentation	125
45	No Load Lube Test Conditions	126
46	Gear Pattern Development Test Conditions	127
47	Strain Survey Test Conditions	129

LIST OF TABLES (Cont'd)

TABLE		PAGE
48	Load Sharing Survey Test Conditions, Steel	130
49	Transmission Error Survey Test Conditions	130
50	Housing Strain Survey Test Conditions	132
51	Endurance Test Spectrum	132
52	Overtorque Development Test Spectrum	134
53	Bearing Test Set-Up Conditions	135
54	Test Survey Loads and Speeds	136
55	Fretting Fatigue Test Summary	137
56	No Load Lube Test Results, Ambient Temperature (°F)	139
57	No Load Lube Test Results, Elevated Temperature (°F)	140
58	Steel Homing, Strain Survey Results	162
59	Endurance Test, Cumulative Test Test Time	162
60	Typical Stabilized Temperatures @ 100% Torque	168
61	Overtorque Test #1, Cumulative Test Time	171
62	Overtorque Test #2, Cumulative Test Time	172
63	Typical Stabilized Temperatures @ 120% Torque	175
64	Tooth Root Temperature Distributions	177
65	Comparison of Typical Vibration Levels	179
66	Steel vs Ceramic Bearings, 250 Hour Proof Test	181
67	Housing Strain Survey Test Conditions	192
68	Composite Housing Strain Survey Results	193

SUMMARY

The objectives of the Advanced Rotorcraft Transmission program were to develop the technology necessary to advance the state-of-the-art in helicopter transmission design and achieve a 25% reduction in weight, a 10 dB cabin noise reduction, and a 5,000 hour mean time between removals (MTBR), representing approximately a two to one improvement in reliability. Sikorsky chose as the baseline to which all work would be compared, a three engine Army Cargo Aircraft (ACA) of 85,000 pound gross weight. The ACA was designed to carry a payload of 25,000 pounds on a 500 KM mission radius. The baseline transmission configuration was the CH53E with a nose gearbox input, main bevel combining gear, and two stage planetary but sized to the 115:1 overall reduction ratio and 16030 HP input of the ACA.

Preliminary designs were conducted of split path and split torque transmissions to evaluate the weight, reliability, and noise and compare the improvements to the program goals. A split torque gearbox with a high reduction ratio double helical output gear was determined to be 23% lighter, greater than 10 dB quieter, and almost four times more reliable than the baseline two stage planetary design. The improvements were attributed to extensive use of composites, spring clutches located at the transmission input, advanced high hot hardness gear steels, the split path configuration itself, high reduction ratio, double helical gearing on the output stage, elastomeric load sharing devices, and elimination of accessory drives.

Detail design studies were conducted of the chosen split path configuration and drawings were produced of a 1/2 size gearbox consisting of a single engine path of the second stage spur mesh, and output stage double helical gear mesh. Fabrication and testing was then conducted on the 1/2 size gearbox. In a parallel effort, McGill Bearing Co., Valparaiso, Indiana designed, fabricated, and tested an angular contact spherical roller bearing. Bearings with steel rollers as well as ceramic rollers were fabricated and tested. The testing showed that ceramic rollers performed better than steel rollers especially under marginal lubrication regimes and outperformed the steel rollers under lost oil survivability testing. In other parallel efforts, Ohio State University developed methodology to analyze the transmission error in a double helical gear mesh and the Sikorsky materials department conducted fretting tests of Pyrowear 53 high hot hardness gear steel with and without thin dense chrome plating. No difference in allowable was found for 9310 with fretting, Pyrowear 53 with fretting and Pyrowear 53 with thin dense chrome plate with fretting.

The 1/2 size gearbox testing proved that the concept of the split path gearbox with high reduction ratio double helical output gear was sound. Topological tooth modifications permitted the high face width to diameter ratio double helical pinions to operate with good load distribution. Measured gearbox operating temperatures and vibration levels were low throughout the testing. Measured load sharing with the elastomeric load sharing device was excellent but the material chosen was not able to withstand the internal gearbox operating environment and further development is required. Measured load sharing without any load sharing device was acceptable so long as tolerances of the bearing bore locations and index tooth timing were tightly controlled. Testing also showed that the double helical gear is susceptible to surface deterioration effects from low EHD oil films inherent in the design.

INTRODUCTION

Traditional development of helicopter engines and transmissions have followed divergent paths in terms of development test time. Engines have been tested for thousands of hours prior to first flight whereas it is common for a helicopter transmission to have only hundreds of hours of testing. This has led to a reluctance on the part of transmission designers to advance the state-of-the-art in favor of more established and proven approaches. The ART program was designed to permit development of high risk items without involvement in success oriented schedules and production commitments. It was a highly coordinated effort by the government to structure a program incorporating key material and component technologies for advanced rotorcraft transmissions. The intent was to make a large improvement in the state-of-the-art by accumulation of test time on components with high payback in the areas of reduced weight, reduced noise, and increased reliability. The effort concentrated on high gain and comparatively high risk items that were systematically evaluated to solve problems prior to full scale development. Therefore many advanced and innovative concepts were tested.

The major thrust of the ART contract was the development of a high reduction ratio, torque splitting output stage. For minimum weight, the output stage of the split path design has a high aspect ratio of face width to diameter. For minimum noise, a double helical output stage was chosen. The double helical stage also alleviates some of the problems of high face width to diameter pinions since there are now two pinions which can be corrected for deflection separately. Split path designs have been used in production helicopters in the Soviet Union in their Mi-26 helicopter and in Great Britain at Westland in their Lynx helicopter. These production split path designs use quill shafts in the torque splitting branch to achieve load sharing. Westland has also accomplished design work on their "Advanced Engineering Gearbox" showing the weight advantages of split path designs with very high output stage reduction ratios. In the ART split path design, load sharing was achieved with an elastomeric load sharing device which achieved excellent load sharing but could not withstand the helicopter gearbox environment, and by the use of no load sharing device at all, relying instead on accurate bearing location and indexing of gear teeth. The load sharing achieved without any device was acceptable and can be likened to the load sharing between pinions of a planetary gearset which rely on accuracy of manufacture. Elimination of the quill shaft load sharing method, used in previous production helicopters, saves two bearings per shaft (four per engine), and replaces three major components with one.

The present ART program was divided into nine tasks. Task 1 consisted of selection of the ACA aircraft, the choice of three GE-38 engines as the powerplant, definition of the CH-53E transmission as the baseline (uprated to the reduction ratio and power requirements of the ACA), determination of the baseline performance, and definition of the methods to be used to quantify the baseline and advanced designs. Task 2 was the preliminary design phase of the program. Split path and split torque main transmission designs were completed through the layout stage. For each type of transmission two layouts were

completed, one having an output reduction ratio of approximately 8 to 1 and one design having an output reduction ratio of approximately 10 to 1. Advanced technology was incorporated into these designs in as many areas as possible. In task 3, the advanced designs were evaluated and compared to the baseline. A split path design, with a reduction ratio of 9.77 to 1 was chosen based on 23% reduced weight, 4 to 1 improvement in reliability and greater than 10 dB reduction in cabin noise level. In the task 4 detail design phase, those elements of the advanced split path design that would be tested were chosen and detail designs conducted. Because of the cost impact of full sized ACA components, a 1/2 scale test article consisting of the second and third stage of a single engine path of the split path gearbox was selected for evaluation. In addition, angular contact spherical roller bearings, double helical gear transmission error, and fretting of Pyrowear 53 gear material was selected for further assessment. Task 5 consisted of preparation of test plans while task 6 was fabrication of test facilities and test rigs, and task 7 was fabrication of test components. Testing was carried out in task 8 in three areas. Fretting tests were conducted on Pyrowear 53 steel with and without thin dense chrome plating to determine allowables compared to baseline 9310 steel and to see if thin dense chrome plating afforded any benefits. Testing was accomplished to determine if a single angular contact spherical roller bearing could replace the current state-of-the-art ball/roller combination in a high speed application having radial and thrust loads. Finally, a 1/2 size gearbox was tested to determine load sharing characteristics and operation of high face width to diameter double helical gear set. The final task was reporting.

This report is written to document the work, describe the results, and present conclusions reached.

SELECTION OF EVALUATION PROCEDURES

Baseline Aircraft

The Army Cargo Aircraft (ACA) was chosen as the baseline aircraft for which all studies were directed. At the time the baseline aircraft was chosen, the projected ACA requirements were given in the U. S. Army draft Operational and Organizational (O&O) Plan dated 18 March 1988. Requirements for the ACA defined at that time resulted in a solution in excess of 100000 pounds gross weight.

Recognizing the ACA size and cost implications of the O&O plan requirements, the Army awarded a contract to Sikorsky Aircraft in September of 1988 to study the most cost effective size for the ACA consistent with the spectrum of combat lift requirements. The resulting ACA requirements were found to be less demanding than the O&O plan but still beyond what could be met by a reasonable growth of the CH-47 or CH-53E

Figure 1 shows a plot of payload vs radius of action for various ambient conditions and also shows how the gross weight of the ACA solution will vary with payload and radius of action. The plots are made on the assumption of 1995 airframe technology, scaled engines of the MTDE technology, and a disc loading of 10 pounds per square foot. A payload of 25,000 pounds at 500 km mission radius was chosen as a reasonable compromise between the most demanding requirements of the O&O plan and an affordable ACA solution. Gross weight is between 80,000 and 85,000 pounds for this aircraft.

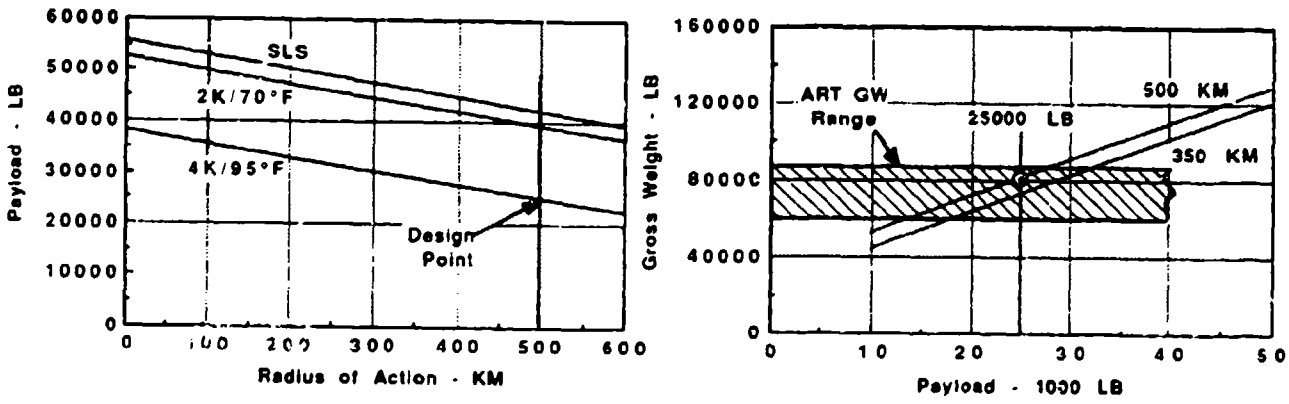

Figure 1. ACA Gross Weight, Payload, and Performance

The selected ACA design criteria are summarized as follows:

- Design Mission of 25,000 lb/500 km Radius of Action
- 1995 Airframe and Rotor Technologies Using Composites. Fly-by-Wire, Bearingless Main Rotor, etc.
- Cabin With C-130/C-141 Cross Section
- Rotor Sized to Provide 200 fpm VROC at 95% IRP, 4K/95°F
- Transmission Rated at Power Required for HOGE at 2K/70°F with Full Fuel and 150% of Design Mission Payload

Three General Electric GE38 growth engines with a sea level standard day intermediate rated power (IRP) of 6180 HP each were selected for the ACA design. The selection process included a survey of potentially available engines in the required power class and determination of the lightest weight, most fuel efficient ACA solution consistent with engine availability in the time frame of the advanced transmission technology.

Potential engines are listed in Table 1 along with their power ratings, specific fuel consumption, and qualification status. Figure 2 compares the nominal engine power requirements for two and three engine ACA solutions, considering both the design takeoff condition and the one-engine inoperative (OEI) hover in ground effect requirement. Clearly, a two engine solution is unattractive, requiring about double the engine size of a three engine solution. Three engines provide a good match between the takeoff and engine out conditions.

Table 1. Potential ACA Engines

	SEA LEVEL STD IRP/SFC	4000 FT 95°F IRP/SFC	ENGINE STATUS
T64-GE-419	4560/.470	3492/.485	1991 H-53E Prod
T55-L-714	4527/.502	3350/.524	1989 Qualified
YT406-AD-400	6150/.435	4940/.431	Prototype for MV-22
T406 PLUS	6150/.411	4940/.407	1992 Qualification
GE 38	6180/.367	4549/.379	1995 Qualification
XT701-AD-700	8079/.471	6416/.472	Inactive HLH Engine
JTAGG-L	8000-10000 SHP CLASS		Undefined

ACA solutions were sized using the Helicopter Design Model which calculates helicopter design attributes, weights, and performance. Candidate engines used for sizing were four T64-GE-419's, three T406 plus's, three GE38's, and four GE38's. In all cases projected advanced transmission weight savings of 25% were assumed compared to the current CH53E transmission. The results are summarized in Table 2. The three engine GE38 solution was selected based on lightest weight and lowest fuel consumption.

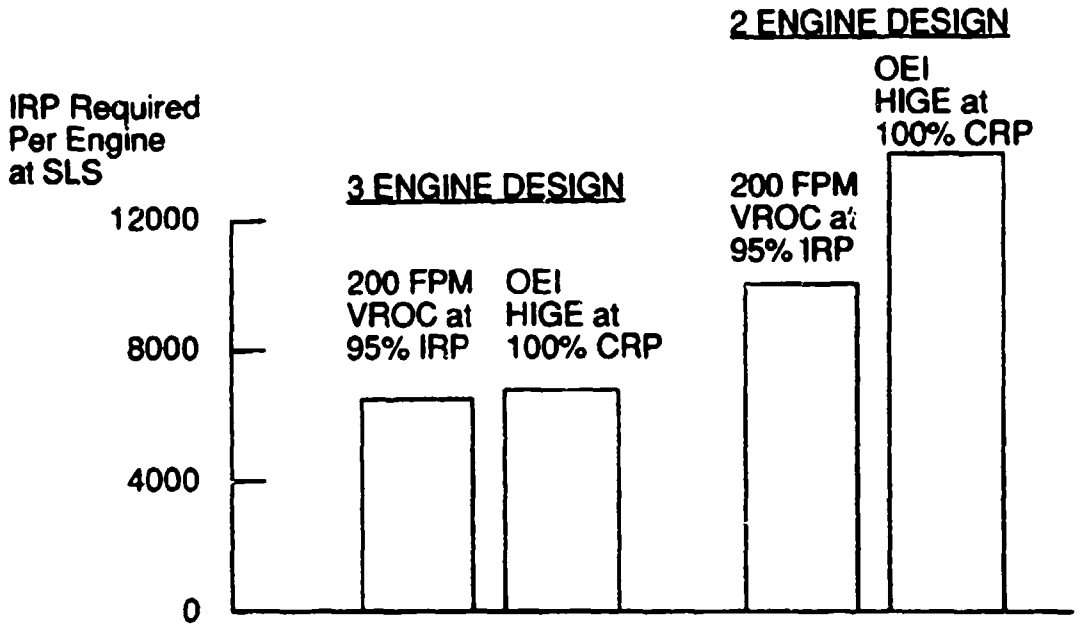

Figure 2. Power Required for Climb and OEI, 2 vs 3 Engines

Table 2. Aircraft and Engine Parameters for Various Engines

	(4) T64-GE-419	(3) T406 PLUS	(3) GE-38	(4) GE-38
Total 4K/95 IRP	13,968	14,820	13,647	18,196
SFC - Lb/HP-Hr	0.485	0.407	0.379	0.379
Mission Fuel - Lb	21,400	17,500	15,650	18,100
Weight Empty - Lb	44,400	41,400	39,900	41,900
Gross Weight - Lb	91,800	84,900	81,500	86,000
Disc Loading - PSF	8.3	10.9	10.0	16.0
Rotor Diameter - Ft	122.5	102.6	104.9	85.6

Using three GE38 engines in an ACA with a gross weight of approximately 85,000 pounds and a payload of approximately 25,000 pounds, a baseline aircraft was designed. Performance at sea level at 59°F standard day and at 4,000 feet at 95°F are compared in Figures 3 and 4. A plot of payload vs radius of action is shown in Figure 5. A three view drawing of the baseline ACA is depicted in Figure 6 while Table 3 shows aircraft design attributes, Table 4 is a summary of weight, and Table 5 is a mission analysis summary.

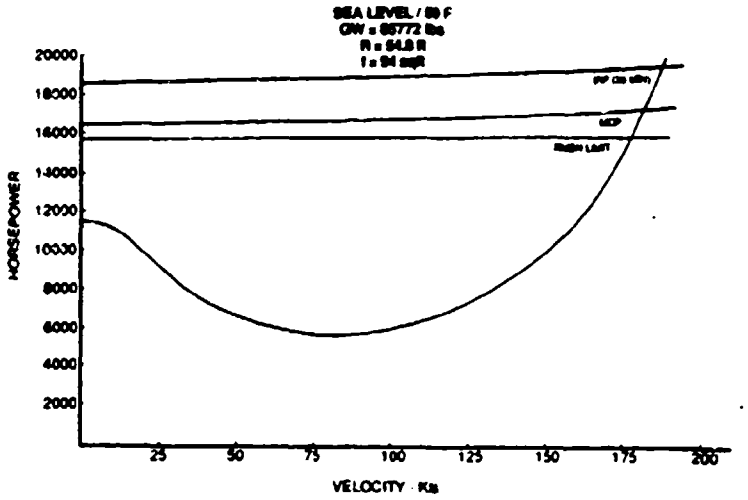

Figure 3. ACA Baseline, Power Required vs Airspeed at Sea Level

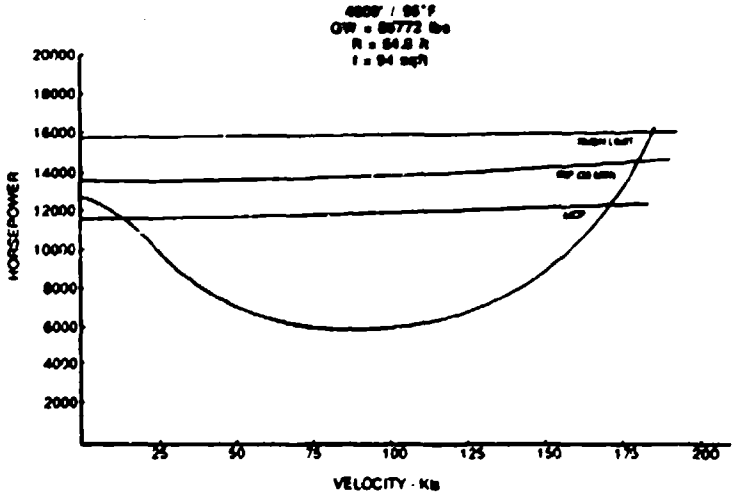

Figure 4. ACA Baseline, Power Required vs Airspeed at 4000 Feet

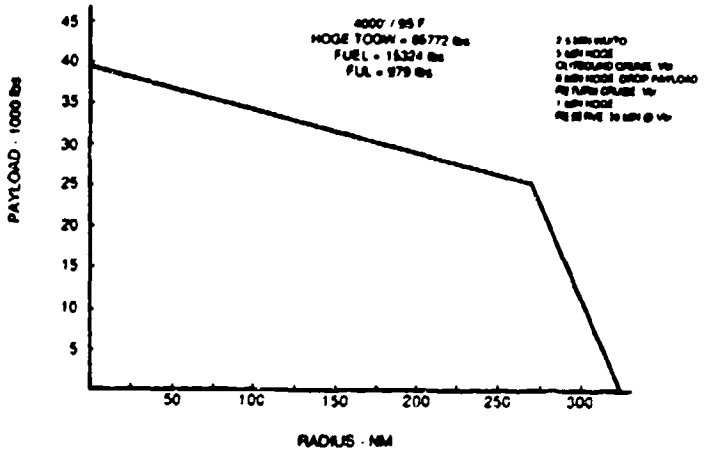

Figure 5. ACA Baseline, Payload vs Radius

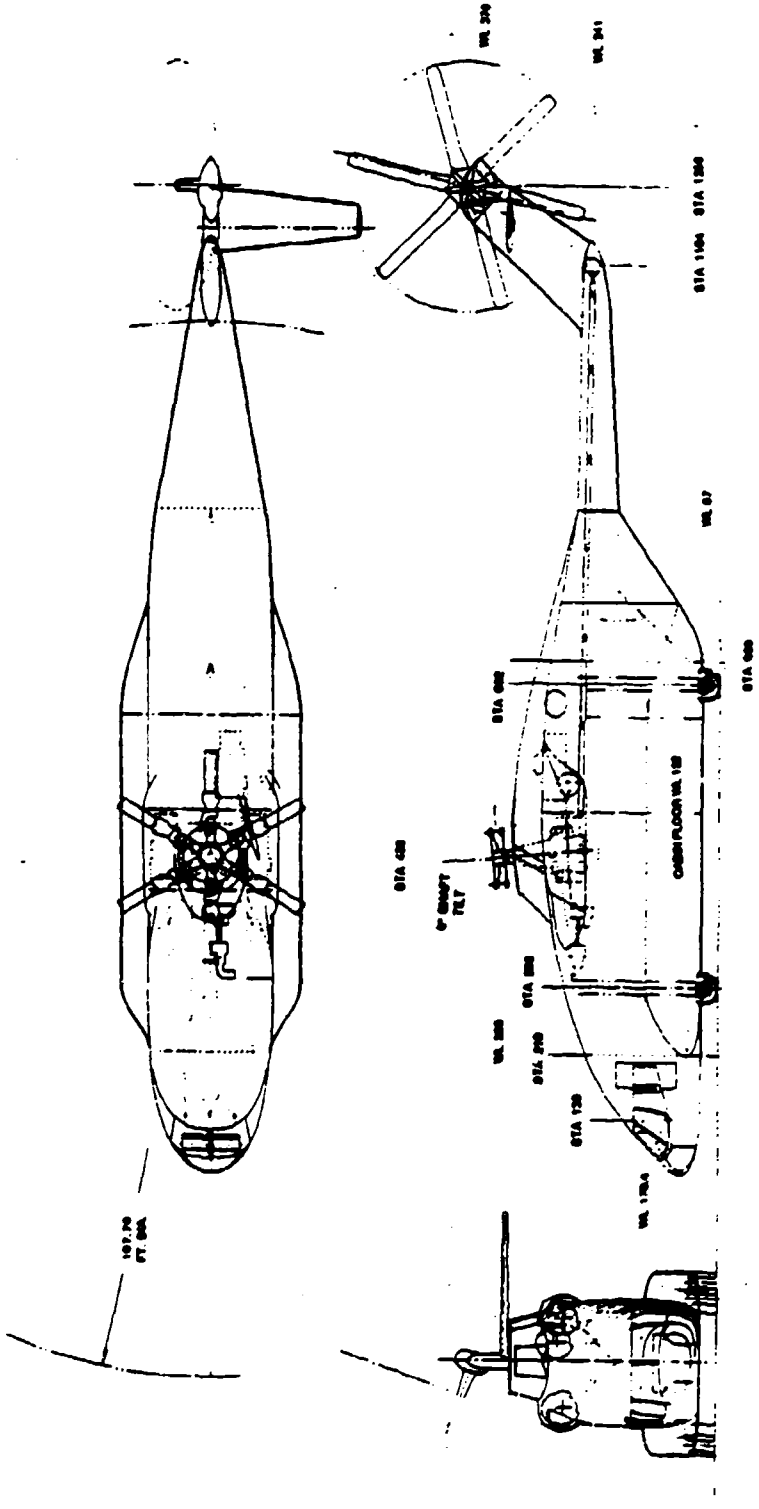

Figure 6. ACA Baseline Aircraft

Table 3. Baseline Aircraft, Aircraft Design Attributes

General		Main Rotor		Tail Rotor	
Des G.W. (Lb)	85772	Radius (Ft)	54.80	Radius (Ft)	12.01
Payload (Lb)	25000	Aero Chord (Ft)	3.200	Chord (Ft)	1.587
Wgt Empty (Lb)	44469	Geom Chord (Ft)	3.200		
Fuel (Lb)	15324	No of Blades	6	No of Blades	5
Hover HP	12609	Rotor Solidity	.1113	Sdty/Act Fac	.2104
Climb HP	12961	Tip Speed (FPS)	725.0	Tip Speed (FPS)	725.0
MR Design HP	10924	Aero Asp Ratio	17.123	Aspect Ratio	7.566
SLSS HP/Eng	9270	Geo Asp Ratio	17.123		
Par Drag (Sq Ft)	94.0	CT/Sigma	0.0840	CT/Sigma	0.0800
Vertical Drag	0.07000				
TR Cant (Deg)	20.00	MR Lift (Lb)	8334.5	TR Lift (Lb)	2437.5
MR Disc (PSF)	9.46	Figure of Merit	0.7571	Figure of Merit	0.6962
MGB Design HP	15651	Bl Area (Sq Ft)	1052.3	Bl Area (Sq Ft)	95.3

Baseline Transmission

The baseline transmission system for the ACA aircraft is based on the technology of the CH53E. The ACA transmission system has the same configuration as the CH53E but has been resized to the requirements of power and speed of the ACA. The gear and bearing sizing is based on the same level of reliability as the CH53E and has similar stresses, deflections, and lives. The transmission system consists of a number 1 and number 3 engine nose gearbox which connect to the main gearbox thru input drive shafting. The number 2 engine drives through a series of spur gears in the rear cover of the main gearbox to the main bevel mesh which then combines power from all three engines. A shaft transmits power from the combining output bevel gear shaft to the sun gear of the first stage planetary. The first stage planetary carrier drives the second stage planetary sun gear. Finally the second stage planetary carrier drives the main rotor shaft. Both the first and second stage planetary ring gears are fixed to the main transmission housing through a common shaft. Drive shafting from the rear cover area of the main gearbox transmits torque through a series of drive shafts to the intermediate gearbox, up the pylon shaft, and to the tail gearbox whereupon the tail rotor is driven.

The installation of the baseline CH53E type transmission system in the ACA aircraft is shown in Figure 7. A cross sectional layout of the ACA baseline main gearbox having the configuration of the CH53E is depicted in Figure 8 which also shows the rpms, reduction ratio's, numbers of teeth, and pitch diameters for the main meshes. This gearbox has been sized to the speed and power requirements of the ACA.

Table 4. Baseline Aircraft, Summary Weight Statement

Group	Weight (Lb)		% GW
Main Rotor Group		8569	9.99
Tail Group		1072	1.25
Tail Rotor/Fan	564		0.66
Tail Surfaces	508		0.59
Body Group		9599	11.19
Alighting Gear		1966	2.29
Flight Controls		1907	2.22
Engine Section		534	0.62
Propulsion Group		15575	18.16
Engines	2790		3.25
Air Induction	174		0.20
Exhaust System	91		0.11
Fuel System	1456		1.70
Engine Controls	74		0.09
Starting System	193		0.23
Drive System	10797		12.59
Auxiliary Power Unit		288	0.34
Instruments		140	0.16
Hydraulics		230	0.27
Electrical Group		750	0.87
Avionics		963	1.12
Armament Group		145	0.17
Furnishings		610	0.71
Air Conditioning and Anti-Ice		380	0.44
Auxiliary Gear		850	0.99
Contingency		889	1.04
Weight Empty		44469	51.85
Fixed Useful Load		979	1.14
Pilot	233		
Co-Pilot	233		
Fuel Trapped	80		
Mission Equipment	200		
Other Ful.	233		
Payload		25000	29.15
Useable Fuel		15324	17.87
Gross Weight		85772	

Transmission Design Data

The basic transmission design parameters for the baseline as well as for the advanced split torque and split path transmissions are shown in Table 6. Since one engine inoperative (OEI) power is felt all the way to the final stage bull gear mesh in the split path type of arrangement, the gearbox is essentially sized to OEI conditions. For the bull gear mesh, tail power and losses are removed from the input power and the bull gear is designed to somewhat lower requirements. The accessory units are assumed to be identical to those used on the CH53E in terms of type, number, speed, and power and are listed in Table 7.

Table 5. Baseline Aircraft, Mission Analysis

Mode	Gr Wgt (lb)	Speed (Kts)	VStall (Kts)	Dist (NM)	Time (Min)	SHP	Fuel (Lb)	SFC
WU/TO	85684	-	-	-	2.5	11577	199	.389
Hover	85371	-	-	-	5.0	12550	424	.383
Cruise	81712	152.4	179.8	270.1	106.3	8618	6765	.418
Hover	78203	-	-	-	5.0	11066	385	.394
Hover	52928	-	-	-	3.0	6775	165	.458
Cruise	49909	143.2	234.3	270.1	113.2	6266	5813	.464
Hover	47008	-	-	-	1.0	5957	50	.477
Res Cr	46219	143.3	241.7	71.6	30.0	6164	1523	.466

Total Mission Fuel is 15324 Lbs
Total Mission Time is 236.1 Minutes

Notes:
Total Gross Weight = 85783 Lbs, Rotor Radius = 54.8 Ft,
Parasite Drag = 94.0 Sq Ft, Temperature = 95°F, Altitude = 4000 Ft.

Table 6. Summary of Transmission Design Parameters

Engine RPM	15000
Main Rotor RPM	130
Overall MGB Reduction Ratio	115.38
MGB Input HP	16030
MGB Input HP (Limit)	32060
Engine HP (OEI)	6209
Main Rotor HP	14825
Main Rotor HP (Limit)	29650
Tail Rotor RPM	580
Tail Rotor HP (Gears)	2400
Tail Rotor HP (Limit)	4328

Methodology

Baseline gearbox weight was determined using statistical weight equations that utilize rudimentary weight parameters such as design torque and reduction ratio. Layout weight calculations were conducted on the advanced split path and split torque designs to obtain the individual component weights and to enable identification of bulk items which the layout does not include such as hardware, protective coatings, sealants, bosses on castings, lubrication system components, oils, etc. Once identified, the bulk item weights are estimated using values obtained from systems of similar design. These layout calculations are compared to the analytical weight and differences resolved.

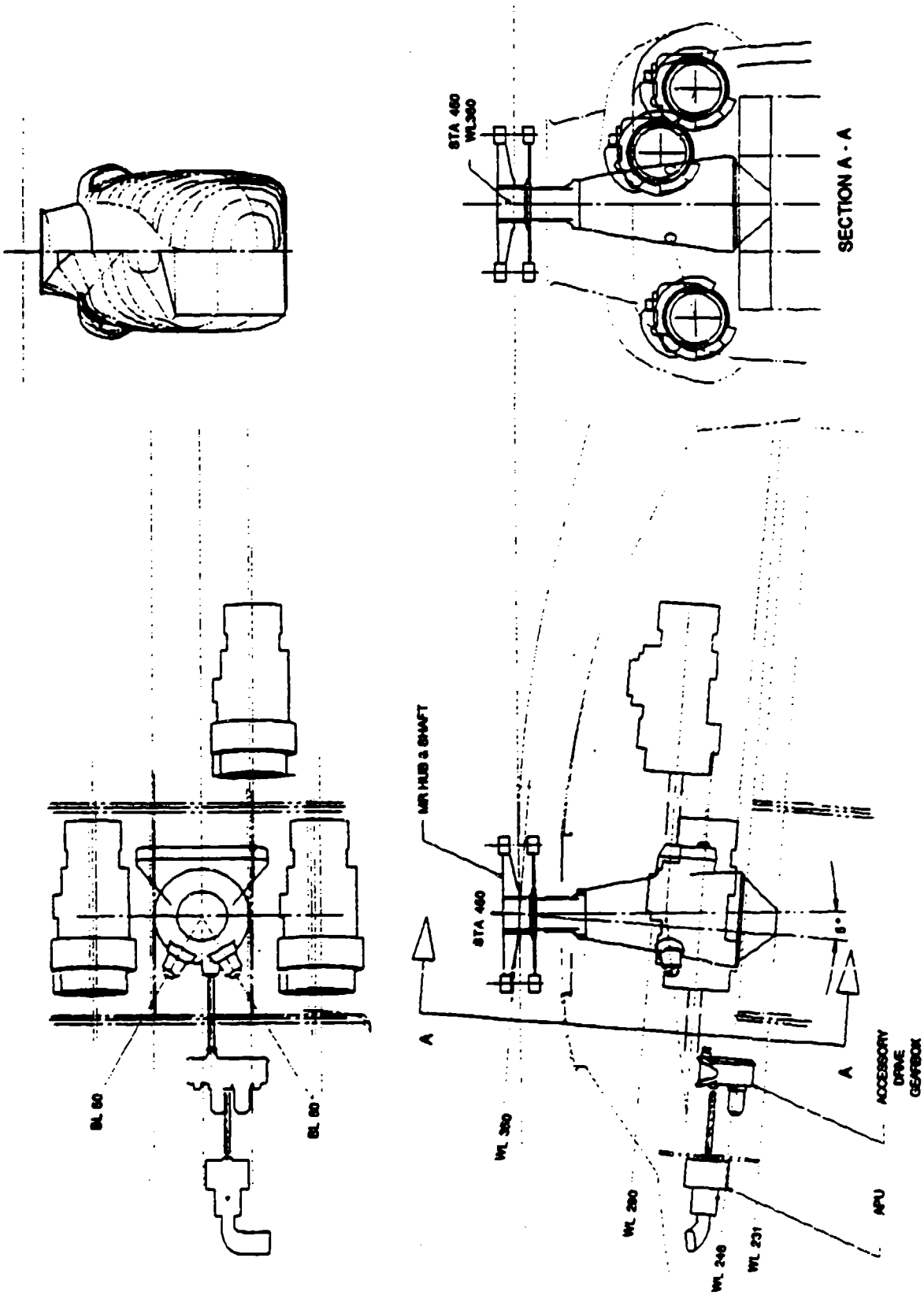

Figure 7. Baseline Transmission Installation

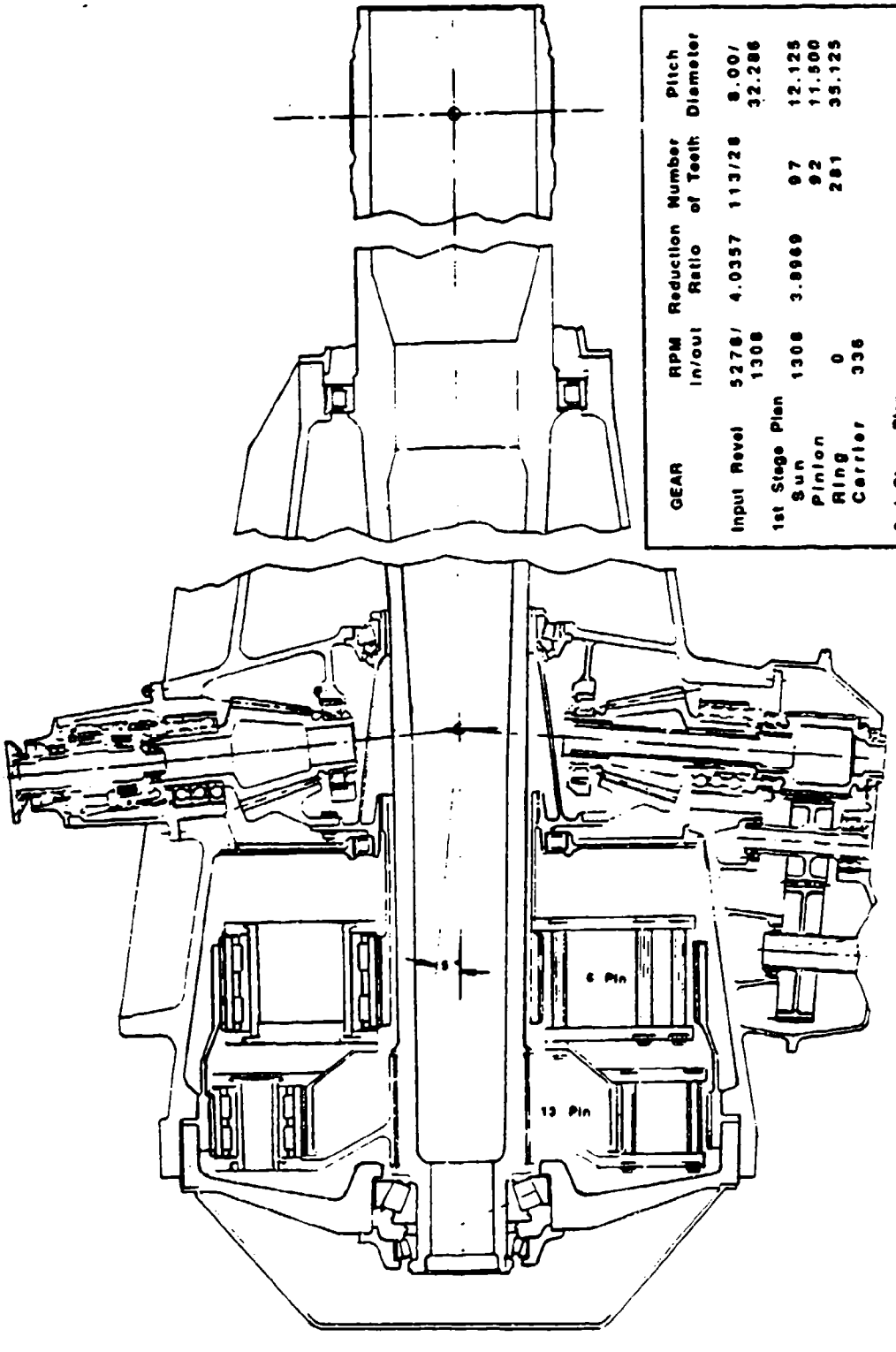

GEAR	RPM In/out	Reduction Ratio	Number of Teeth	Pitch Diameter
Input Revol	5278/ 1308	4.0357	113/28	8.00/ 32.286
1st Stage Plan				
Sun	1308	3.8969	97	12.125
Pinion			92	11.500
Ring	0		281	35.125
Carrier	336			
2nd Stage Plan				
Sun	336	2.5816	141	23.500
Pinion			41	6.833
Ring	0		223	37.167
Carrier	130			

Figure 8. ACA Baseline Transmission

Table 7. Accessory Units Required for ART

Unit	HP	RPM	Location
Generator #1	107	6019	Accessory Gearbox
Generator #2	107	6022	Accessory Gearbox
Generator #3	107	5987	Main Gearbox
Utility Pump	32	4047	Accessory Gearbox
2nd Stage Servo Pump	54	4111	Accessory Gearbox
Primary Servo	54	4419	Main Gearbox
Tachometer, Main Rotor	1	4419	Main Gearbox
Oil Cooler	100	6291	Main Gearbox
MGB Lube Pump #1	4	1983	Main Gearbox
MGB Lube Pump #2	2	2379	Main Gearbox
Acc. Gearbox Lube Pump	2	5180	Accessory Gearbox
Engine Tachometer (3)	1	4082	Nose(2), MGB (1)
Fuel Control Tach (3)	1	3794	Nose(2), MGB (1)
Hoist Pump	100	5755	Accessory Gearbox
Engine Start Pump	110	4316	Accessory Gearbox
Auxiliary Power Unit	110	8354	Accessory Gearbox

The ART noise evaluation methodology encompasses three major elements needed to determine the effects of design tradeoffs on ART noise levels and in cumulative noise reduction benefits achieved. These elements are largely sequential and include; (1) the application of established gear noise characteristics during the preliminary and detail design efforts to evaluate design parameters. (2) the application of gear noise, finite element, and gear design models to more accurately predict and subsequently reduce ART source noise levels, and (3) Component testing to refine and validate the analytical estimates of ART noise levels. Rotorcraft interior noise levels are ultimately determined by a combination of source, energy transmission path, and receiver (aircraft interior) characteristics The ART noise evaluation methodology concentrates on acoustic evaluations of gearbox design configurations and parameters. Since characterization of the vibration transmission paths in the airframe and aircraft interior are beyond the scope of the ART design effort, estimates of the total noise reduction requirement for ART was achieved by estimates in reduction of source level noise. These reductions were estimated by comparing similar designs of spur gears, high contact ratio spur gears, helical gears, and herringbone gears with high helix angles.

MTBR was calculated by the hazard function analysis method which uses historical helicopter transmission failure rate data that has been gathered from examination of gearboxes at overhaul. Weibul and statistical analyses are used to account for every different type of failure mode in each component of the transmission. Reliability of gears and bearings, the major components which have an effect on MTBR, are calculated from analysis of gear stress and bearing life. Other failure modes, such as free wheel unit wear, housing cracks/fracture/corrosion, o-ring leakage, sheared bolts, plugged jets, loose nuts, seal leakage, etc. are accounted for by using the historical data base. Note that only failure modes which cause gearbox removals are counted against removal rates. For example, seal leakage is not counted if the seal is field replaceable.

Baseline Weight, Noise, MTBR

The baseline transmission system weight derived from historical weight trending equations is shown in Table 8. Gearbox removal data for the CH53E main gearbox is shown in Table 9. An observed MTBR of 1400 hours is seen from the data showing 85 removals in 119,000 flight hours. The theoretical calculated MTBR for the CH53E transmission is 963 hours using the hazard function analysis method which results in a correlation factor of 1.41 to be applied to the calculations for the baseline ACA, and split path and split torque designs. The calculated baseline ACA transmission MTBR is 997 hours using the correlation factor of 1.41 from the observed data. The baseline cabin and cockpit noise estimates are shown in Table 10.

Table 8. Baseline Transmission System Component Weights

Item	Weight (Lbs)
Main Gearbox	6882
Main Rotor Shaft	1412
Nose Gearboxes (2)	676
Accessory Gearbox	280
Intermediate Gearbox	209
Tail Gearbox	596
Tail and Pylon Shafts	484
Other Shafts	150
Rotor Brake	108
Total Weight	10797

Table 9. Baseline Transmission, CH53E MGB Removals

Item	Number of Removals
1st Stage Planetary Bearings	16
No 2 Free Wheel Unit Assembly	13
Retainer Clip	9
Laminated Shim Stock	8
2nd Stage Planetary Bearings	8
No 2 Gimbal Assembly	7
F.O.D.	2
Main Rotor Shaft Timken Bearing	1
Auxiliary Oil Pressure Loss	1
Number 2 Bevel Triplex Bearing	1
High Speed Roller Bearing	1
Main Bevel Case/Core Fracture	1
Oil Leakage	1
Bull Gear Rim Fracture	1
Sheared Accessory Take-Off Gear	1
Others	14
Totals	85

85 CH53E main gearbox removals in 119000 flight hours

Table 10. Baseline Transmission, Cabin and Cockpit Noise Estimates

Center Freq (Hz)	Cabin OGE Hover Octave Level (dB)	Cabin 150 KIAS Octave Level (dB)	Cockpit OGE Hover Octave Level (dB)	Cockpit 150 KIAS Octave Level (dB)
63	110	112	105	107
125	106	110	101	103
250	104	106	97	100
500	106	108	97	100
1000	110	115	104	102
2000	110	112	102	100
4000	104	105	94	92
8000	95	97	85	85
16000	88	89	81	84
dBA	114	118	108	105
SIL-4	108	110	99	99

PRELIMINARY DESIGN

Four preliminary designs were completed in the preliminary design phase of the program. Designs of split path and split torque gearboxes were completed for a high output bull gear reduction ratio of 10.85:1 (141/13) and a lower ratio of 8.15:1 (106/13) for a total of two ratios of split torque and two ratios of split path designs. Later during the detail design phase of the program, the maximum ratio was reduced to 9.77:1 (127/13) when detail analysis showed high stresses in the bull pinion shaft. Weight, noise, and MTBR were then evaluated for these four designs and compared.

Split Torque

The split torque gearbox is characterized by an input planetary system that acts as a differential to assure load sharing. Figure 9 is a schematic of the arrangement. Power is input from each engine to the sun gear of the differential planetary. The ring gear is used as an output to a bevel pinion which drives one torque splitting branch while the carrier drives a second bevel pinion to the other torque splitting branch. The advantage of this arrangement is that torque is inherently balanced since any tendency for maldistribution of torque split will be balanced by a slight rotation of the carrier relative to the ring gear to thus make up the difference. The disadvantage is that the entire engine drive is lost if either branch is lost. Note that the bevel pinions are arranged on opposite sides of the bevel gears to obtain the correct direction of rotation since the ring gear and carrier of the planetary rotate in different directions. Each output bevel gear drives one bull pinion which then combines power onto the output bull gear.

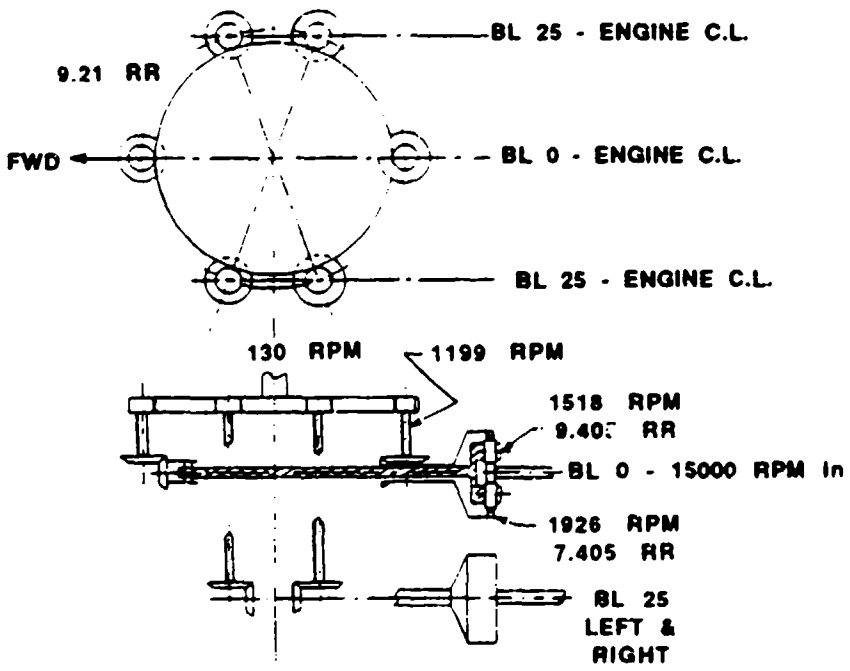

Figure 9. Schematic of Split Torque Main Transmission

The #2 engine carrier drive shaft must pass across the bull gear on butt line 0 to connect the second bevel pinion of the #2 engine. The only place that this is possible is under the bull gear since the main rotor shaft must transmit torque upward to the rotor head on top of the bull gear. Placing the carrier drive shaft under the bull gear proved to be a large disadvantage for the three engine split torque gearbox. For a two engine design, the requirement goes away since the carrier shafts can pass along side of the main rotor shaft. The differential planetary itself can achieve a relatively high reduction ratio since there is no fixed member. The lowest weight, however, is achieved by the largest reduction at the last stage. Therefore the high reduction ratios possible with the torque splitting planetary is of little advantage.

Figure 10 is a cross section of the split torque main gearbox designed to the requirements of the ACA. The output bull gear has been set at 48 inches in diameter to accommodate manufacturing. Although gear grinding equipment exists for this size, there is no quench press equipment for holding the bull gear during the quenching cycle of carburization. It was felt that a quench press for this size could be manufactured and the gear carburized. Other processes were considered such as induction hardening but the weight increase created by reduced allowables did not justify the change. The output bull gears of both the split torque and split path designs are all made with 48 inch pitch diameters (approximately).

Engine power for the split torque gearbox is input directly to a spring overrunning clutch located at the input. The spring clutch design is common to all preliminary gearbox designs. For the #1 and #3 engines, the output of the spring clutch drives the sun gear of the differential planetary. For the #2 engine, 2 stages of bevel gears are required so that the #2 engine can be located at the correct waterline, and still have room for the tail-take-off to be located under the #2 engine. The bull gear is designed as a herringbone or double helical mesh with opposing hands of helix. This arrangement permits the use of high helix angles for reduced noise and yet does not create bearing problems since the thrust cancels. One basic problem with the split torque design is that the herringbone pinions are on the same shaft as the 2nd stage bevel gears. The bevel gears require that the mounting be fixed so that the bevel gear pitch apex point can be located at the intersection of the bevel pinion and gear. On the other hand the designer would like the herringbone pinions to float while the single bull gear remains fixed axially such that the thrust loads would equilibrate. If the bull gear floats, each fixed bull pinion would have to be shimmed so that all the intersections between left and right hand helix members lie in a plane. A literature search showed that no designs of herringbone gears could be found that had fixed multiple pinions. A solution would be to fix the second stage bevel gear and to permit the herringbone pinions to float using an axially compliant coupling between the members.

The tail-take-off (TTO) for the split torque gearbox also required an extra spur gear mesh to get the TTO bevel gear set away from the input bevel gear set. The additional gearing required for the #2 engine input and TTO mesh also reduced the reliability of the split torque design. Thus the advantage of the inherent load sharing is offset by the disadvantages of extra gearing

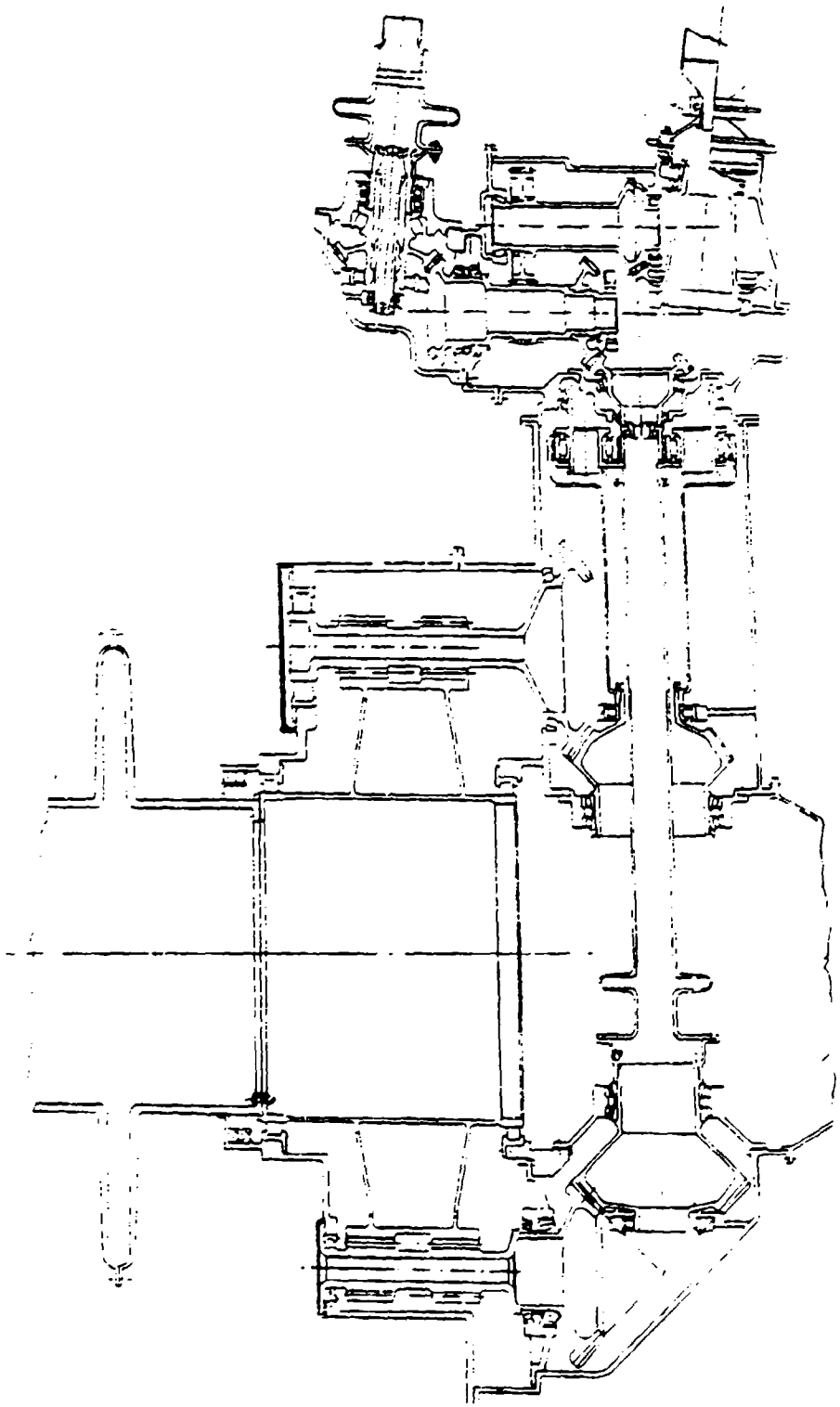

Figure 10. 11:1 Split Torque Cross Section

required for the #2 engine input. This showed up in the weight and MTBR calculations that will be reviewed in subsequent sections of this report.

Split Path

The split path gearbox is characterized by a "closed loop" of gearing where an integer number of teeth must be designed to fit in a circular arc path that is common to the the bull gear and 2nd stage spur pinion and either the 2nd stage bull gear or the bull pinion depending on the choice of teeth by the designer (See "Load Sharing Devices" section of this chapter for an explanation of the closed loop). If any member in the path is lost, the drive will still continue through the other path. Figure 11 is a schematic of the split path gearbox.

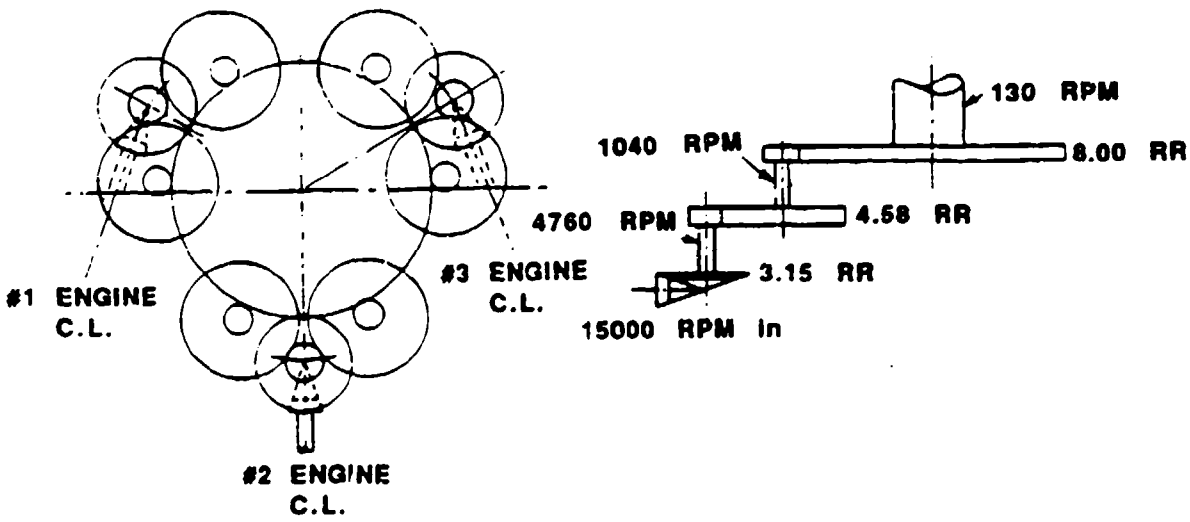

Figure 11. Schematic of Split Path Main Transmission

In the split path design power is input to an overrunning spring clutch and then directly into a bevel pinion. The output bevel gear centerline is parallel to the main rotor shaft centerline. The second stage of gearing is a parallel axis gear set where the torque is split in two for each engine drive. The output stage herringbone bull pinions are driven directly by the parallel axis output gear. As in the split torque design, the output bull gear combines power from each engine and transmits torque to the main rotor by means of the output quill shaft.

Figure 12 is a cross section of the split path gearbox. Load sharing between torque splitting assemblies must be controlled in the split path gearbox. A new load sharing device is shown in Figure 12 located on the flange of the spur gear and between the spur gear and herringbone pinion. The device shown contains alternate layers of rubber and metal forming a torsionally soft but radially and axially stiff member (See "Load Sharing Devices" section of this report for further discussion). A plan view of the split path gearing arrangement is shown in Figure 13. Since the bull pinions are equally spaced in groups of three about the bull gear, the resultant bearing reaction is zero if

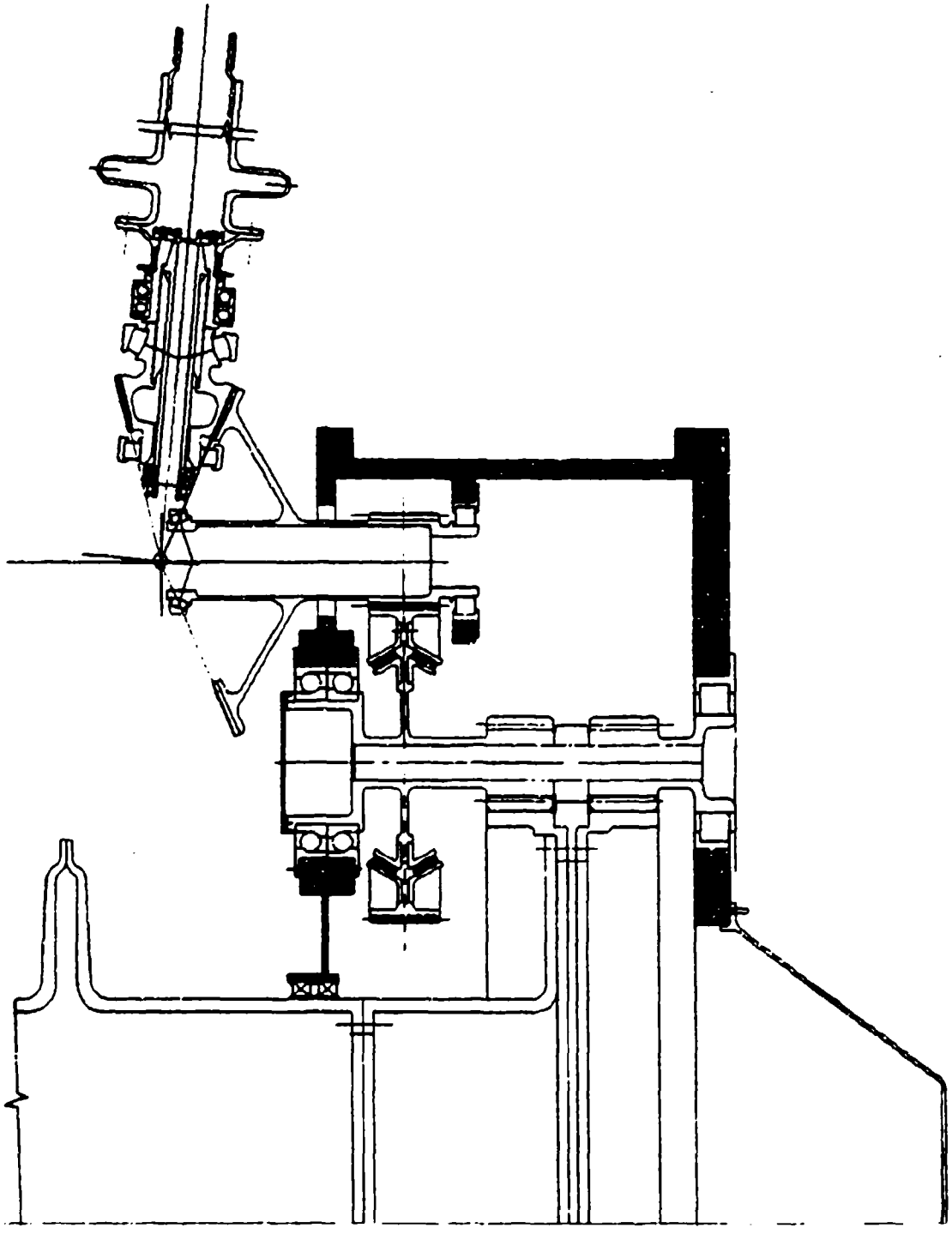

Figure 12. 11:1 Split Path Cross Section

all inputs have the same power. For this reason a design was developed for a bull gear without any bearings that relies for support on the central rings which are the same size as the pitch diameters of the gears. Under normal conditions, the rings do not touch because of deflections of the rims. Under OEI conditions, the bull gear will be forced to one side and the rings will act as supports through the bull pinion shafts. (See "Bearingless Bull Gear Design" section of this report for further discussion). If a spur gear is used in the second stage, the shaft assembly consisting of the second stage gear and bull pinion can be designed to float on roller bearings and the bull gear can be fixed. This is the normal state-of-the-art method of load control between halves of a herringbone gear set. When using this design however, the bearingless bull gear can not be used since by definition the bull gear must be free to float. In the final detail design as will be seen, the bearingless bull gear design was not used so that the bull gear could be fixed and the bull pinions floating. The output composite quill shaft is approximately 24 inches in diameter and transmits only torque to the main rotor. Main rotor loads are reacted by the upper truss assembly (See "Composite Main Rotor Shaft/Quill/Standpipe" section of this report).

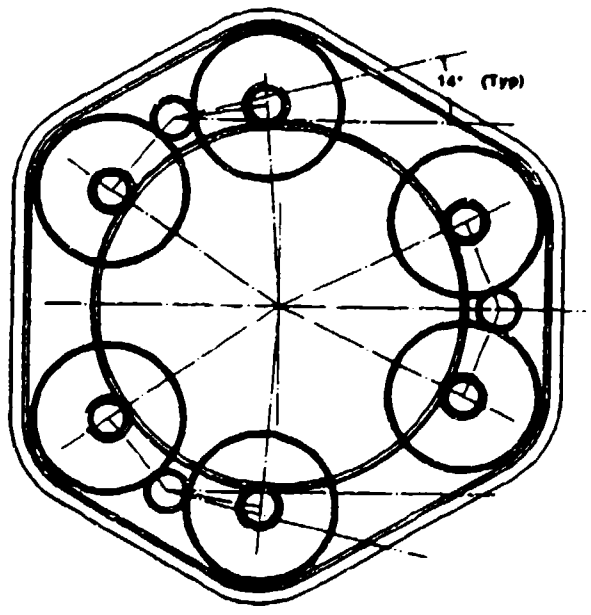

Figure 13. Split Path Top View

Trade-Off Studies

Trade off studies were conducted on various details of both the split torque and split path designs to determine the best approach to use. The following sections of the report discuss the details of the more important trade off studies.

Load Sharing Devices

Split path designs must rely on load sharing methods for successful operation. Prior to selection of a load sharing device for the ART gearbox, many devices were examined. Figure 14 shows why load sharing devices are required. The arc length abcde in Figure 14 times 2 (for the two halves) must be divisible by an integer number of teeth or the gears will not assemble or operate properly. The line cd in Figure 14 represents an angular relationship between teeth of the spur gear and herringbone pinion. It can be seen that manufacturing errors in the angular relationship between teeth can cause one half of the mesh to be in contact while the other half is not depending on the stiffness of the parts. For infinitely rigid parts, even small errors would cause all the load to travel to one path of the split path design and no load to the other path. To overcome this, transmission designers have placed torsionally compliant members between the spur gear and output pinion.

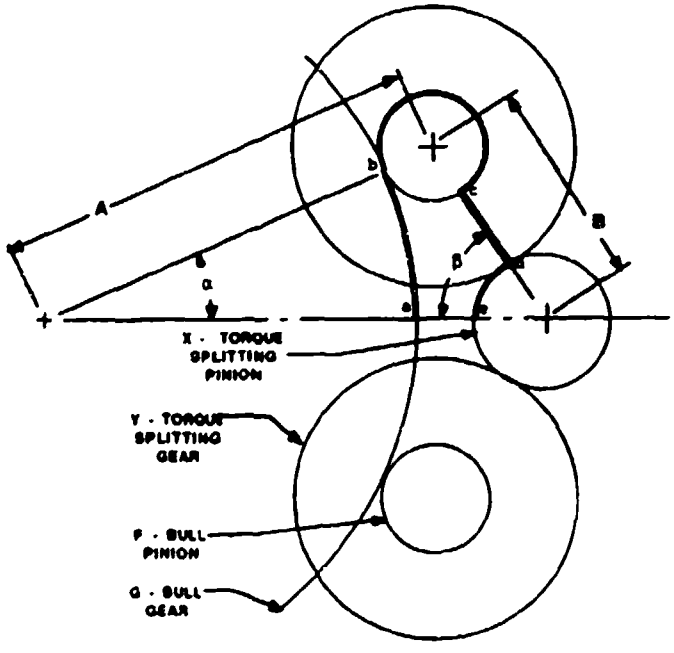

Figure 14. Tooth Geometry Relationships for Torque Splitting Drive

State-of-the-art split path designs used in England by Westland Helicopters and in Russia on the MIL-26 helicopter have used a quill shaft to provide the torsional compliance between members as shown in Figure 15. A helical spline and shim arrangement provide accurate indexing to control the angular relationship between teeth. It is more important that each assembly have the same relationship between teeth than is the actual magnitude of the angle. The quill shaft twists under load to reduce the torsional stiffness and share load in proportion to the spring rate, transmitted load, and error between two assemblies.

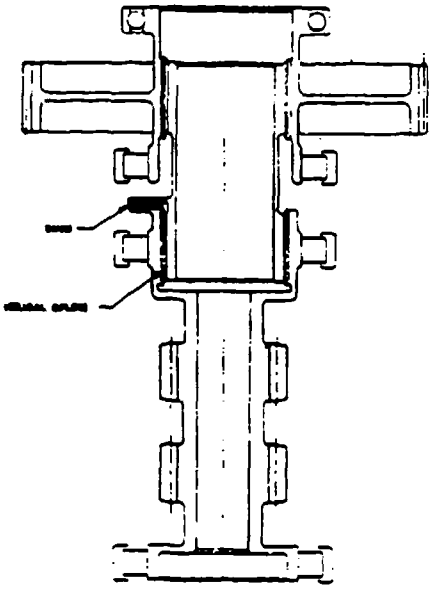

Figure 15. Quill Shaft Load Sharing Device

Another method is depicted in Figure 16 which depends on balance of thrust loads between helical gear members having opposite hands of helix. This method produces inherent load sharing because the helical pinions, connected by a common shaft will shift axially until the thrust load, and hence torque, is equal on each half. This method has been used previously in turboprop gearboxes by Pratt and Whitney, Canada. Note the use of the axially compliant coupling between the bevel gear and left and right hand helical pinions. This coupling permits the helical pinions to move axially without disturbing the

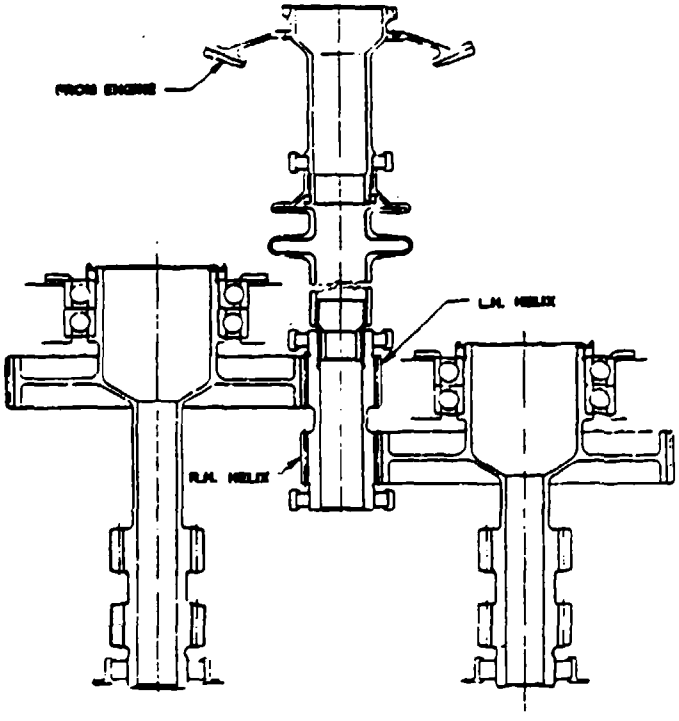

Figure 16. Helical Gear Load Sharing Scheme

bevel gear location. Extra bearings, one extra pinion, and the extra coupling are required for this design which decreases reliability and adds weight. The largest drawback, however, is the fact that the herringbone pinions can not float with this design and therefore load sharing between herringbone halves is affected.

Another design of merit is depicted in Figure 17. This is a new configuration that received consideration during the preliminary design phase. Individual composite blocks are formed and placed between internal and external toothed conical members. Under load, the composite blocks have a high deformation in the tangential direction and relatively low in the other directions. The cone permits preloading of the blocks to put the material in compression. Alternate layers of rubber/metal or rubber/fiber can be used as can many other types of resin/fiber materials. The design was eventually eliminated because of the complicated machining required for the slots used to drive the blocks.

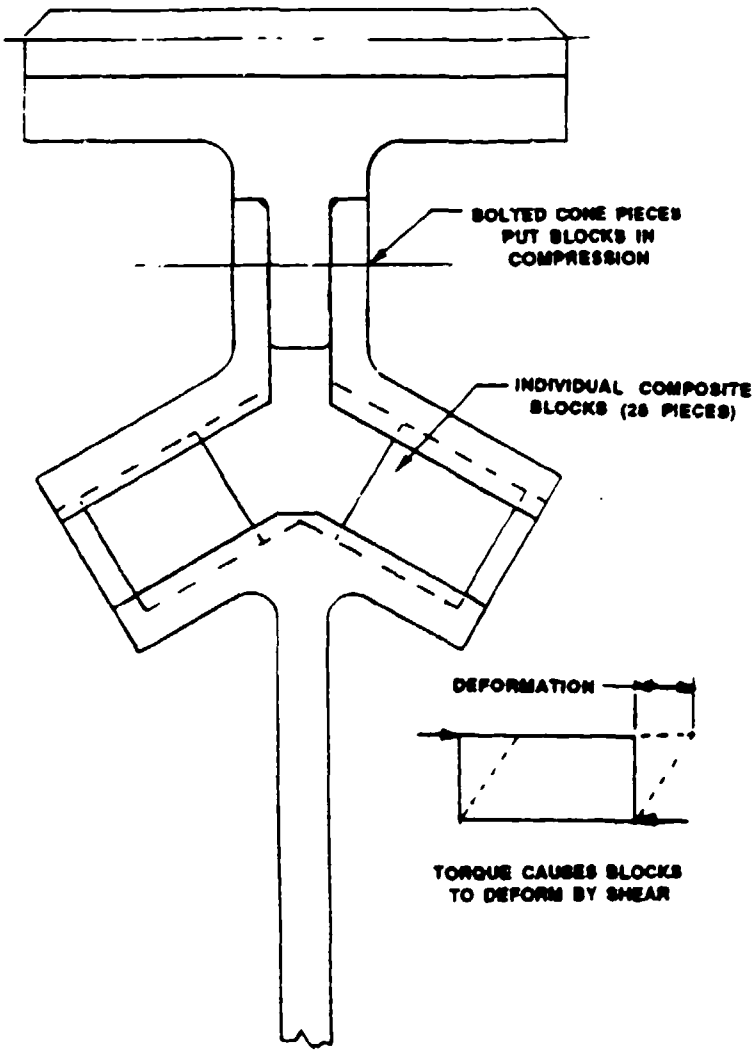

Figure 17. Composite Block Load Sharing Device

The load sharing device that was eventually selected is shown in Figure 18. A preliminary design is shown that has two bolt circles and an inwardly sloping angle making the device also soft in a bending sense. The final design is shown in Figure 19 with only one bolt circle and an outwardly sloping angle. The initial design had the advantage of making each isolator half as a separate molded assembly with the rubber molded to the metal at all locations. In the final design, the rubber is molded only to the inner side plate and torque is carried by friction on the outer part between the gear rim and isolator. Even for a small preload, a large pressure is formed between the gear rim and outer layer of the isolator and torque is transmitted by friction coefficient times the load produced by the pressure. A second feature of the selected isolator is the redundant spline drive. In normal operation, a clearance exists between teeth of the internal and external splines. At 140% torque, the splines touch and any further application of torque is carried by the spline teeth. The spline also acts as a limiting device to limit static strain produced in the rubber. Shims are ground at assembly to produce the proper preload and keep the rubber in compression at all times. Eighteen, 3/8 inch diameter bolts are used to overcome preload and provide high clamping loads to reduce fretting at the bolt holes.

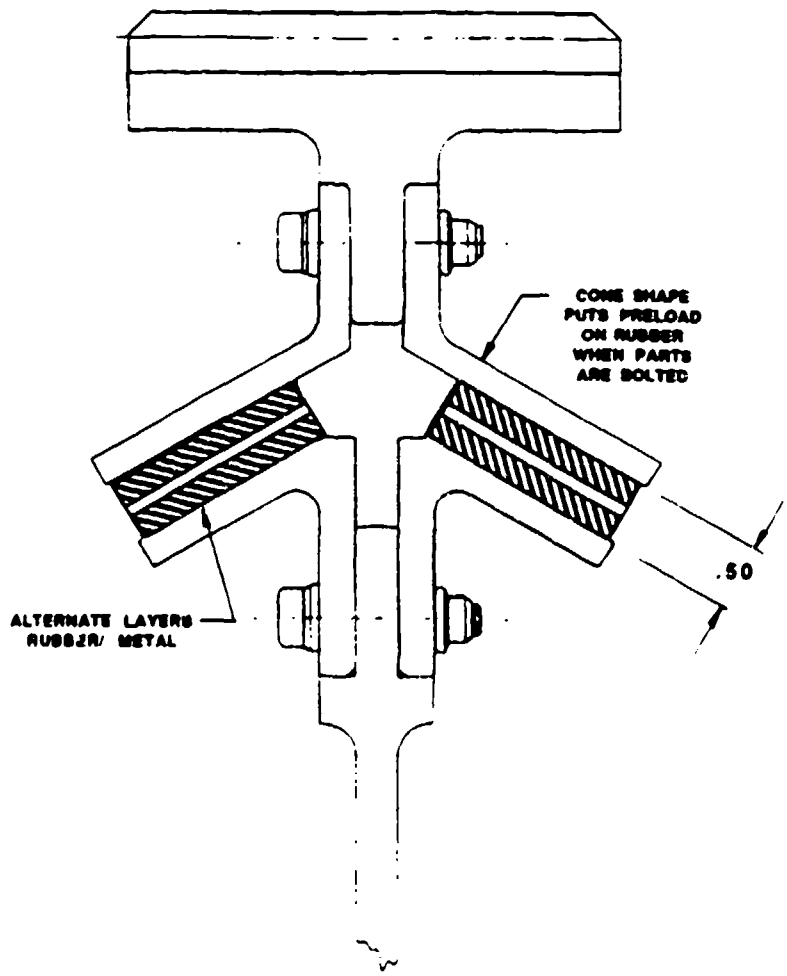

Figure 18. Elastomeric Torsional Load Sharing Device

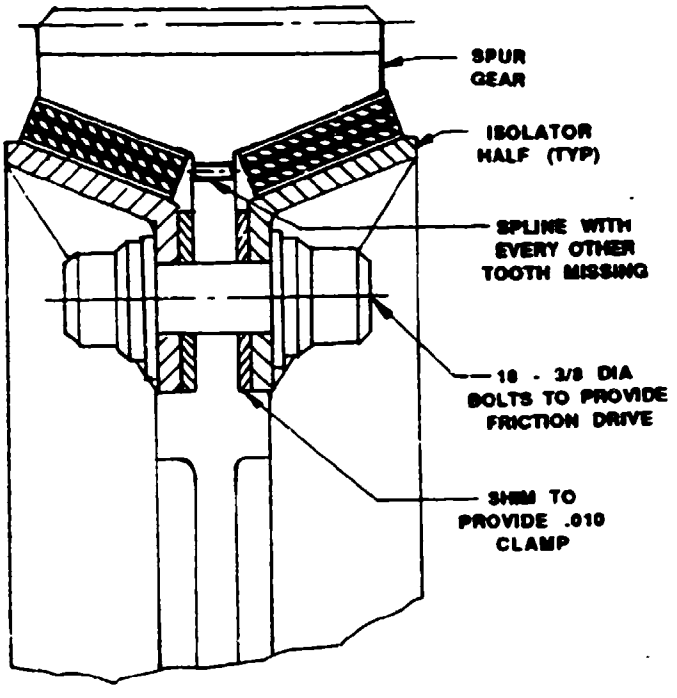

Figure 19. Inverted Elastomeric Torsional Load Sharing Device

Other schemes were also examined such as hydraulic devices, belleville washers, etc. but are not worthy of description.

To examine the benefits of the elastomeric torsional isolator compared to the conventional quill shaft used in other split path transmissions, the two designs are shown side by side in Figure 20. In the conventional design, the spur gear and the herringbone pinion are each mounted on their own bearings independent of each other. The quill shaft is then placed between the two shafts and tangential motion is achieved by the spring rate of the quill shaft. In the ART design, tangential motion is achieved by rotation of the spur gear about the pinion through the spring rate of the elastomeric isolator. Note that compared to the ART design there are two additional bearings per shaft times two shafts per engine times the number of engines. For the ACA, this amounts to 12 extra bearings for the conventional design. Since bearings are a major driver of MTBR, The ART design has an advantage of higher reliability. There may also be a noise benefit for the elastomeric design since it acts to isolate the spur gear from its support.

Spring Clutch on Input

The spring clutch is a type of helicopter overrunning clutch that has been tested at high speed. Although this type of clutch is affected by centrifugal load, the degree is much less than the conventional sprag or ramp roller type of overrunning clutch. A side by side comparison of the sprag, ramp roller, and spring clutch would show that the weight would be about the same for each design when the same torque is used. Since the spring clutch can operate at higher speed, it can be designed for lower torque and hence be lighter.

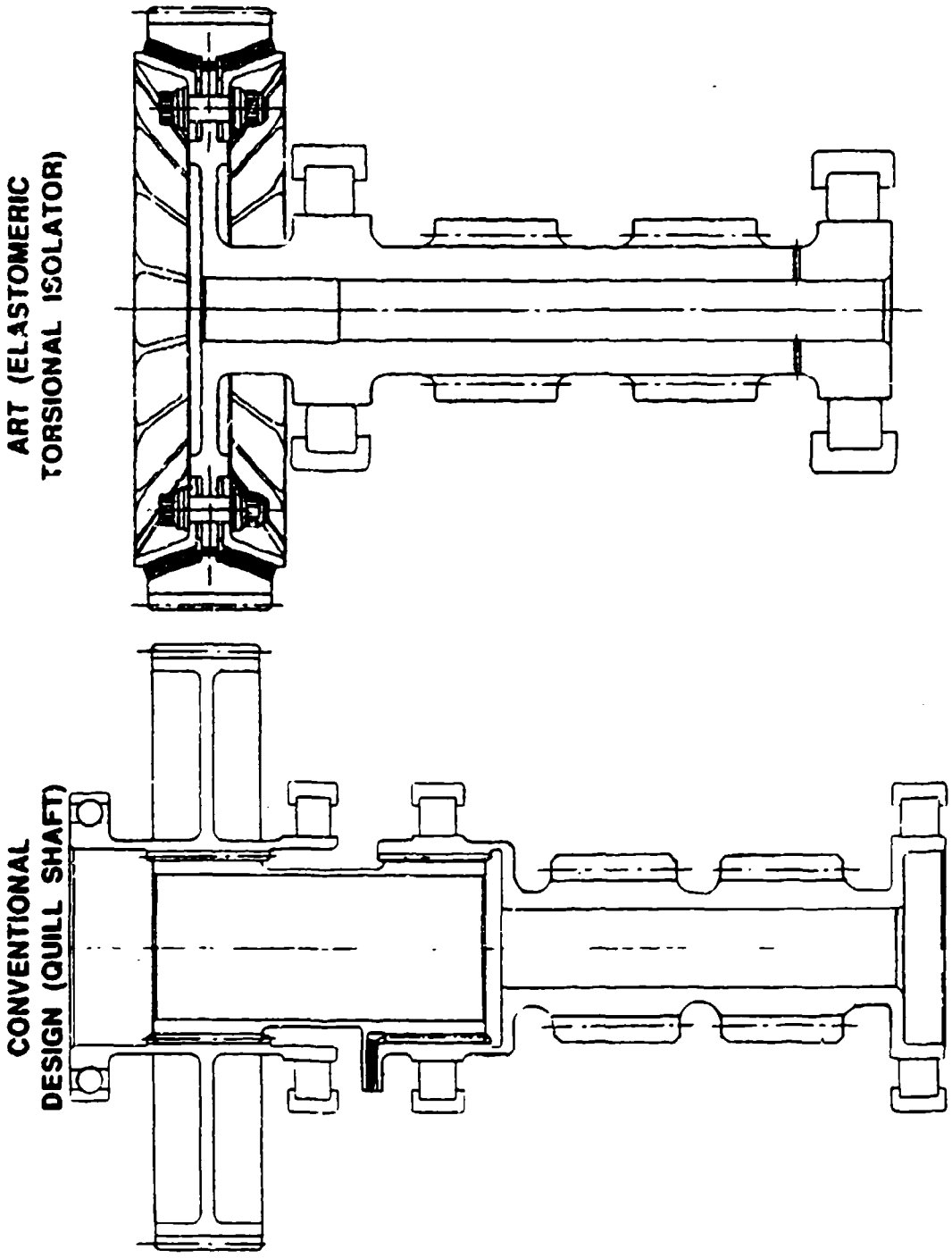

Figure 20. Comparison of ART and Conventional Load Sharing Devices

The principle of operation of the spring clutch is shown by the simplified sketch as seen in Figure 21.

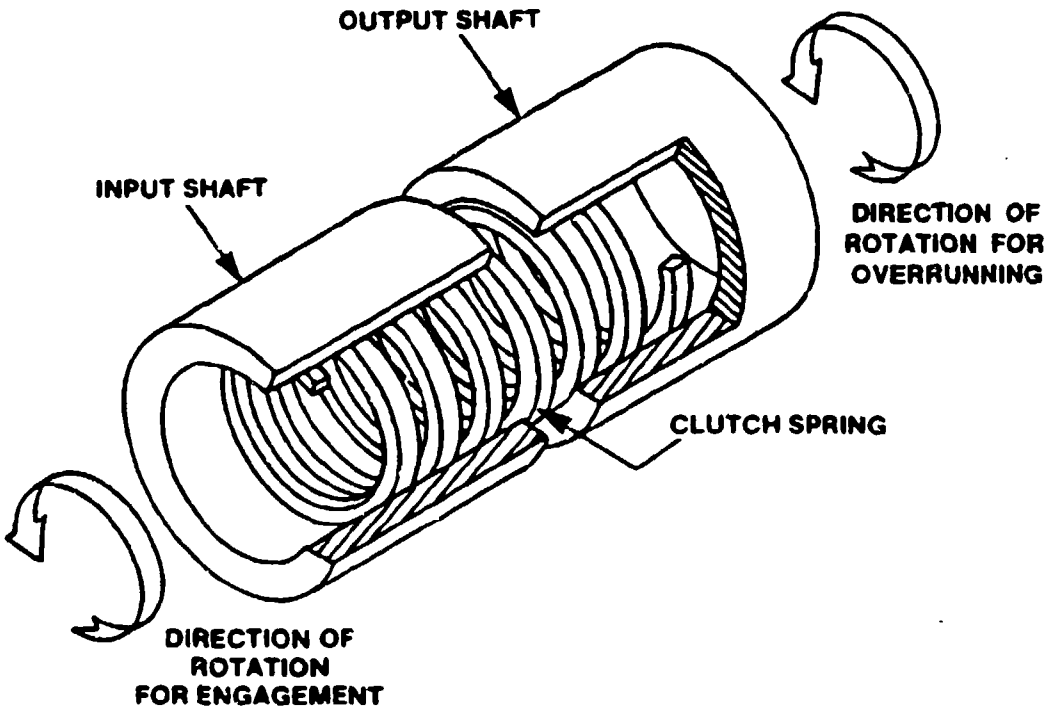

Figure 21. Principle of Spring Clutch Actuation

The input and output housings of the spring clutch are formed by concentric cylinders. The end coils of the rectangular section spring are slightly larger in diameter than the center coils such that the end coils are interference fit with the housings while the central coils are clearance fit. When torque is applied to the input shaft in a counterclockwise direction as shown, and the output shaft is fixed, the spring tends to expand. As each coil expands outward, the outside diameter of the spring coil grips the inside diameter of the housing and torque is gradually transmitted across each coil in an exponential manner. At the center of the spring, all the torque is transferred across the center coil across the gap from the input to the output housing. Torque then dispenses on the output housing in an equal and opposite manner to the input housing. When torque is reversed such that the input shaft is fixed and the output shaft is rotated in the same direction as shown

in Figure 21, the spring now has a tendency to contract. Eventually, the end coil that is interference fit with the housing on the output side will slip and overrunning will occur.

The actual spring has exponentially varying thickness coils for constant stress and to make the spring smaller. The end coils also vary in thickness as well as width. The last four coils on each end are the "teaser coils" that are interference fit with the outer housings. Figure 22 is a sketch of a helicopter spring for a spring clutch showing design features.

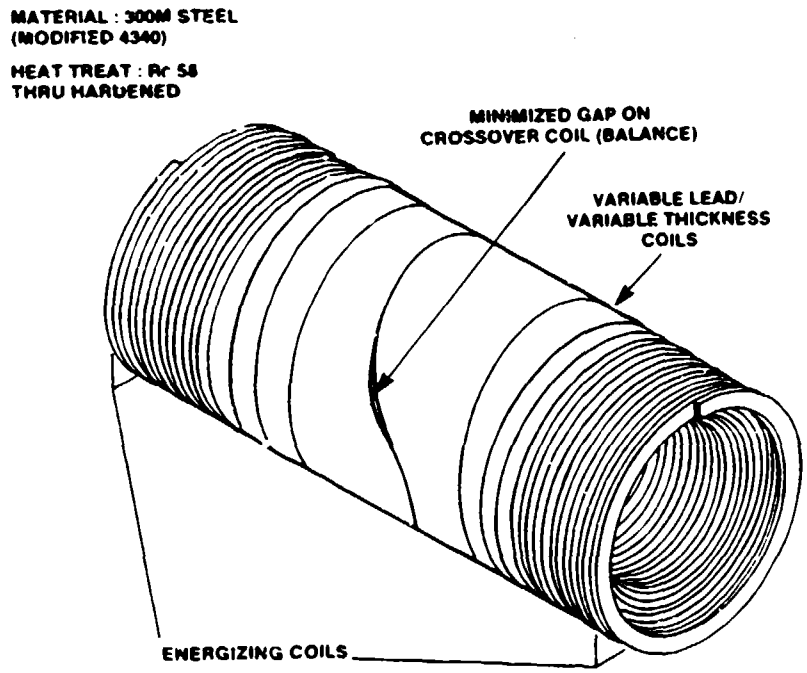

Figure 22. Spring Design Features

A layout of the spring clutch on the input section of the ART main gearbox is shown in Figure 23. An arbor is used to support the spring during overrunning. The inside diameter of the spring is interference fit with the arbor when there is no torque tending to unwind the spring. The arbor acts as a guide to keep the coils straight in the overrunning mode. A squeeze film damper is provided at the outside diameter of the duplex bearing set to reduce the spring rate of the bearing support and to provide damping for the first rigid body mode that the spring/input shaft/and engine drive shaft system must traverse on the way to operating speed. The spring arbor extends through the input bevel pinion and has a support bearing at the end. This bearing provides a large bearing spread and acts in conjunction with the duplex bearing to support the engine drive shaft. The input bevel pinion shaft forms the spring clutch output housing. A single angular contact spherical tapered roller bearing carries combined thrust and radial load and replaces the conventional state-of-the-art ball/roller combination used normally. The spherical bearing is manufactured with an outer land guided cage and the inner race is integral with the input pinion shaft.

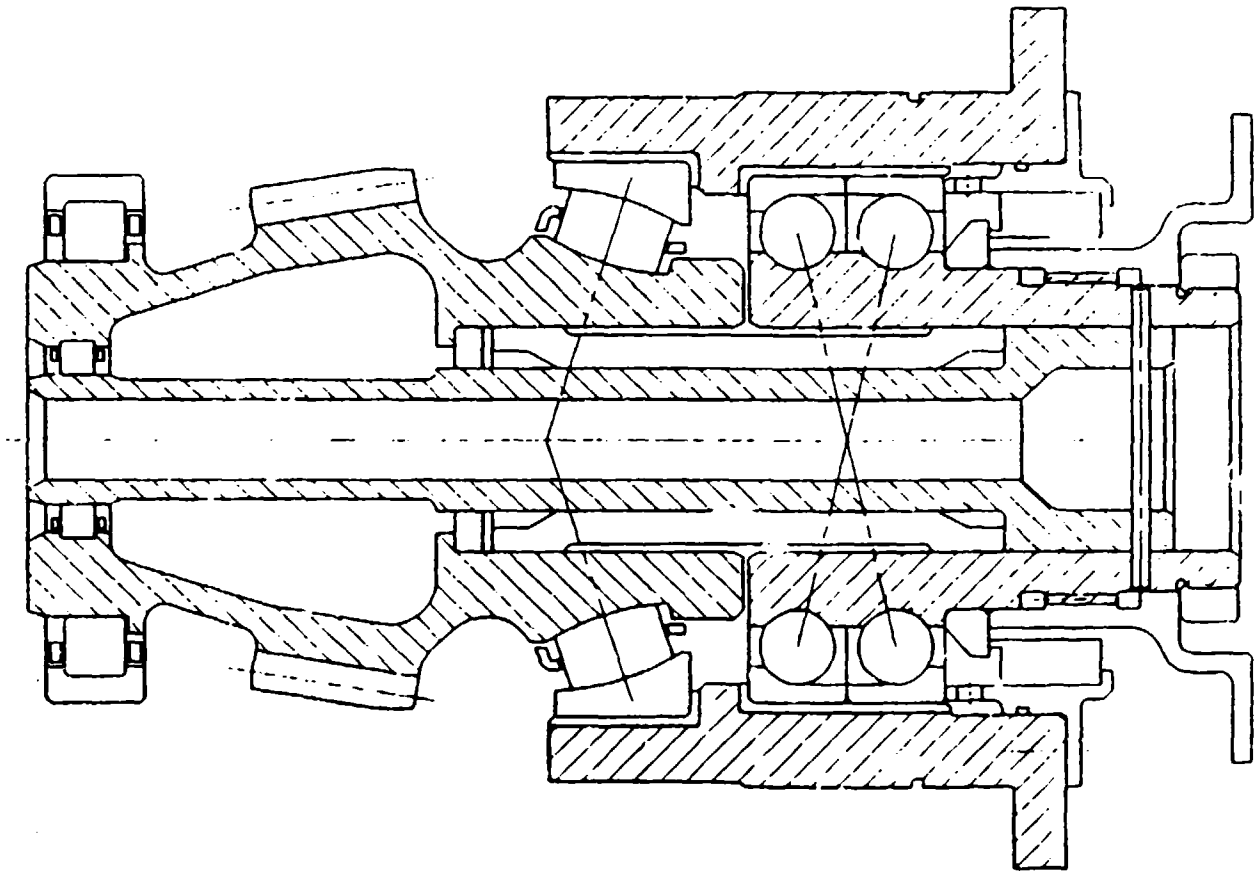

Figure 23. ART Input Bevel Pinion With Spring Clutch

The preliminary designs of the spring clutch assembly were weighed. Each input spring clutch was found to be 38.45 pounds for a total of 115.35 pounds for the 3 engine aircraft. For comparison purposes, a ramp roller clutch was designed to operate on the input bevel gear. The input bevel gear rotates at 4,935 rpm vs 15,000 rpm for the pinion where the spring clutch operates. A layout was made of the ramp roller clutch at the bevel gear and it was found to weigh 161.59 pounds per engine for a total of 484.77 pounds for the aircraft. Thus the spring clutch on the input bevel pinion is 369 pounds lighter than a conventional ramp roller clutch on the output bevel gear. Considering that the baseline main gearbox weighs 6882 pounds, the savings in weight for the spring clutch alone amounts to 5.4% of the main gearbox weight and also represents 3.4% of the entire transmission system weight.

High Contact Ratio/Buttress/Herringbone Gears

The output bull gear is a parallel axis gear set with the need for a large reduction ratio and also the need for reduced transmission error to reduce noise generated at the gear clash frequency. Types of gearing considered for this mesh were conventional spur gear, high contact ratio spur gear, helical gear, high contact ratio helical gear, double helical gear, high contact ratio double helical gear, and conformal circular arc gear (Novikov). Spur gears,

high contact ratio spur gears, and conformal gears were eliminated for noise reasons as it was felt that the 10 dB noise reduction could not be met with these types of gears. This is especially true when considering that transmissions with output bull bull gears (S76) tend to have the highest noise generated internally at the output stage of gearing. Helical gears and high contact ratio helical gears (transverse contact ratio greater than 2) were eliminated because the thrust load produced at the large gear radius induced high bending moments into the bull gear support structure and bearings. This left as the design choice double helical gears which offer the benefit of cancellation of thrust load and thus permit even higher helix angles to be used. By making the transverse contact ratio greater than 2, even higher overall contact ratios could be achieved and in the final design, overall contact ratios approaching 4 have been attained. A matrix of designs is presented in Table 11. Each of the bull gear meshes listed in Table 11 were run through a helical gear computer program to calculate bending stress, contact stress, and scoring. Scoring was not a problem owing to the low output speed of 130 rpm. A helical gear with zero helix angle is of course a spur gear. The upper four designs were for approximately an 11:1 reduction ratio while the lower four deigns were for 8:1 ratio. From the matrix of bull gear designs run it was found that contact stress was the dominant design condition and thus the lightest design resulted when the teeth could be made as large as possible to reduce bending stress. Figure 24 illustrates this point by plotting the ratio of factor of safety on bending to contact stress vs number of teeth in the pinion. All data assumes a 48 inch pitch diameter bull gear (Set by manufacturing considerations).

Table 11. Matrix of Bull Gear Designs

No of Teeth	Pres Angle	Helix Angle	Face Width
13/141	20°	0°,10°,20°,30°,40°	4.0, 5.5
15/167	20°	0°,10°,20°,30°,4	4.0, 5.5
17/186	20°	0°,10°,20°,30°,4	4.0, 5.5
19/226	20°	0°,10°,20°,30°,40	4.0, 5.5
13/106	20°	0°,10°,20°,30°,40°	4.0
15/125	20°	0°,10°,20°,30°,40°	4.0
17/137	20°	0°,10°,20°,30°,40°	4.0
19/156	20°	0°,10°,20°,30°,40°	4.0

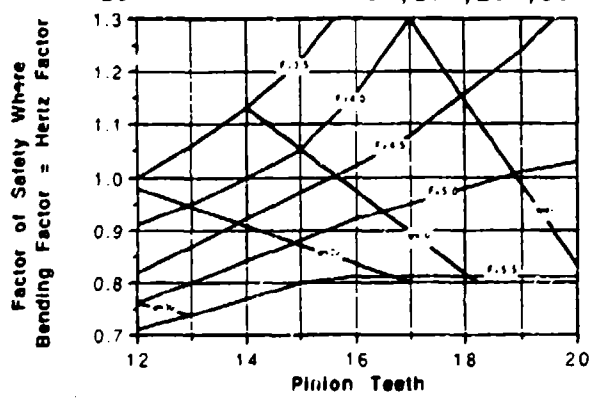

Figure 24. Variation of Bending and Contact Stress With Helix Angle

A typical result can be seen in Figure 25 which is a plot of stress divided by the allowable stress (or factor of safety) vs helix angle The plot is for the 13/141 mesh. As helix angle increases, contact stress continues to decrease whereas bending stress decreases slightly to about 20°, then increases slightly to about 30°, and then increases sharply above 30°. This is a typical plot for all designs. The maximum helix angle used was reduced as a result of this phenomenon to approximately 30°.

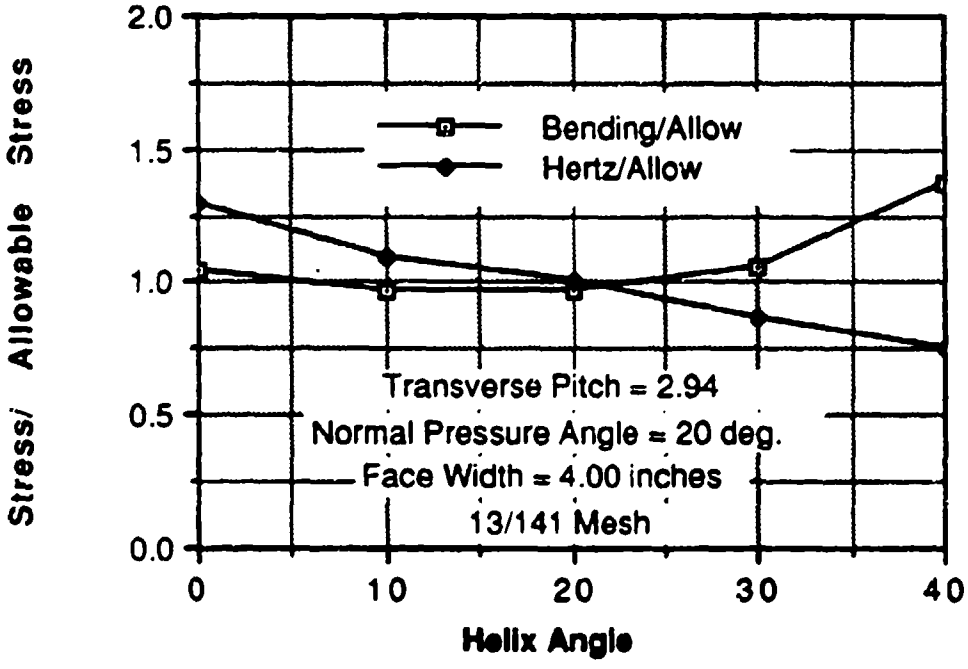

Figure 25. Herringbone Gear Mesh Design Parameters

Preliminary layouts were prepared for 8:1 and 11:1 ratio bull gears. It was found that last stage reduction ratio had a profound effect on weight. This fact is illustrated in Figure 26. The reason for the weight savings can be realized when considering for a moment what happens when the output bull gear is left alone and the bull pinion pitch diameter is decreased. First of all, the bull gear face width remains the same since the output torque, and hence output tangential tooth load has not changed. Secondly, the weight of the bull pinions themselves is reduced since the size of the pinion is smaller. Lastly, the reduction ratio is increasing and hence the speed of the bull pinions is increasing. This results in less torque on the bull pinions and in fact, all stages prior to the bull gear can now have reduced ratios and reduced weight because of the lower torque and lower reduction ratio requirements. Therefor, increasing the reduction ratio at the last stage has the direct effect of reducing sizes of all gearing prior to the output bull gear.

It was also found that the reduction ratio of the output bull gear mesh is limited by the basic diameter of the pinion when considering induced fatigue bending in the pinion shaft. Bending of the pinion is influenced by geometry and such basic considerations as to where to put the support bearings. Figure 27 illustrates what happens to the bending stresses in the shaft section

between left and right hand helix members when the bearing is located on the outside of the spur gear or when the bearing is located between the spur gear and herringbone pinion. The bull gear pitch diameter was fixed at 48 inches for the calculations. The configuration with the bearing between gears reduces the peak stress by approximately 30% and was selected for this reason. Note that the critical stress occurs on different sides of the torque splitting pairs depending on configuration. In all cases the highest stress on the selected configuration is lower than the lowest stress on the outboard bearing configuration. This is a somewhat surprising result since transmission designers often select "straddle mounted" designs for improved rigidity.

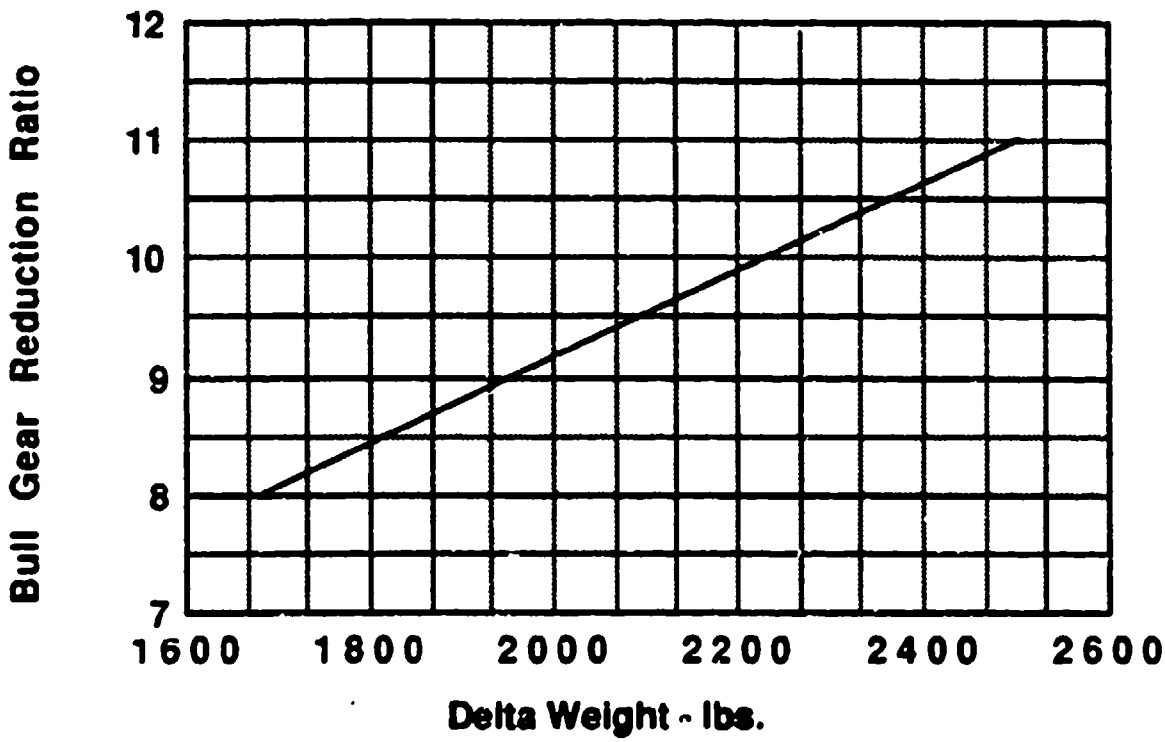

Figure 26. ART/ACA Weight Savings vs Reduction Ratio

The second stage gearing of the split path gearbox is also a parallel axis mesh. A decision was made to make the second stage a spur gear set to allow the assembly consisting of the herringbone pinions and parallel axis gear to float axially. For reasons of noise reduction and weight savings, it was decided to also make the mesh a high contact ratio spur. A high contact ratio gear design was also used for the differential planetary of the split torque design.

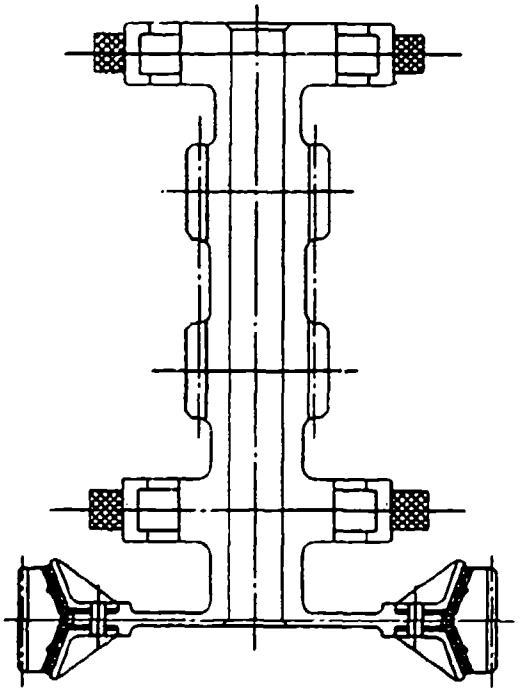

REDUCTION RATIO	R.H. Kf x lb	L.H. Kf x lb
11.09	60590	51300
10.08	40590	35030
9.77	34230	29110
9.50	30780	26310

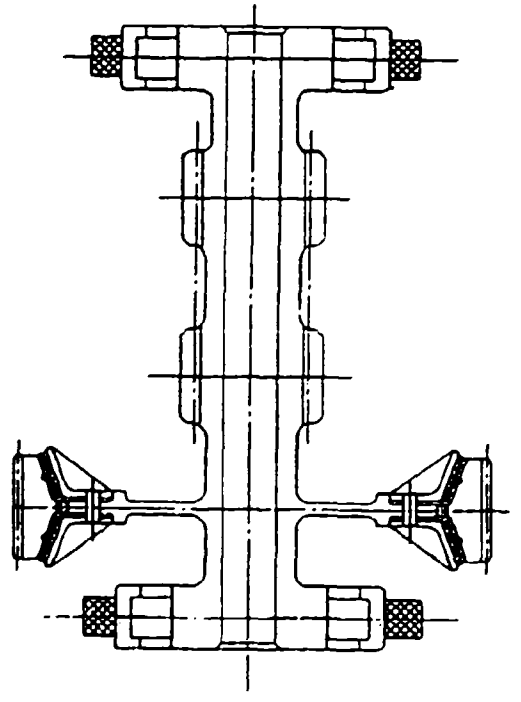

REDUCTION RATIO	R.H. Kf x lb	L.H. Kf x lb
11.09	41330	50540
10.08	25120	30720
9.77	21890	26950
9.50	19260	23690

SELECTED DESIGN

Figure 27. Bull Pinion Bearing Configuration Comparison

Bearingless Bull Gear Design

A trade off study was conducted on the method of mounting of the herringbone gear and herringbone pinion/spur gear assembly of the split path gearbox. A herringbone gear set has the unique attribute of central alignment of one member to the other since any maldistribution of tooth load tends to be self correcting. Therefor if one member of the set is permitted to float axially as for example on roller bearings, the loads between left and right hand helix members will be identical. Another distinctive virtue of the ART herringbone bull gear is that the bearing load is essentially zero most of the time. With these peculiarities in mind, various design options for supporting structure of the bull gear mesh were examined. Table 12 lists the configurations.

Table 12. Bull Gear Support Trade Off Study

Design	Bull Gear Fixity	Bull Pinion Fixity	Bearing Life @ OEI (hrs)	Weight (lbs)
S.O.A.	Fixed	Floating	28670	Baseline
2 Timken	Fixed	Floating	28670	-131
1 Roller	Floating	Fixed	15220	-389
Rings	Floating	Fixed	3800	-458

Figures 28, 29, and 30 show the reactions of the bull gear for 3 engines operative, one engine inoperative, and two engines inoperative respectively. The reaction is zero when all three engines operate at the same power levels because the spacing of pinions around the periphery of the gear is equal in groups of three. When one or two engines are inoperative, a reaction load is induced at the inoperative engines herringbone pinion pitch points. Figure 31 summarizes the magnitudes of reactions.

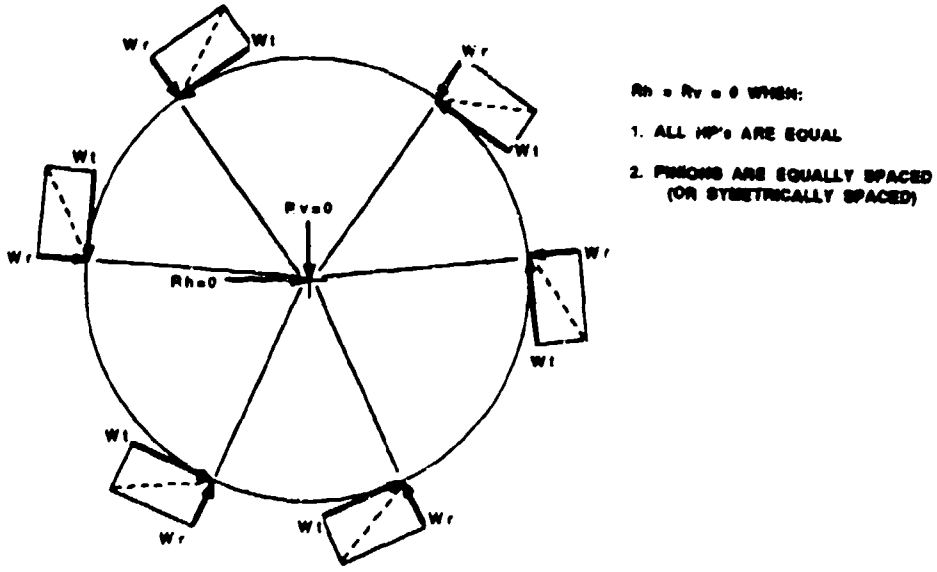

Figure 28. Bull Gear Reaction, All Engines Operative

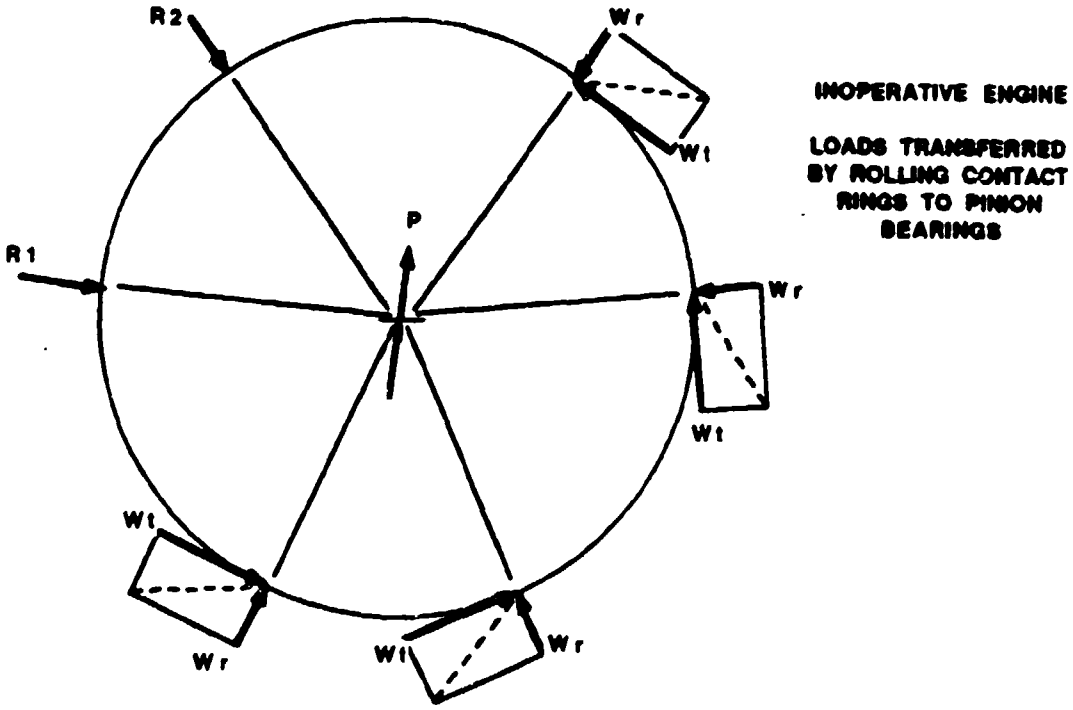

Figure 29. Bull Gear Reaction, One Engine Inoperative

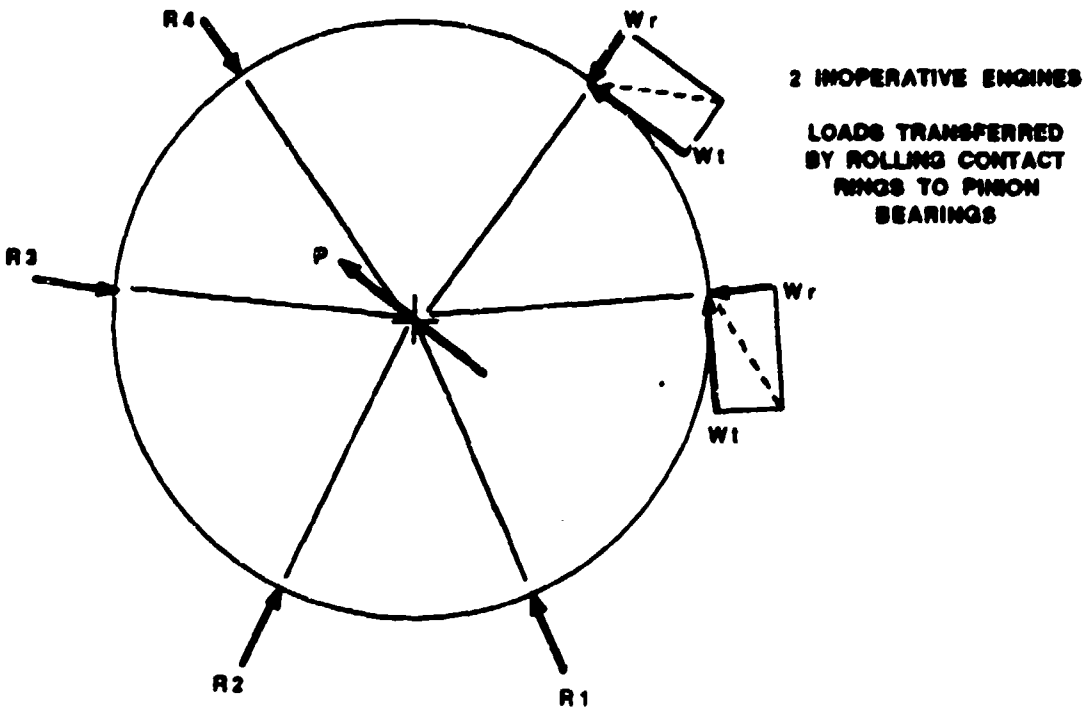

Figure 30. Bull Gear Reaction, Two Engines Inoperative

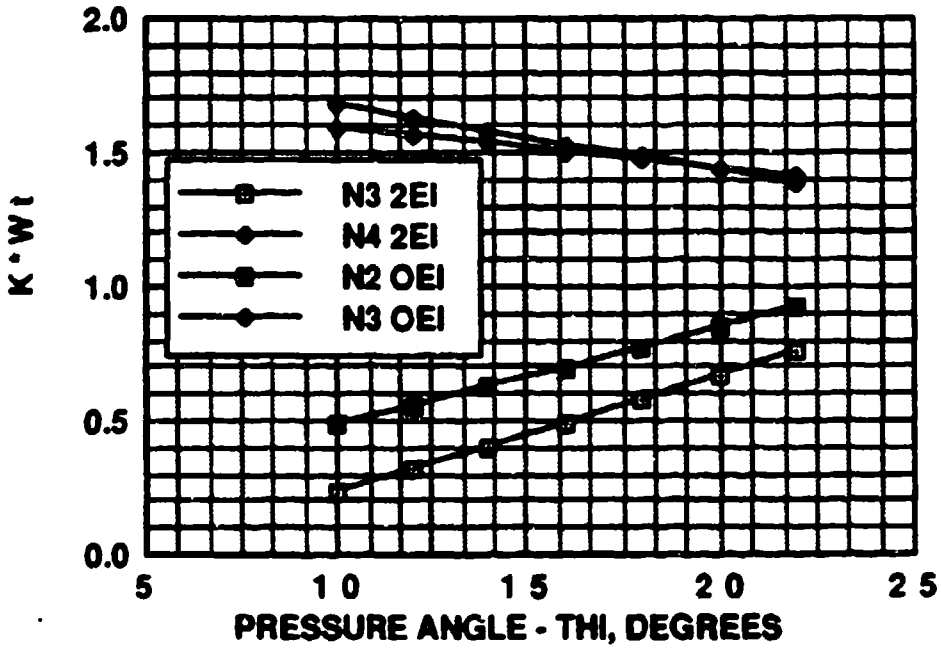

Figure 31. Bull Gear Reactions as a Function of Tangential Tooth Load

The state-of-the-art design, "S.O.A.", of Table 12 consists of a conventional centralized gear web on the bull gear which is then connected to a bull gear shaft with bearings at each end. This is the heaviest solution of those examined. In the "2 Timken" design, the 2 tapered roller bearings are placed directly under the center of the bull gear and are relatively large in diameter such that the conventional gear shaft is eliminated. A fixed shaft then transfers the bearing load to the supporting end plates. This design permits floating pinions and saves some weight compared to the baseline but is still a heavy solution. The "1 roller design" is identical to the 2 Timken design except that the back-to-back Timken bearings are replaced by a single roller bearing. By the nature of the roller bearing, the bull gear becomes a floating member in this design and the pinions must be constrained axially. Since there are six pinions, they would all have to be shimmed in a plane so that the bull gear could follow the path thus formed. Individual axial adjustments of the bull gear in this design will effect neighboring pinion load sharing. A literature search showed that when herringbone gears are used with multiple pinions, the pinion members are always the floating part. The "ring" design has a rolling element ring placed in the space between left and right hand helix members of the pinion and gear. The diameter of the rings are equal to the pitch diameter of the gears. Under normal operation the rings will not make contact since small deflections that are present will tend to separate the contacts slightly. Under conditions of differing power from each engine, such as OEI operation, the bull gear will shift slightly towards the direction of the resultant load until the rings of the gears on the inoperative engine side will contact. The rings will then act as supports through the pinion bearings and the mesh will continue to operate. When one examines the magnitude of the load as shown previously in Figure 31, it is seen that the maximum ring load is approximately 1.42 times the tangential tooth load. This is a

substantial bearing load since the tangential tooth load is in the order of 63,000 pounds during OEI conditions. The contact stresses on the ring are quite high for theses magnitudes of load even though the rings are very large in diameter. A ring life of 3800 hours during OEI conditions represents unlimited aircraft life since OEI occurs only for a small percent of the time. Figure 32 depicts the bearingless bull gear design. To manufacture the pinion central rings the design shown uses electronic beam (EB) welding. The gears are finish ground prior to welding, and the ring welded and ground concentric to the pinion. The ring used in the bull gear does not require welding because the gears are manufactured separately and bolted together. The central ring is bolted with the same flange as the gears. An alternate design is shown in Figure 33 which eliminates the welding of the pinion rings. Full recess action pinions are used. The pinion has the entire working profile of the tooth above the pitch diameter i.e., the dedendum is negative. On the gear, the entire working profile is below the pitch diameter. Hence the pinion ring can be made integral with the pinion and all teeth and the rings ground without grinding wheel interference. On the gear, the ring is not required to be integral. The technical risk of operation is considered very high for any designs which use fixed pinions and floating bull gear and for this reason, the final design chosen was the 2 Timken arrangement.

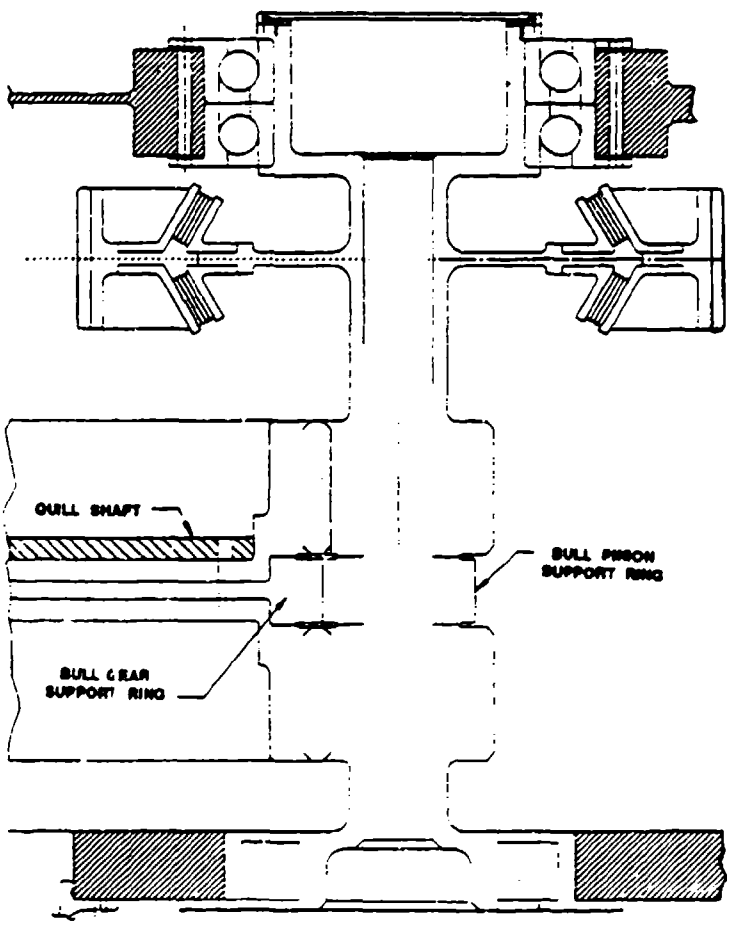

Figure 32. Bearingless Bull Gear Design

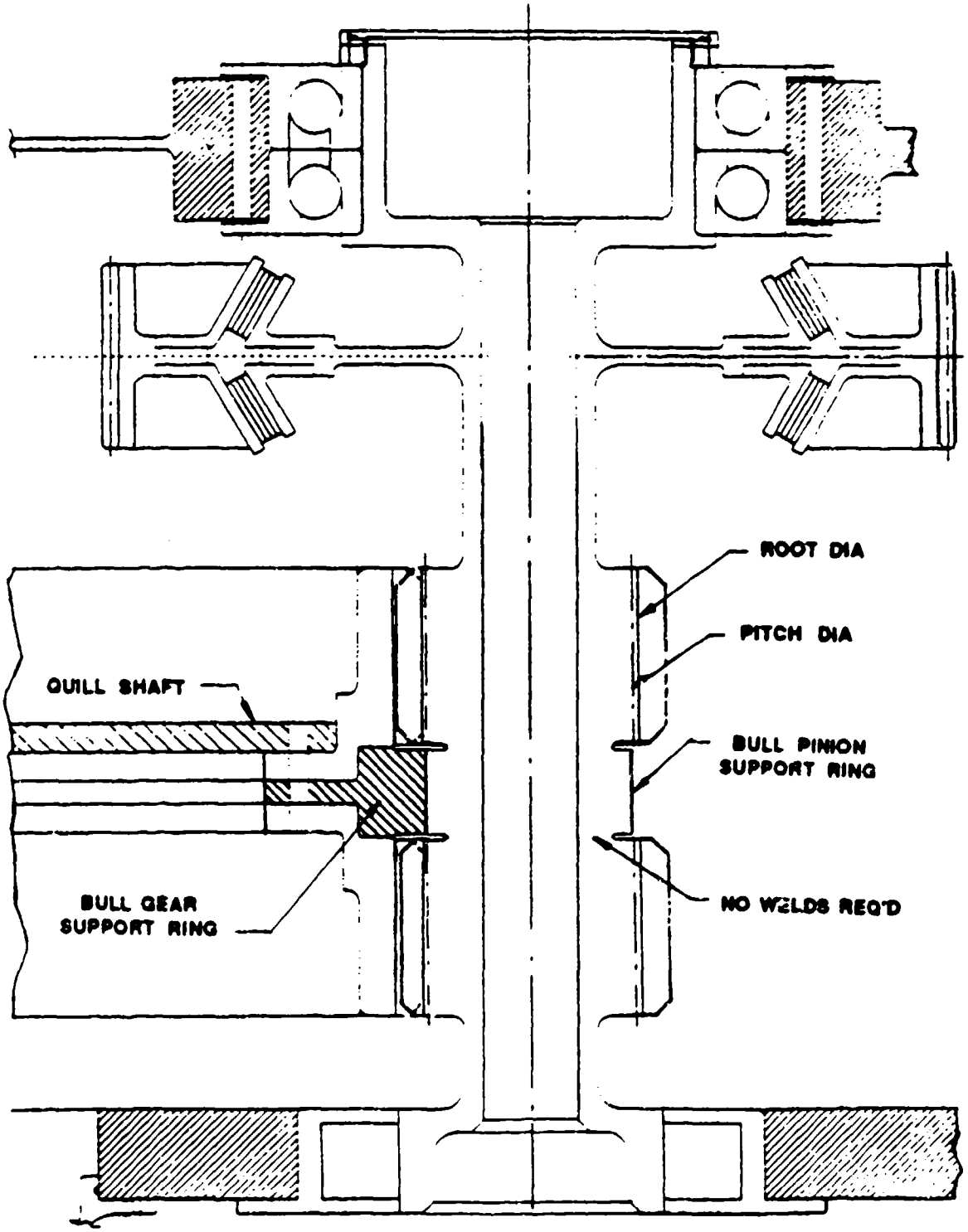

Figure 33. Bearingless Bull Gear With Full Recess Action Pinions

High Hot Hardness Gear Steels

During the preliminary design phase of the program, gear steels were reviewed to determine if any of the high hot hardness gear steels would offer any benefits. Gear steels under consideration were SAE 9310 (baseline), VASCO X2M, Carpenter Pyrowear 53, and CBS 600. After examination of static properties, fatigue bending allowables, contact stress allowables, scoring resistance, fracture toughness, heat treat requirements, and machinability, Carpenter Pyrowear 53 was selected. All of the high hot hardness gear steels offer improvements in surface related distress such as scoring resistance and contact (Hertz) stress improvements. Pyrowear 53 was chosen based on its excellent fracture toughness being even better than the baseline 9310.

Angular Contact Spherical Roller Bearings

A good deal of research has been directed at development of a single, high speed bearing to take the place of the current state-of-the-art ball/roller combination for reaction of combined thrust and radial loads. Figure 34 illustrates some configurations that have been investigated including the cylindrical roller bearing with spherical thrust shoulder, and high speed tapered roller bearings. In the ART program a single row angular contact spherical roller bearing was investigated. Testing has shown that the major difficulty in development of a single bearing designed to carry thrust and radial load is in the heat generation after loss of oil and resultant bearing survivability characteristics. Both the tapered roller bearing and the cylindrical roller bearing with thrust capability use a thrust shoulder to react axial load. After loss of oil the heat buildup at the thrust shoulder is generally very rapid and the bearing fails at that point. In the angular contact spherical roller bearing, there is no thrust shoulder as axial loads are transmitted as shear loads across the rollers. It is expected that the survivability characteristics of this bearing after loss of oil will be improved for this reason.

Another technology improvement used in the angular contact spherical roller bearing is the use of ceramic rolling elements. For high speed bearings the reduced roller mass of ceramic rollers results in increased life since the reduction factor for centrifugal load is reduced. The density of the silicon nitride ceramic used is .116 pounds per cubic inch vs .283 pounds per cubic inch for steel.

The reduced density also educes another benefit in the form of reduced heat generation again from the fact that the centrifugal roller load is reduced. The latter benefit can help the lost oil survivability characteristics by reducing temperature generation. The lower heat generation may be the most important advantage of ceramic rollers. A plot of bearing life for various contact angles for steel and ceramic rollers is shown in Figure 35. The bearings on this graph are the roller bearing and the single row angular contact spherical roller bearing located on the input bevel pinion. The speed is 15,000 rpm corresponding to the speed of the GE-38 engine. For a smaller helicopter than the ACA, the life improvements for ceramic rollers compared to steel rollers would be more dramatic since rpm is generally in the range of 20,000 to 24,000 rpm and centrifugal effect will be more severe.

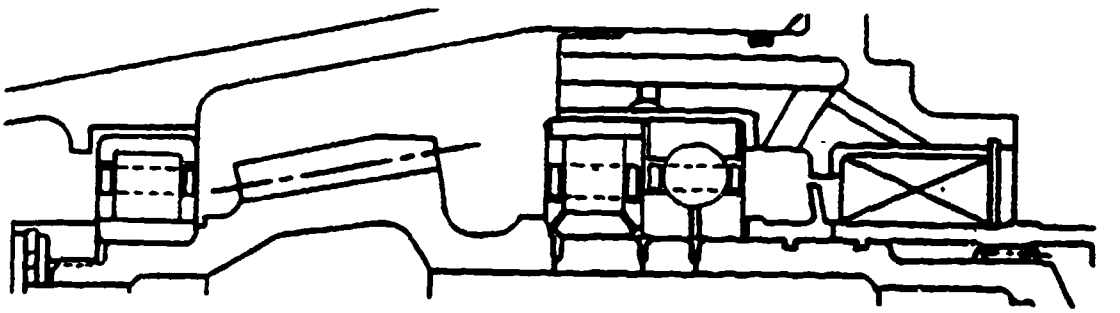

BALL/ ROLLER BEARING COMBINATION

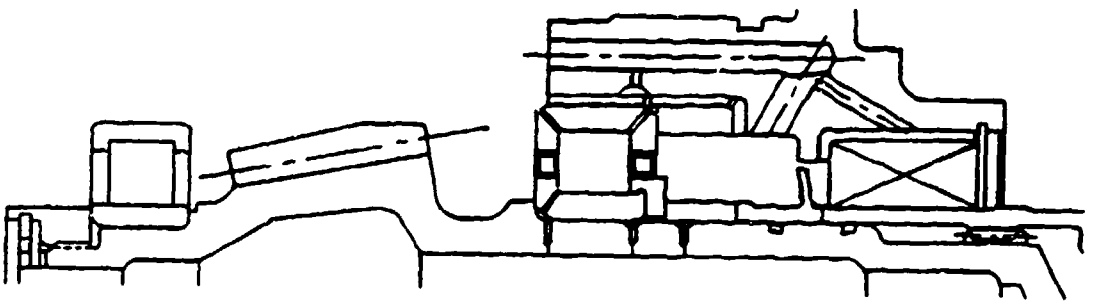

CYLINDRICAL ROLLER BEARING WITH THRUST CAPABILITY

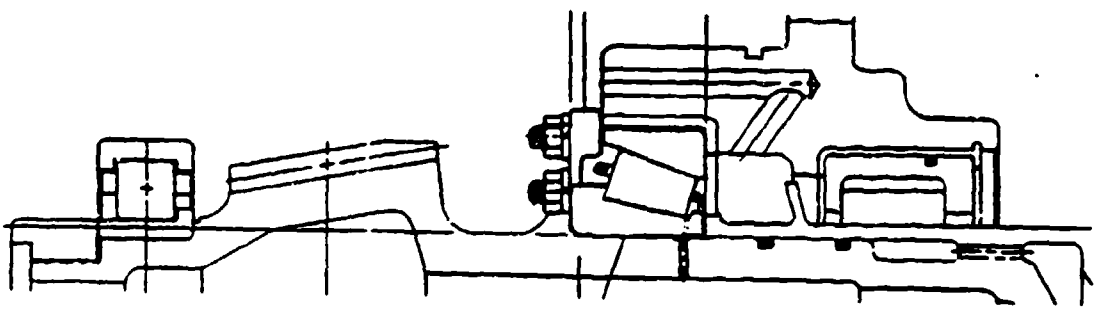

TAPERED ROLLER BEARING

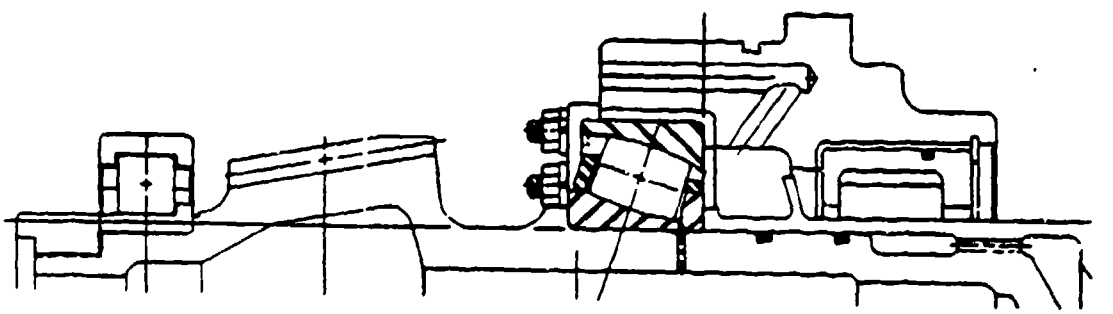

SINGLE ROW ANGULAR CONTACT SPHERICAL ROLLER BEARING

Figure 34. Single Bearing Configurations Which Replace Ball/Roller

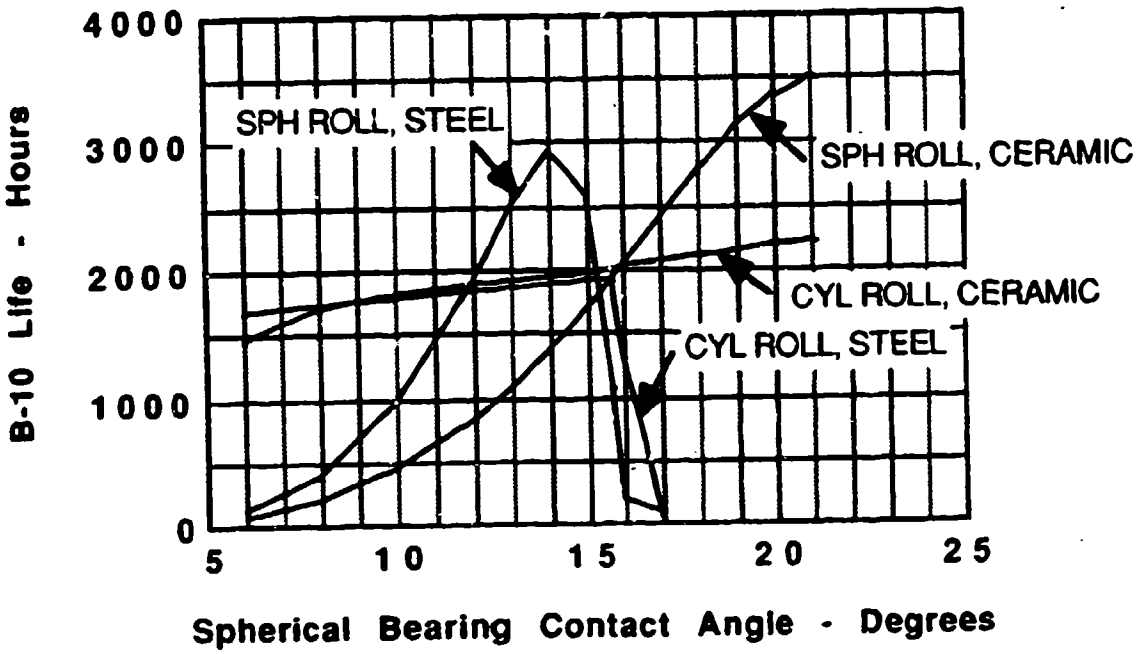

Figure 35. Bearing Life for Steel and Ceramic Rollers

The mounting of the angular contact spherical roller bearing is shown in Figure 36. The cross section shows how the bearings are arranged in a typical input pinion configuration. The spherical bearing has its inner race integral with the pinion shaft as does the roller bearing at the other end.

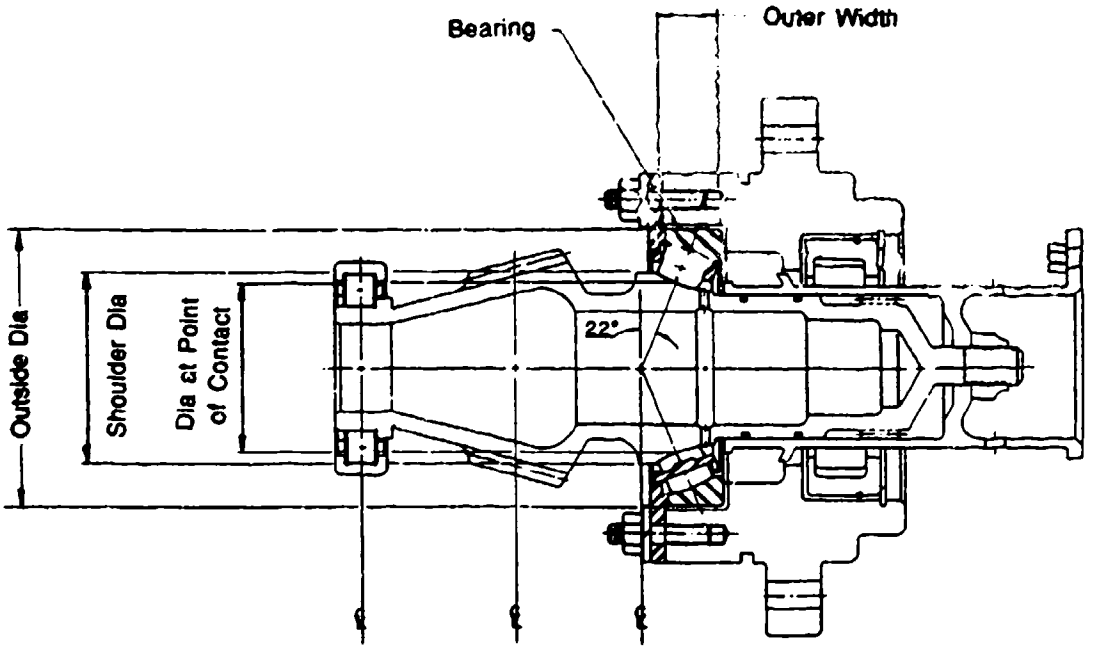

Figure 36. Mounting of Angular Contact Spherical Roller Bearing

Composite Main Rotor Shaft/Quill/Standpipe

The ART system is arranged with a truss member to react rotor loads. The truss is a composite structure with six legs attached to the airframe. A sketch is shown in Figure 37. In the upper portion of the truss, a housing contains the main rotor shaft and bearings. Head moment, torque, thrust, and side load are reacted in the main rotor shaft as in a conventional design. The main gearbox only carries torque to the main rotor shaft. There will of course be some rotor load fed through the quill shaft to the main gearbox since it is a redundant structure and this must be accounted for. The main rotor shaft is titanium and oil is supplied from the main gearbox system through tubing to the main rotor shaft bearings whereupon it then drains back to the main gearbox. A schematic of the standpipe structure separate parts is shown in Figure 38 showing how the individual components are fabricated. The rough tube sizes are shown varying from 10 x 10 inches at the upper end to 5 x 5 inches at the lower end. Many of the parts are resin transfer molded (RTM). The final assembly is bonded and co-cured.

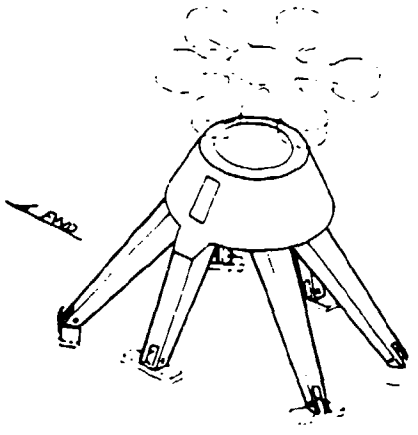

Figure 37. Standpipe structure, ART/ACA

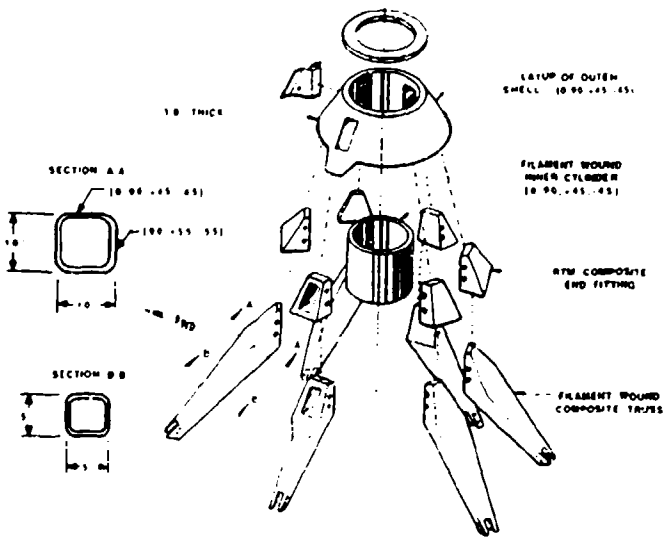

Figure 38. Schematic of Standpipe Structure Separate Parts

A cross section showing the main rotor shaft, quill shaft, rotor head, and upper truss section is shown in Figure 39. The layout shows that the quill shaft attaches to the rotor head through a bolt flange. Thus torque does not flow through the main rotor shaft in this design. Later, it was decided to move the quill shaft bolt flange to the bottom of the main rotor shaft because it was too difficult to fabricate the opposing composite flanges on the rotor head connection. In the new design (See detail design chapter), torque is transmitted through the main rotor shaft. Since the diameter is large, torsional stress is low. The composite quill shaft from the main transmission contains a composite coupling between the main gearbox and main rotor shaft. This coupling is designed to remove any misalignment between the rotor and transmission and must also be capable of transmitting torque.

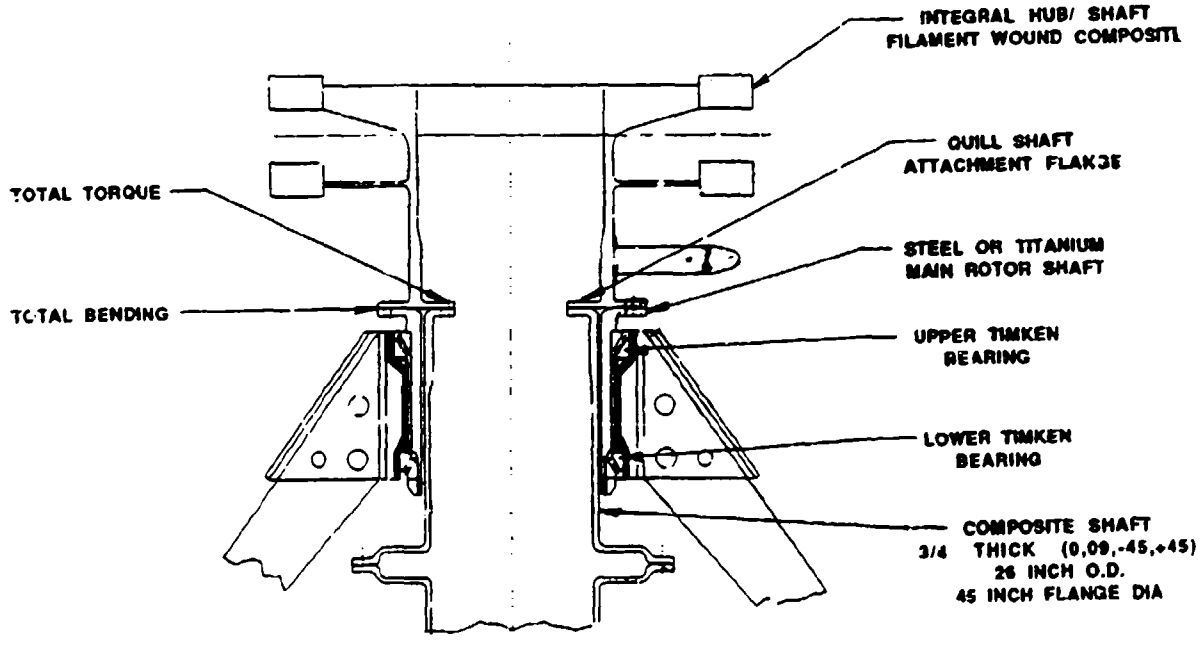

Figure 39. ART/ACA Main Rotor/Quill Shaft

An alternate arrangement of main rotor shaft and quill shaft is shown in Figure 40. Here the composite rotor head extends downward to form the main rotor shaft. It was felt that the main rotor shaft bearings could not be installed directly onto the composite material. Rotating bearing races have a tendency to creep under load when the load is alternating on the raceway and the ring materials are relatively thin as is the case for the main rotor shaft bearings. The tendency to creep is overcome by very high press fit in aircraft designs. Sikorsky has successfully used the "Keller" criteria developed in-house and verified by years of successful field operation. The ART bearings are very large and thin and require a very high press fit to meet the no-creep criteria. The stresses become too high in composites for the high fits required. The design shown in Figure 40 overcomes this by using metal liners between the composite shaft and bearings. A metal piece is also used on the lower end of the main rotor shaft to hold the lower bearing and at the same time the metal piece permits the use of a nut to clamp the lower bearing and carry the weight of the helicopter. The metal piece is dowelled to the composite shaft just above the lower bearing and to the metal liner used for the upper bearing. The dowel is used in this location because the bending stress is low here being zero at the center of the lower bearing. The parts are also tapered for tighter fits during the curing process. This design was eventually eliminated in favor of the metal main rotor shaft as shown in Figure 39 for reasons of the high technical risk associated with fabrication.

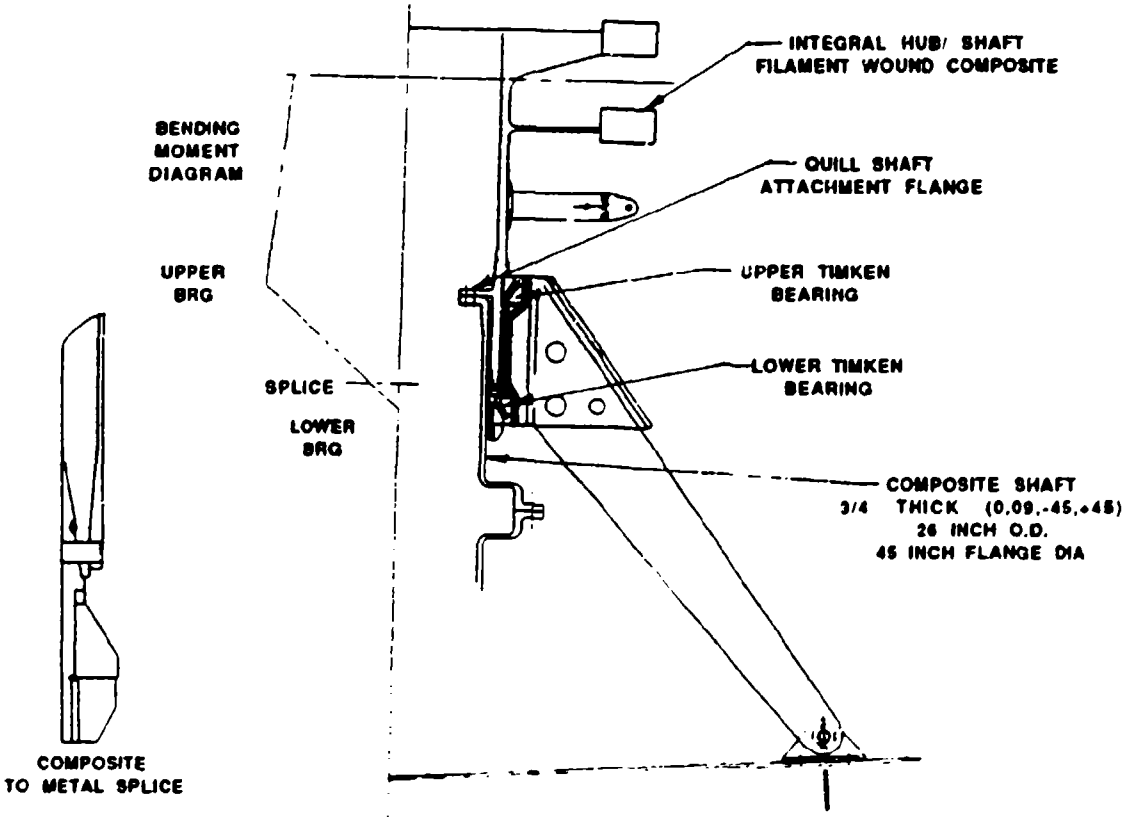

Figure 40. ART/ACA Main Rotor/Quill Shaft, Alternate Arrangement

Composite Housings

Composite housings are used throughout all of the ART transmission system. The material selected is graphite polybismalimide which is suitable for operation in an oil environment at high temperatures. The method of manufacture is resin transfer molding (RTM) although areas next to bearings and other machined surfaces are made by injection molding with chopped fibers and thermoplastic resins such as PEEK. A cross section of the transmission showing only the housings can be seen in Figure 41.

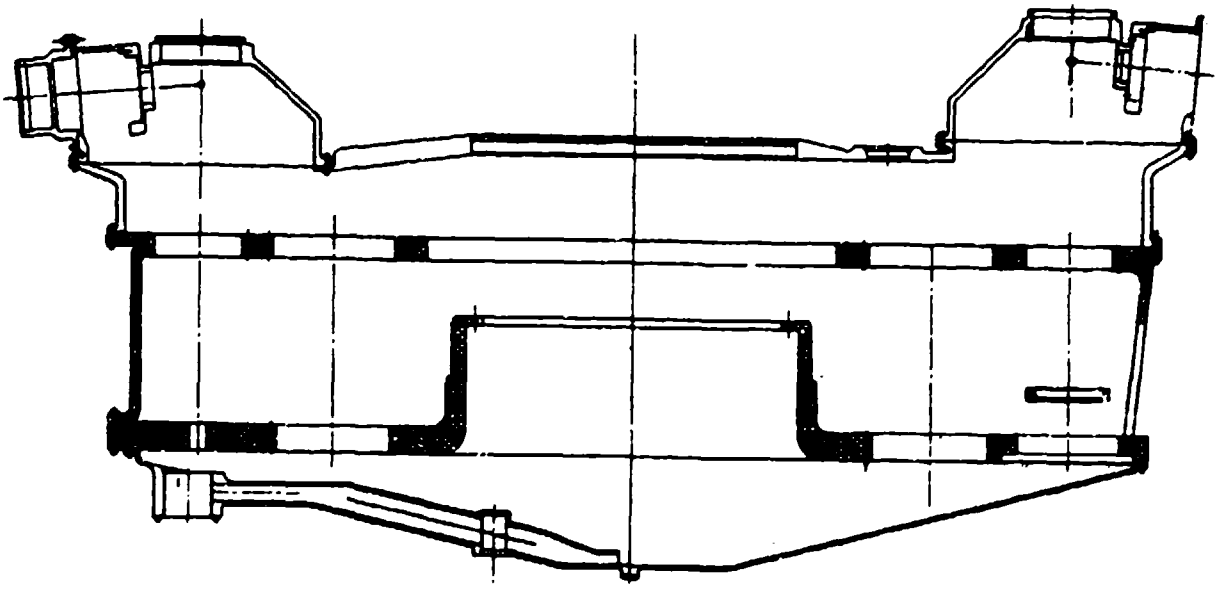

Figure 41. Schematic of ART/ACA Composite Housing Assembly

The split path gearbox readily lends itself to composite design since the bearing locations for the last two stages of gearing essentially form two planes. Thus flat plates can be designed in these planes to react the bearing loads and carry them to the periphery of the housing where they then transfer to the airframe mounting attachments.

The design of composite housings is an integrated part of the design process and must be conducted concurrent with the design of gears and shafting. Initial designs for ART were developed using finite element analysis with quasi-isotropic material properties assuming layups such as +45°, -45°, 0°, 90° and designing as if the material were isotropic. Refinements were then made in the analysis by inputting fiber oriented properties. Material was added and fiber orientation varied to develop stiffness along load paths reducing deflections. In the ART program, it was found that deflection and not strain was the controlling design parameter. It is sometimes difficult to stiffen composite housings since ribs can not be used with RTM because of cost considerations.

Graphite polybismalimide housing are used in the ART program to save weight and solve the corrosion issue prevalent with magnesium housings. The composite material chosen is also good for higher operational temperature than current state-of-the-art magnesium housings. Even considering advanced magnesiums such as WE43, an alloy of ittrium and rare earth which have improved corrosion resistance and can operate at higher temperatures, composites offer weight advantages.

Candidate Transmission Selection

After completion of the four preliminary designs of split torque and split path gearboxes, the weight, noise, and MTBR were analytically evaluated by the methods previously outlined. The results are summarized in Table 13.

Table 13. Preliminary Design Weight, MTBR, and Noise

Configuration	Weight (lbs)	% Wgt	MTBR (hrs)	% MTBR	Relative Noise
Baseline	10,795	-	997	-	Baseline
11:1 Split Path	8,287	-23%	3,890	+390%	-10dB+
8:1 Split Path	9,111	-16%	3,330	+334%	-10dB+
11:1 Split Torque	8,751	-19%	2,950	+296%	-10dB+
8:1 Split Torque	9,430	-13%	2,600	+261%	-10dB+

Examination of the results shows that the 11:1 ratio split path design is a clear choice over the others. It has the lowest weight and highest MTBR. In terms of noise, all designs met the goal of 10 dB noise reduction because each design utilized a herringbone output bull gear and high contact ratio spur gear set. Hence noise drops out of the evaluation procedure. The split torque designs are inferior for a three engine design such as used on the ACA. Perhaps the gaps in weight and MTBR would shorten for a two engine arrangement since the complications of the central engine TTO and drive shaft located under the bull gear would be avoided. Based on selection of the split path gearbox arrangement, all detail design studies were conducted on that design.

Revised Aircraft Power Train Arrangement

The split path transmission installation in the ACA is shown in Figure 42 while the split torque is shown in Figure 43.

The installation of the split torque design is complicated by the need to raise the #2 engine. A higher engine location is required because the vertical distance from the engine input to the TTO is greater in the split torque design and the TTO location is fixed. Also the higher gearbox tends to block the flow of air for the engine inlet.

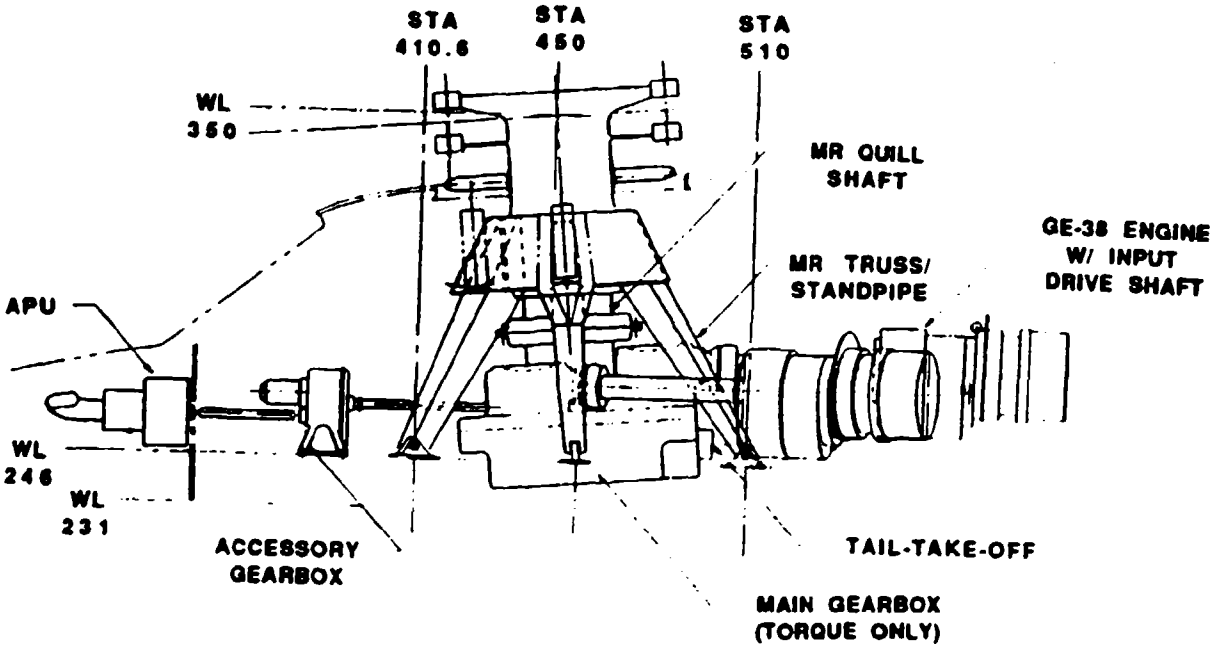

Figure 42. ACA Aircraft Installation of Split Path Gearbox

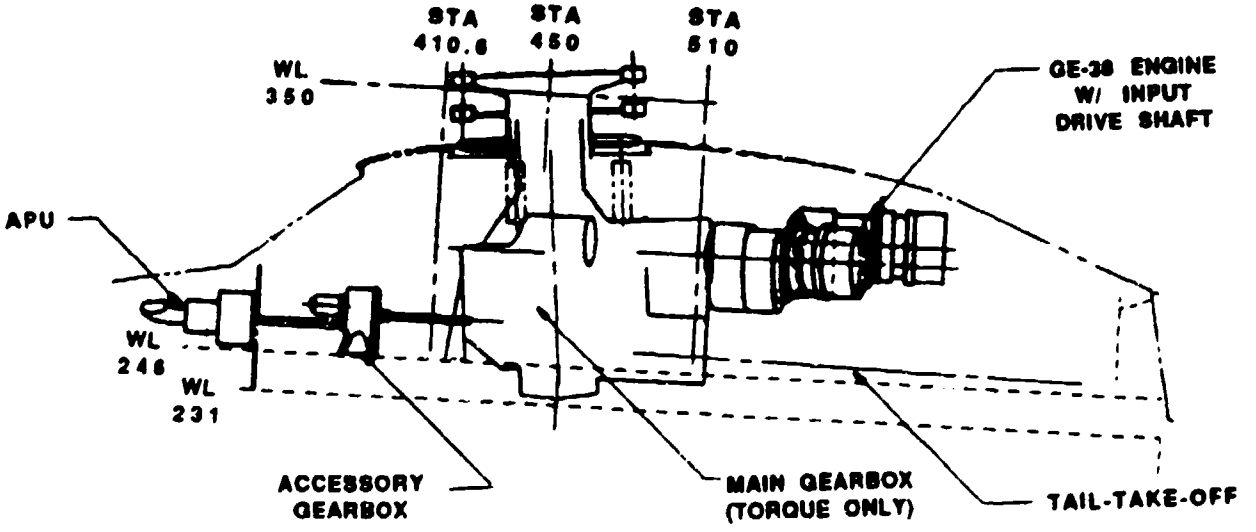

Figure 43. ACA Aircraft Installation of Split Torque Gearbox

Figure 44 is a typical engine installatic [illegible] the ART/ACA. The pivot point of the gimbal mount is located at [illegible] f the input drive shaft coupling center. Thus any deflections [illegible] frame at the aft engine support relative to the transmission support are removed at the coupling as a misalignment angle. The angle is kept small because the distance from the gimbal to the aft engine support is large.

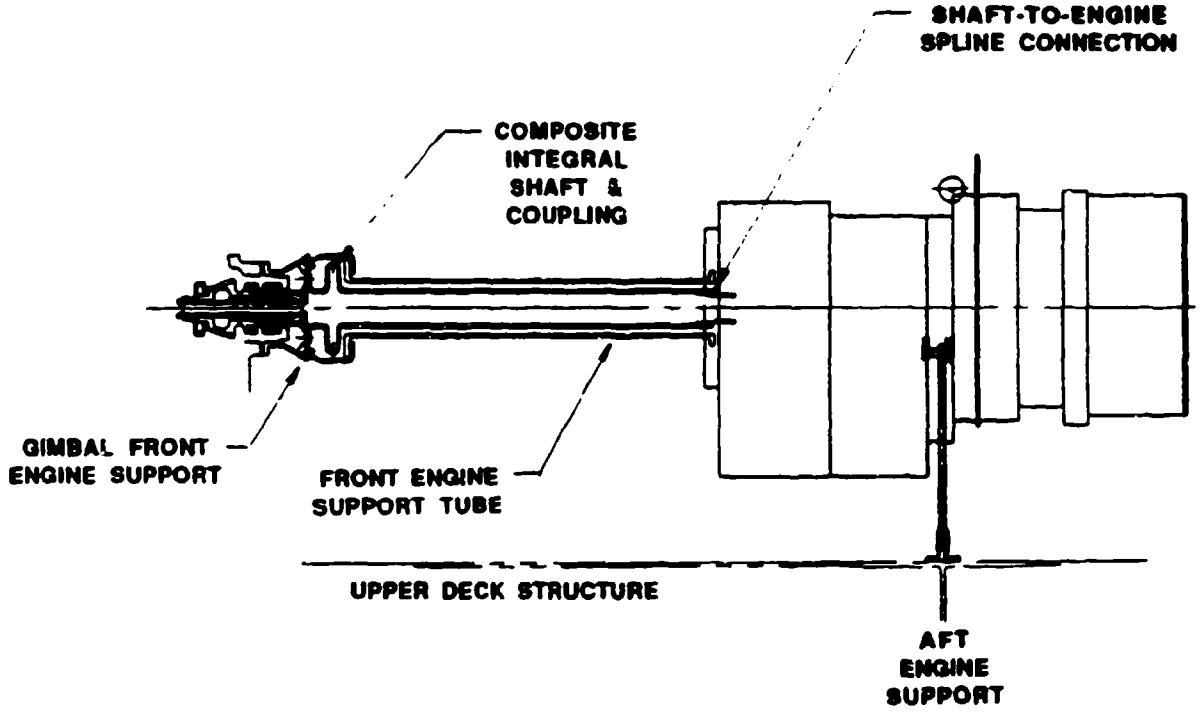

Figure 44. ART/ACA Engine Installation

SYSTEM PERFORMANCE EVALUATION

Approach and Methodology

The ART weight savings results in additional reductions when the ACA aircraft is downsized for the same payload and performance. Weight savings from the transmission alone is 2,508 pounds. If the aircraft size is not changed, the payload will increase by the transmission weight savings. If the payload is kept constant, the aircraft can be downsized. The results are shown in Table 14.

Table 14. Weight Savings by Downsizing Aircraft for Same Payload

Parameter	Baseline	Baseline w/ART	Downsized w/ART
Gross Weight	85,764	85,764	81,957
Payload	25,000	27,508	25,000
Mission Fuel	15,316	15,316	15,218
Weight Empty	45,448	42,940	41,739

Note that the weight empty is reduced by 2,508 pounds for the baseline w/ART since this is the savings for the ART transmission system alone. There is however an additional 1,201 pounds savings by downsizing the aircraft for the same payload thus the ART has actually saved 3,709 pounds in the aircraft

When resizing the aircraft for the same payload certain aircraft design parameters were kept constant. The engines, three GE-38's, were fixed for all designs. The cabin size was fixed. The payload/range was kept at 25,000 pounds with a radius of action of 500 kilometers. The takeoff criterion of 200 feet per minute vertical rate of climb at 95% internal rated power, 4,000 feet, 95°F day was kept constant. With the disk loading maintained at approximately 10 pounds per square foot, the main rotor diameter was sized to match the power required with the power available at the takeoff condition.

All aircraft design analysis was accomplished with the helicopter design model (HDM) as shown in Figure 45. The HDM is a computer program which uses basic input data of mission requirements, design criteria, configuration, engine, and technology. The program then calculates dimensions, weights, powers, performance parameters, and costs. The HDM uses experience factors for calculation of many of the outputs. For example, weight trending equations are provided for the main gearbox, main rotor shaft, main rotor blades, intermediate gearbox, tail gearbox, and tail drive shafting. These equations use parameters such as horsepower, rpm, and reduction ratio with coefficients derived from previous designs to calculate weights. Figure 46 shows the excellent correlation achieved not only with Sikorsky designs but for all helicopter drive systems.

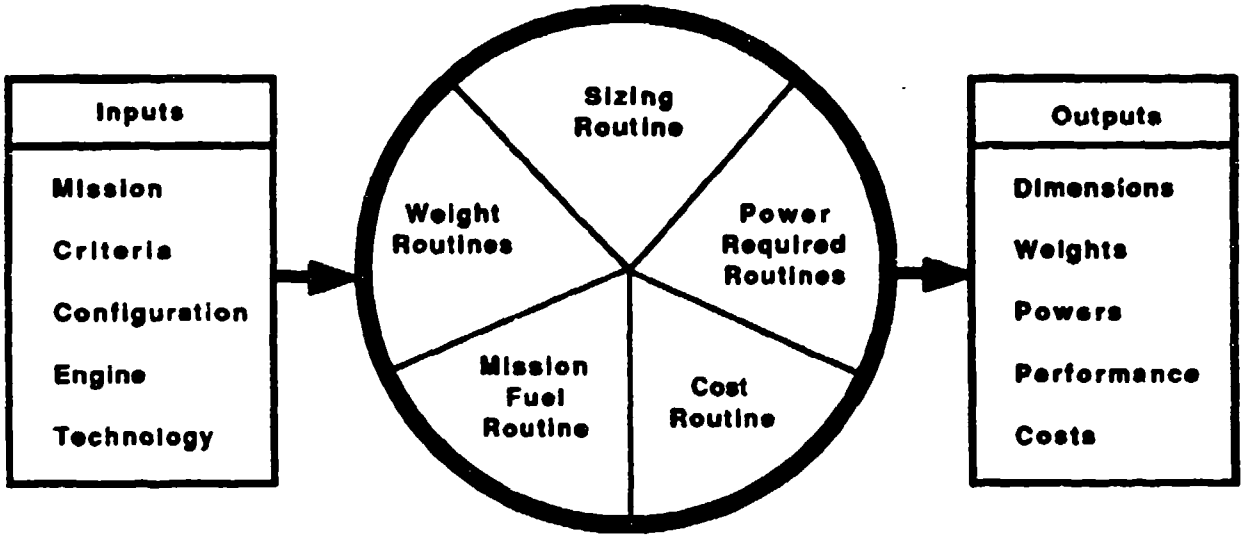

Figure 45. Helicopter Design Model

Aircraft Size, Weight, and Performance

Using the HDM, the baseline ACA aircraft was downsized with the 11:1 split path advanced transmission system. Since this resizing results in changes to the design parameters for the transmission system such as reduced reduction ratio, the transmission system itself is resized. This iteration is continued until a final solution is reached. This results in a smaller, lighter aircraft as shown in Table 15.

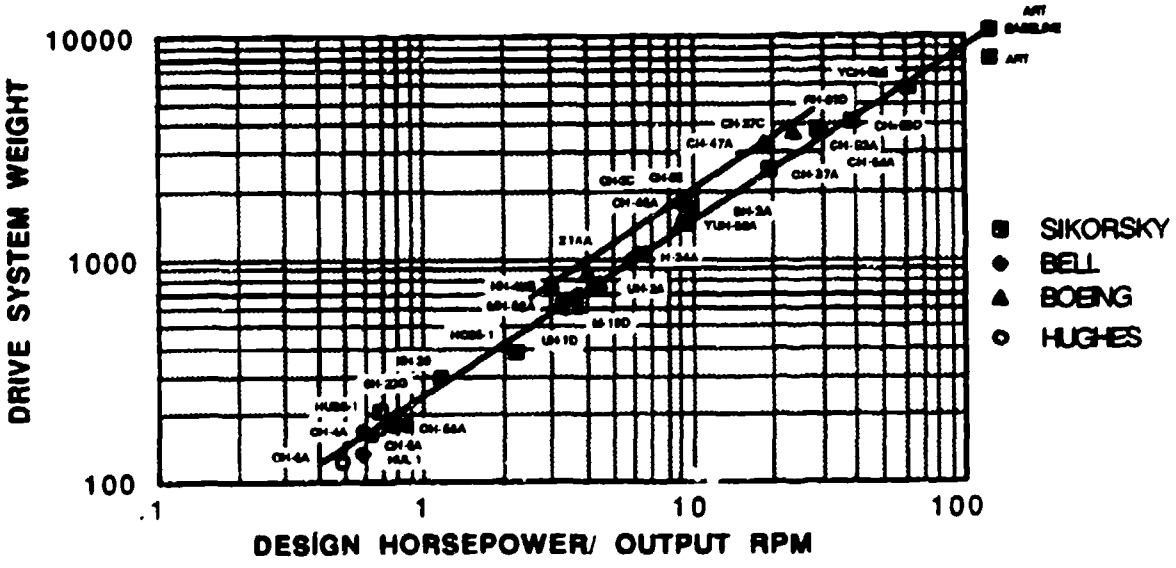

Figure 46. Correlation of Parametric and Actual Drive System Weight

Table 15. Downsized Aircraft and Transmission

Parameter	Baseline	Downsized
Gross Weight (lb)	85,764	81,957
Weight Empty (lb)	44,469	40,760
Main Rotor Dia (ft)	109.6	101.8
Blade Chord (ft)	3.20	3.29
Disk Loading (psf)	9.46	10.46
Main Gearbox Rating (HP)	15,650	15,650
Main Rotor rpm	130	140
MGB Reduction Ratio	115	107
Drive System Weight	10,795	7,870

Note that the transmission is now 2,925 pounds lighter than the baseline vs 2,508 pounds lighter without designing to the reduced size aircraft. In addition to the transmission savings, the weight reductions associated with other components are listed in Table 16.

Table 16. Aircraft Weight Savings w/Downsized ART

Item	Baseline	Downsized w/ART	Saving
Main Rotor	8,569	8,321	248
Tail Rotor	564	555	9
Tail Surfaces	510	512	(2)
Body	9,599	9,286	313
Landing Gear	1,966	1,896	70
Flight Controls	1,907	1,844	63
Engines	2,790	2,790	
Engine Related Items	1,066	1,066	
Fuel System	1,456	1,447	9
Drive System	10,795	7,870	2,925
Other*	4,358	4,358	
Contingency	889	815	74
Weight Empty	44,469	40,760	3,709

The objective of downsizing the aircraft was to achieve essentially the same performance. As seen in Table 17, this goal has been achieved.

Table 17. Performance at 4,000 ft, 95°F Day

Item	Baseline	Downsized w/ART
Gross Weight	85,764	81,957
VROC at 95% IRP (FPM)	200	200
Best Range Speed (kt)	152	153
Max Cruise Speed (kt)	170	170
Dash Speed (kt)	180	180
Cruise Fuel Consumption (lb/hr)	3,450	3,440
Useful Load w/Cabin	39,466	39,993(+527)
Soundproofed to MIL-STD-1294		

Other benefits are derived from the ART weight savings. These are generally small but are in the right direction. The aircraft will have reduced detectability by virtue of increased atmospheric attenuation from higher main rotor rpm. Higher main rotor rpm also reduces blade "flicker" which reduces visual detection. The smaller sized aircraft will also have smaller static and doppler radar returns. Several survivability benefits are also inherited by virtue of increased ballistic survivability from the wider blade chord, increased agility from lower inertia, and greater crashworthiness from the standpipe configuration. Aircraft availability is improved since transmission maintenance is decreased. Smaller, lighter components also require less field support and improve deployability.

Life Cycle Cost

Life cycle aircraft costs include development costs, production costs, operating costs, and support costs. Life cycle costs have been calculated for the ACA with the ART transmission system. Several assumptions were required to project forward in estimating the future cost of the ACA. All costs have been normalized to 1990 year dollars. The development program is assumed to start in 2010 and lasts five years. Three flying prototypes have been included in the development phase as well as associated ground test articles. Engine development costs have been assumed to be paid prior to this program.

Production runs from the year 2015 through 2026. A production run of 600 total aircraft with associated spares was anticipated, beginning at a rate of 15 aircraft per year and building up to a peak of 75 per year. Operating and support costs have been determined over a 35 year period. Representative peace time attrition rates and a utilization rate of 240 flight hours per aircraft per year were used in the analysis. The Time phased relationship of development, acquisition, and operational costs are shown in Figure 47.

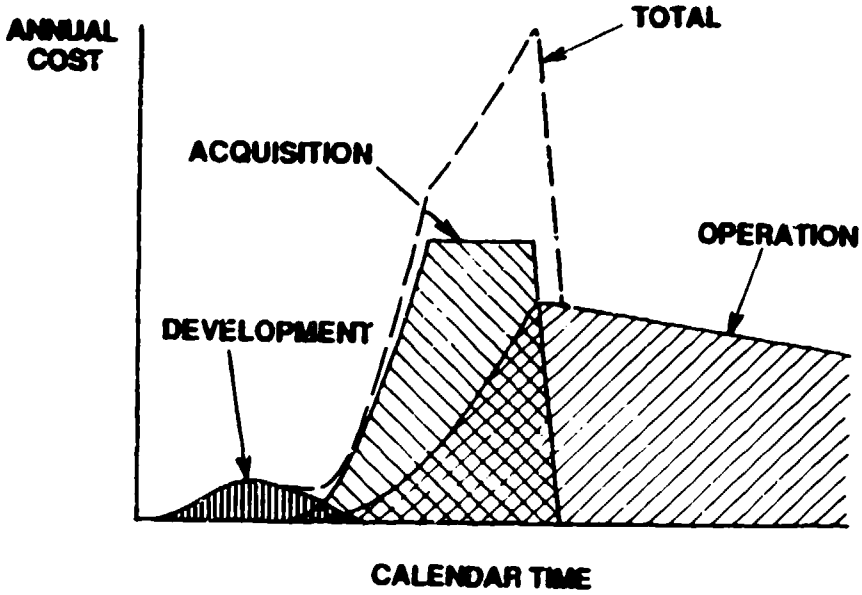

Figure 47. Time Phased Elements of Life Cycle Cost

Since the interest in the ART program is in the transmission area, the life cycle cost of the transmission system was determined in more detail than the other areas. Transmission parameters affecting life cycle cost are listed in Table 18.

Table 18. Transmission Parameters Affecting Life Cycle Cost

Item	Baseline	Baseline w/ART	Downsized w/ART
Weight	9,077	6,276	6,322
Cost Per Pound	$144	$157	$157
MTBR (FH)	997	3,890	3,890
MMH to Remove	14	10	10
MMH to Install	28	20	20
MMH to Repair at Depot	3,328	2,059	1,943
Material $ to Repair at Depot	$310K	$192K	$181K
Initial Cost of GSE	$410K	$336K	$317K
Replenishment Cost of GSE	$571K	$468K	$441K
Cost of Shipping Container	$34K	$25K	$24K
Cost to Prepare and Ship	$1,678	$1,374	$1,296
MMH/FH at Depot	2.710	0.489	0.463
MMH/FH Other	0.301	0.281	0.281
Total MMH/FH	3.011	0.770	0.744

The largest difference seen is in the area of depot maintenance. This is solely because the MTBR is so much higher with the advanced designs. High MTBR was achieved in the advanced split path designs by elimination of parts and by designing to increased life requirements. Whereas in the CH53E (baseline) era, the bearing design criteria was to have all individual B10 lives above 1,000 hours, in the ART program 15,000 hours was used. Designing to such a high life is a trade off with weight. The ART gearbox was able to achieve both a weight decrease and an MTBR increase.

Typically, depot overhaul costs are more than 50% of a new gearbox production cost. Since the ART main transmission is very expensive, the overhaul cost will also be expensive. If the rate of depot maintenance for the split path transmission is reduced to one fourth of the baseline value, it is easily seen that tremendous cost reductions are achieved. Maintenance man hours per flight hour at depot is also a direct measure of the MTBR increase. Table 19 shows the large differences in transmission operating cost per flight hour.

Table 19. Transmission Operating Cost Per Flight Hour

Item	Baseline	Baseline w/ART	Downsized w/ART
Depot Maintenance	$360	$65	$61
Other Maintenance	3	3	3
Shipping	2	1	1
Replenishment Spares	34	24	23
Total Trans Operating Cost	$399	$93	$88
Savings	-	$306	$311

As seen from Table 19, the cost saving is in excess of $300 per flight hour for the transmission alone. In the downsized aircraft, there are other savings in addition to the transmission maintenance and spares savings. This is shown in Table 20.

Table 20. Aircraft Operating Cost Per Flight Hour

Item	Baseline	Baseline w/ART	Downsized w/ART
Personnel	$1239	$1239	$1239
Fuel, Oil, Lubricants	555	555	554
Maintenance	598	302	283
Replenishment Spares	374	364	341
Other	1046	1046	1046
Total A.C. Operating Cost	$3812	$3506	$3463
Savings	-	$306	$349

The savings achieved in the transmission system translate into large aircraft fleet life cycle cost savings of over one billion dollars as depicted in Table 21. The transmission weight savings and reliability increase have therefore resulted in substantial life cycle cost savings.

Table 21. Aircraft Fleet Life Cycle Cost

Item	Baseline	Baseline w/ART	Downsized w/ART
Development	$0.5B	$0.5B	$0.5B
Acquisition	11.8B	11.6B	11.2B
Operation	11.1B	10.2B	10.0B
Totals	$23.4B	$22.3B	$21.7B
Savings	-	$1.1B	$1.7B

DETAIL DESIGN

Full Size Aircraft Gearbox

Detail design studies were conducted on the full size aircraft high reduction ratio output herringbone gear, split path gearbox to define all components to the point where detailed estimates could be made of weight, noise, and MTBR. Detail layouts were made of the main gearbox to sufficient detail level to permit accurate weight assessment. Detailed structural analysis was performed to assure that all components were structurally adequate. As will be discussed in subsequent paragraphs, detail drawings were made of all components associated with the second stage high contact ratio spur gear mesh and the output herringbone mesh to be used for a 1/2 size test. As will be shown, stress and deflection are identical for the full size aircraft component and for the 1/2 size test component when 1/8 power is used. Thus, structural analysis for some components was conducted for the full sized hardware while other analysis was performed for the 1/2 sized test hardware.

The detail layout cross section is shown in Figure 48. The components are very similar to those in the preliminary layout except for variations as a result of section beef up or reduction based on the detailed structural analysis. The top view is shown in Figure 49 depicting the mounting feet and some of the main gearbox mounted accessories. Power is fed from each of three GE-38 engines directly to the input side of a spring type overrunning clutch. The output side of the clutch drives a spiral bevel pinion at 15,000 rpm. The spiral bevel gear axis is parallel to the main rotor shaft axis. Torque splitting takes place at the spur gear mesh pinion. The mesh is a high contact ratio spur and there is one pinion and two gears per engine. Each spur gear drives a herringbone pinion which in turn transfers and combines power to the output bull gear. The bull gear is fixed axially and the herringbone pinion assemblies are floating to assure load sharing between left and right hand helix halves of the herringbone mesh. Load sharing between pairs of spur gears on the same engine path is provided by a soft torsional isolator. The isolator is shown mounted between the spur gear and herringbone pinions and contains alternate layers of rubber and metal that are precompressed between the steel outer and inner members by a controlled gap shim using bolts for preloading. The torsional spring rate of the elastomeric device is low relative to the axial and radial spring rate.

Trade off studies were conducted on various aspects of the main transmission design to establish low weight/high reliability solutions. The tail-take-off drive was examined with regard to minimum number of extra meshes. The design chosen uses only one extra bevel gear mesh for the tail-take-off. Trade off studies were also conducted on options for driving accessories. The split path design is well suited for direct drive of accessories without the need for a great deal of extra gearing. All gears use Pyrowear 53 material, a high hot hardness carburizing gear steel which retains its hardness at higher temperature than the baseline 9310 steel. The housings are fabricated by resin transfer molding (RTM) of graphite fibers in a matrix with polybismalimide. These housing composite materials have been tested under a composite housing development CR&D program and were chosen based on strength, resistance

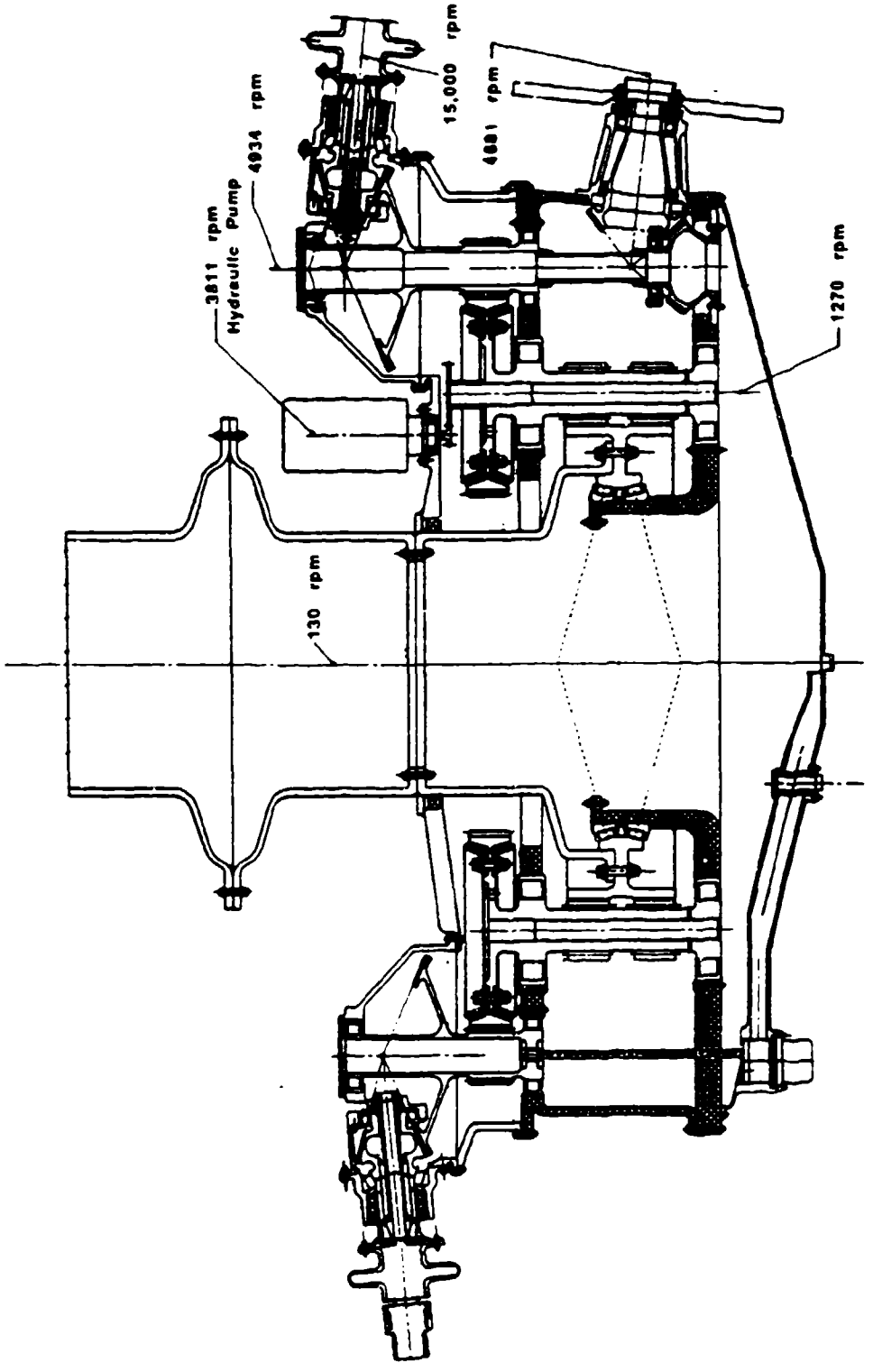

Figure 48. ART Main Gearbox Cross Section

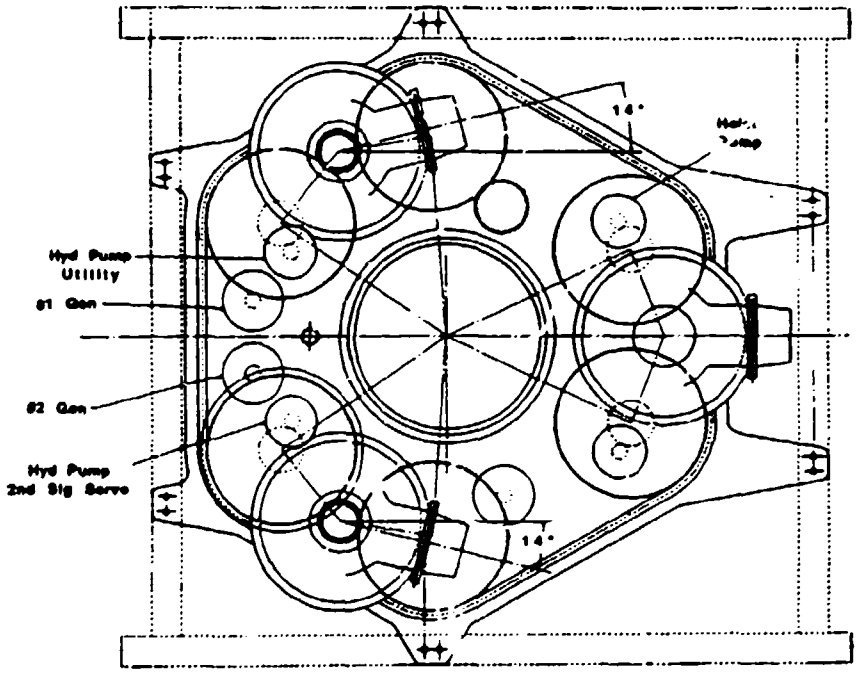

Figure 49. ART Main Gearbox Top View

to corrosion, temperature capability, hot oil resistance, and suitability for RTM fabrication. Table 22 lists the advanced or new technology concepts used for the ART transmission.

Table 22. ART Technology Advances

Advanced Technology	Parameters Impacted
Split Power Gear Concept	Weight, Noise, MTBR, Cost
Canted 3 Engine Arrangement	Balanced Climb/OEI Requirements
Herringbone Gear Mesh - 10:1 RR	Weight, Noise
Composite Housings	Weight, MTBR, Depot Maint, Spares
Composite MRS Truss	Weight
Composite MRS/Quill Shaft	Weight
Pyrowear 53 Gear Material	Weight, MTBR, Lost Oil Surv.
Topological Gear Grinding	Weight, Noise, MTBR
Load Sharing Elastomeric Spring	Weight, Noise
Composite Tail Drive System	Compatibility w/Airframe
Comp. Int. Shaft/Coup. Eng. Shaft	High Angle, Tamper Proof Balance
Ceramic Rolling Element Brgs.	Weight, MTBR
Squeeze Film Damper on Input	MTBR
Spring Clutch on Input	Weight, MTBR
Integral Race Roller Bearings	Weight, MTBR
Spherical Tapered Roller Bearing	Weight, MTBR, Survivability
Flanged Outer Race Bearings	MTBR
Increased Operating Temperature	Weight
3 Micron Oil Filtration	MTBR

Gearing

Basic gear data for the ART full sized aircraft transmission main gearbox is shown in Table 23. Table 24 lists gear bending stress, contact stress, and scoring temperature rise for the major meshes. Bending and contact stresses are calculated by the American Gear Manufacturers Association (AGMA) methodology as shown in ANSI/AGMA 2001-B88 for spur and helical gears and in ANSI/AGMA 2003-B86 for bevel gears. The scoring temperature rise for bevel gears is calculated by the Gleason method whereas for spur gears, the method is based on the work of Blok and Kelley as shown in ANSI/AGMA 2001-B88, Appendix A.

Table 23. Full Sized ART, Basic Gear Data

Gear	Number of Teeth	Pitch Dia	rpm	Pressure Angle	Spiral (Helix) Angle
Input Bevel Pinion	25	6.6667	15,000	20°	25°
Input Bevel Gear	76	20.2667	4,934	20°	25°
2nd Stage Spur Pinion	26	5.0268	4,934	18°	-
2nd Stage Spur Gear	101	19.5271	1,270	18°	-
Herringbone Pinion	13	4.9134	1,270	20°	31°
Herringbone Gear	127	48.0000	130	20°	31°
TTO Bevel Pinion	37	9.0024	4,934	20°	30°
TTO Bevel Gear	39	9.4891	4,681	20°	30°
Hyd Pump Spur Gear	60	6.0000	1,270	22.5°	-
Hyd Pump Spur Pinion	20	2.0000	3,810	22.5°	-
Generator Spur Pinion	11	2.1267	11,663	22.5°	-
Oil Cooler Spur Pinion	34	6.5706	3,773	22.5°	-

Table 24. Bending and Contact Stress, and Scoring Temperature Rise

Gear	Gear Design HP	Bending Stress (psi)	Contact (Hertz) (psi)	Scoring Rise (°F)
Input Bevel Pinion	5,343	29,990	184,150	234
Input Bevel Gear	5,343	24,700	184,150	234
Input Spur Pinion	2,671	45,490	143,250	137
Input Spur Gear	2,671	47,120	143,250	137
Output Herringbone Pinion	1,296	56,710	176,130	139
Output Herringbone Gear	1,296	55,090	176,130	139
TTO Bevel Pinion	2,400	30,080	193,890	73
TTO Bevel Gear	2,400	29,670	193,890	73

Bearings

Basic bearing life is calculated by the methods outlined by AFBMA. Standard envelope dimensions were used for all bearings. Factors for material and EHD lubrication were used to determine the B-10 bearing lives. The results for the full sized aircraft main gearbox are shown in Table 25. The prorated power was used to establish the bearing life calculated in Table 25. The prorated power is defined as that power which if applied continuously, would give the same life as a spectrum of power and percent time. An estimated usage spectrum of power and percent time was used to calculate the prorated power. For the ART, the prorated input power used was 64.26% of the maximum , and the prorated main rotor power was 61.30% of maximum. The tail drive system prorate was 48.92% of the maximum tail rotor power.

Table 25. Full Sized ART, Basic Bearing Summary

Position	rpm	Load @ Prorate (lbs)	B-10 Life (hrs)
Input Clutch Duplex (3)	15,000	20	very high
Input Bev. Ang. Con. Sph. Roll (3)	15,000	5,960	50,060
Bevel Pinion Roller (3)	15,000	2,900	42,610
#1 Bev Gear/Spur Pin Tapered Roll	4,934	3,400	73,030
#1 Bev Gear/Spur Pin Roller	4,934	2,120	5,400,000
#2 Bev Gear/Spur Pin Tapered Roll	4,934	3,930	44,010
#2 Bev Gear/Spur Pin Roller	4,934	7,640	71,040
#3 Bev Gear/Spur Pin Tapered Roll	4,934	4,290	32,740
#3 Bev Gear/Spur Pin Roller	4,934	5.960	165,400
#1 Herringbone Pinion Upper Roll (3)	1,270	12,500	195,140
#1 Herringbone Pinion Lower Roll (3)	1,270	19,700	22,400
#2 Herringbone Pinion Upper Roll (3)	1,270	25,200	16,800
#2 Herringbone Pinion Lower Roll (3)	1,270	16,900	38,300
Herringbone Gear Tapered Roller (2)	130	4,420	1,160,000
TTO Pinion Tapered Roller	4,934	4,780	22,630
TTO Pinion Roller	4,934	3,530	122,120
TTO Gear Tapered Roller	4,681	3,280	81,650
TTO Gear Roller	4,681	1,360	3,290,000

The bearing lives of Table 25 can be summed using probability theory to find a system B-10 life. For this calculation, there are three sets of input bevel pinion bearings, and three sets of herringbone pinion bearings. The lives listed are all different for the #1, #2, and #3 engine input to the bevel gear/spur pinion shaft because of the angular orientation of the bevel gear input (aligned with the engine) and the spur pinion (aligned with the bull gear). Similarly the angular orientation is different for each branch for each engine on the spur gear/herringbone pinion mesh. The B-10 system life is calculated to be 1965 hours. This represents a mean bearing system life of 9825 hours.

Lubrication

Lubrication system design begins with the calculation of the heat generated. For the ART, the heat generated was calculated for the 100% input power design condition with 16,030 HP input. Table 26 summarizes the heat generation calculations.

The total heat generated of 18,360.1 BTU/min corresponds to a loss of 432.9 HP. For 16030 HP input, an efficiency of 97.3% is calculated which is representative for a three stage helicopter gearbox.

The required flow is determined by using the assumption that all of the heat generated will be transferred to the oil and assuming a temperature rise of the oil. A typical helicopter gearbox oil was assumed at 210°F with a specific heat of 0.455 BTU/lb°F and a density of 0.0331 pounds per cubic inch. The required flow was then calculated as that flow which would produce a temperature rise of 40°F in the oil. The actual flow may be more than the required flow because of the limitation of using a minimum jet diameter of 0.032 inch. Given a pressure of 70 psig, a flow of 0.18 gallons per minute (gpm) is calculated for a 0.032 inch jet. If the required flow is less than 0.18 gpm, extra oil is put into the system. For a large gearbox such as the ACA, the theoretical and actual flow will not be too different because most jets are required to be larger than 0.032 inch but as size decreases, more and more minimum size jets will be used and the actual flow can reach more than 2 times the required flow. A summary of actual and theoretical flow is shown in Table 27.

The oil cooler has been sized to reject 16,200 BTU/min on a sea level standard day. This is based on past designs where some amount of heat will be rejected through the gearbox housings by conduction and convection (radiation is usually small). For the ART, 10% of the heat is assumed to be rejected through the housings. By taking 90% of the heat generated at the 100% power condition on a standard day, the cooler is sized to keep the sump temperature at approximately 200°F for most of the time. At high power conditions on a hot day, the oil will heat up slightly.

The lubrication pumps have been sized for 65 gpm each (2 pumps) at 70 psig. From previous experience, the sump usually contains an amount of oil in gallons equal to 0.4 times the flow in gallons per minute. Therefore the sump for the ACA is estimated to contain 52 gallons of oil. This would normally be adjusted during the no load lubrication survey which is generally the first test to be run on a new transmission.

Table 26. Full Sized ART, Heat Generation Summary

Description	Individual BTU/Min	Qty per box	Total BTU/Min
Input Bevel Duplex Ball Bearing	215.3	3	645.9
Input Bevel Ang. Cont. Sph. Roller	425.5	3	1276.5
Input Bevel Roller Bearing	150.0	3	450.0
Spring Clutch Arbor Duplex Ball	19.6	3	58.8
Spiral Bevel Gear Mesh	1747.0	3	5241.0
#1 Bev Gear/Spur Pin Sph Roller	89.2	1	89.2
#1 Bev Gear/Spur Pin Roller	69.5	1	69.5
#2 Bev Gear/Spur Pin Sph Roller	98.6	1	98.6
#2 Bev Gear/Spur Pin Roller	132.1	1	132.1
#3 Bev Gear/Spur Pin Sph Roller	135.5	1	135.5
#3 Bev Gear/Spur Pin Roller	113.1	1	113.1
High Contact Ratio Spur Mesh	1595.8	3	4787.4
TTO Pinion Ang. Cont. Sph. Roller	159.3	1	159.3
TTO Pinion Roller Bearing	59.7	1	59.7
TTO Gear Ang. Cont. Sph. Roller	176.1	1	176.1
TTO Gear Roller Bearing	32.7	1	32.7
TTO Spiral Bevel Mesh	422.6	1	422.6
#1 Upper Herringbone Pinion Roller	60.0	3	180.0
#1 Lower Herringbone Pinion Roller	80.6	3	241.8
#2 Upper Herringbone Pinion Roller	112.0	3	336.0
#2 Lower Herringbone Pinion Roller	71.0	3	213.0
Herringbone Gear Mesh	524.9	6	3149.4
Timken Bearings, Herringbone Gear	21.6	2	43.2
Generator	66.3	3	198.9
Hoist Pump	20.8	1	20.8
2nd Stage Servo	11.2	1	11.2
Primary Servo	11.2	1	11.2
Utility Pump	6.6	1	6.6
Grand Total			18,360.1

Table 27. Full Sized ART, Actual and Theoretical Flow

Description	Req'd Flow (gpm)	Jet Dia (in)	Qty Per Box	Total Actual (gpm)
Input Bevel Duplex Ball Bearing	1.54	.094	3	4.66
Input Bevel Ang. Cont. Sph. Roller	3.04	.136	3	9.75
Input Bevel Roller Bearing	1.07	.078	3	3.21
Spring Clutch Arbor Duplex Ball	0.14	.032	3	0.54
Spiral Bevel Gear Mesh	3.12	.136	12	39.00
#1 Bev Gear/Spur Pin Sph Roller	0.64	.062	1	0.68
#1 Bev Gear/Spur Pin Roller	0.50	.055	1	0.53
#2 Bev Gear/Spur Pin Sph Roller	0.70	.064	1	0.72
#2 Bev Gear/Spur Pin Roller	0.94	.073	1	0.94
#3 Bev Gear/Spur Pin Sph Roller	0.97	.078	1	1.07
#3 Bev Gear/Spur Pin Roller	0.81	.070	1	0.86
High Contact Ratio Spur Mesh	2.85	.128	12	34.54
TTO Pinion Ang. Cont. Sph. Roller	1.14	.081	1	1.15
TTO Pinion Roller Bearing	0.43	.052	1	0.48
TTO Gear Ang. Cont. Sph. Roller	1.26	.086	1	1.30
TTO Gear Roller Bearing	0.23	.040	1	0.28
TTO Spiral Bevel Mesh	1.51	.094	2	3.10
#1 Upper Herringbone Pinion Roller	0.43	.052	3	1.43
#1 Lower Herringbone Pinion Roller	0.58	.060	3	1.90
#2 Upper Herringbone Pinion Roller	0.80	.070	3	2.58
#2 Lower Herringbone Pinion Roller	0.51	.055	3	1.59
Herringbone Gear Mesh	0.47	.052	48	22.88
Timken Bearings, Herringbone Gear	0.15	.050	3	1.32
Generator	0.47	.052	3	1.43
Hoist Pump	0.15	.032	1	0.18
2nd Stage Servo	0.08	.032	1	0.18
Primary Servo	0.08	.032	1	0.18
Utility Pump	0.05	.032	1	0.18
Grand Total Actual Flow				136.66
Grand Total Theoretical Flow				131.87

(Theoretical Flow = Sum of Req'd Flow x Qty)

Composite Housings

The split path main gearbox design is ideally suited for the use of composite housings. There are essentially two flat plates through the gearbox which hold the majority of the bearings and carry the majority of the loads. Sizing of thicknesses for the composite housing was accomplished by conducting a finite element analysis of the complete housing assembly. The free body of the housing has loads applied to it at each bearing location. Reactions are through the mounting feet which are constrained to ground. The FEA model is shown in Figure 50.

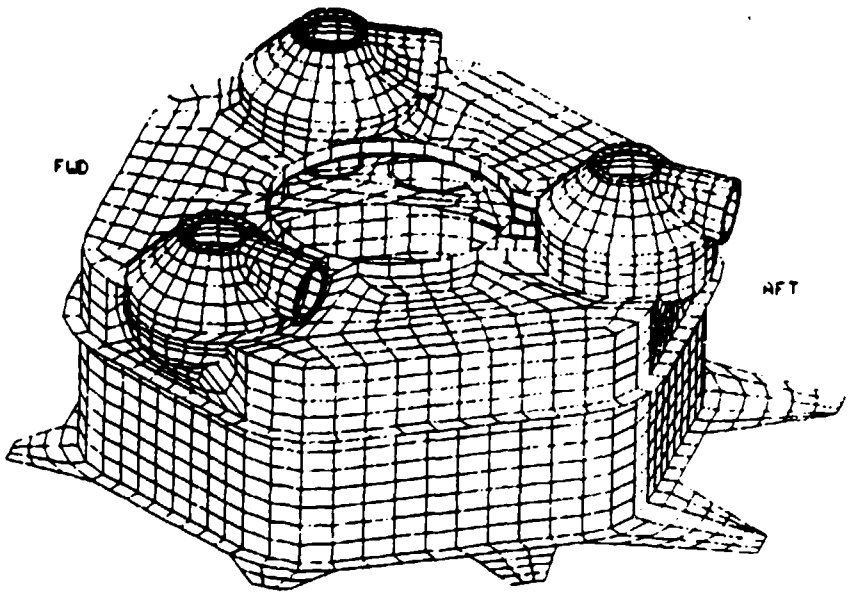

Figure 50. Composite Housing Finite Element Model

The material used for the housings is graphite fibers in a matrix of polybismalimide. Approximately a 50% fiber volume can be achieved by resin transfer molding (RTM) wherein dry fibers are placed inside a closed mold and the resin is injected to extrude through the fibers and fill the mold. A temperature/time cycle is applied after injection to solidify the material. The part is removed from the mold and is subjected to a final temperature/time cycle for final curing. The matrix material can achieve a tensile modulus of 10 million for a quasi-isotopic layup of +45°, -45°, 0°, 90°. By altering the directions of the layups, the properties can be tailored to achieve selective stiffness. This was done to some extent in the ART housings. It was found that deflection was the governing design condition rather than strain. The highest strain calculated was for the number 1 engine input housing. Its value was .0019 versus an allowable strain of .004 inch per inch for the graphite polybismalimide material used. The deflected housing shape is depicted in Figure 51. As seen, the highest deflections occur on the upper cover in the area of the input attachments. This is a difficult area to stiffen without the use of ribs. Ribs are not practical with the RTM process because they complicate the mold, complicate the layup of the graphite and add to the cost. Upper cover deflections are shown in Figure 52 and input housing major principal strain is shown in Figure 53.

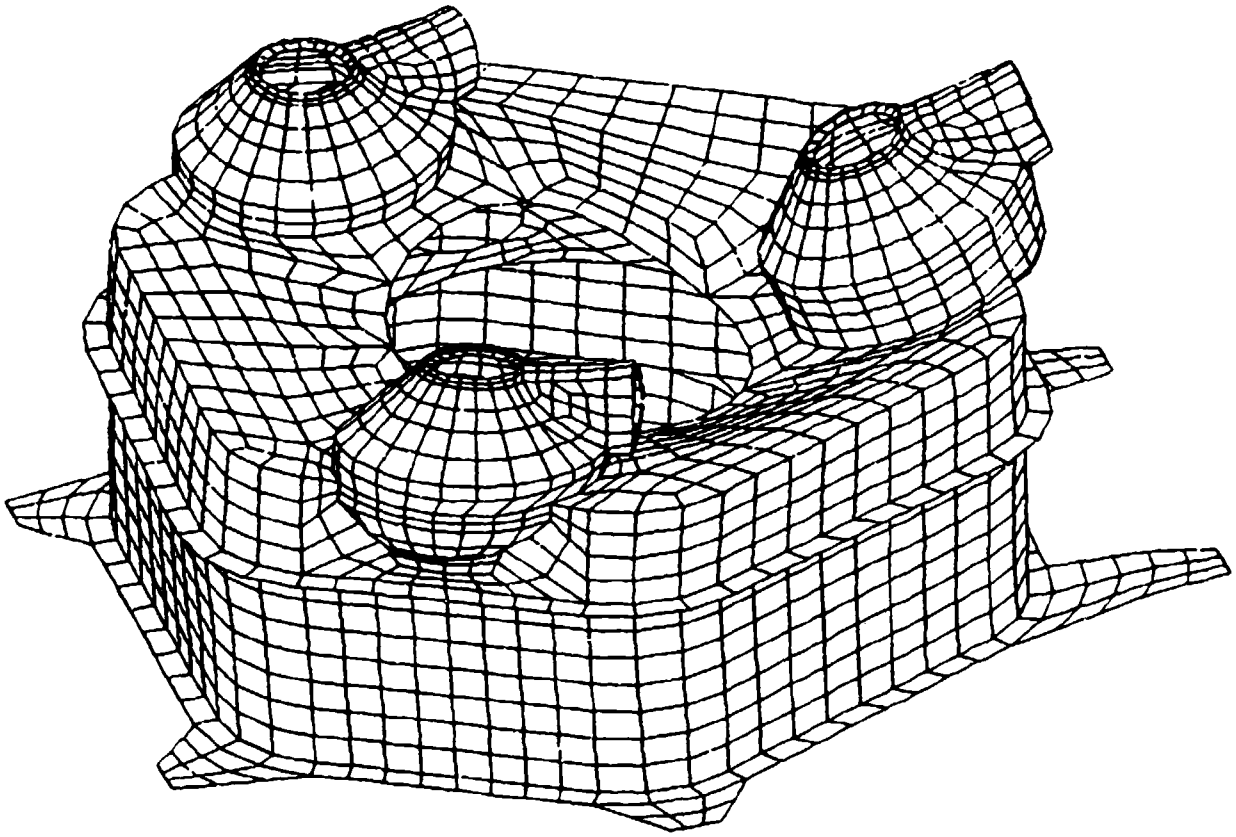

Figure 51. Composite Housing Deformed Shape Plot

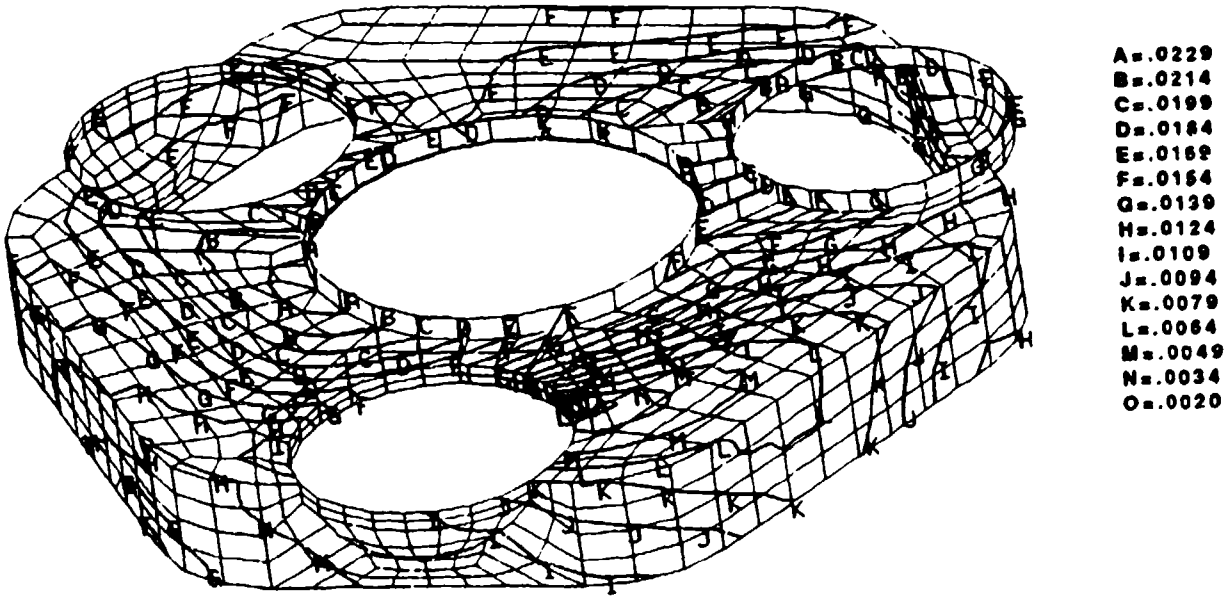

Figure 52. Upper Cover, Total Deflection

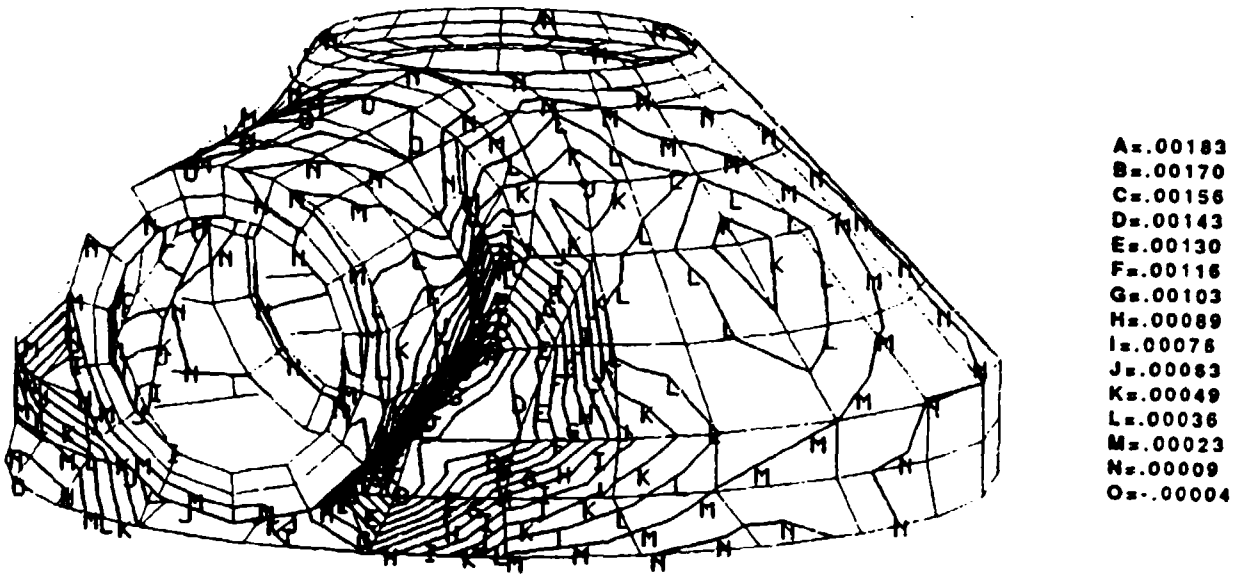

Figure 53. Input Housing, Major Principal Strain

Composite Main Rotor Shaft/Quill/Standpipe

Torque is transferred from the main gearbox to the main rotor by means of a composite quill shaft on the ART/ACA. The quill shaft is 26 inches in diameter and is 0.8 inch thick. It carries over 7 million inch pounds torque at the 100% power condition transmitting 14825 HP. A titanium main rotor shaft is located inside of a composite housing with six truss member legs which attach to the airframe. A cross section of the truss, main rotor shaft, rotor head, quill shaft and main transmission are illustrated in Figure 54. Rotor loads are transmitted from the rotor head to the main rotor shaft, through the main rotor shaft bearings into the truss structure. Since there is some bending stiffness to the quill shaft assembly, some moment will be redundantly transmitted to the quill shaft. The bolted connection with integral coupling is intended to reduce the redundant load carried by the truss. A finite element analysis of the structure was conducted. The model is exhibited in Figure 55. The analysis showed that in forward flight at the limit rotor load condition with limit head moment, limit thrust and limit side load applied, the quill shaft reacts only 0.1% of the moment (3,450 inch pounds moment compared to the head moment of 3,020,000 inch pounds). The finite element analysis load conditions are listed in Table 28.

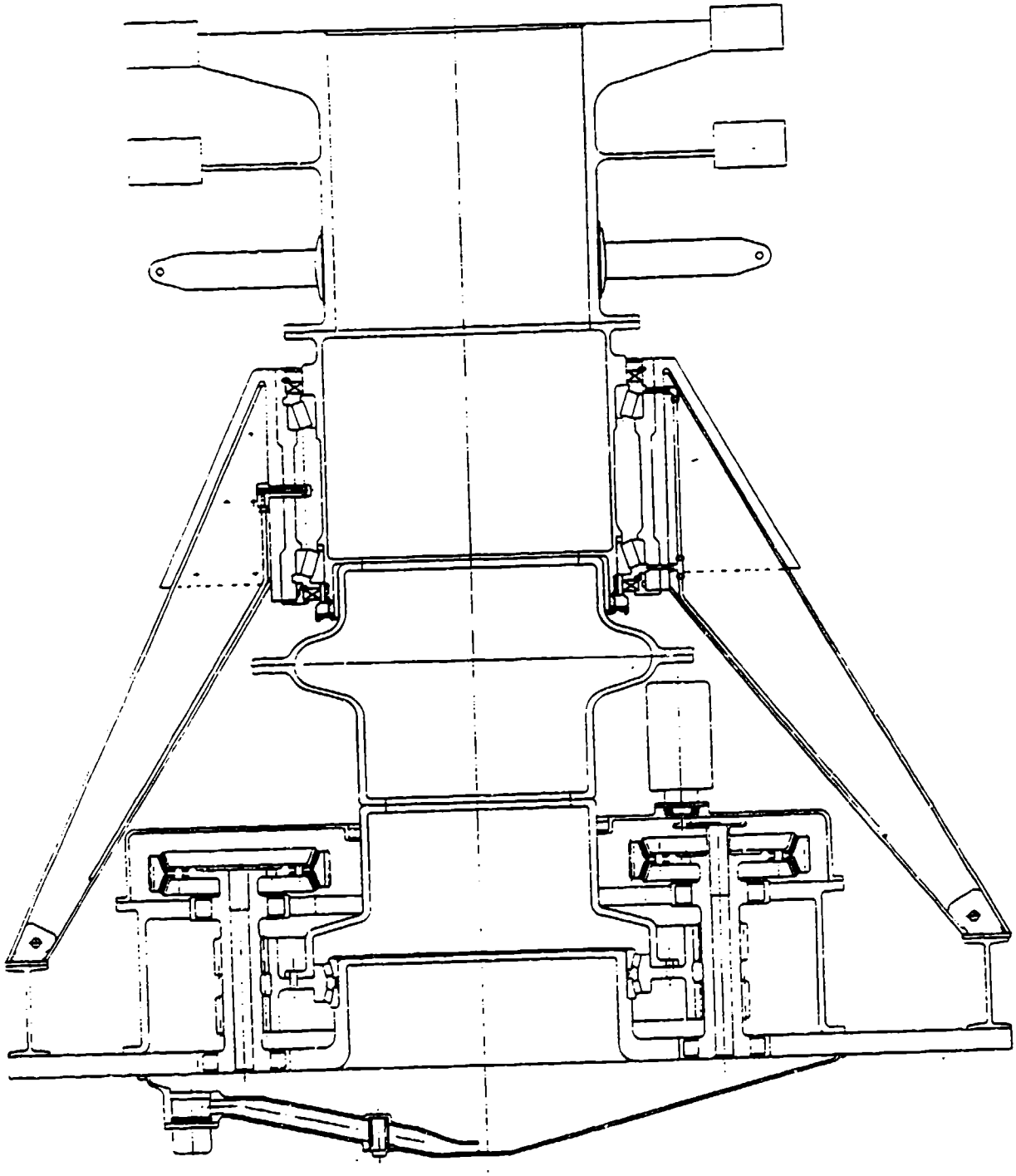

Figure 54. Composite Quill, Main Rotor Shaft, Truss Cross Section

Table 28. Composite Quill, Main Rotor Shaft, Truss Load Conditions

Condition #	Name
1	20g Forward Crash (174,900 lb @ rotor)
2	20g Down Crash (174,900 lb @ rotor)
3	10g Side Crash (87,450 lb @ rotor)
4	Limit Forward Flight Limit Head Moment = 3,020,000 in-lb Limit Side Load = 17,920 lb Limit Thrust = 154,000 lb Limit Torque = 14,400,000 in-lb Limit Servo Load = 80,000 lb
5	Limit Rearward Flight (Same magnitudes as #4 but acts to rear)
6	Limit Side Flight (Same magnitudes as #4 but acts to side)

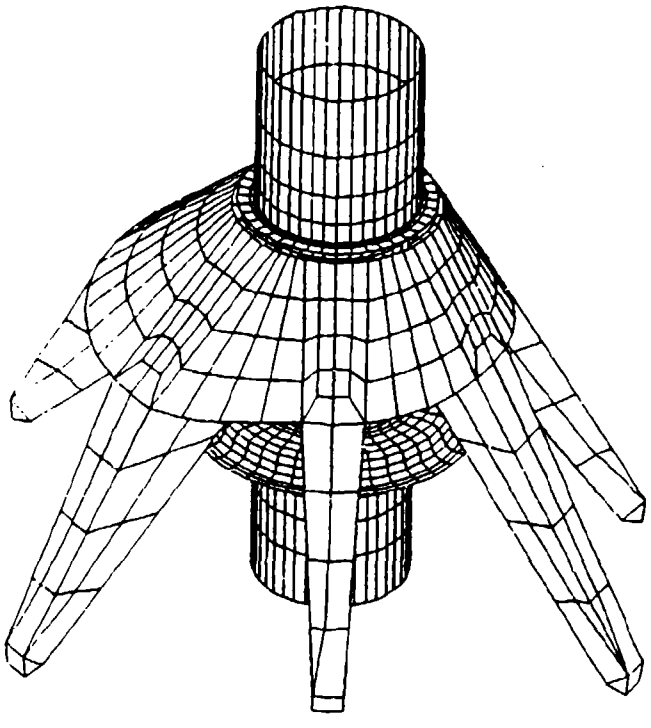

Figure 55. Composite Standpipe/Truss FEA Model

The composite truss is designed by strain rather than deflection. The deflection can be relatively high in the truss member since no gearing is involved. Figure 56 shows deflection levels of .676 inch maximum. This deflection occurs at the center of the forward servo mount and is caused by the limit servo load of 80,000 pounds. This magnitude of deflection is in the direction of the applied servo loads and merely causes an extra extension of the servo. The deflection at the rotor head of .256 inch is low relative to other Sikorsky helicopters considering the size of the structure.

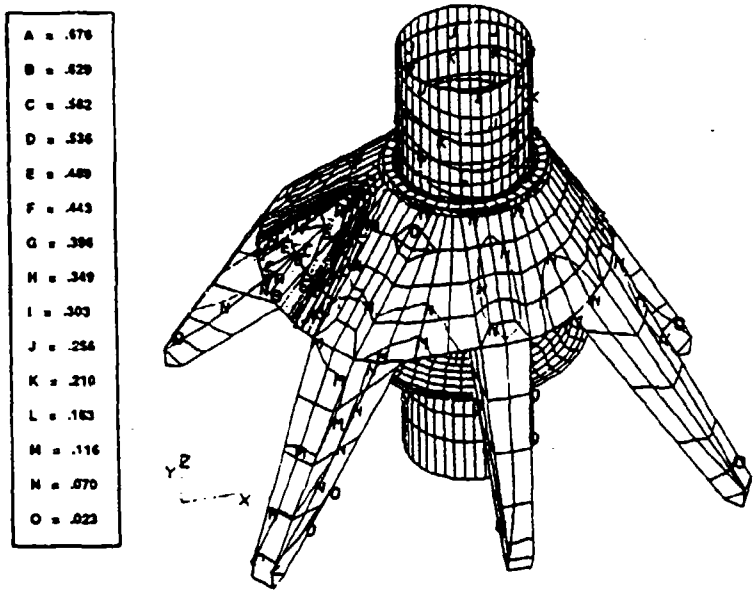

Figure 56. Composite Standpipe/Truss Total Deflection

Figure 57 presents the strain values for the assembly. The maximum strain of approximately .008 inch per inch is caused by the method of constraint used and does not represent a true value. This conclusion is based on the extremely confined area of the high strain concentrated at the point where the multipoint constraint equations are written. The real strain in the part is closer to the values shown by "E", or 0.001 inch per inch which is well within the allowable of .004 inch per inch. The material used is the same as for the gearbox housings, graphite-polybismalimide.

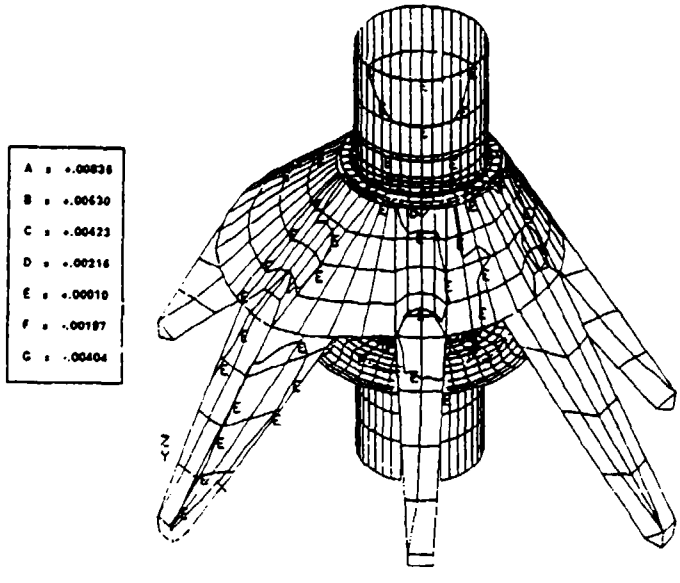

Figure 57. Composite Standpipe/Truss Strain in the Y Direction

Spring Clutch

The spring clutch was analyzed by convention methods as outlined in "Helicopter Freewheel Unit Design Guide", USAAMRDL-TR-77-18. The spring coils have variable thickness for the first 9 coils on each end and have variable width for the central 7 coils. There are 33 coils all together. The central coil widths vary exponentially to produce constant stress. The variable thickness and variable width of coils greatly reduces the size of the spring required but increases cost and manufacturing complexity. The overall dimensions of the spring are 2.714 inches outside diameter x 1.729 inches inside diameter x 6.156 inches long. The coil width at crossover is 0.783 inch and the coil thickness at crossover is 0.493 inch. The 100% design condition is taken to be the one engine inoperative (OEI) case of 6209 HP at the input at 15,000 rpm. Testing of spring clutches has shown that the static torque capability is greater than four times the design value. The spring is guided by an arbor located on the inside diameter of the spring. The initial fit between the spring and arbor is 0.015/0.0175 inch interference. The growth from centrifugal force is 0.0143 inch at 125% rpm so the the spring will remain on the arbor until the rpm of the output tends to exceed the rpm of the input at which time the clutch will engage and the coils will leave the arbor and transfer to the outer housing.

The method of operation of the spring clutch and the weight advantages were previously discussed in the preliminary design chapter of this report. The weight savings of a spring clutch located on the transmission input at 15,000 rpm compared to a conventional ramp roller clutch located at the output bevel gear at 4935 rpm is 123 pounds per engine. The total weight savings per aircraft is 369 pounds and represents 3.4% of the weight of the entire transmission system. This is a significant weight saving for a single component such as the freewheel unit.

Engine Drive Shaft

The engine drive shaft uses an integral shaft and coupling concept. The coupling and shaft are fabricated from composite material using the RTM process. The inner mandrel of the integral shaft and coupling is covered with dry fabric using the braiding process. Braiding is selected because the weave of material is much more tolerant to ballistic damage than other methods of fabrication. Ballistic tolerance is a major concern with drive shafts because they are traditionally the weak link in the drive system. High speed shafting also suffers from degradation of balance characteristics when the shaft and coupling are separate and are field removable. The integral shaft and coupling will retain its original balance throughout its lifetime since there are no loose pieces that can cause parts to shift or parts which can be removed or changed. An additional advantage is that the angular misalignment capability and critical speed characteristics can be enhanced by selective use of stiff materials such as 0° graphite in the shaft and compliant materials such as high angle fiberglass in the coupling.

The ART engine drive shaft has the integral shaft and coupling on the transmission input side and a metal spline on the engine output side. The metal male spline is bonded and riveted to the composite shaft on the engine end. An elastomeric gimbal is located on the transmission input with the center of rotation at the center of the integral coupling. The engine is supported at the transmission through the gimbal and at the rear of the engine by struts. Any motion induced during flight is transferred to the coupling as an angular misalignment only, without any axial or side motions. Figure 58 displays some of the basic dimensions of the final composite shaft and coupling design.

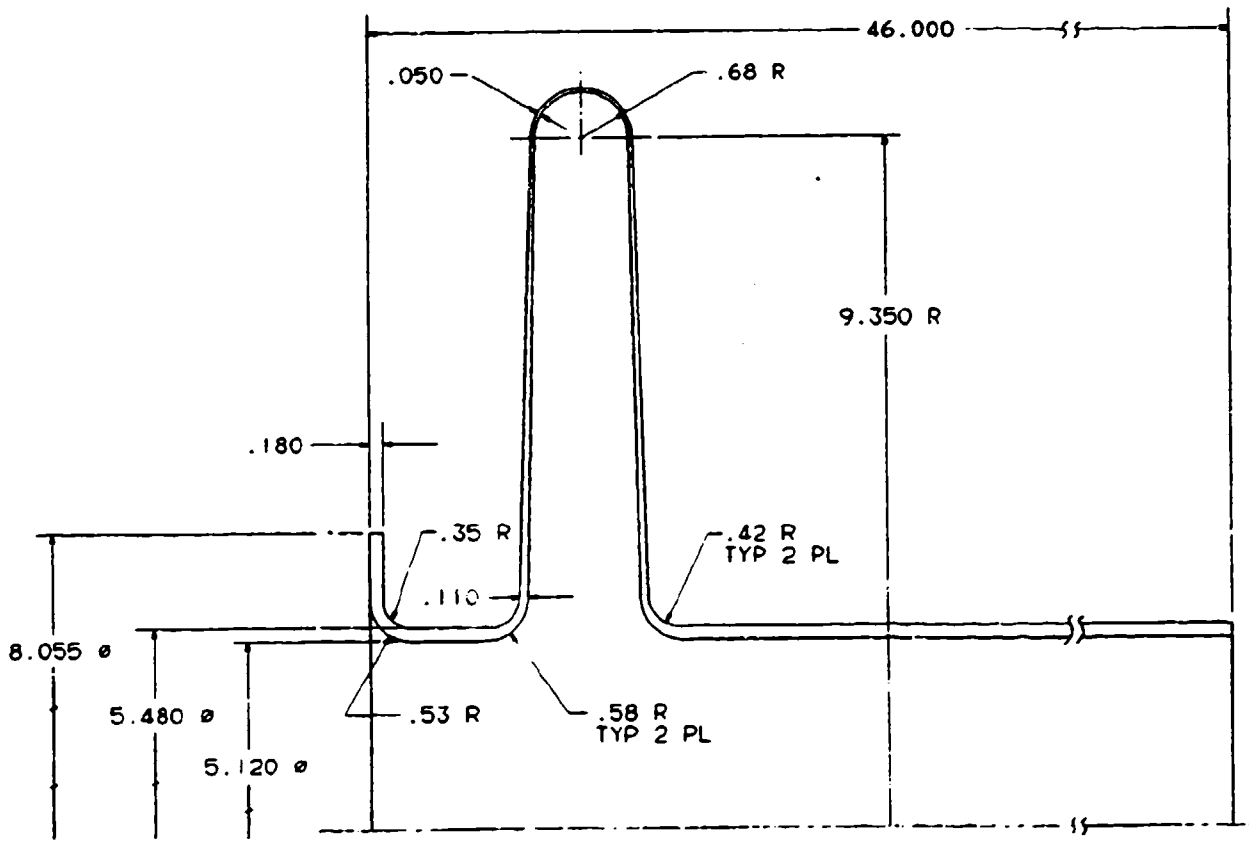

Figure 58. Composite Integral Shaft/Coupling Basic Dimensions

A finite element analysis was conducted of the integral shaft and coupling to determine structural adequacy for transmitting torque and for angular misalignment capability. Figure 59 shows the deflected position for enforced angular misalignment.

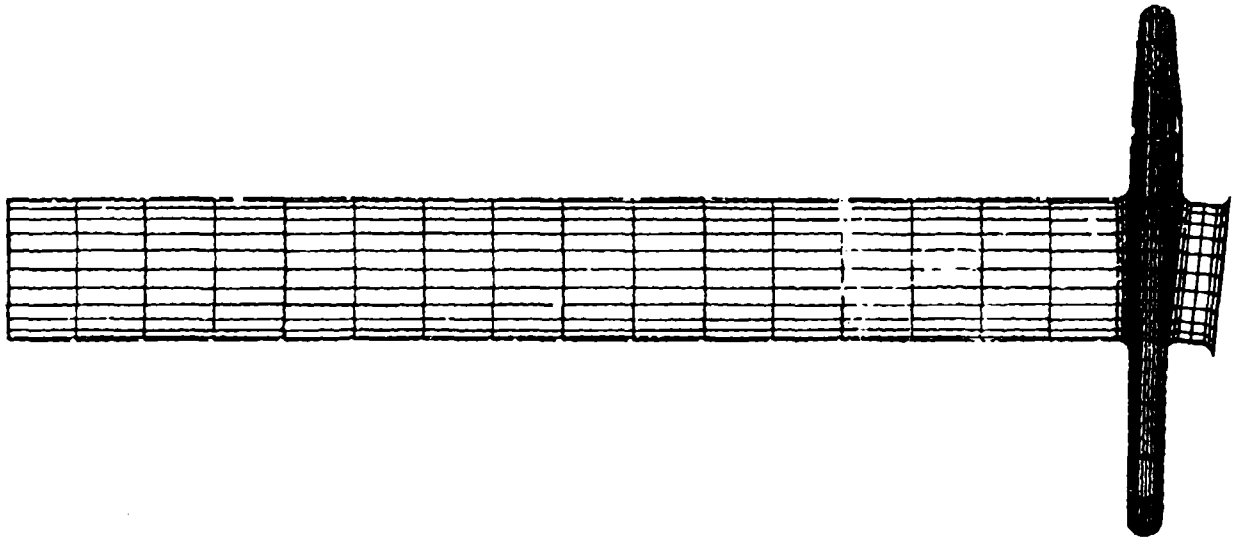

Figure 59. Composite Integral Shaft/Coupling Angular Misalignment

Spring rates of the assembly were calculated for use in conducting dynamic analysis. In the side or lateral direction, the spring rate was calculated to be 1985 pounds per inch. In the bending direction of angular misalignment, a rate of 4715 inch pounds per radian was found. The torsional spring rate was found to be 1,083,000 inch pounds per radian. The maximum shear strain was calculated to be 0.0018 inch per inch in the tube part of the shaft which is well within the allowable for the composite material.

A shaft dynamics analysis was conducted to determine mode shapes and frequencies. The results are shown in Figure 60. There are two rigid body modes, labeled "1st mode" and "2nd mode" in Figure 60, which must be traversed during run up from engine start at zero speed to ground idle at approximately 60% speed. These modes occur at relatively low speed and therefore have low energy. Moreover, the transmission input duplex bearings are mounted in a squeeze film damper which will limit the amplitude of vibration (see discussion of spring clutch). The third mode, also a rigid body mode, is well above the operating speed range and is unaffected by shaft length. The 4th mode is the "first bending" mode of the system since the drive shaft takes on the characteristic bending shape. This mode is highly influenced by shaft length and limits the length of shaft that can be used. Shaft diameter can be increased to raise the shaft length but this increases the angular misalignment spring rate and hence decreases angular misalignment capability. A compromise of 48 inches shaft length was selected based on the needs of the engine for air inlet purposes.

Accessories

Trade off studies were conducted to determine the best method for mounting of accessory drives. The baseline CH53E transmission uses a separate accessory gearbox with some main gearbox mounted accessories for redundancy. The ART gearbox has convenient locations both on top of the box and underneath the box to mount accessories directly with splines into available shafts. This method eliminates accessory gearing completely and is a major advantage for the split path gearbox. For the ACA, there are three positions available on the top of the box and three positions available on the bottom of the box at 4934 rpm. This is a suitable speed for oil pumps and hydraulic pumps but is too slow for generators. There are also available six positions on top and six positions

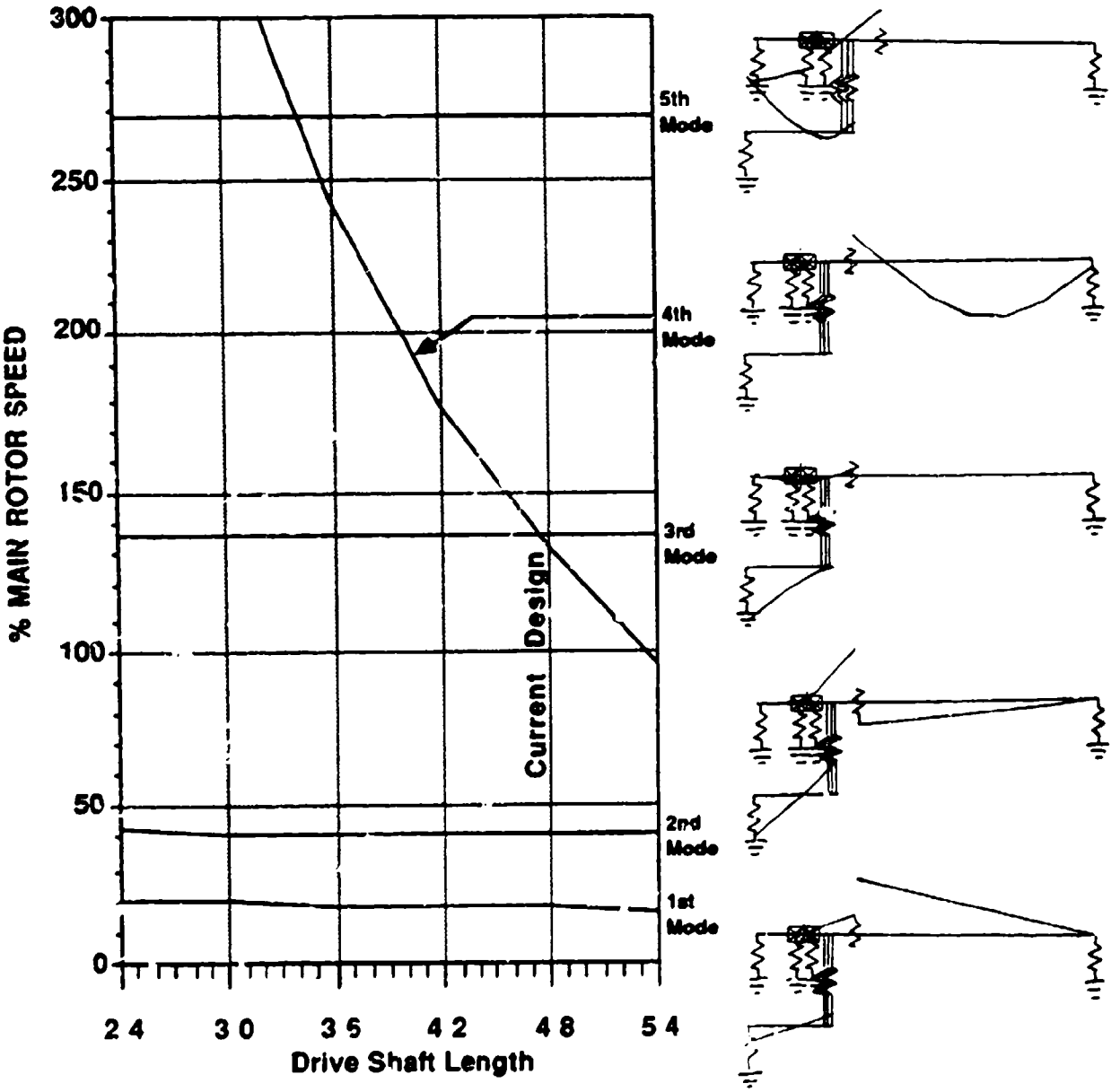

Figure 60. ART Engine Input Dynamic Analysis

on the bottom of the box rotating at 1270 rpm. This speed is generally too slow for accessories. Schemes were developed for increasing the speed of the accessory when driven from one of these locations.

A planetary system was examined since it offered a coaxial drive method with the speed increasing ratio desired. Figure 61 is a cross section. The ring gear of the planetary is 3.55 inches and is fixed by bolting to the housing in the area of the bearing supports. The sizes of the gears in this planetary are small and the parts are not critical because the stresses are low. The planetary was eliminated from consideration however, because it contained too many parts resulting in reduced reliability and although the parts are small, there was also a cost consideration.

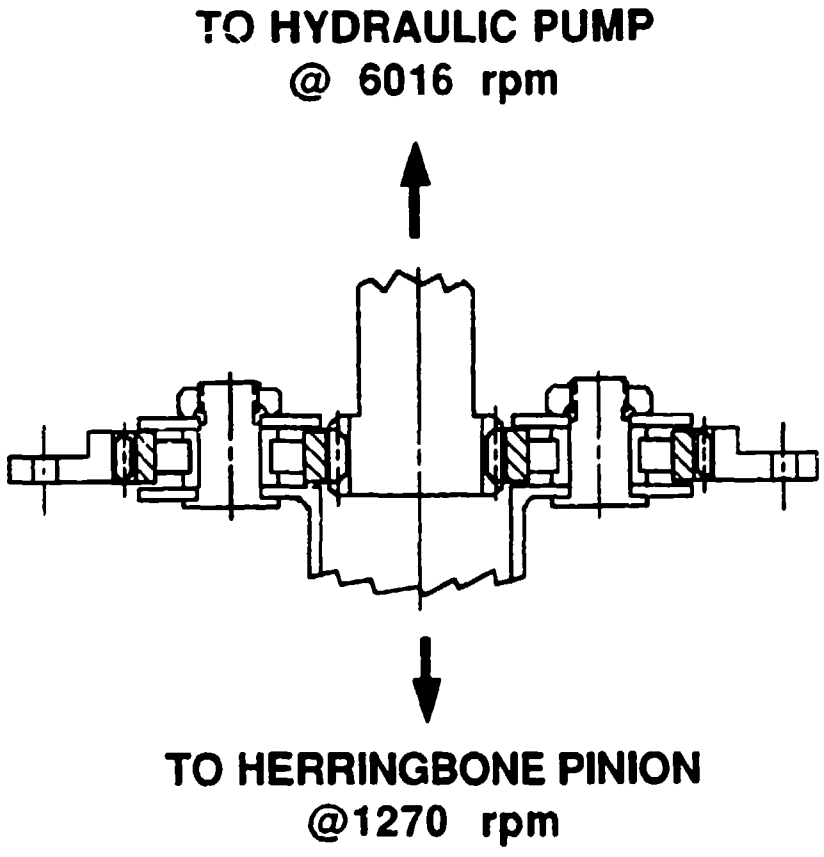

Figure 61. ART/ACA Planetary accessory Drive

Another accessory drive method added a small spur gear directly onto the end of one of the vertical shafts. The accessory then has its own spur pinion to mesh with the gear. The accessory is offset from the center of the gear by the center distance of the small spur set. Figure 62 illustrates the design concept. With a 3:1 to 4:1 ratio, the 1270 rpm herringbone pinion shafts become suitable for pump drives. There are no extra bearings or shafts required since gear reactions are carried by the main bearings on the herringbone pinions and by the bearings in the accessory.

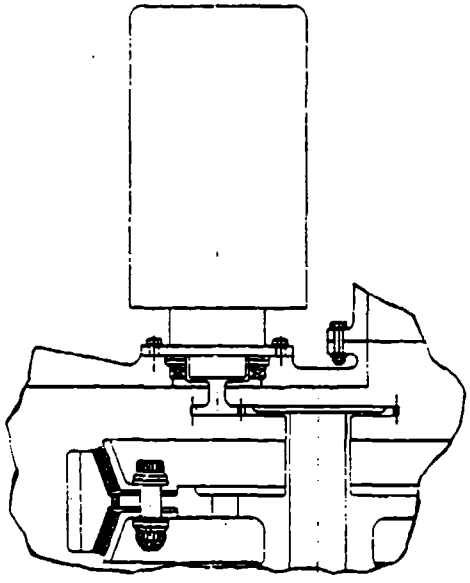

Figure 62. ART/ACA Accessory Drive Using Additional Gear

Another accessory drive method examined was to use an existing gear, such as the high contact ratio spur gear as the driver and to attach a spur pinion onto the accessory drive shaft. For the ART/ACA gearbox, this method proved useful to obtain the high speed necessary to drive a generator. Figure 63 demonstrates the concept. For both the additional spur gear method examined above in Figure 62 and the existing gear method shown in Figure 63, the accessory must be designed to react the gear loads through its own bearings. Also the pinion on the output shaft would be special such that the accessory could only be used for the ART transmission. This is not a difficult disadvantage to overcome because the benefits of reduced weight outweigh the disadvantage of a special output shaft. Also, misalignment problems often encountered with accessories using quill shafts, would be eliminated. This benefit alone warrants their use.

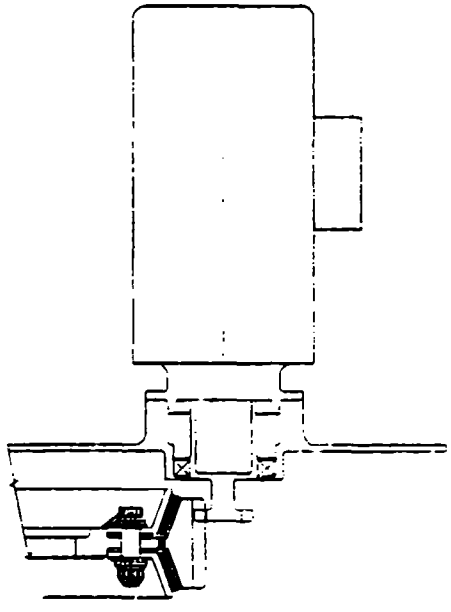

Figure 63. ART/ACA Accessory Drive Using Existing Gear

Rotor Brake

The ART rotor brake is mounted at the tail-take-off area with the rotor brake disk being attached to the flange of the tail-take-off output bevel gear shaft. A carbon disk is used for weight saving. The rotor brake worst case design condition is an emergency stop from full rpm. The rotor kinetic energy is 11,660,000 foot pounds for this condition. With a brake torque of 71,000 foot pounds, the rotor can be stopped in 30 seconds. During the stop, all of the rotor kinetic energy is transferred to heat in the disc. The carbon brake disc is sized at 28 inches in diameter and is 1 inch thick.

Tail-Take-Off

The tail-take-off (TTO) drive consists of a single spiral bevel gear mesh with the pinion driven from the input bevel gear at 4934 rpm. Since this is almost the desired speed of the tail drive shaft, the reduction ratio of 1.054 is low, producing a tail drive shaft speed of 4681 rpm. The tail-take-off is positioned so that the tail drive shaft passes under the #2 engine. The TTO pinion is driven from a splined quill shaft attached to the 2nd stage spur pinion. Both the pinion and gear use angular contact spherical roller bearings so that the bevels can be accurately positioned by shimming in the axial direction. The angular contact spherical roller bearings react both thrust and radial loads.

Diagnostics

The ART main transmission diagnostic system must address mechanical elements including gears, bearings, drive shafts, flanges, freewheel units, seals, elastomeric springs, rotor brake, pumps, generators, oil cooler, oil filter, and oil jets. In addition, the design makes use of many novel features to meet the goals of reduced weight, improved reliability, and reduced noise. All of these combine to pose a significant challenge to the transmission diagnostic system. The ART diagnostic system makes use of present and new diagnostic technology to meet the goal of a safe, reliable, and affordable transmission.

There are several diagnostic strategies that are customarily used to detect and to locate degradation mechanisms within a transmission system. These include parametric exceedance (over torque, over temp, low oil pressure, etc.), life assessment based on hours of use, and oil debris monitoring. In addition, certain off line methods are in regular use including spectrographic oil analysis programs (SOAP), and traditional inspection methods like visual, magna-flux, zy-glow, and other dye penetrant methods. Since the focus of this analysis is on the on-board, on-site monitoring of the ART transmission, no detail reference to these methods is made. Eventual deployment, however, would rely on methods such as these in conjunction with the diagnostic system resident on the aircraft.

Diagnostic technology has made advances in other areas as well. These have been made possible by the common use of microprocessor based systems that greatly increase the computational power of a human operator. Advances

include multi-parameter exceedance (envelope exceedance), vibration analysis, real or near real time prognosis, actual usage analysis for life assessment, and new sensors for oil borne debris monitoring and analysis.

The design of the ART diagnostic system began with the breakdown of the transmission system into its constituent components and the analysis of each component for its failure modes. The failure modes were then combined with specific diagnostic strategies and the results are shown in Table 29. Table 29 does not show all components in the ART transmission but rather deals with generic parts i.e., a gear has the failure modes of spalling, pattern loss, and fatigue. Under gear spalling, the diagnostics are listed under vibration, life, prognostics, and debris monitoring, etc.

The ART diagnostic system includes all aspects of the diagnostic process including sensors, signal conditioning, conversion, data, information processing software and hardware, and information display. The data and information processing software and hardware include both on-aircraft and off-aircraft sub-systems. The diagnostic system is shown conceptually in Figure 64.

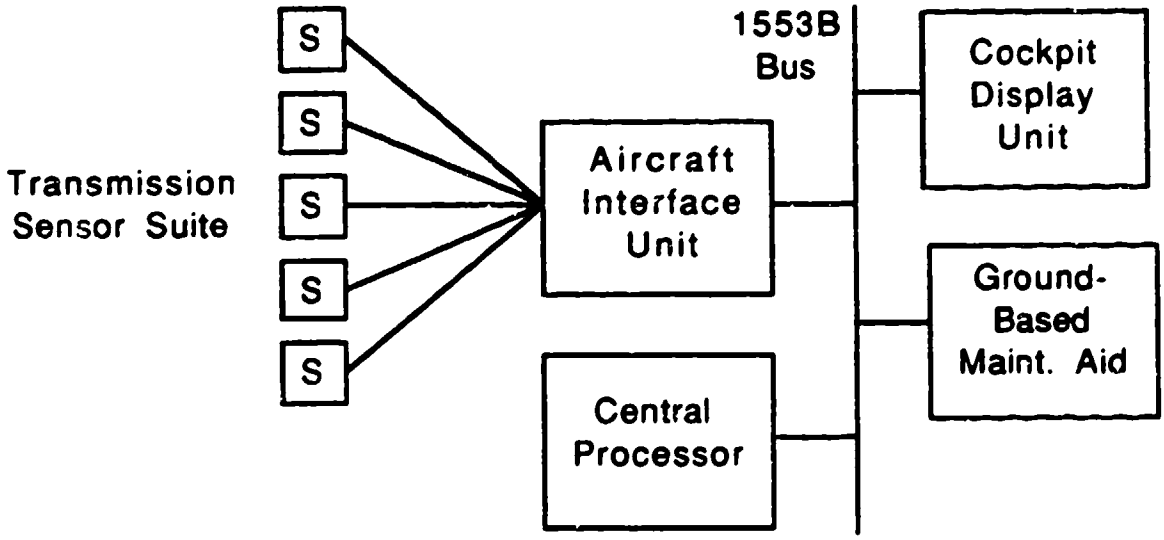

Figure 64. Generalized Diagnostic System

Table 29. Diagnostic Strategies

Generic Component	Mode	Vib	Exc	Life	Prg	Deb
Bearing (Any Type)	Spalling	x		x	x	x
	Cage Failure	x			x	
	O/R Spinning					x
Bearing Retainer	Torque Loss					x
Elastomeric Device	Delamination	x		x	x	x
Elastomer Side Plates	Fatigue	x		x	x	
Elas Clamp Bolts	Fatigue	x		x	x	
	Torque Loss	x				
FWU Spring Clutch	Fatigue	x	x	x	x	
	Wear/Fretting			x	x	x
Gear (Any Type)	Spalling	x		x	x	x
	Pattern Loss	x				
	Fatigue	x		x	x	
Gear Flange	Fatigue	x		x	x	
Gear Shaft	Crack/Fracture	x		x		
Housings (Composite)	Ck/Fract/Delam	x		x		
	Torque Loss	x		x		
Input Drive Shaft	Crack/Fracture	x		x		
	Unbalance	x				
	Overload		x			
Input Flange	Crack/Fracture	x				
	Torque Loss	x				
	Bolt Loose/Cracked	x				
Lube Filter	Plugged		x		x	
Lube Pump	Pressure Loss	x	x	x	x	x
Nuts	Torque Loss	x				x
Oil Cooler Core	Leakage				x	
	Clogged		x			
Oil Cooler Thermostat	Stuck		x			
Oil Cooler Shroud	Cracked	x				
Oil Cooler Fan	Cracked	x			x	
Oil Jet	Plugged		x			
O-Ring	Leakage			x	x	
Quill Shaft	Crack/Fracture	x		x		
	Wear/Fretting	x		x		x
Rotor Brake Actuators	Leakage		x			x
Rotor Brake Calipers	Crack			x	x	x
Rotor Brake Disk	Wear			x	x	x
Rotor Brake Pucks	Wear			x	x	x
	Fire	x				x
Rot Disk Attach Bolts	Torque Loss				x	
Seal	Leakage			x	x	
Spline	Wear/Fretting			x		
Tachometer	Signal Loss			x		

Processing is divided between three processors: the aircraft interface unit, the central processor, and the ground-based processor or maintenance aid. The workload for each of these processors is shown in Table 30.

Table 30. Diagnostic System Processor Workload

Unit	Workload
Aircraft Interface Unit	Signal Conditioning Conversion Vibration Analysis Preprocessing
Central Processor	Exceedance Monitoring Prognosis for Propagating Modes Performance Assessment Oil Debris Monitoring Vibration Analysis Life Usage
Maintenance Aid	Analysis of Onboard Data Elapsed Time Tracking Long Term Prognosis Exceedance Remaining Life Computation Maintenance Action Reporting Expert System Fault Isolation

Weight, Noise, MTBR

The weight, noise, and MTBR of the detail design was reevaluated and compared to the baseline and preliminary design values. Noise and MTBR did not change for the split path design from the preliminary and detail designs since basics such as gear teeth and bearing sizes did not change. There were substantial changes in weight however as a result of detail analysis and design. In the overall summary, the transmission system increased by 1%. The details are shown in Table 31. It can be seen from the table that the input section weight decreased as a result of detail analysis whereas the second stage spur gear and third stage bull gear weight increased.

One reason for the weight increase in the bull gear mesh was the decision early in the detail design to eliminate the bearingless bull gear concept and to utilize a bearing support for the bull gear. The decision was based on an industry survey of commercial and marine drives with double helical gearing which showed that in all cases with multiple pinions driving a central gear, the pinions are always designed as the floating member. The bearingless bull gear design (see preliminary design section) requires that each individual pinion be shimmed to a central plane that defines the path of the bull gear. Any errors in shimming would cause load maldistribution Also, any tendency of the bull gear to deflect would be resisted by the fixed locations of the bull pinions which would in turn induce unequal gear loading. Another area of weight increase after detail design was in the composite truss and main rotor shaft. This was caused by beef up of the structure as a result of detail analysis.

Table 31. Weight Comparison

	Growth Baseline	Split Path Prelim Des	Split Path Detail Des
Main Gearbox	6183	4820	4804
Input Section #1	220	320	220
Input Section #2	532	320	220
Input Section #3	208	320	220
Rotor Drive	853	-	-
Bull Gear Installation	-	799	1033
Spur Gear/Bull Pinion	-	1412	1645
Gimbal Mount	103	-	-
Scissors/Standpipe	66	-	-
Housings and Rear Cover	1451	1088	1061
Sumps/Pumps	125	125	83
Main Shaft Bearings	292	255	224
Planetary	2146	-	-
Accessory Gearbox TO	22	21	-
Rear Cover Gearing/Etc	150	150	88
Plumbing Provisions	15	10	10
Main Rotor Shaft/Truss	1412	1116	1513
Lube, MGB	698	690	716
Drive Shafts	634	594	584
Rotor Brake	108	100	100
Nose Gearbox	676	-	-
Accessory Gearbox	280	243	-
Intermediate Gearbox	208	191	191
Tail Gearbox	596	533	533
TOTAL DRIVE SYSTEM	10795	8287	8441
% Savings	Baseline	23%	22%

1/2 Size Test Gearbox

Test hardware consists of a portion of the aircraft gearbox and is designed to be 1/2 the size of the aircraft components. One half size was chosen to save the cost of fabrication of a 48 inch diameter bull gear. A 48 inch gear is beyond the current manufacturing capabilities for a carburized and ground gear and is limited by current quenching press sizes. The 1/2 size test gearbox consists of one engine branch of the second stage spur pinion, splitting to two second stage spur gear/herringbone pinions, and then combining onto the output bull gear. The input bevel pinion is not included in the test hardware and the test box has only a single branch of the torque splitting gearbox. The main objectives of the test were to determine the load sharing between torque splitting halves, test the large reduction ratio, topologically ground herringbone gearset, and to test the durability of the elastomeric isolator. Secondary test objectives were to test the split power gear concept, test of Pyrowear 53 gear material scoring index at elevated temperature, and to correlate finite element analysis stress distributions, tooth root stresses, and transmission error.

A cross section of the 1/2 size test gearbox is shown in Figure 65. The test gearbox is highly instrumented. Each shaft has provisions for a slip ring drive and alternatively, the angular measurement device used to measure transmission error. The numbers of teeth, pressure angles, and helix angles are identical to the full size aircraft hardware. The relationships of the teeth and the angles formed between gear centers are identical to the full size components. The gear diametral pitches of the one half size components are twice those of the aircraft gears resulting in one half of the pitch diameters. Tooth proportions both in the radial and transverse directions are similarly reduced to one half.

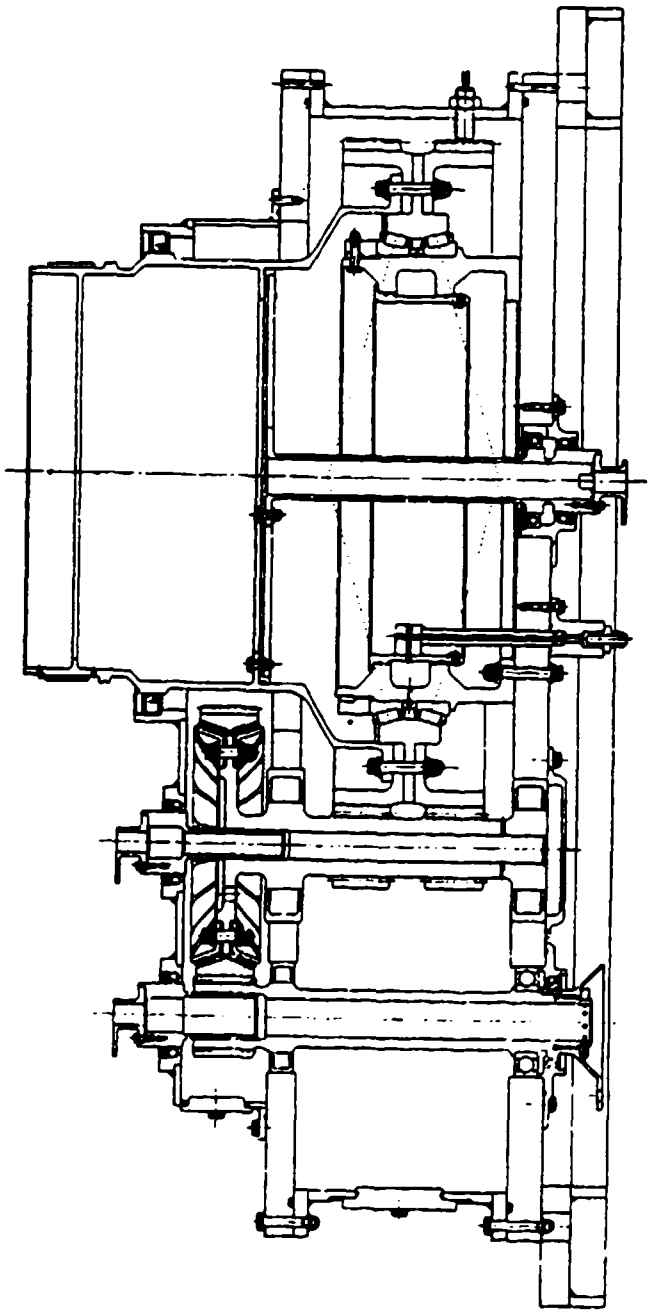

Figure 65. Cross Section of 1/2 Size Test Gearbox

A finite element analysis was conducted of the 1/2 size test gearbox mounted in the test fixture used to hold the gearbox to the test stand. A view of the finite element model element breakup is shown in Figure 66. The analysis was used to determine stresses and deflections in the mounting frame as well as in the test gearbox housings. Deflection and stress results are shown in Figures 67 through 70. As seen by the results, the highest deflection occurs at the outer edge of the test fixture and is 0.017 inch. This deflection occurs in a very localized area between mounting bolts. Internal to the gearbox, the deflections are very low with a maximum reading of 0.0036 inch occurring on the lower plate which is the highest loaded member. The stresses in the test fixture and lower plate are very low for steel.

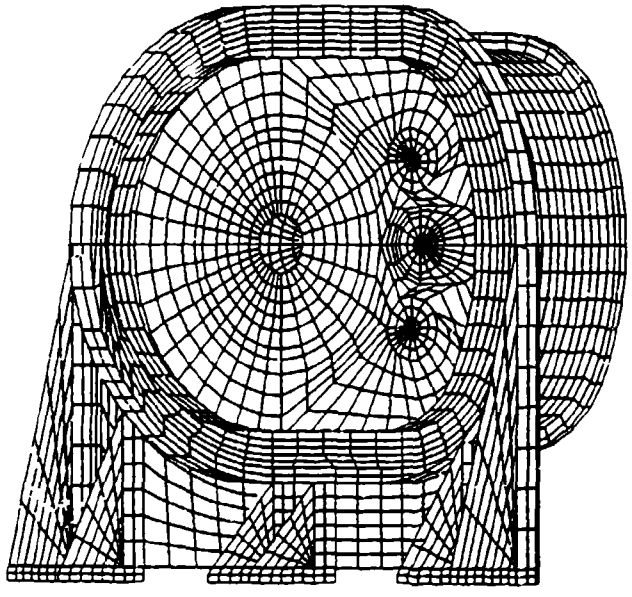

Figure 66. Finite Element Model of Test Gearbox in Fixture

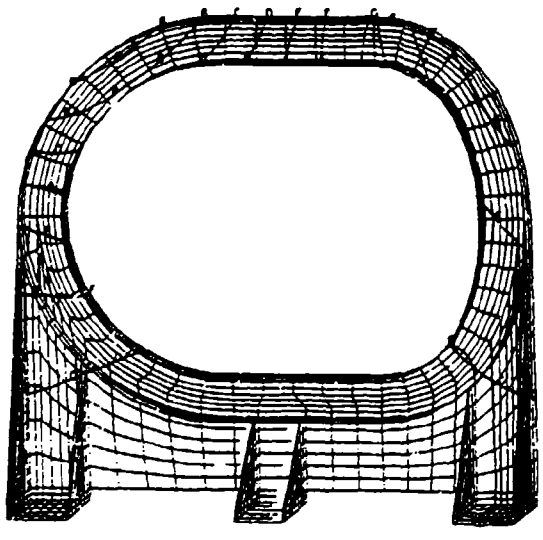

TOTAL DEFLECTION	
.0170	A
.0143	B
.0117	C
.0091	D
.0065	E
.0039	F
.0013	G

Figure 67. Test Fixture Total Deflection

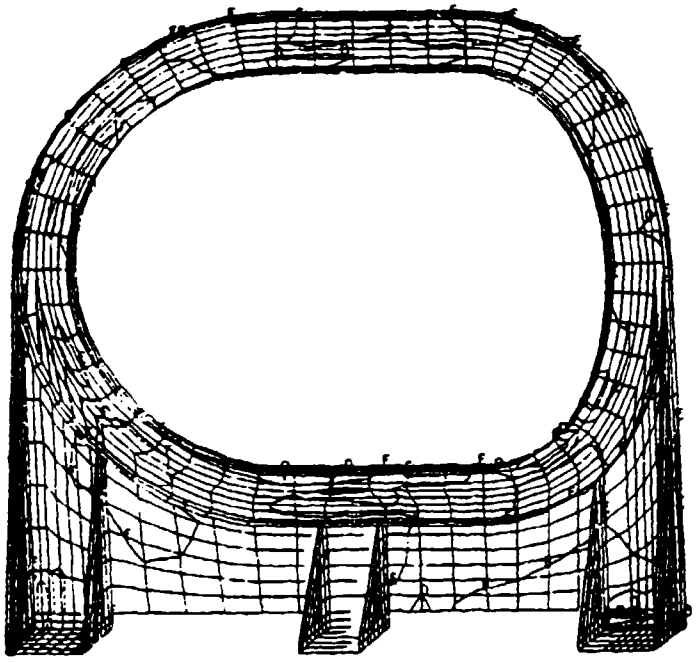

MAX PRINCIPAL STRESS	
2970	A
2370	B
1770	C
1170	D
570	E
-40	F
-640	G

Figure 68. Test Fixture Maximum Principal Stress

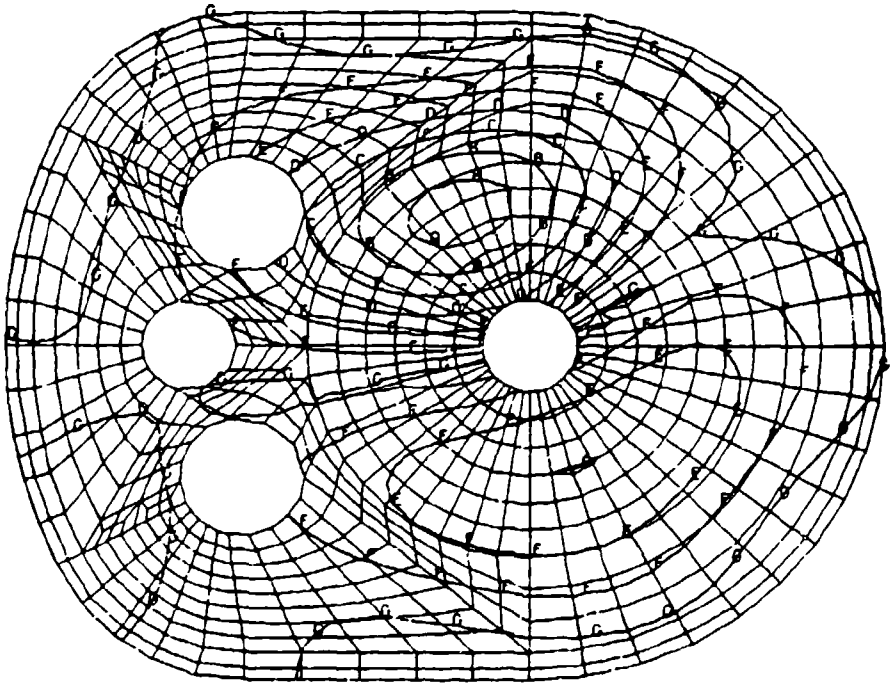

TOTAL DEFLECTION	
.0036	A
.0030	B
.0025	C
.0019	D
.0014	E
.0008	F
.0003	G

Figure 69. Test Gearbox Lower Plate Total Deflection

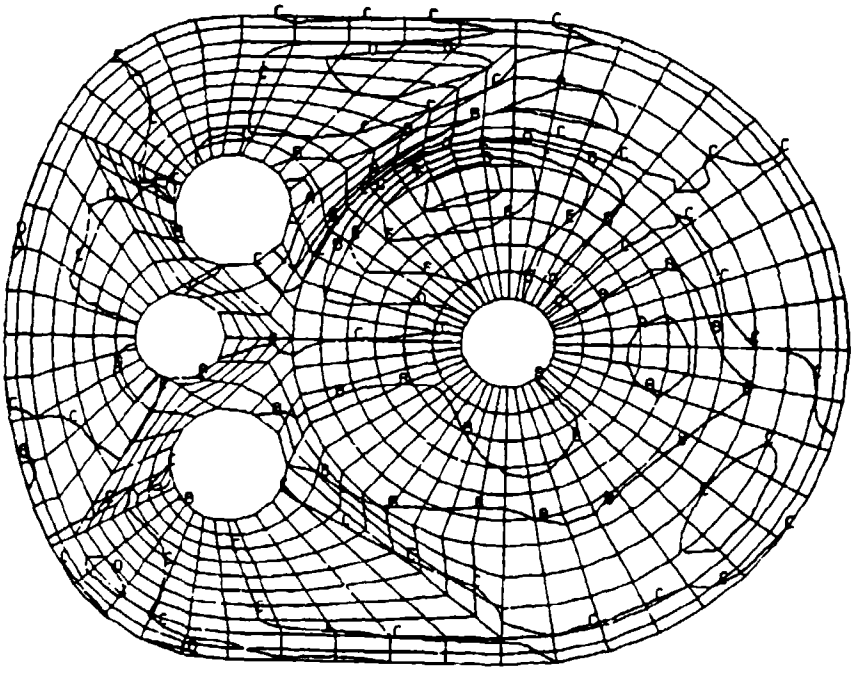

MAX PRINCIPAL STRESS	
2260	A
1180	B
100	C
-980	D
-2060	E
-3140	F
-4220	G

Figure 70. Test Gearbox Lower Plate Maximum Principal Stress

Scaling Attributes

A one half size model was selected to conduct ART testing. For the half size tests to be representative of the full sized aircraft hardware care was taken in selection of the load scaling factors. First, the physical geometry was made exactly to 1/2 size. Secondly, all rotational speeds were kept the same. With these two conditions of 1/2 size and the same speed, most of the important design parameters are the same in the 1/2 and full size components if power is reduced to 1/8 in the 1/2 size model. Table 32 illustrates the relationships.

When comparing the full sized hardware to the 1/2 size hardware operating at 1/8 power and the same rpm, gear tooth bending, Hertz stresses, and tooth deflections are identical but scoring temperature rise is less in the 1/2 size test components. Temperature rise in the mesh is lower as a result of lower pitch line velocity in the 1/2 size gearbox. Shaft and housing stress and deflection are identical in both cases. Bearing lives are slightly higher in the 1/2 size box because bearing capacity does not decrease at the same rate as the load decrease when going to 1/2 size. Therefore, most important parameters scale identically except for gear scoring which is about 1/2 of the full size gearbox scoring and bearing life which is slightly higher in the 1/2 size gearbox.

Table 32. Relationship of Design Parameters

Parameter	Full Size Aircraft	1/2 Size Test
Horsepower	HP	HP/8
Torque	T	T/8
Tangential Tooth Load	Wt	Wt/4
Tooth Fatigue Bending Stress	fb	fb(Identical)
Tooth Compressive (Hertz) Stress	fc	fc(Identical)
Gear Tooth Deflections	Δ	Δ(Identical)
Pitch Line Velocity	PLV	PLV/2
Tooth Temperature Rise	Δt	Δt/2
Shaft Fatigue Bending Stress	fs	fs(Identical)
Shaft Deflection	Δs	Δs(Identical)
Housing Stress	fh	fh(Identical)
Housing Deflection	Δh	Δh(Identical)
Bearing Dynamic Capacity	C	C/3.61
Bearing Load	P	P/4
Bearing Life (Roller Bearing)	Lroll	1.41 Lroll
Bearing Life (Ball Bearing)	Lball	1.51 Lball

The other available choice for the 1/2 size test gearbox was to make all components 1/2 size and to run at two times the speed of the full size gearbox. The test would then be conducted at 1/4 horsepower. This amounts to the same torque as the 1/2 size components tested at 1/8 power and the same speed. For two times the speed, the pitch line velocity will be identical in both the full size and 1/2 size boxes. Gear design parameters of tooth bending, contact, and temperature rise would now be identical at 1/4 horsepower. Also, the shaft and housing deflections and stresses would be identical. When looking at bearings however, the life is reduced to less than 10% of the life of the full sized bearings. This was unacceptable and the compromise position of approximately the same bearing life was accepted by testing at 1/8 power and the same speed.

Gearing

The gearing design data for the 1/2 size test gearbox is listed in Table 33 while stresses are tabulated in Table 34. The basic design data is identical to that shown in Table 23 except for the pitch diameters which are 1/2 of those for the full size aircraft. The gear stresses are similar to those shown in Table 24. The input spur gear is slightly different because in the aircraft gearbox the input spur is designed for 2671 HP whereas the equivalent of the test gearbox is (648 x 8)/2 = 2592. This difference is the result of losses being subtracted from the inputs on the aircraft gearbox and being neglected in the 1/2 size gearbox. Note that the herringbone mesh stresses are identical because the horsepowers are 1296 for the aircraft vs an equivalent of (648 x 8)/4 = 1296 per herringbone mesh half. The scoring temperature is based on a surface finish of 10 RMS.

Table 33. One Half Sized ART, Basic Gear Data

Gear	Number of Teeth	Pitch Dia Angle	rpm	Pressure Angle	Spiral (Helix)
2nd Stage Spur Pinion	26	2.5134	4,934	18°	-
2nd Stage Spur Gear	101	9.7636	1,270	18°	-
Herringbone Pinion	13	2.4567	1,270	20°	31°
Herringbone Gear	127	24.0000	130	20°	31°

Table 34. Bending and Contact Stress, and Scoring Index

Gear	Gear Design HP	Bending Stress (psi)	Contact (Hertz) (psi)	Scoring Rise (°F)
Input Spur Pinion	324	44,140	141,120	69
Input Spur Gear	324	45,730	141,120	69
Output Herringbone Pinion	162	56,710	176,130	69
Output Herringbone Gear	162	55,090	176,130	69

Bearings

The bearing lives for the 1/2 size test gearbox are listed in Table 35. The lives shown are not prorated but are shown for 100% load. Since the total test time is not expected to exceed 500 hours and the maximum test load is 120%, the chance of a bearing B-10 type spalling failure during the test is low.

Table 35. One Half Sized ART, Basic Bearing Summary

Position	rpm	Load @ Prorate (lbs)	B-10 Life (hrs)
Spur Pinion Roller Bearing	4,934	3,640	1,980
Spur Pinion Ball Bearing	4,934	688	43,760
#1 Herringbone Pinion #312 Roller	1,270	5,930	19,980
#1 Herringbone Pinion #313 Roller	1,270	9,380	2,370
#2 Herringbone Pinion #312 Roller	1,270	12,210	1,730
#2 Herringbone Pinion #313 Roller	1,270	8,120	3,700
Herringbone Gear Tapered Roller (2)	130	15,410	17,400

Internal Shafting

The internal shafting for the ART transmission is designed for unlimited life at the highest expected operating condition. The critical section is at the center of the herringbone pinion between the left and right hand helical pinion members. In fact, it is this section that essentially limits the center distance and reduction ratio and sizes the split path gearbox output stage. Stresses in the shaft of the 1/2 size pinion at 1/8 power and full speed are identical to the full size hardware at full power and full speed. The margin of safety from the combined conditions of helical pinion thrust, shaft bending, and torsion is zero in this section. The outside of the shaft has been shot peened for added margin of safety. All other sections of shafting in the ART transmission have positive margins of safety.

Elastomeric Isolator

The elastomeric isolator for the 1/2 size test gearbox has the same stress and deflection as its full sized counterpart with the scaling factors established. Analyses were conducted using closed form solutions as a first approximation followed by finite element analysis. The analyses results are shown in Table 36.

Table 36. Spring Rate and Strain Summary for Elastomeric Isolator

Parameter	Closed Form Solution #1	Closed Form Solution #2	Finite Element Analysis
Ka - axial #/in	1,490,000	1,000,000	-
Kr - radial #/in	2,750,000	3,780,000	2,550,000
Kt - torsion in #/rad	570,000	679,000	680,000
Max Princ Strain in/in	.450±.110	.372±.058	.421±.026

Two closed form solutions are given. The results were calculated by two different methods from two different references. The final proof of spring rate is of course the test results. The finite element model was used to check the stress and deflection in the isolator side plates as well as in the rubber itself. Figure 71 shows the elements of the model used for the side plates. It was found that the ribs were required because the deflection in the rim created by the application of 10,000 pounds preload on the bolts was too high. The addition of ribs greatly reduces the resulting deflection. Figure 72 shows that the maximum deflection with the addition of ribs is .015 inch occurring at the point of gear load application. Away from the gear load, the deflection drops to .0035 inch in the same location. Since the gear load is stationary in space and the isolator is rotating, the resultant gear load creates a vibratory strain in the rubber and isolator side plates. The torsion is steady in theory but also produces a small vibratory because of localized bending effects. Figure 73 shows the compressive nature of the stress distribution in the isolator. This compressive stress is induced by the 10,000 pound axial preload used. Figures 74 through 76 show the shearing strains in the rubber in the three principal directions. The highest strain is produced in the R-Ø direction and is caused by the application of torque. The

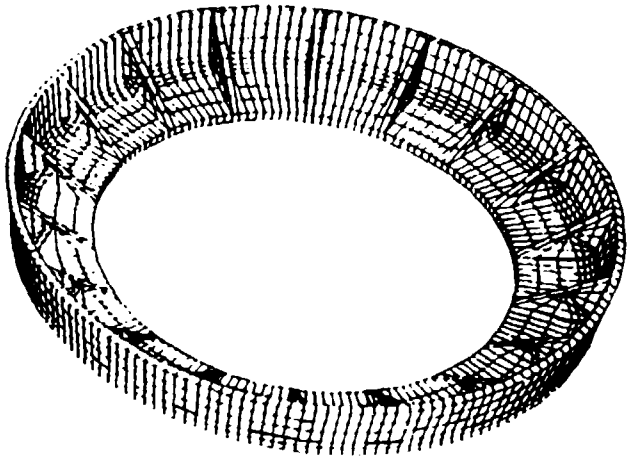

Figure 71. Finite Element Model of Elastomeric Isolator Side Plate

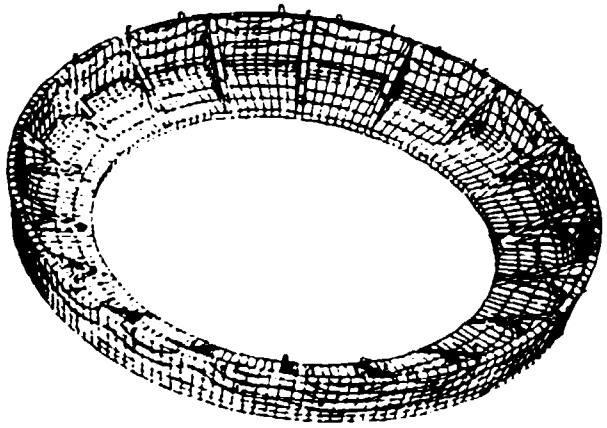

DEFLECTION	
.0150	A
.0127	B
.0104	C
.0081	D
.0058	E
.0035	F
.0011	G

Figure 72. Elastomeric Isolator Side Plate Deflections

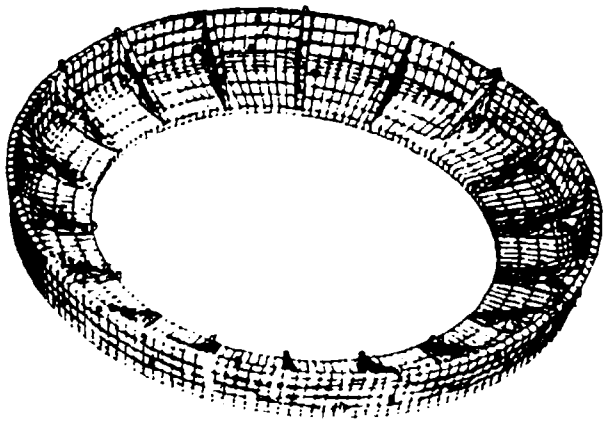

HOOP STRESS	
6000	A
-7000	B
-20000	C
-33000	D
-46000	E
-59000	F
-72000	G

Figure 73. Elastomeric Isolator Side Plate Hoop Stresses

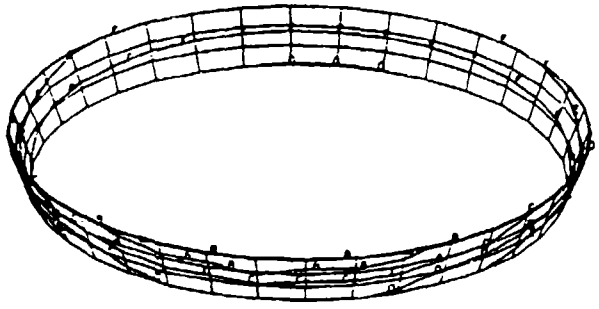

SHEARING STRAIN (R-Ø)	
.441	A
.431	B
.421	C
.411	D
.401	E
.391	F
.381	G

Figure 74. Elastomeric Isolator Rubber Shear Strain in R-Ø

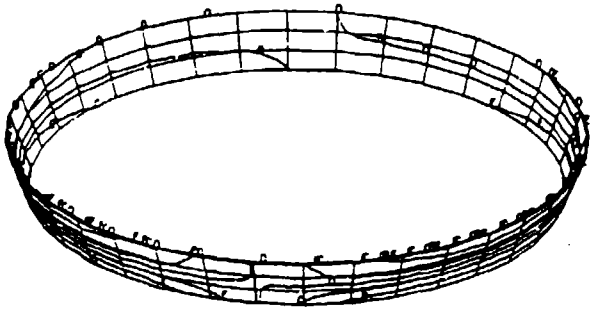

SHEARING STRAIN (Ø-Z)	
.0463	A
.0314	B
.0166	C
.0017	D
-.0131	E
-.0279	F
-.0428	G

Figure 75. Elastomeric Isolator Rubber Shear Strain in Ø-Z

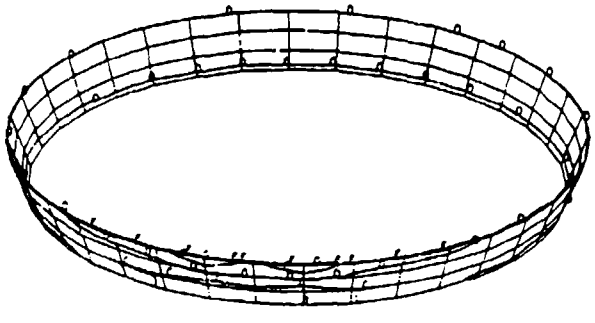

SHEARING STRAIN (R-Z)	
.0002	A
.0001	B
.0000	C
-.0001	D
-.0002	E
-.0003	F
-.0004	G

Figure 76. Elastomeric Isolator Rubber Shear Strain in R-Z

shearing strain in the Ø-Z direction is caused by the gear loads and in the R-Z direction by the preload. The maximum principal shear strain is plotted in Figure 77. Vibratory strain from the applied gear loads was a concern during the design of the isolator. The finite element analysis shows that the vibratory strain is low and shows how the rubber attempts to "spread" the load more so than metal parts would do.

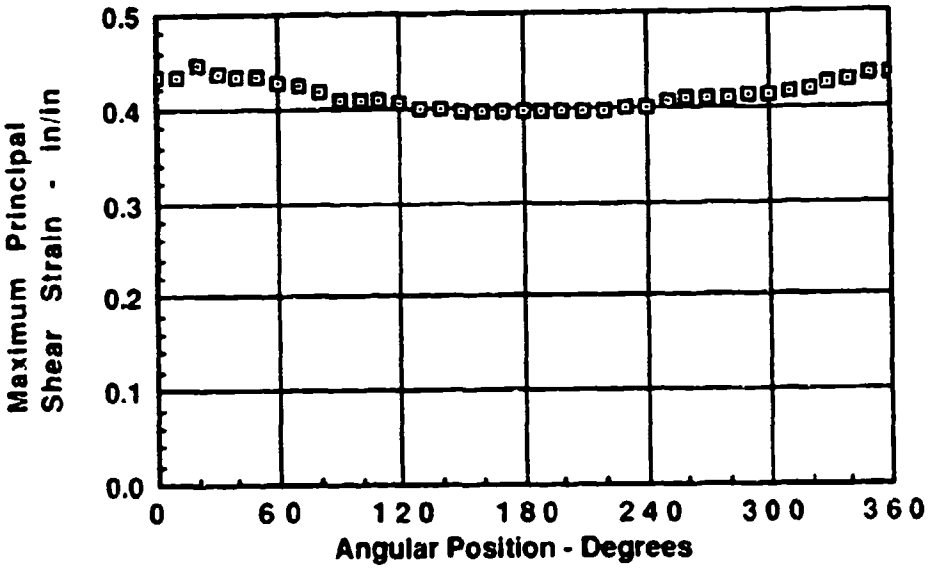

Figure 77. Maximum Principal Shear Strain vs Angular Position

Lubrication

For the ART 1/2 size gearbox lubrication system, the heat generated was calculated for the 100% test power design condition of 648 HP input. Table 37 summarizes the heat generation calculations. The heat generation of 352.59 BTU per minute corresponds to 8.3 HP and makes the calculated efficiency equal to 98.7%. Remember however, that this only represents two stages of the three stage gearbox.

Table 37. One Half Sized ART, Heat Generation Summary

Description	Individual BTU/Min	Qty per box	Total BTU/Min
Input Spur Pinion Ball Bearing	5.94	1	5.94
Input Spur Pinion Roller Bearing	16.73	1	16.73
High Contact Ratio Spur Mesh	68.91	2	137.82
Herringbone Pinion Input Roller	8.87	2	17.74
Herringbone Pinion Output Roller	7.50	2	15.00
Herringbone Gear Mesh	53.05	2	106.1
Timken Bearings, Herringbone Gear	26.63	2	53.26
Grand Total			352.59

It is assumed that all of the heat generated will be transferred to the oil. MIL-L-23699 oil was used at 210°F with a specific heat of 0.455 BTU/lb°F and a density of 0.0331 pounds per cubic inch. The required flow was then calculated as that flow which would produce a temperature rise of 40°F in the oil. The actual flow may be more than the required flow because of the limitation of using a minimum jet diameter of 0.040 inch. Given a pressure of 60 psig, a flow of 0.26 gallons per minute (gpm) is calculated for a 0.040 inch jet. If the required flow is less than 0.26 gpm, extra oil is put into the system. A summary of actual and theoretical flow is shown in Table 38. As seen, almost all jets are oversized and are based on the minimum 0.040 inch diameter. The location of the -101 through -104 jets is shown in Figure 78.

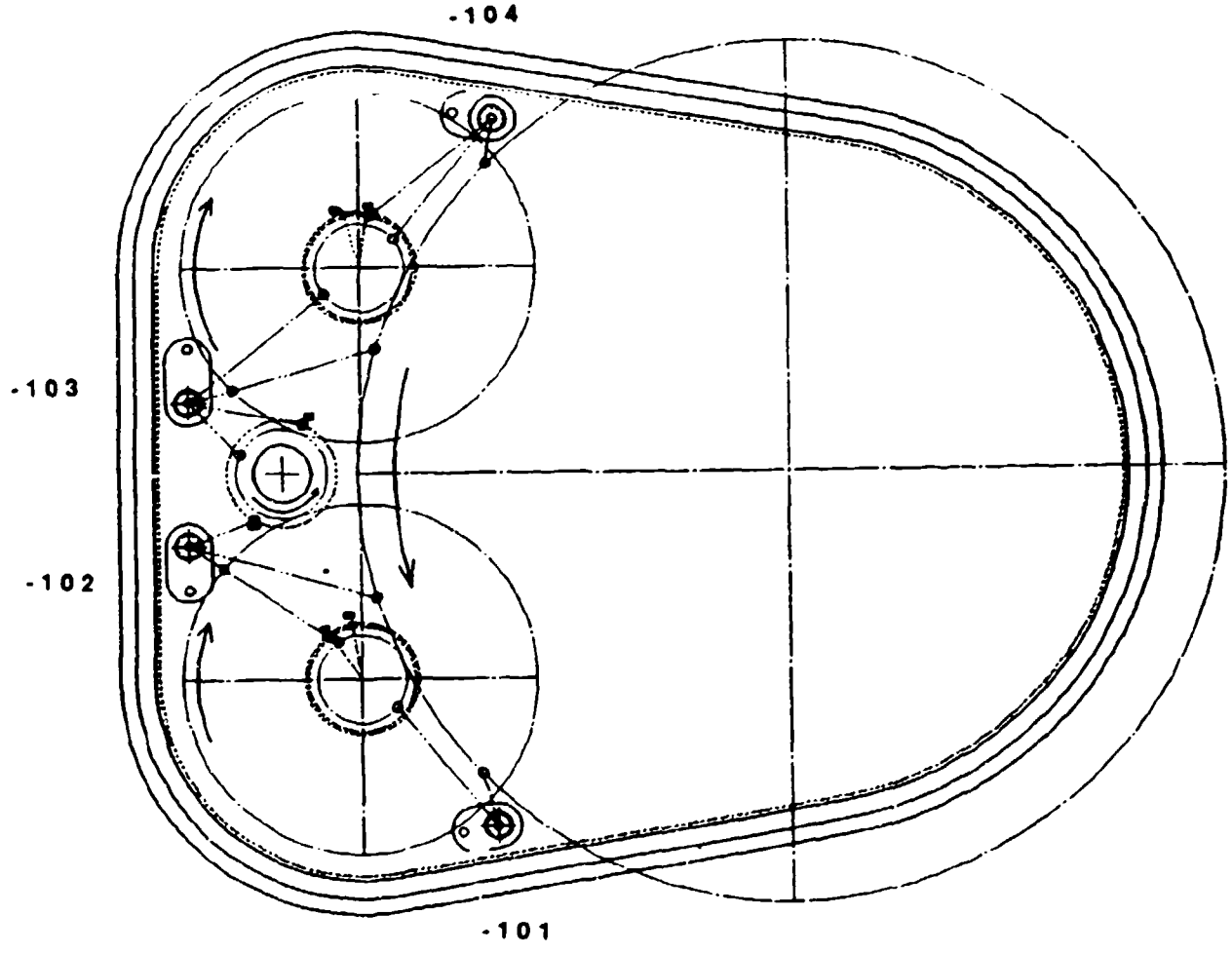

Figure 78. 1/2 Size Gearbox, Location of Jets

Table 38. One Half Sized ART, Actual and Theoretical Flow

Description	Req'd Flow (gpm)	Jet Dia (in)	Qty Per Box	Total Actual (gpm)
-101 Jet (4 Outlets)				
Upper Herringbone Pin (After Mesh)	0.047	.040	2	0.520
Upper H.B. Gear (After Mesh)	0.047	.040	2	0.520
-102 Jet (8 Outlets)				
Upper H.B. Pinion (Before Mesh)	0.047	.040	2	0.520
Upper H.B. Gear (Before Mesh)	0.047	.040	2	0.520
Upper Spur Gear (Before Mesh)	0.246	.055	1	0.492
Spur Pin Brg (Output Side) MR211	0.120	.040	1	0.260
Up Spur Gear Brg (Input Side) MR312	0.072	.040	1	0.260
Up Spur Gear Brg (Out. Side) MR313	0.054	.040	1	0.260
-103 Jet (7 Outlets)				
Lower Spur Gear (Before Mesh)	0.246	.055	1	0.492
Lower H.B. Gear (Before Mesh)	0.047	.040	2	0.520
Lower H.B. Pinion (Before Mesh)	0.047	.040	2	0.520
Spur Pin Brg (Output Side) MR211	0.042	.040	1	0.260
Spur Pin (After Up & Before Low)	0.492	.078	1	0.990
-104 Jet (6 Outlets)				
Lower H.B. Gear (After Mesh)	0.047	.040	2	0.520
Lower H.B. Pinion (After Mesh)	0.047	.040	2	0.520
Lower H.B. Pin Brg (In Side) MR312	0.063	.040	1	0.260
Lower H.B. Pin Brg (Out Side) MR313	0.100	.040	1	0.260
Timken Jet				
Tapered Roller Bearing LL566800	0.190	.040	1	0.260
Grand Total Actual Flow				7.954
Grand Total Theoretical Flow				2.377
(Theoretical Flow = Sum of Req'd Flow x Qty)				

The test gearbox uses a dry sump lubrication scheme as shown in Figure 79. A separate oil tank is used to hold the test gearbox oil rather than using the gearbox sump itself. This was done so that the oil in the separate tank could be heated for the high temperature testing without disturbing the test components. The oil tank also contains an oil cooler for normal operation. A scavenge pump is sized to pump all the oil in the gearbox sump to the oil tank. The dummy gearbox has its own independent oil system identical to the test gearbox system except there is no heater in the dummy gearbox oil tank.

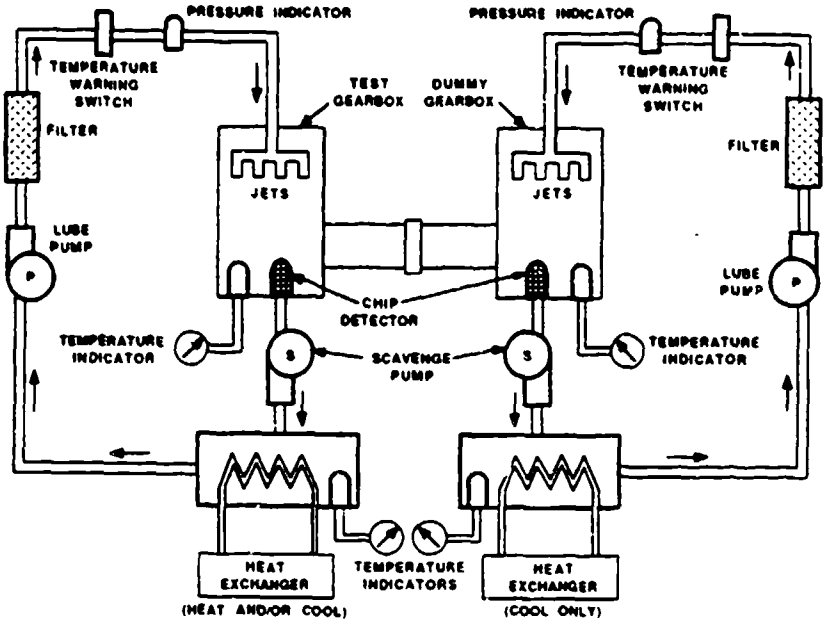

Figure 79. 1/2 Size Gearbox Lubrication System Schematic

Topological Gear Grinding

The gear teeth of the 1/2 size test gearbox have been topologically modified with the objective of achieving a uniform load distribution at a selected load. The 100% load condition of 648 horsepower input was selected as the uniform load design point. A high percentage of test time was spent at the 100% load condition with some testing at higher and some at lower loads. Normally, for the aircraft gears, a condition such as cruise would be selected as the design point which generally runs about 85% load. It should be noted that the uniform load condition will only exist at that particular value of load which produces deflections of the same magnitude as the corrections. For this reason, it is desirable to keep the deflection low so that load distributions at loads away from the design point will not be too severely maldistributed. Ideally, it is desired to have zero deflection but of course this is not possible. The light weight structure of the ART gearing design induces greater deflections than would be the case in commercial gearing. Therefore the topological tooth modifications become even more important in the ART transmission.

With the advent of computer numerical control (CNC) gear grinding machines, the gear designer has more latitude in making topological tooth modifications. In the past, corrections were limited to profile modifications, crowning, and lead modifications. A new dimension has been added with CNC form grinding machines which can now also control the "in feed" of the wheel with respect to the face width. This new correction has been termed "root line modification". There are also single point grinding machines which can control the tooth contour at will. These machines are generally too slow for production applications. One interesting aspect of CNC machining is the ability of the machinist to easily make grinding corrections after the first piece is ground to correct for manufacturing errors. Another relatively recent invention, the coordinate measuring machine (CMM) has also made the use of the CNC gear grinders feasible since there is now a method for inspection of the modified profiles.

Finite element analysis has provided a method for prediction of the deflections of the teeth to determine what modifications are required. The teeth of the initial gears are topologically ground, corrected by test, reground, and retested until the desired load distribution is achieved. The finite element analysis, correlated by the test data permits the final corrections to be arrived at in a scientific manner with less time required in trial testing. In the past, it was not uncommon to make more than six grinding corrections before the final tooth form is established. Each grinding correction requires disassembly of the gears, regrinding, touch up of finishes, inspection, reassembly and retest. By using initially corrected teeth and a correlated FEA, it may be possible to achieve load sharing on the initial grind or with only one grinding correction which saves manhours but more importantly saves calendar schedule time.

There are several types of finite element analysis which can be conducted to determine topological tooth corrections. The most direct form of analysis consists of modeling a single gear and shaft, fixing the shaft to ground at the bearings, and applying a uniform tooth load across the face. The topological corrections are then made equal and opposite to the deflections at the pitch line across the tooth face. The assumption is that when the tooth corrections are of the proper magnitude and direction, the load will be uniform hence the load is applied uniformly in the analysis. This method neglects the influence of housing deflections which can be significant. To determine the influence of housing deflections, the gear and shaft are placed in a model of the housing. Moreover the loads from each shaft in the assembly can have an influence on the deflection of every other shaft.

The FEA model for the ART 1/2 sized transmission contained the housing as well as the input pinion, two assemblies consisting of the input gear and herringbone pinion, and the output bull gear. Loads were applied uniformly to each tooth of each mesh in the gearbox all at once. The assumption is that when the proper corrections are applied to the teeth, the load distribution will be uniform therefore a uniform distribution can be applied in the beginning of the analysis. Small changes in stiffness from the material removed for the topological corrections are neglected. The teeth were loaded using five separate positions representing one diametral pitch of roll angle through the mesh and five separate load cases were run. Since the teeth on each side of the loaded teeth were also modeled, these represent the loaded teeth at earlier or later times during the mesh cycle. The housings, shafting, gear webs, and other areas not located in the immediate vicinity of the loaded gear teeth are modeled with a coarse mesh and simple elements such as plates and beams. The loaded gear teeth are modeled with a fine mesh using three dimensional solid elements. Figures 80 through 83 depict the fine mesh areas of the teeth on the spur pinion and gear and herringbone pinion and gear. Note that in Figure 80 two groups of five teeth each are modeled. This represents the spur pinion load splitting points. Similarly, the herringbone output gear contains two segments of five teeth each with only one of the segments showing in Figure 83. At the intersections of the coarse and fine models of the FEA mesh, multi point constraint equations were written for each common connection. These constraints equate slopes and deflections at the interfaces. The gear shafts were also constrained to the housings using multi point constraint equations in addition to gap elements. Gap elements make the solution of the

equations of equilibrium non linear. To model a bearing with gap elements, only compressive loads are permitted to be transferred from the shaft, across the bearing, and into the housing. This is how a bearing works since tensile forces can not be transmitted across rolling elements.

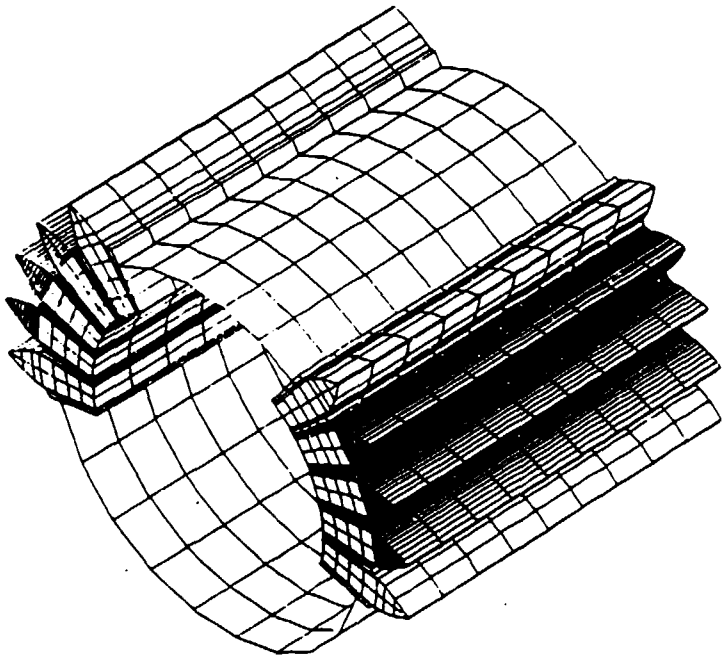

Figure 80. FEA Model of Input Spur Pinion

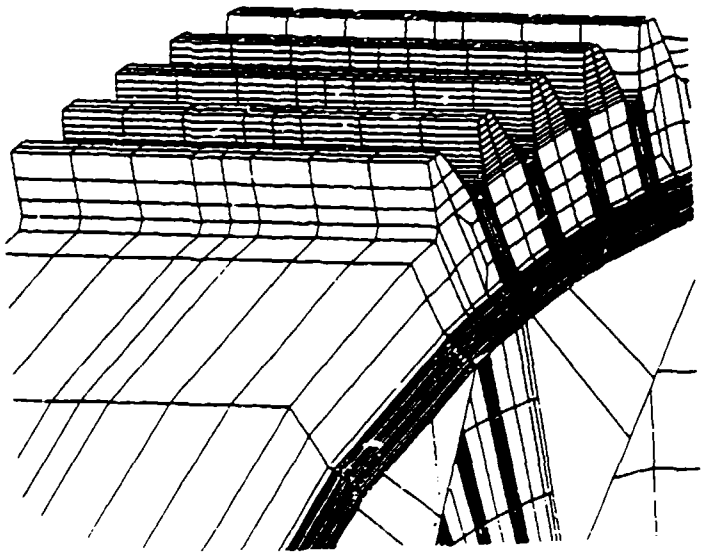

Figure 81. FEA Model of Input Spur Gear

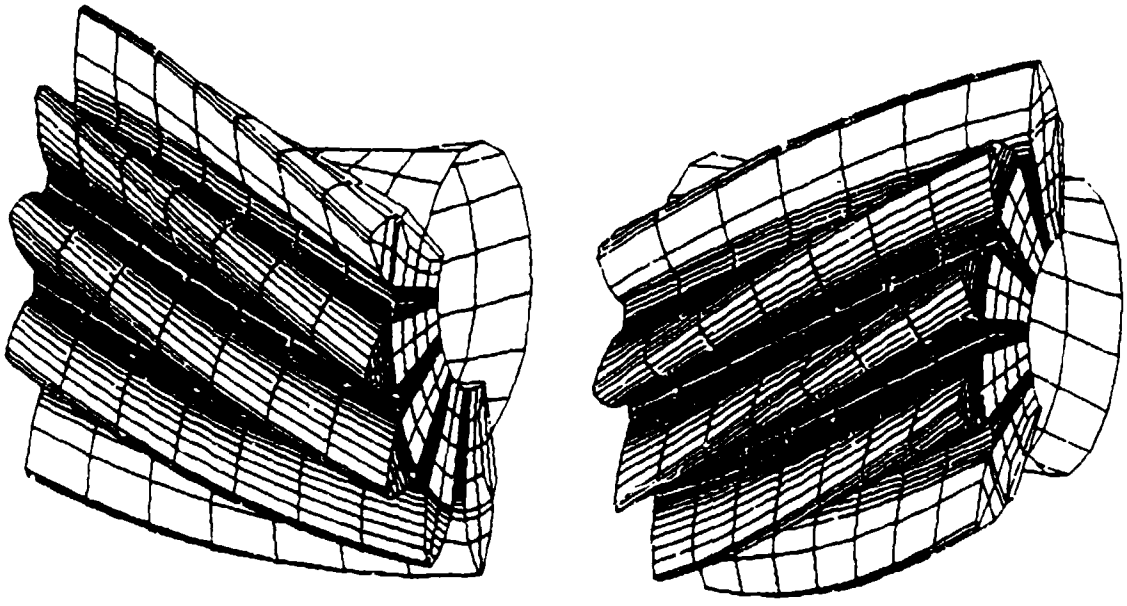

Figure 82. FEA Model of Herringbone Pinion

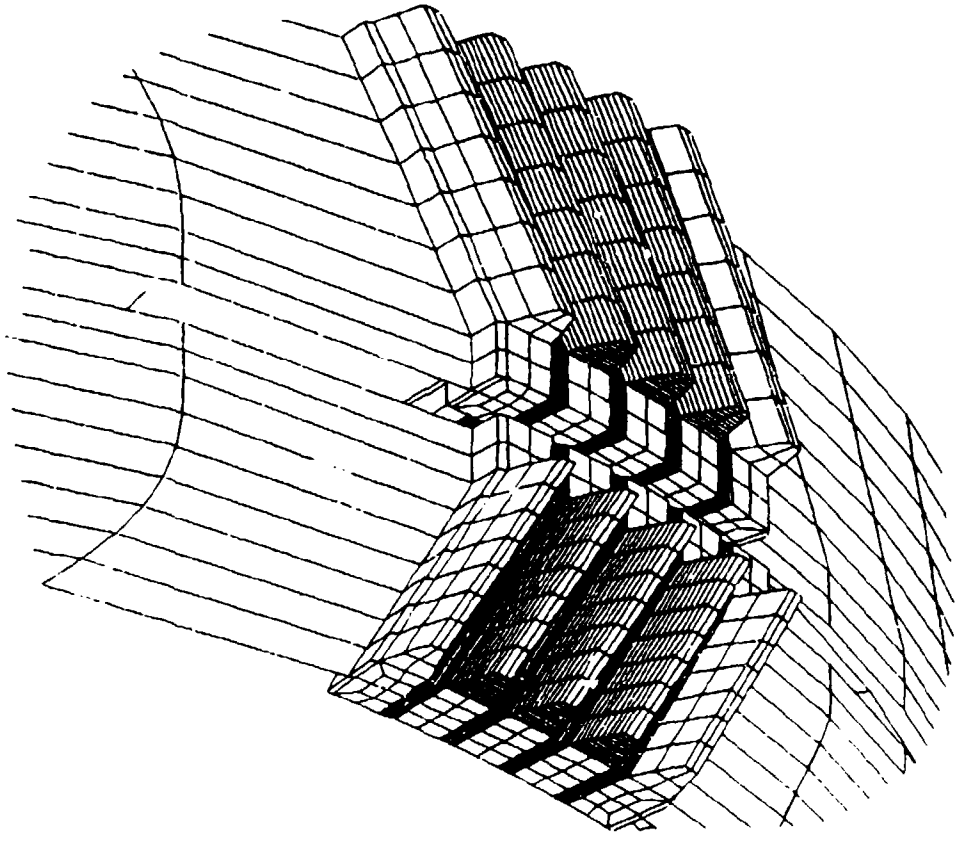

Figure 83. FEA Model of Herringbone Gear

The resulting model was divided into seven sub elements or "super elements" so that each portion of the model could be run separately. If any geometric changes were made, only the super element containing the changed geometry had to be rerun. Even for the 1/2 size gearbox which contained only one engine path and only the gears of the second and third stages, the resulting finite element model was of gigantic proportions. The model contained 72,000 grid points, 53,000 elements, and 432,000 degrees of freedom. It required approximately 3 gigabytes of memory and took approximately 5.5 hours of CPU time on the very fast IBM 3090-600 to decompose the seven super elements. Each load case could be run in approximately 30 minutes after decomposition. If a complete aircraft gearbox is to be run, a new procedure must be developed since the model will become too large for state-of-the-art computers. A simple case which models each member of a mesh separately is recommended.

A step beyond what was analyzed for the ART transmission is to conduct a three dimensional contact analysis to determine load distribution. In the three dimensional contact analysis, no assumptions about load distribution are made. Only the input torque is applied and the output is restrained. The teeth themselves are permitted to slide across each other as would be the case for real meshing gears and the load is permitted to seek its own equilibrium in the deflected state. Topological corrections can then be applied to the model and the mesh reanalyzed, etc. Large models might be handled by analyzing only one mesh at a time and can still contain a model of the housing. To accomplish this, a coarse model without teeth can be used for meshes not being analyzed. Loads can be applied to the rims of these coarse gear models. The influence of the loads on housing deflections is then determined. The teeth of the mesh being analyzed is broken down into a fine grid mesh. With this type of a model, a large gearbox can be analyzed using three dimensional contact analysis and accounting for all factors which influence load distribution such as shown in Table 39.

Table 39. Factors Affecting Gear Tooth Deflections

- Tooth Deflections
  - Bending of the gear tooth
  - Deflection from Hertzian pressure
  - Shear deflection
  - Temperature differences throughout the tooth
  - Stiffness as the teeth roll through mesh
  - Manufacturing errors
- Shaft and Gear Deflections
  - Bending of shafts
  - Torsion of shafts
  - Temperature differences throughout the shaft and web
  - Centrifugal deflection
  - Manufacturing errors
- Position of Gear Axis in Casing
  - Deflection of bearings
  - Deflection of housings
  - Temperature differences throughout the housing
  - Differential thermal expansion of different materials
  - Assembly errors
  - Manufacturing errors

FABRICATION

Angular Contact Spherical Roller Bearing

Manufacture of angular contact spherical roller bearings was performed by McGill Manufacturing Company of Valparaiso, Indiana. Two different bearings were fabricated for testing, being identical except for the rollers which were steel for one bearing and silicon nitride ceramic for the other. Both inner and outer races as well as the steel rollers were manufactured from Carpenter Pyrowear 53 alloy steel. The races were computer numerical control (CNC) turned, carburized, heat treated and fixture quenched with the appropriate cyclic freeze and draws. The faces of the outer race were rough ground on a rotary table grinding machine, and the O.D.'s and races rough ground on a microcentric and CNC bore grinder to obtain the proper spherical profile. After a stress relief operation, the faces, O.D. and races were finish ground. The races were then polished to the required 4 RA finish and inspected The cross section of the bearing with key dimensions is shown in Figure 84.

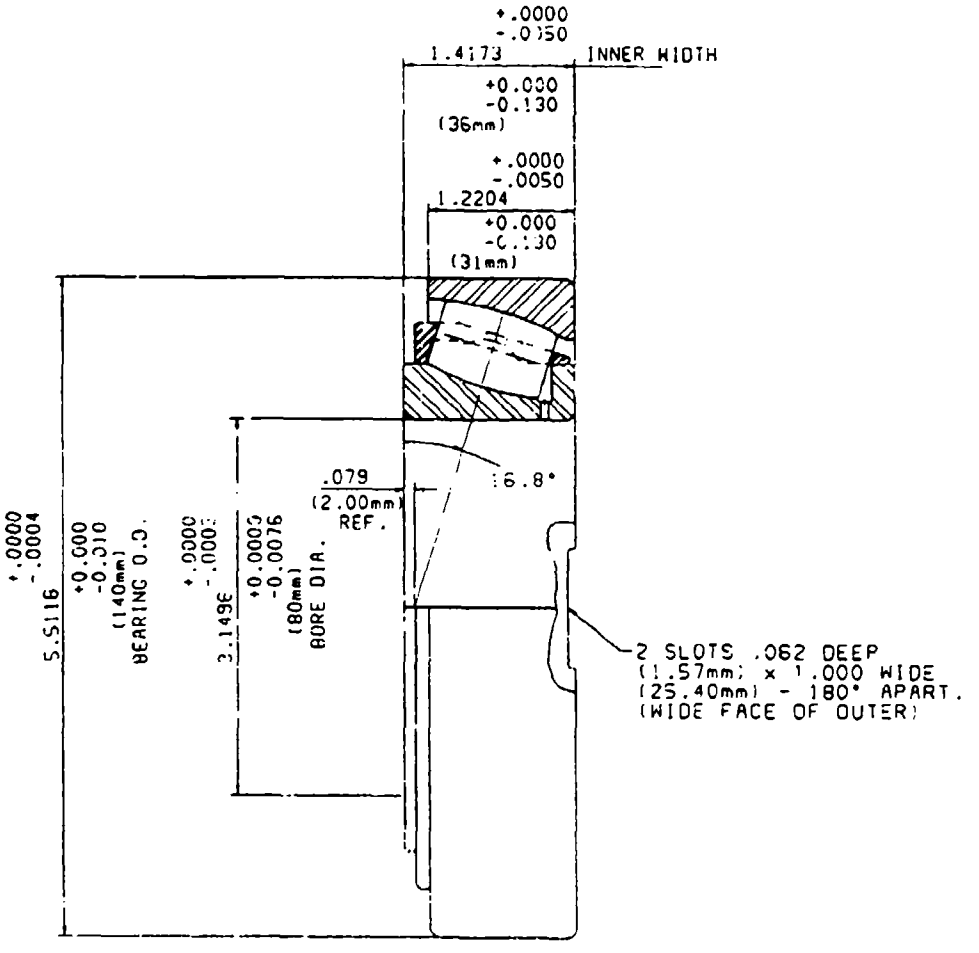

Figure 84. Angular Contact Spherical Roller Bearing

Retainers for the spherical rollers were CNC turned from 8620 steel. The roller pockets were broached, bore ground, checked for imbalance, inspected, and silver plated.

The steel rollers were turned, carburized, and cyclic heat treated prior to being straight O.D. ground. Roller O.D.'s were straight ground so that they could be held squarely when they are face ground in frames on the rotary table. The O.D.'s were rough and finish ground on the microcentric grinder, stress relieved, inspected, and microfinished to the 3 RA requirement.

The silicon nitride rollers were fabricated by GTE-Valenite. The hipped silicon nitride rollers were ground by Erie Industries. To obtain the correct radius of curvature, a special tool room setup with a diamond wheel was employed. The cost for production manufacture of the ceramic rollers is estimated at approximately $90.00 each for roller blanks with a machining cost of $320.00 each making the estimated finished roller cost $410.00 each. Thus, the advantages of ceramic rollers vs steel rollers must offset the additional cost to be useful for production helicopter transmissions.

1/2 Size Test Gearbox

Fabrication of the 1/2 size test gearbox components began in May of 1989 with the ordering of bearings, seals, forgings and other material and ended in March, 1991 with the final grinding of the double helical pinions. The material used for all gears in the 1/2 size gearbox was Pyrowear 53, a high hot hardness carburizing gear steel. Gears were heat treated to Rockwell C 60-64 case hardness and Rockwell C 33-45 core hardness.

The easiest gear to manufacture was the input spur pinion shown partially completed in Figure 85. The bearing journal for the roller bearing (nearest to spur gear) was honed to produce a surface finish of 2 to 6 RMS. The journal nearest to the spur gear teeth is the integral race for a roller bearing. The journal was finished to runout, straightness, and roundness requirements similar to a roller bearing raceway. The high contact ratio spur pinion had tip relief but did not have any topological corrections since they are all on the mating spur gears. The teeth of the spur pinion and bearing journals are carburized to produce .020 to .035 inch depth of case in the finished part.

The spur gears and double helical gears were ground on the Phauter Kapp Grinder as shown in Figure 86. This machine is a form grinder and is designed to use cubic boron nitride (CBN) cutting wheels as shown in Figure 87. CBN is a form of "imitation diamond" and is the next hardest material next to a natural diamond. On a relative hardness scale, it is much harder than silicon nitride used in current state-of-the-art grinding wheels. The advantage of CBN wheels is two fold: (1) The wheel is so hard that there is very little wear. There is no wheel dressing but rather the wheel is sent back for replating after a number of gears are ground which can reach to 50 or 100 gears or more, and (2) The majority of the heat generated in the grinding process is transferred to the wheel rather than to the part being ground as in conventional grinding because of the differences in specific heat of the material hence there is little chance of grinding burns. Since there is less

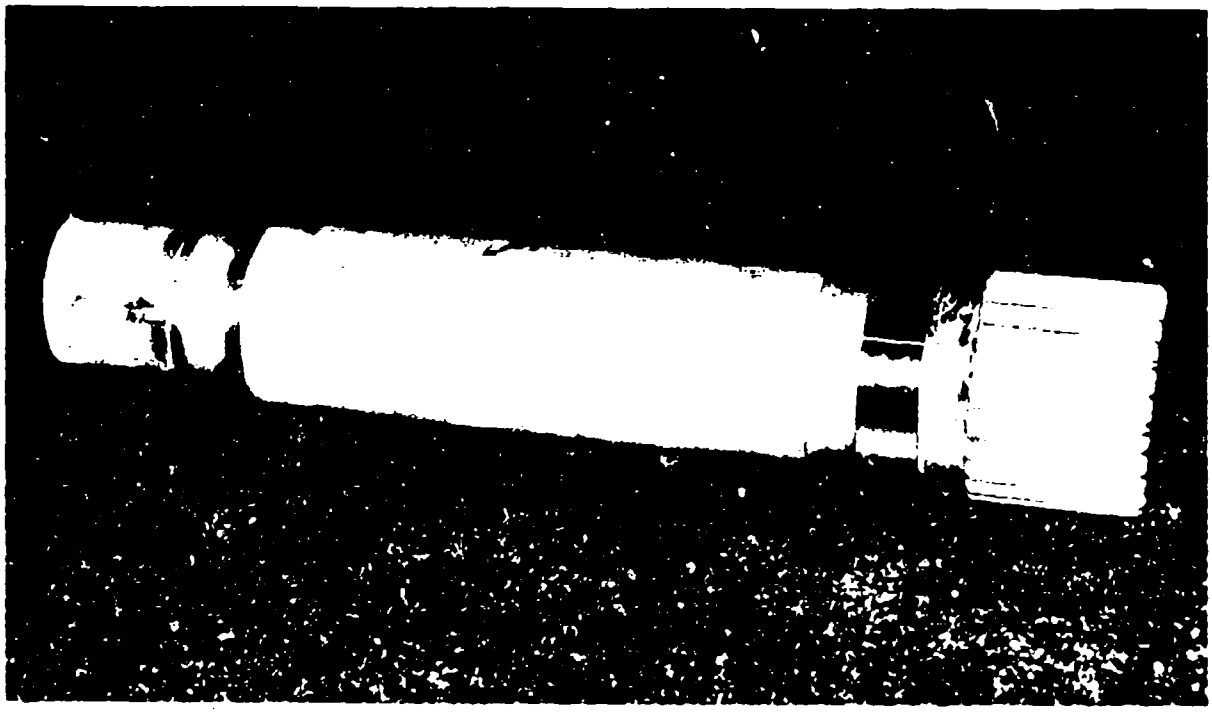

Figure 85. High Contact Ratio Spur Pinion

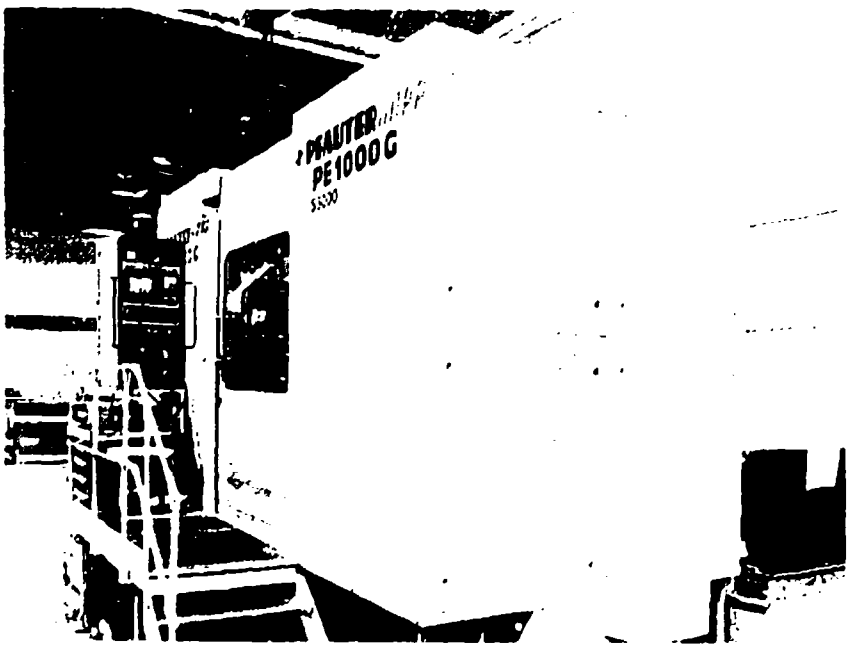

Figure 86. Phauter Kapp Grinding Machine

chance of grinding burn damage, deeper cuts can be taken. Profile modifications are manufactured into the wheel which is unique to the part being manufactured and can not be used for any other part. The numerical control permits off axis corrections such as lead modification and root line modification which can of course vary across the face. Crowning, for example, is obtained by "feeding in" at the ends of the teeth.

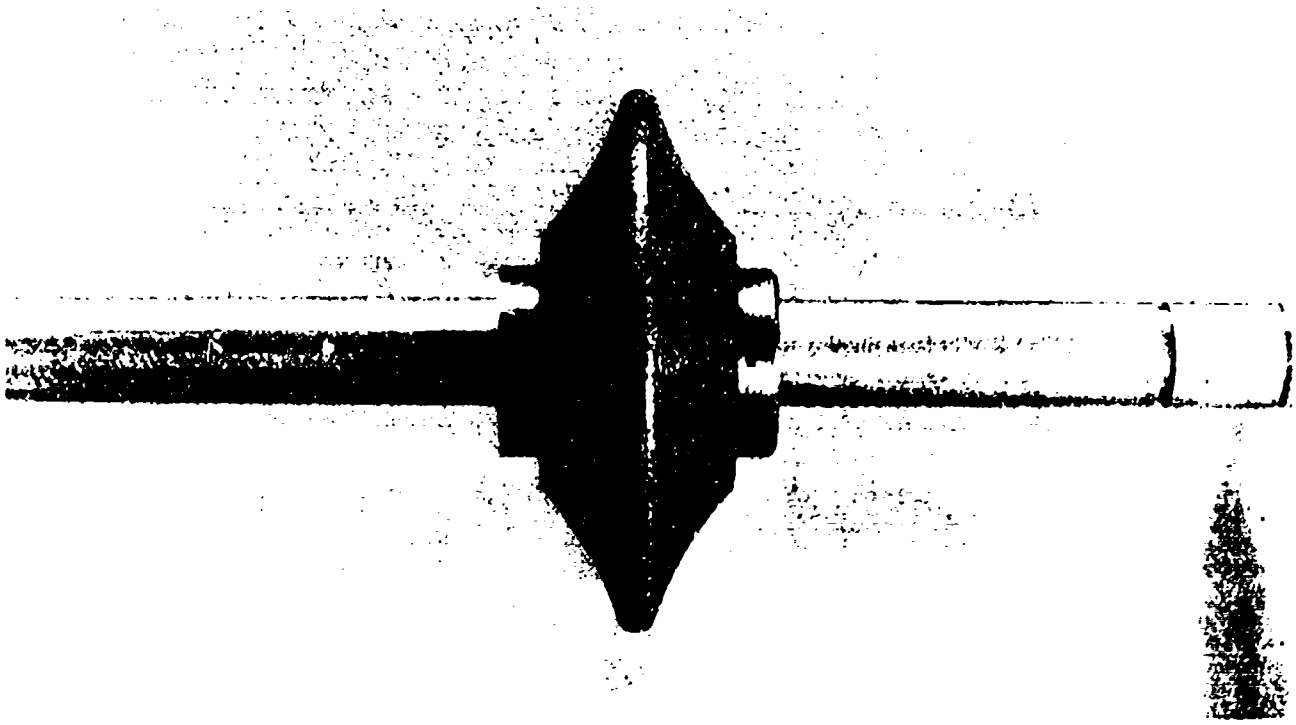

Figure 87. Cubic Boron Nitride (CBN) Form Grinding Wheel

The 1/2 size tapered roller bearing outer race/double helical gear assembly is shown in Figure 88. The helical gears, having a pitch diameter of 24 inches, were form ground using CBN wheels on the Phauter Kapp machine. The two halves of the gear are bolted together thereby permitting individual gear grinding and permitting a large grinding wheel diameter to be used.

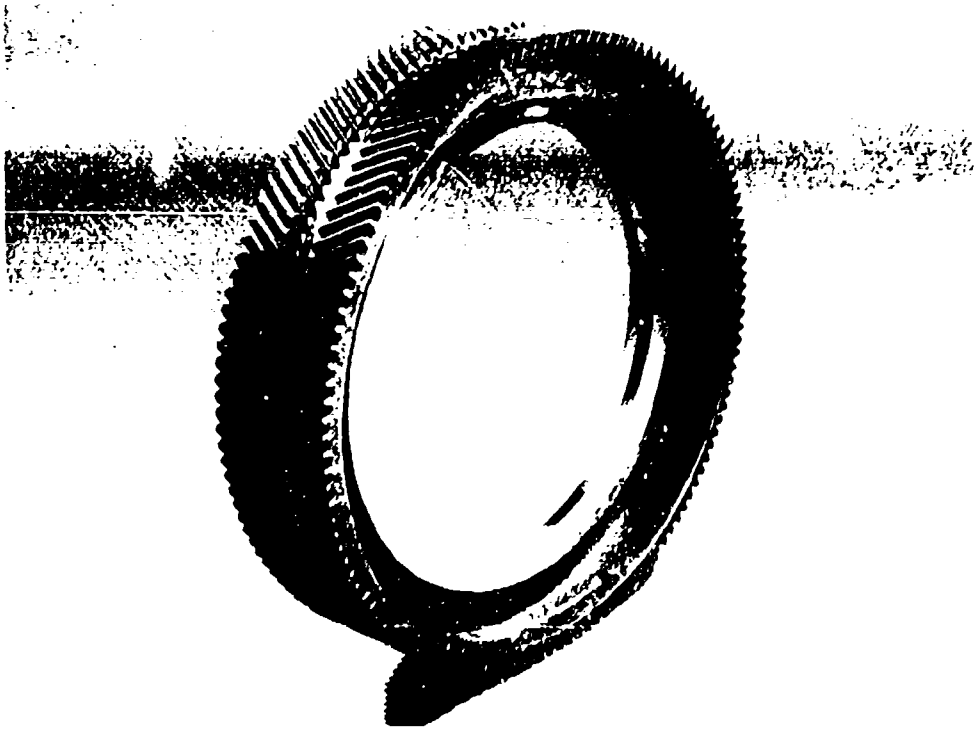

Figure 88. Bearing Outer Race/Double Helical Gear Assembly

Figure 89 is a photograph of the spur gear being hobbed prior to carburization. The gear blank has been previously copper plated so that there will be no carbon infusion on the top lands and end faces of the teeth during the carburizing process. This is important for a high contact ratio gear since the top land is small and "capping" or fracture of the tips of the teeth can occur with too much carbon near the tips of the teeth.

One of the most time consuming parts to fabricate was the side plate of the elastomeric load sharing device. The attachment of the flange to the tapered outer section required ribbing to reduce deflection and stress from preloading of the rubber. The ribs were "hogged out" using a ball end mill. A part is shown in Figure 90 in the milling machine and in Figure 91 as a finished piece. In production, this part could be made as an investment casting to reduce manufacturing cost. The finished side plates were then placed in a mold with three intermediate steel conical shims and an outer steel cone and nitrile rubber injected to form the completed elastomeric load sharing device assembly as shown in Figure 92 along with a semi-finished spur gear. The manufacture of the shims and rubber molding was performed by Lord Corporation, Erie, Pa.

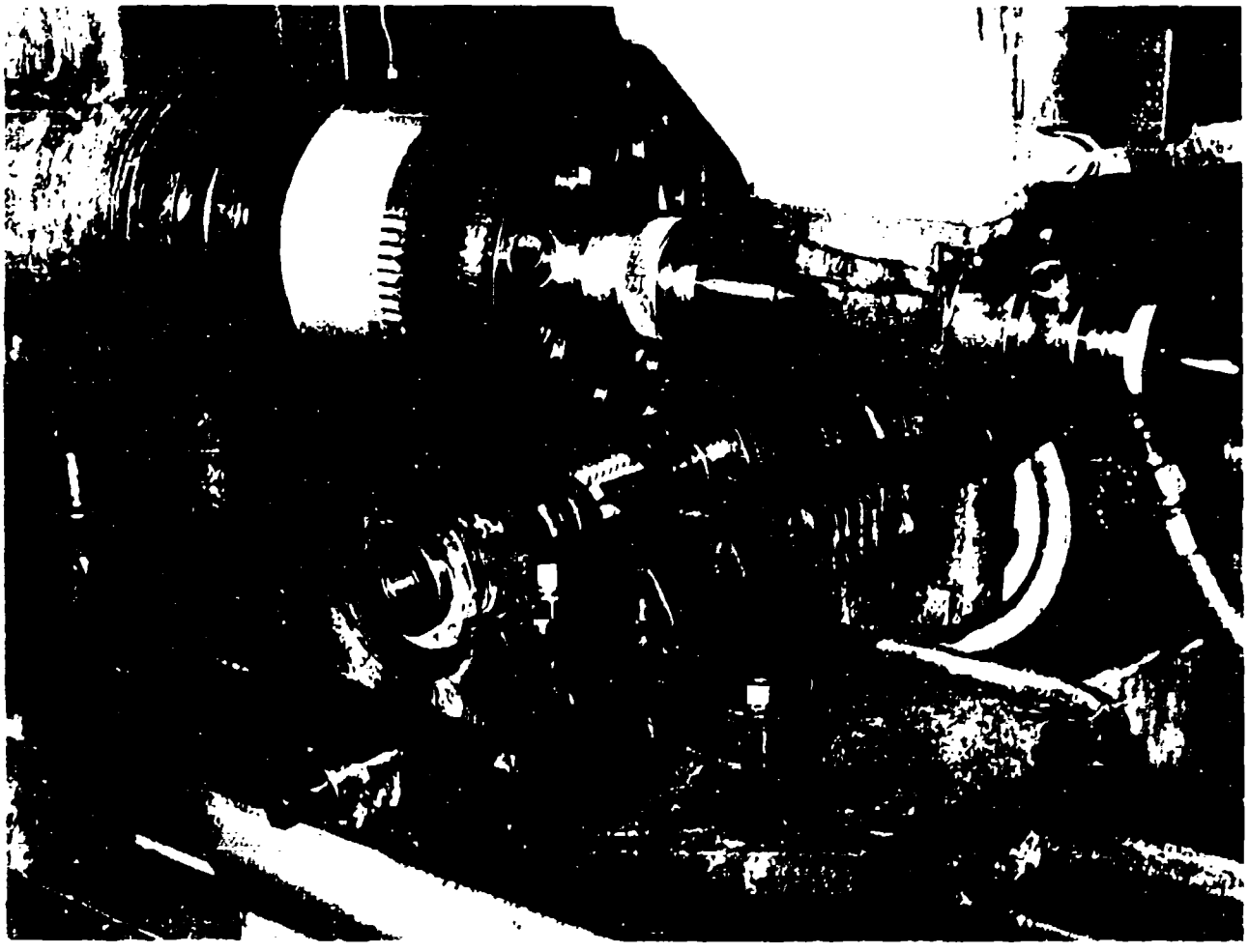

Figure 89. Spur Gear Hobbing Prior to Carburization

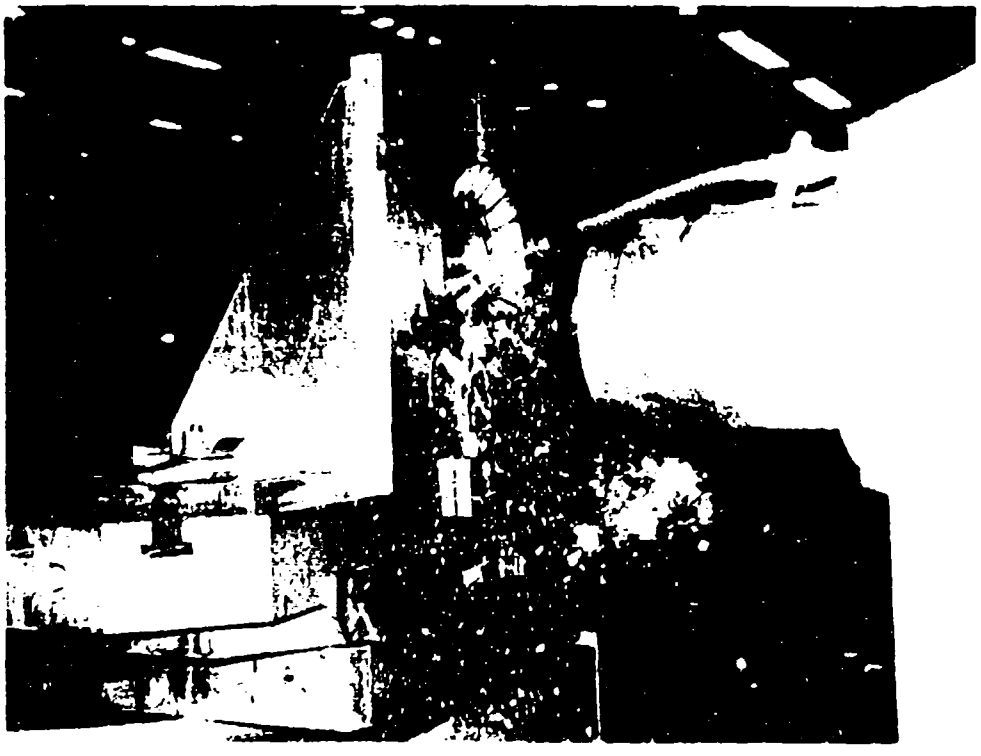

Figure 90. Elastomeric Load Sharing Device Side Plate Pocket Milling

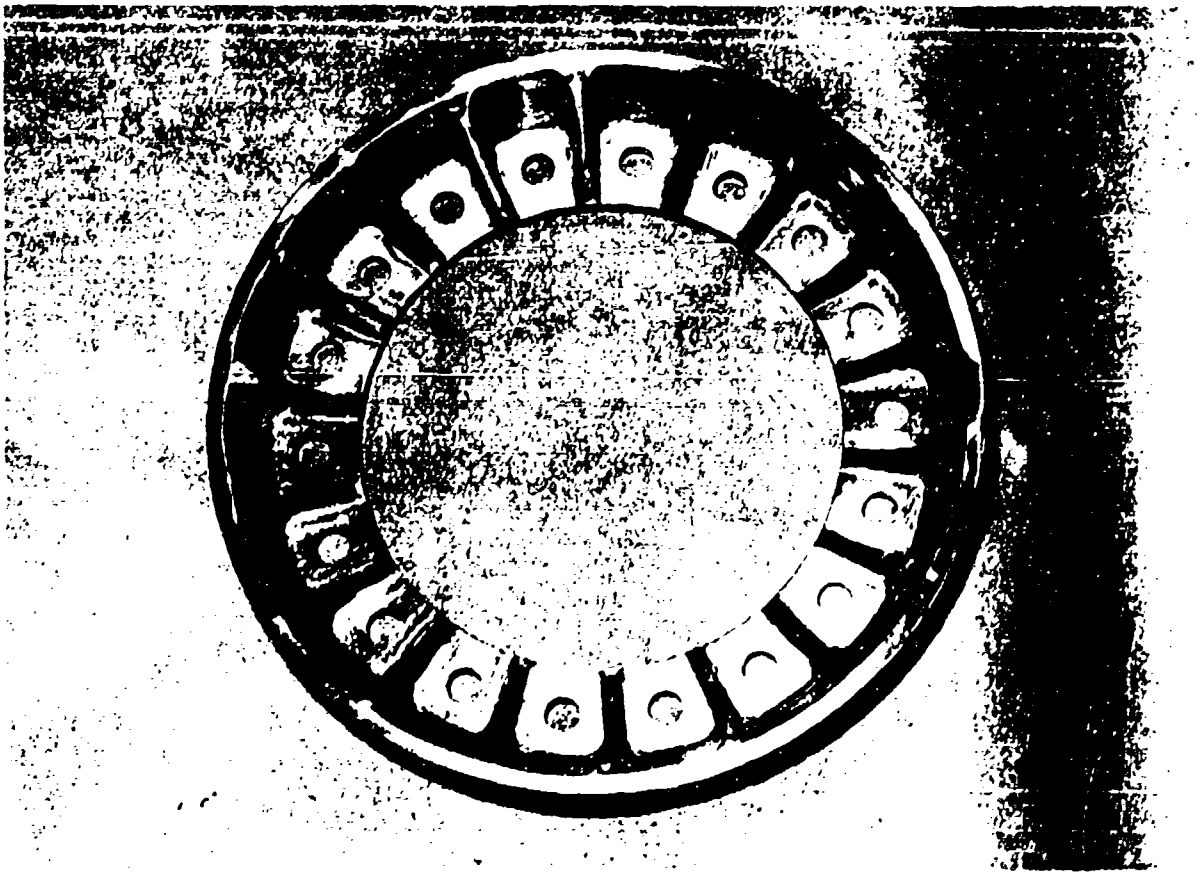

Figure 91. Elastomeric Load Sharing Device Side Plate

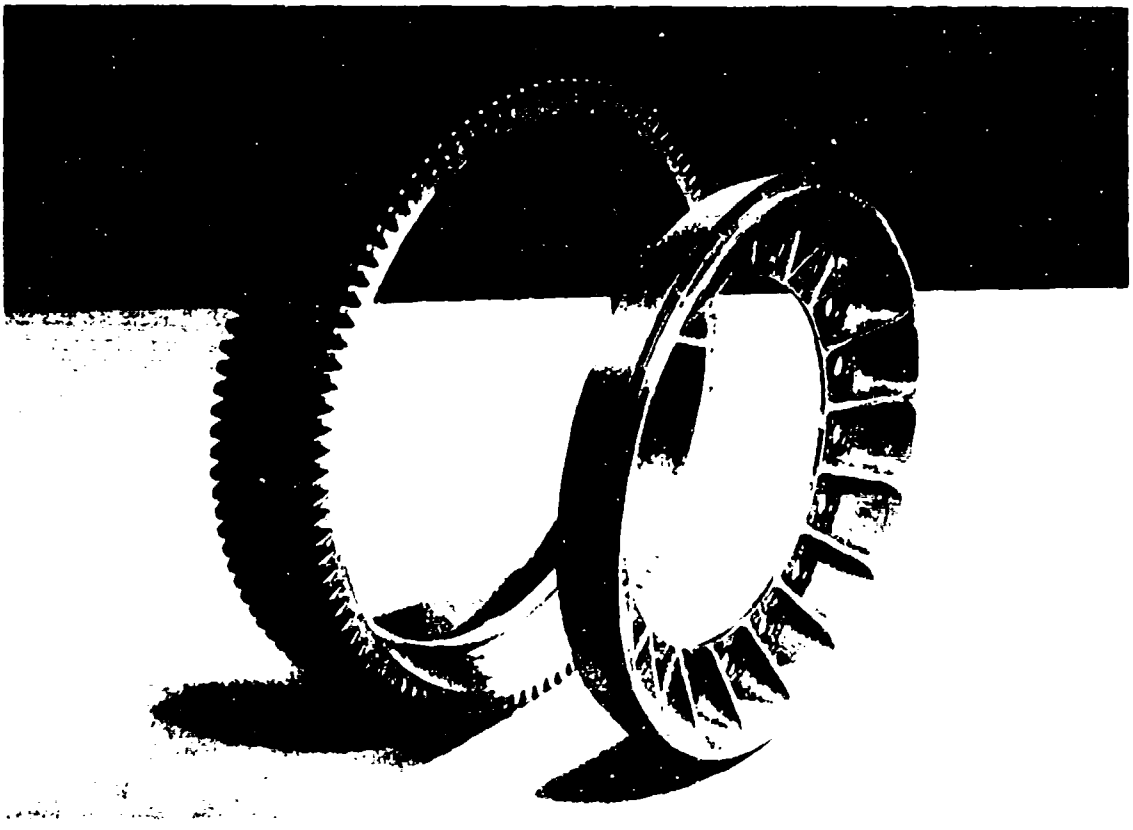

Figure 92. Spur Gear and Elastomeric Load Sharing Device

The double helical pinion at an intermediate point in manufacture is shown in Figure 93. The finished part is shown in Figure 94. The pinion tooth twist appears severe because there are only 13 teeth and the helix angle is 31°. The teeth are modified on the profile, have crowning, helix modification and root modification and the left and right helix angle pairs have different modifications. Similarly, the upper and lower pinions for each engine have different modifications.

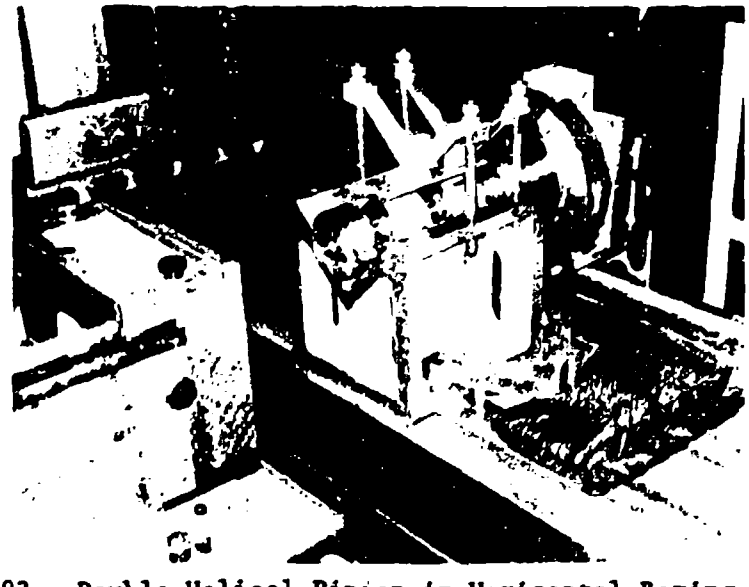

Figure 93. Double Helical Pinion in Horizontal Boring Machine

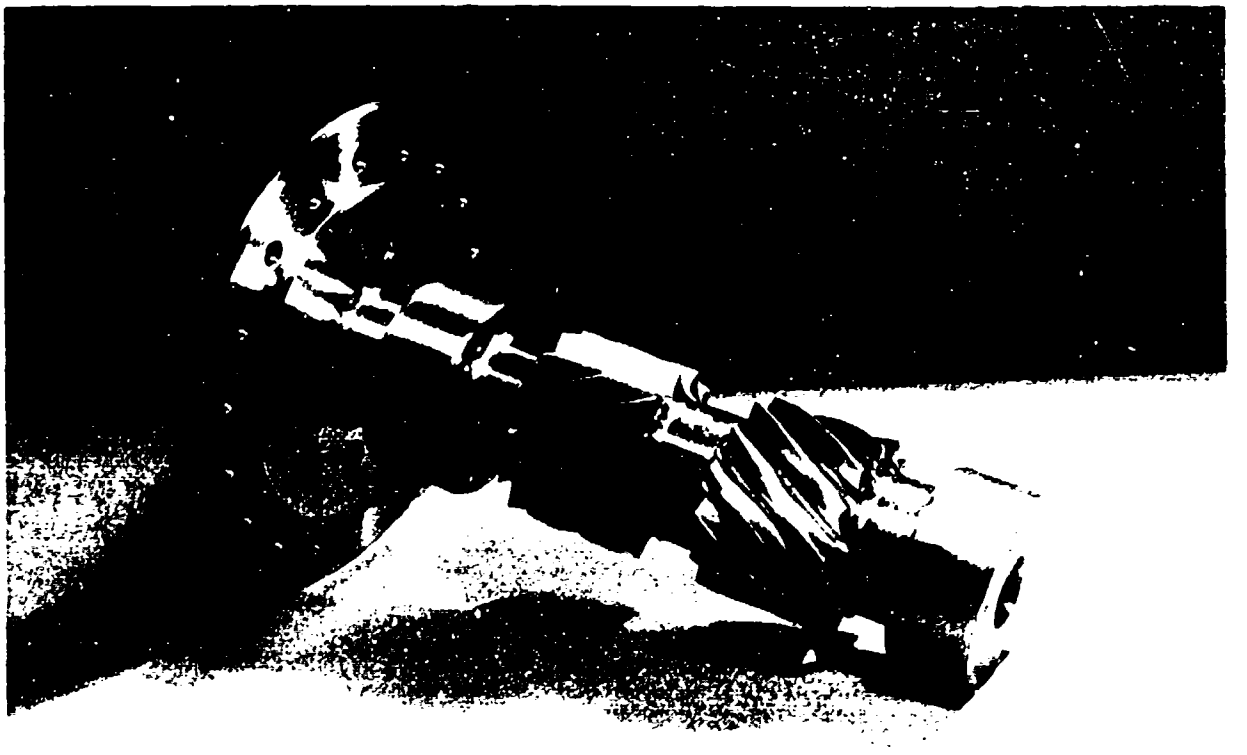

Figure 94. Completed Double Helical Pinion

Components making up the assembly of the spur gear and double helical pinion are shown in Figure 95. The shims between the flange of the double helical pinion and the elastomeric load sharing device side plates are ground to produce the desired clamp up in the axial direction. The most important aspect of the assembly is that the angular relationship between the "x" tooth (or index tooth) of the spur gear must be timed to the "x" tooth of the double helical pinion. To assure load sharing for components in the same assembly, the timing relationship must be the same between the two assemblies regardless of absolute magnitude. The timing relationship was checked using the assembly fixture as shown in Figure 96. Timing was set by setting the backlash between the spline teeth of the internal spline on the spur gear and the external spline on the double helical pinion flange. This spline has every other tooth missing so that there is a wide range of adjustment possible. The backlash gap was set to a value which represented the deflection of the elastomer at 140% torque at 200°F. During manufacture of the spur gears and double helical pinions, tolerances were introduced into the timing relationships so that "perfect" angles between both parts are not obtained necessarily with the same backlash between parts. Adjustments were made to account for these variables. The adjustments were calculated based on detailed measurements taken of the timing of the index teeth and spline teeth of the spur gears and double helical pinions using the Zeiss coordinate measuring machine (CMM) shown in Figure 97. As a final check, the timing of each assembly was checked in the CMM. Although the Zeiss machine is a highly accurate device, the timing check proved to be very difficult to perform and the results were not reliable to the desired accuracy of 0.0005 inch. A better method was developed which consisted of locking out the output bull gear and applying a small torque (by hand) on the input. By hand rotating each spur gear/double helical pinion assembly, it can easily be determined as to which side is contacting and which side is loose. By then applying torque until both sides are in firm contact,

the angular error between the two parts can be calculated if the spring rate is known. This is probably the method that is most amenable to production unless a more reliable measurement technique can be developed.

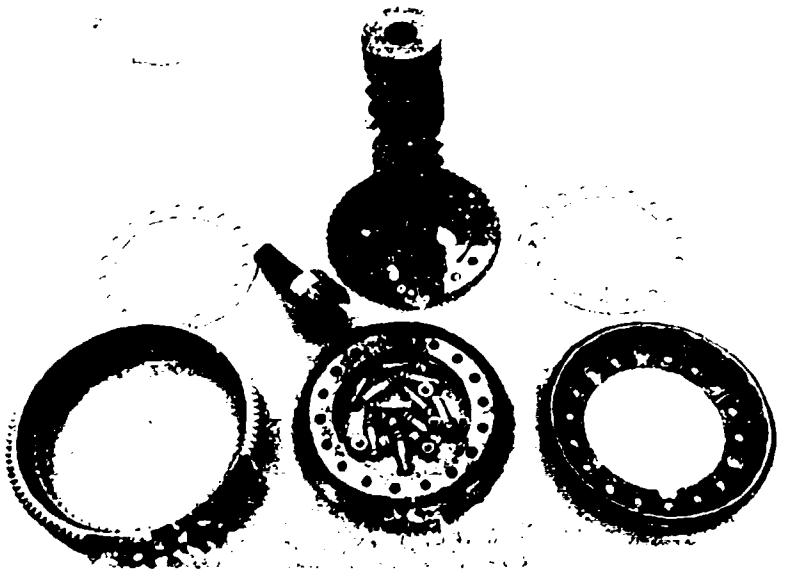

Figure 95. Components of Double Helical Pinion/Spur Gear Assembly

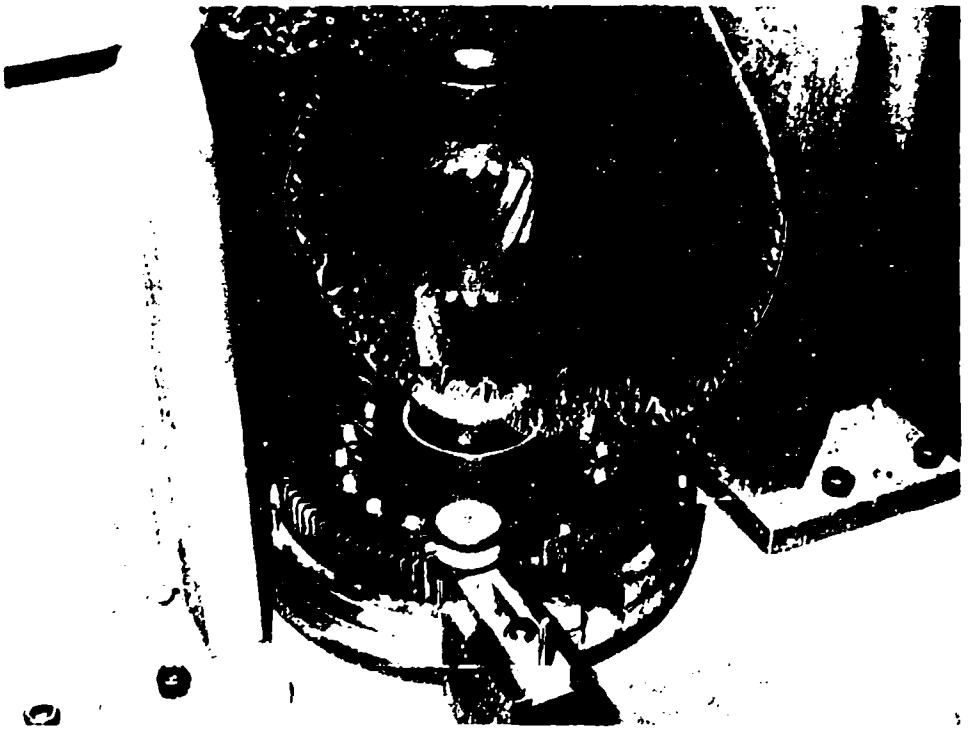

Figure 96. Assembly Fixture, Double Helical Pinion/Spur Gear

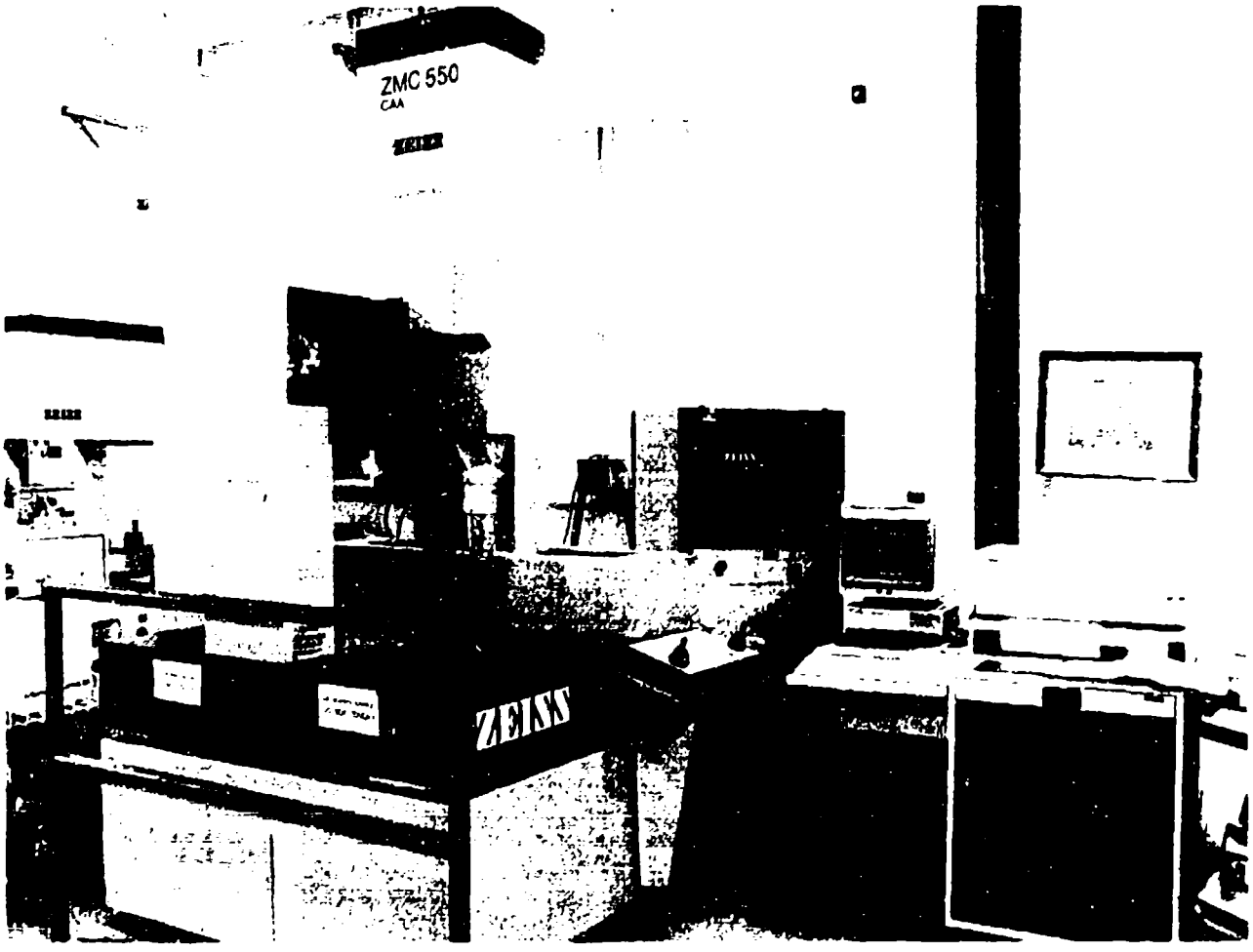

Figure 97. Zeiss Coordinate Measuring Machine

Figure 98 depicts the 1/2 size gearbox housing assembly. The housing is fabricated with two steel plates on the upper and lower halves connected by a welded steel center housing. Steel housings were used to reduce side effects of the housing such as deflection, etc. since the objective of the test program was to develop the internal components. In a separate program, a composite housing was substituted for the steel housing and tested. The double helical bull gear assembled into the housing is shown in Figure 99. All internal components of the test gearbox are shown disassembled in Figure 100.

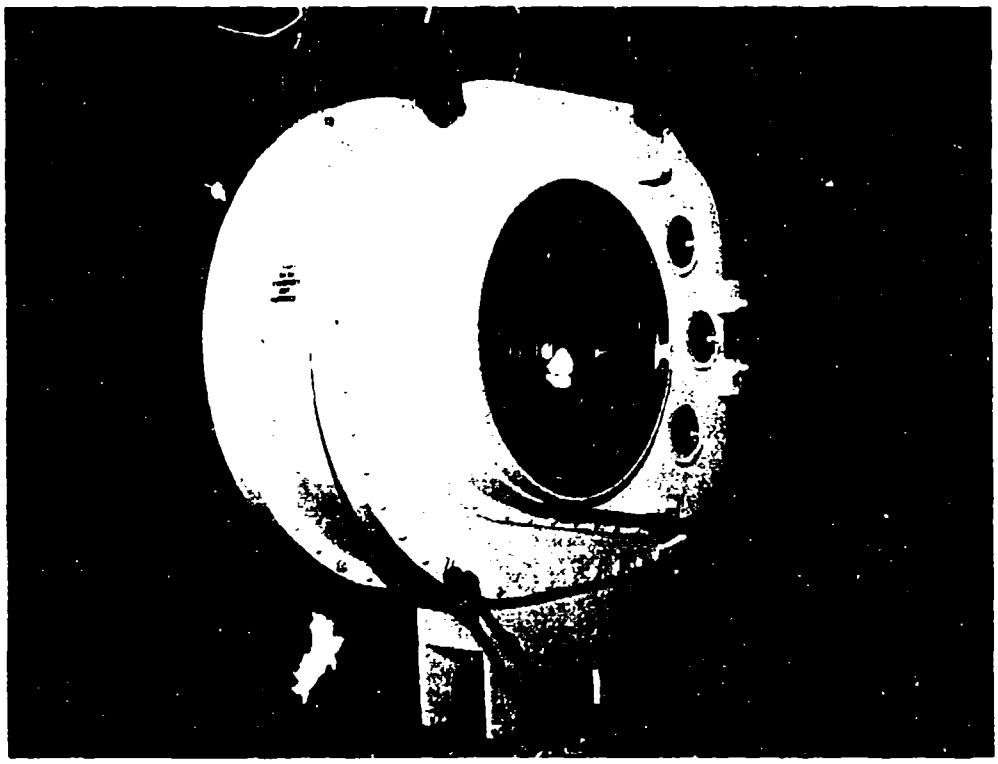

Figure 98. 1/2 Size Gearbox Housing Assembly

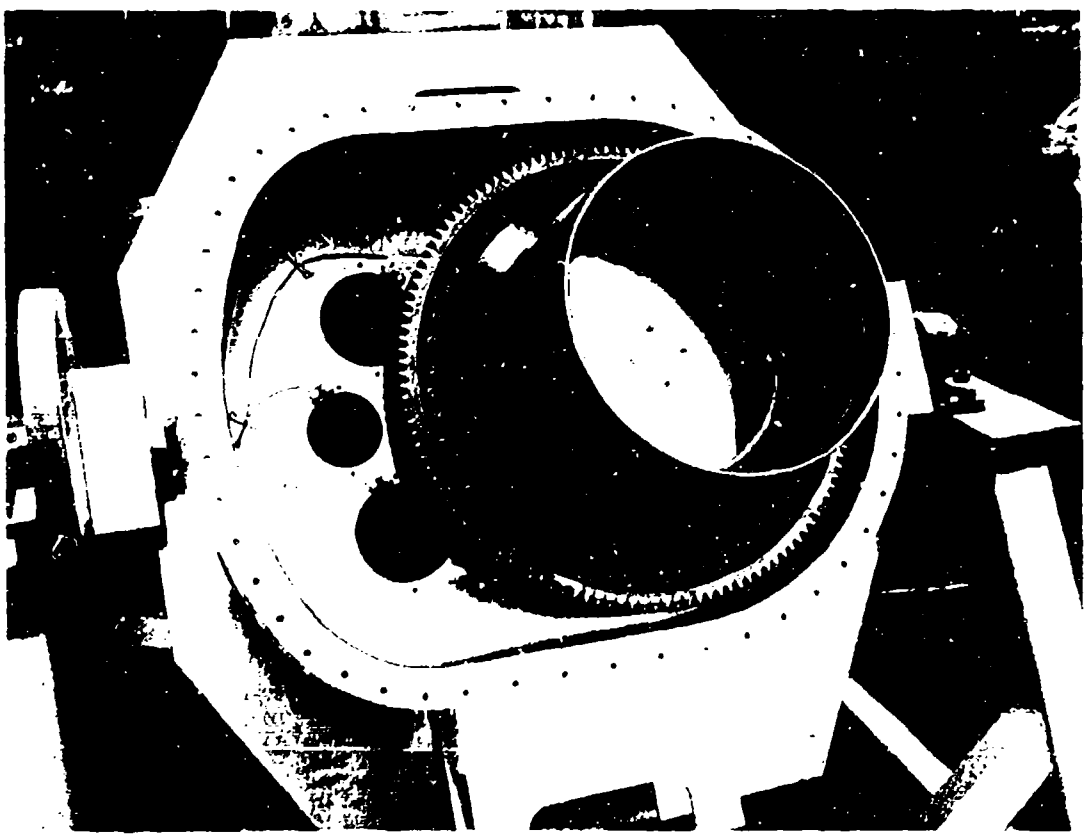

Figure 99. 1/2 Output Double Helical Bull Gear in Housing

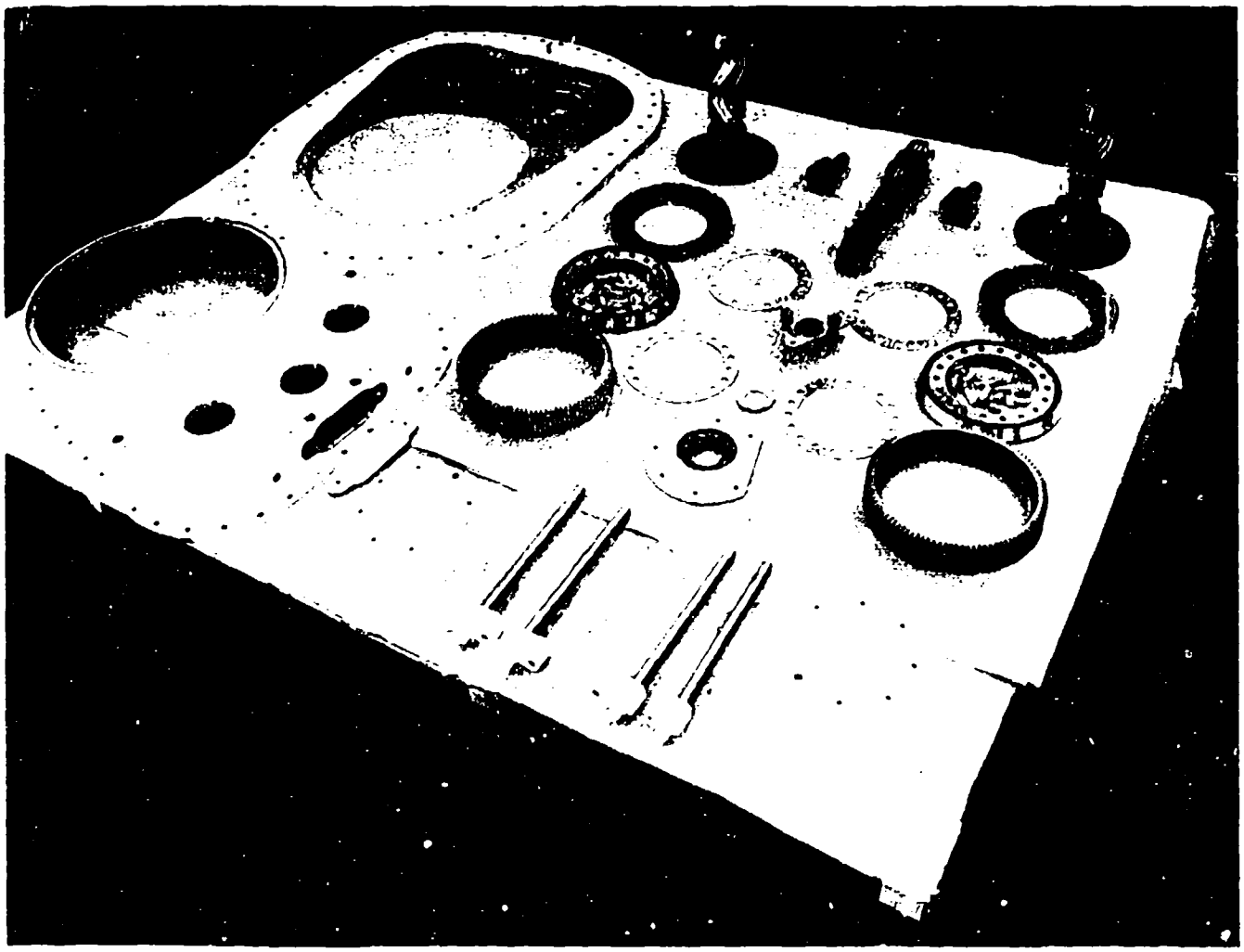

Figure 100. Test Gearbox Components, 1/2 Size Test Gearbox

1/2 Size Gearbox Test Configuration

The test and dummy gearbox each conformed to the requirements of drawing 38072-35000 as shown previously in Figure 65. Throughout testing, minor configuration changes were made. To track these changes, the configurations were numbered according to the order in which they occurred. The basic test configurations differed by the serial number of some components which were changed throughout testing, the backlash measured between the "backup spline" teeth, and the preload used for clamp up of the elastomeric load sharing devices. Table 40 lists the serial numbers of the internal gears and elastomers which made up the 38072-35005 double helical pinion/spur gear assembly. Table 41 lists the spline backlash and preload on the 38072-35008-041 elastomeric load sharing device or on the 38072-35008-042 steel device used to replace the elastomer on the test gearbox of configuration #2 and on the test and dummy gearboxes of configuration #5. Spline backlash was used as a measure of index tooth timing between the double helical pinion and spur gear. Preload was set by shimming to obtain the clamp up required to drive the spur gear in friction.

Table 40. 1/2 Size Gearbox Configuration Serial Numbers

Config Number	Location	Spur Gear 38072-35007 Serial Number	D.H. Pinion 38072-35006 Serial Number	Elastomeric 38072-35008 Serial Number
#1	041 Test	001	002	001/004
	042 Test	010	008	002/003
	041 Dummy	005	004	006/013
	042 Dummy	011	010	009/010
#2	041 Test	001	002	001/002 (1)
	042 Test	010	008	003/004 (1)
	041 Dummy	005	004	006/013
	042 Dummy	011	010	009/010
#3	041 Test	001	002	001/004
	042 Test	010	008	002/003
	041 Dummy	005	004	006/013
	042 Dummy	011	010	009/010
#4 (4)	041 Test	001	002	001/004
	042 Test	010	008	002/003
	041 Dummy	005	001 (2)	006/013
	042 Dummy	011	010	009/010
#5 (4)	041 Test	001	005 (3)	001/002 (1)
	042 Test	010	008	003/004 (1)
	041 Dummy	005	001	005/006 (1)
	042 Dummy	011	010	007/008 (1)

Notes:

1. Solid steel load sharing members, 38072-35008-042 in lieu of elastomeric load sharing devices, 38072-35008-041.

2. Capped tooth on double helical pinion 38072-35006-041 S/N 004 replaced by S/N 001.

3. Spalled tooth on double helical pinion 38072-35006-041 S/N 002 replaced by S/N 005.

4. Composite gearbox installed on dummy side.

Table 41. 1/2 Size Gearbox Configuration Backlash and Preload

Config. Number	Location	Desired Spline Backlash	Actual Spline Backlash	Preload Elas/Steel
#1	041 Test	.0800	.0812	.010
	042 Test	.0804	.0819	.010
	041 Dummy	.0782	.0768	.010
	042 Dummy	.0823	.0832	.010
#2	041 Test(1)	.0825	.0827	.003
	042 Test(1)	.0820	.0819	.003
	041 Dummy	.0782	.0768	.010
	042 Dummy	.0823	.0832	.010
#3	041 Test	.1305	.1349	.033
	042 Test	.1300	.1349	.033
	041 Dummy	.0782	.0768	.010
	042 Dummy	.0823	.0832	.010
#4	041 Test	.1305	.1349	.033
	042 Test	.1300	.1349	.033
	041 Dummy	.1556	.1551	.033
	042 Dummy	.1345	.1345	.033
#5	041 Test(1)	.1490	.1490	.015
	042 Test(1)	.1377	.1378	.015
	041 Dummy(1)	.1556	.1518	.015
	042 Dummy(1)	.1345	.1300	.015

Note:

1. Solid steel load sharing members, 38072-35008-042 in lieu of elastomeric load sharing devices, 38072-35008-041.

Table 41 lists desired backlash and actual backlash. In setting the backlash on the double helical pinion/spur gear assembly, it was not possible to get the exact desired value of backlash because changes in backlash occurred during the process of torquing of bolts to obtain the preload. The difference between the desired and actual backlash is the installed error in index dimension.

For the elastomeric load sharing devices used, the spring rates of the selected serial numbers were determined by bench tests and matched on assembly to give total torsional spring rates between left and right members that were within 5% of each other. Table 42 lists the spring rates of the individual elastomers selected as well as the total spring rate of the two elastomers in parallel (spring rates add in parallel).

Table 42. Elastomeric Load Sharing Device Spring Rates

Location	Elastomer Serial Numbers	Individual Spring Rates (in-lb/°)	Assembly Spring Rates (in-lb/°)
041 Test	001/004	9600/10900	20500
042 Test	002/003	10600/9900	20500
041 Dummy	006/013	10900/9400	20300
042 Dummy	009/010	9900/10400	20300

TEST

Test Facilities/Instrumentation

Material Test Facility/Instrumentation

The material test facility was used to investigate fretting fatigue aspects of gear steels and to determine if improvements could be found with surface coating treatments. Various surface treatments were examined and the most promising coating, thin dense chrome (TDC), was selected for testing. Thin dense chrome plating was evaluated as a coating for Pyrowear 53 high hot hardness gear steel. Two types of specimens were fabricated with the first consisting of polished Pyrowear 53 alloy steel heat treated to core properties (Rc 38). These specimens were not carburized but subjected to the carburizing cycle heat treatment to simulate a non carburized area of a carburized part. The TDC specimens were identical to the polished specimens but with the addition of the thin dense chromeplating performed by Armoloy of Connecticut to the general requirements of AMS 2438; chromium coating, thin, hard, dense deposit. The configuration of the test specimen is shown in Figure 101. To induce fretting in the specimens, Pyrowear 53 pins were fabricated as shown in Figure 102.

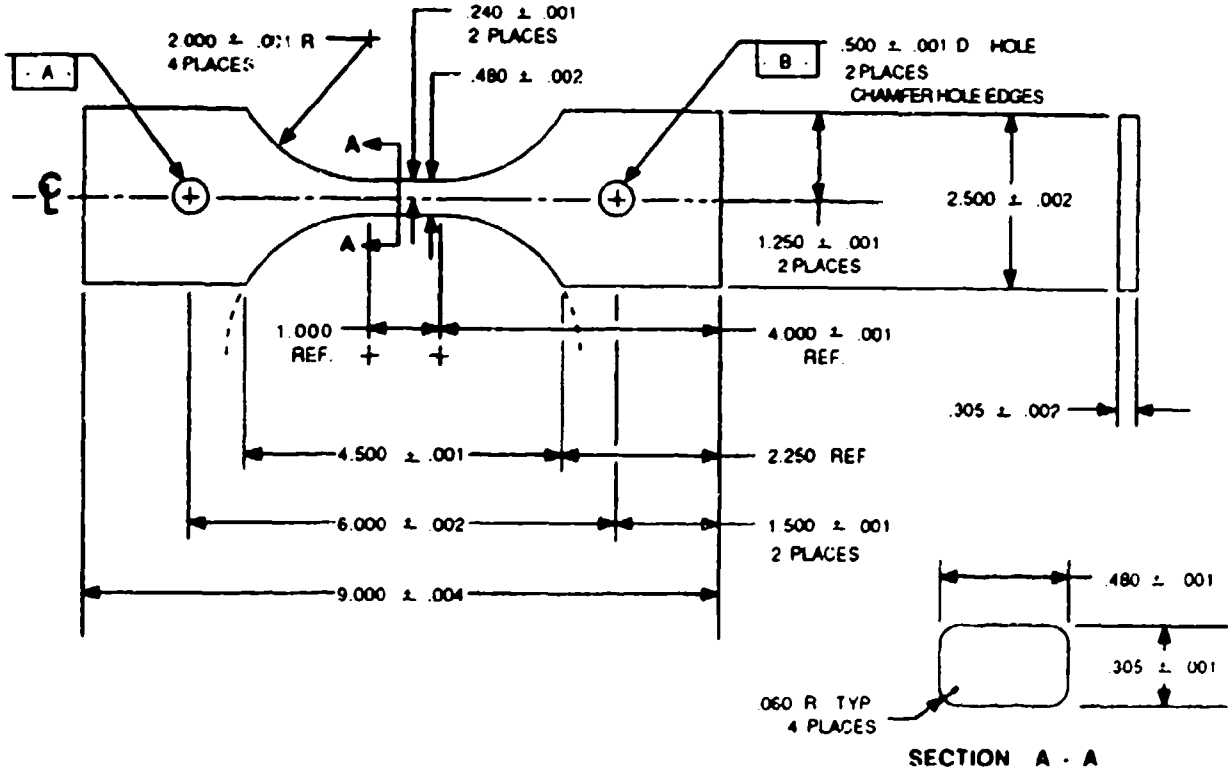

Figure 101. Test Coupon Configuration

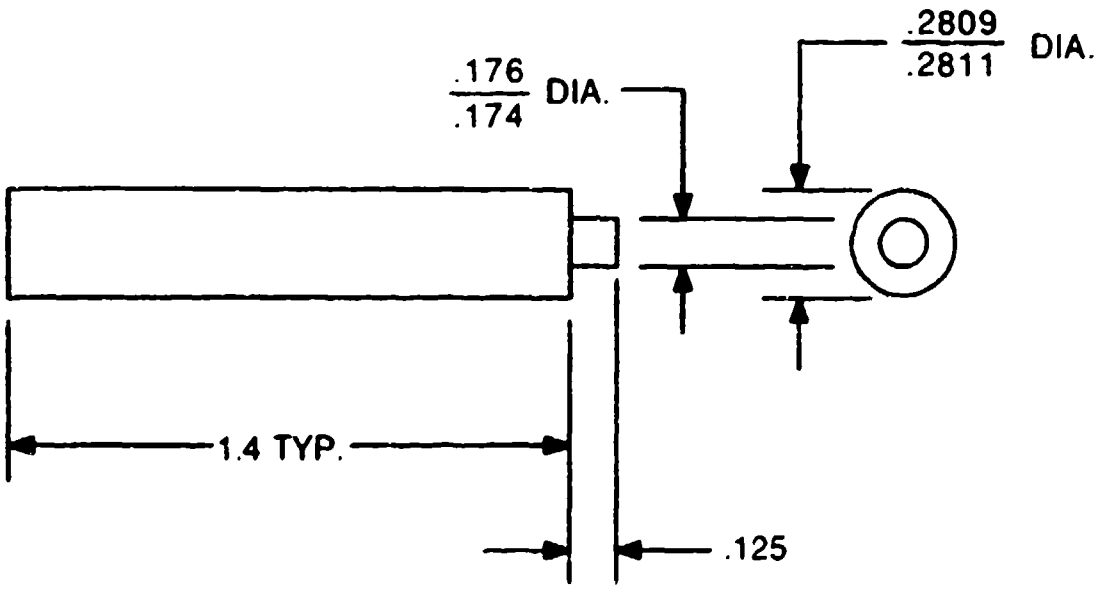

Figure 102. Fretting Contact Pin Configuration

The fretting pins were made from the same material as the test coupons and were subjected to the same heat treatment. The pins were not plated for the TDC tests but polishing of the pin tips was performed.

Fretting fatigue testing was conducted on an MTS Series 810 servohydraulic unit with 20,000 pound capacity as shown in Figure 103. The fatigue test machine applied fatigue axial loads to the test coupon while a special fixture was used to preload the fretting contact pins in a fixed position at the center of the test coupon. The fretting pins were accurately located on each side of the test coupons by means of the special fixture. The pins were preloaded with belleville washers to maintain preload in the event there was any fretting wear. Figure 104 shows the fixture with belleville washers installed. The clamping bars that were used to preload the fretting pins are in three point bending and were calibrated with strain gages on the side of the bar to accurately ascertain the preload magnitude.

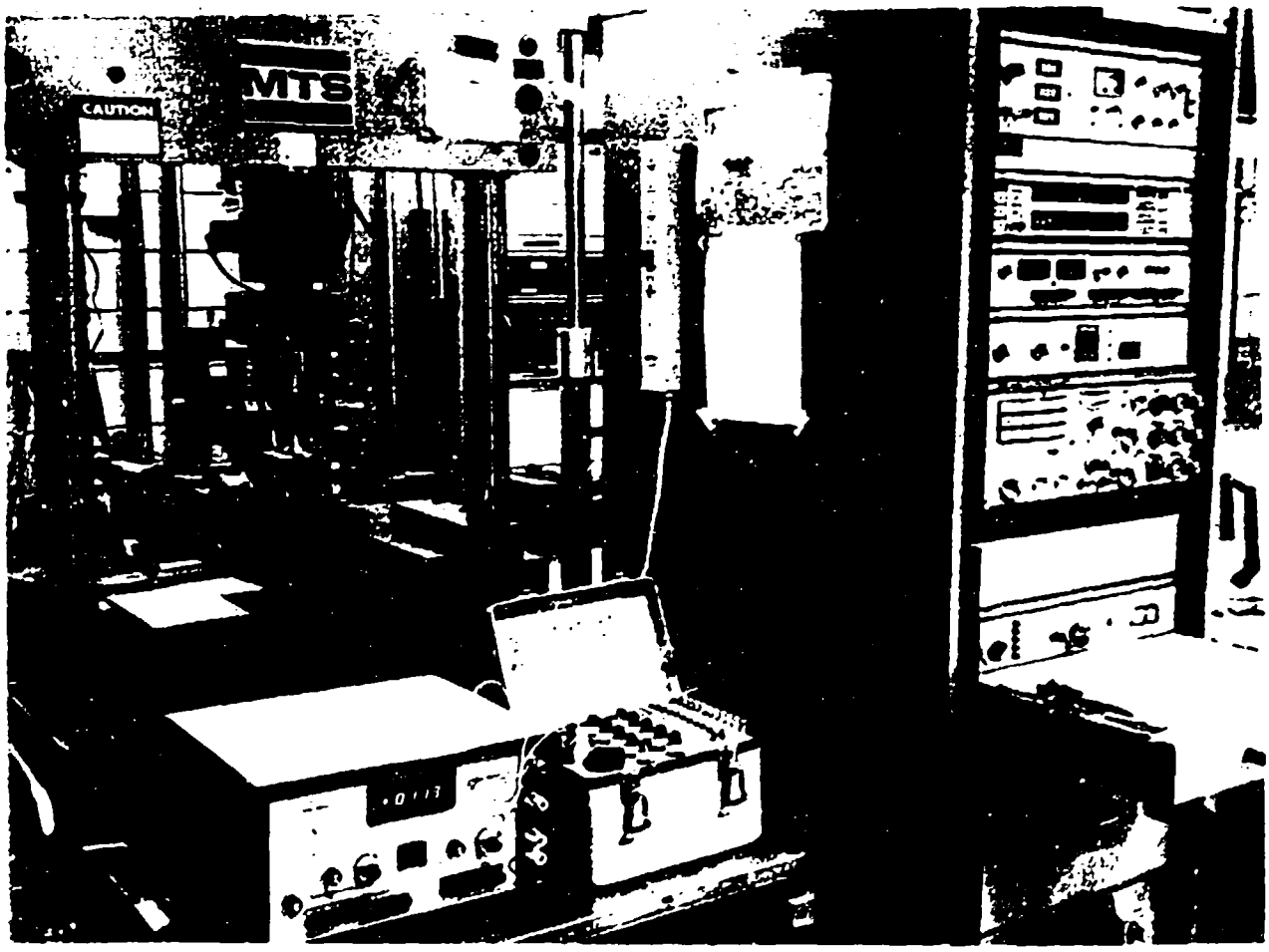

Figure 103. Fatigue Test Machine

A technique was developed for viewing the pin/coupon contact interface for in-situ measurement of fretting slip amplitude. The technique involves attaching a strain gage to the coupon adjacent to the point of pin contact. Micro Measurements Catalog Number EA-06-031EC-350 strain gages were employed. These gages have an extremely fine, repeatable series of parallel lines within the grid pattern which are used as miniature rulers to measure slip amplitudes directly. For each pin to be observed, one gage was carefully trimmed across the grid lines and bonded to the test coupon adjacent to the anticipated contact area. Grid line orientation was transverse to the coupon fatigue loading direction. Using a standard stereo-microscope at 40x magnification and strobe lighting set to correspond to the fatigue loading frequency (30 to 31 Hertz), the fretting slip, if any, was observed in slow motion allowing direct measurement of the peak-to-peak amplitude. Resolution of this method is within approximately 20 microns under ideal conditions. Figure 104 shows the slip amplitude measurement apparatus.

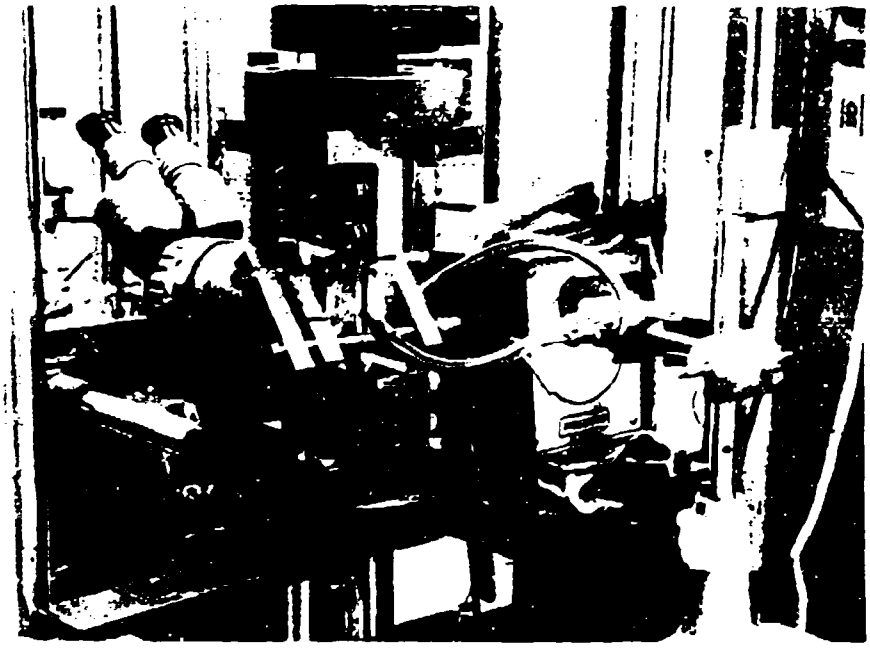

Figure 104. Slip Amplitude Measurement Apparatus

1/2 Size Gearbox Test Facility/Instrumentation

All testing for the 1/2 size gearbox was performed using the tail drive shaft and coupling facility shown schematically in Figure 105. This facility is configured as a regenerative loop powered by a 300 HP electric motor. Variable speeds between 1500 - 8000 rpm were available. A maximum torque equivalent to 2000 HP was also available between a range of 4000 - 8000 rpm. Controls were automated to include integral fault and test parameter monitoring. The operators console is shown in Figure 106.

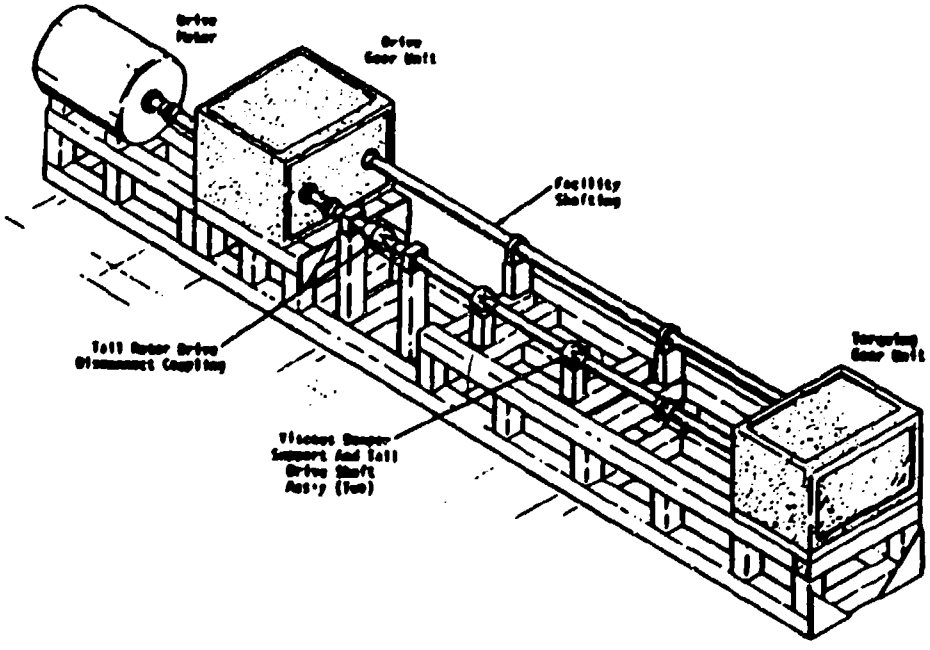

Figure 105. Shaft/Coupling Test Facility

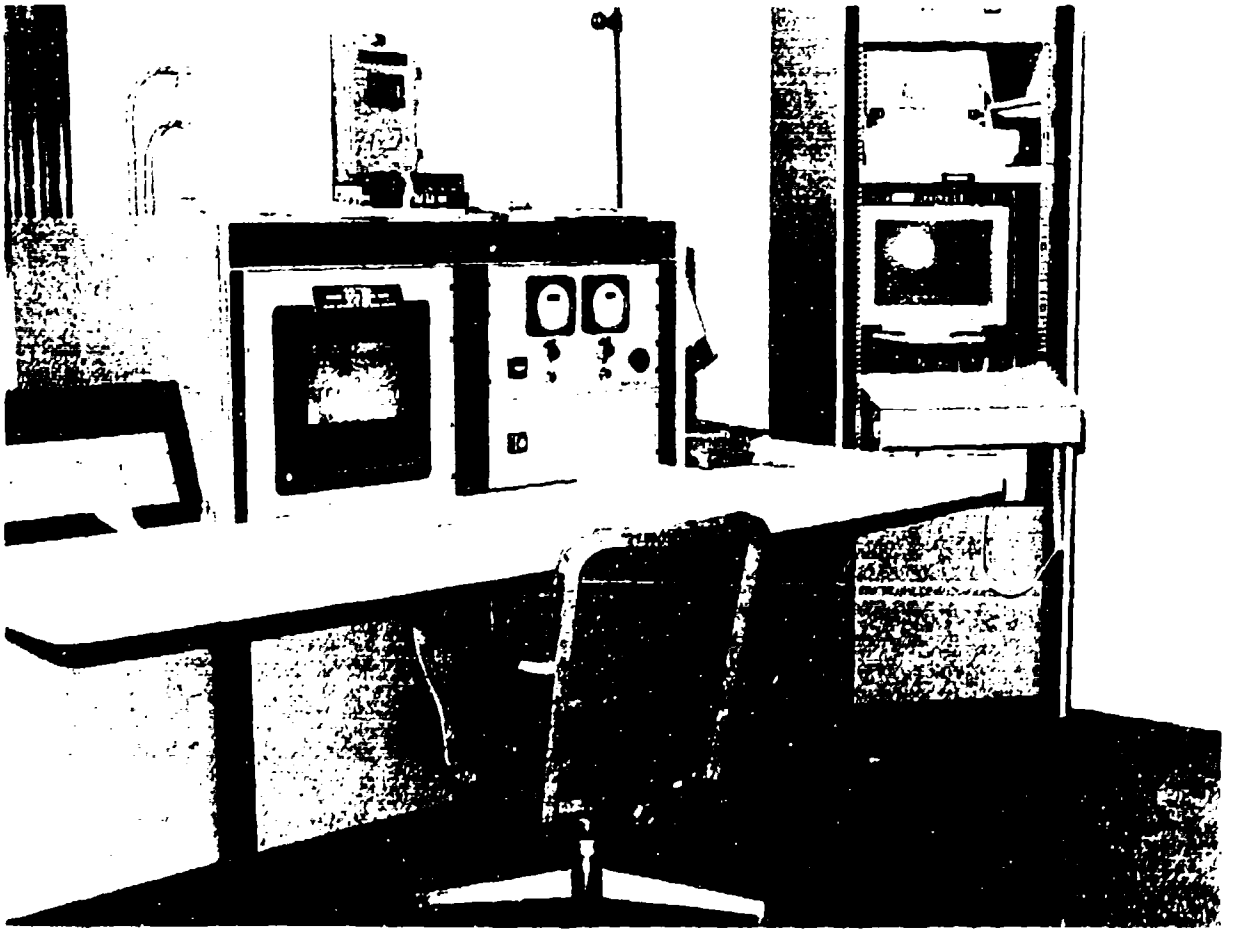

Figure 106. Operators Console

The 1/2 size ART test and dummy gearboxes were installed in the shaft and coupling test facility in a back-to-back configuration, as shown in Figure 107 and in the photograph of Figure 108. The test gearbox input shaft rotated clockwise, looking from the facility torquing gearbox toward the drive gearbox. Maintaining this perspective, both idler shafts rotated counter-clockwise with the output shaft rotating clockwise. In this configuration, the dummy gearbox components rotated backwards with the applied torque contacting the opposite side of the teeth. The opposite rotation and opposite side of the teeth contact put the loads on the dummy gearbox teeth back to the identical position of the test gearbox teeth. Thus all load magnitudes and directions were identical in the test and dummy gearboxes. To accommodate the test stand, each gearbox was installed on its side. The installed orientation had no effect on the development of the transmission components since the lube system was not part of the technology demonstration.

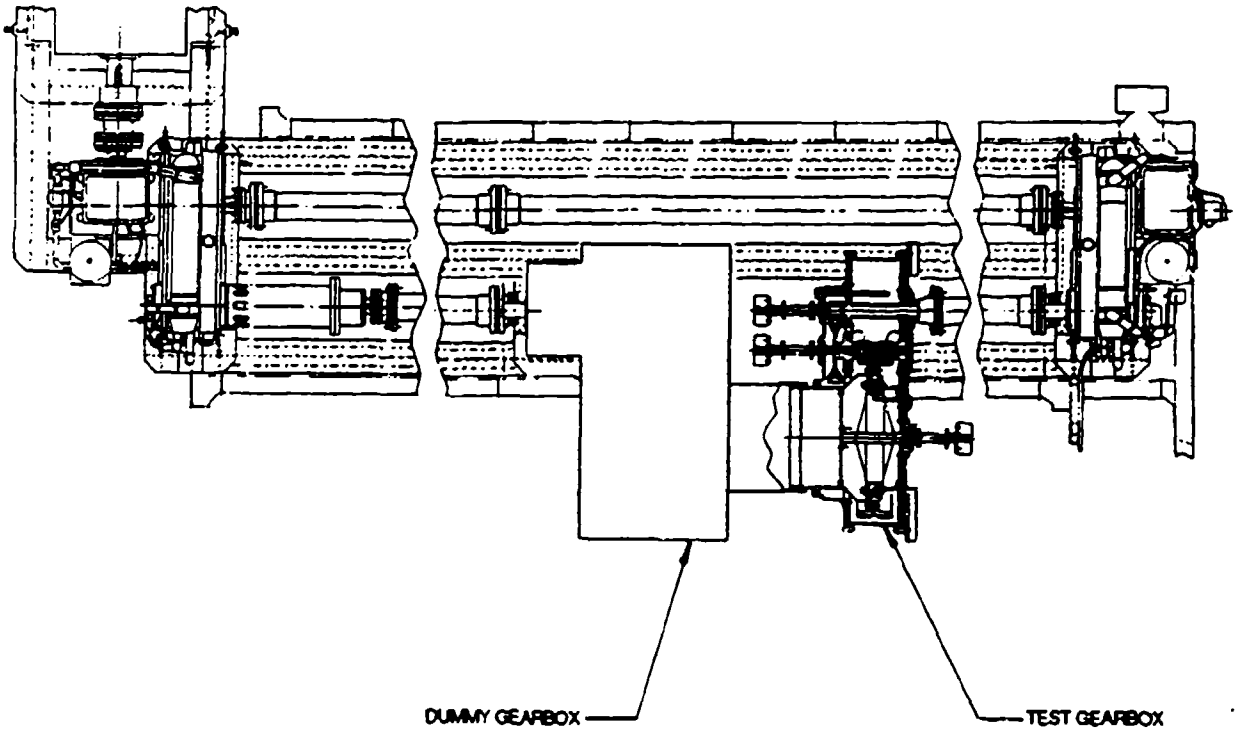

Figure 107. ART Test and Dummy Gearbox Installation

Figure 108. ART Gearbox Installation

Under full load conditions, the ART gearbox used only 32% of the torque the stand was capable of providing. At this reduced power level with respect to the stand capabilities, the gearbox could be run at 100% torque at speeds as low as 500 rpm. The ability to operate the gearbox at these low speeds allowed "quasi-static" data to be collected without resorting to static load application devices. Sleeve bearings in the torquing gearbox prevented further reductions in speed under full load conditions

The test and dummy gearboxes used independent lubrication systems. Each system contained a reservoir, pump and motor, relief valve, 3 micron filter with DP pressure indicator, water/oil heat exchanger, water regulating valve, and a scavenge pump. The test gearbox lube system also provided a thermostatically controlled sump oil heater. The heater was used to raise the oil inlet temperature for the test gearbox to simulate a helicopter gearbox temperature environment. Without the oil heater, temperatures generally ran below 130°F.

The 1/2 size ART gearbox had extensive instrumentation used for data acquisition during the test. Table 43 lists the instrumentation used.

The slip ring installation for the output double helical gear is shown in Figure 109 while the slip ring installation for the input pinion and the upper and lower spur gear/double helical pinion are shown in Figure 110. A view of the instrumentation console for the facility is shown in Figure 111. A photograph of the transmission error encoder installation is depicted in Figure 112.

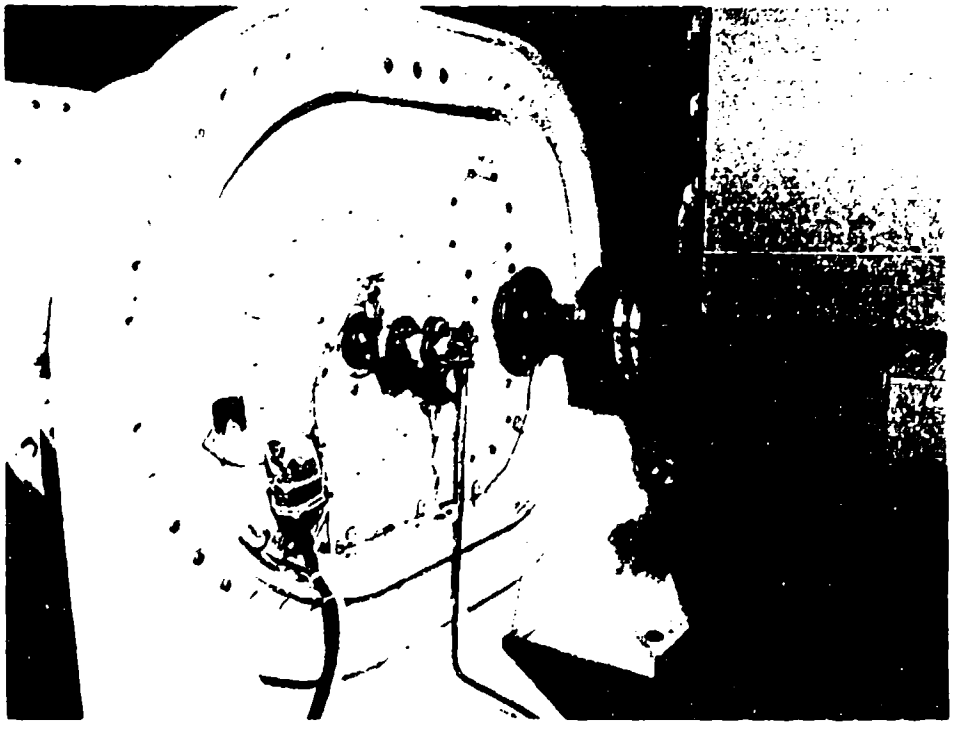

Figure 109. Slip Ring Installation, Double Helical Gear

Table 43. 1/2 Size Gearbox Instrumentation

Measurement	Locations	Qty
Temperature	All Bearings in Test & Dummy	9
	Oil In and Out, Test & Dummy	4
	041 Double Helical Pinion Tooth Roots	6
	042 Double Helical Pinion Tooth Roots	2
	041 Fling off oil	1
Pressure	Lube System Supply, Test & Dummy	2
Flow Rate	Lube System Supply, Test & Dummy	2
RPM	Test Stand Input Shaft	1
Torque	Test Stand Input (Himmelstein)	1
	Test D.H. Pinions (Strain Gage Bridge)	4
Vibration	Housing, Test & Dummy	9
Gear Strain	Input Spur Pinion Tooth Roots, Test	5
	Spur Gear Roots, 041, 042, Test	10
	D.H. Pinion Roots, 041, 042, Test	20
	D.H. Gear Roots, 041, 042, Test	10
Housing Strain	Upper Cover, Lower Cover, Side	9
Displacement	Axial Motion of Spur Gear/D.H. Pinion	2
Chip Detection	Test & Dummy Gearboxes	2
Trans Error	T.E. of Each Gear Mesh (4 meshes)	2

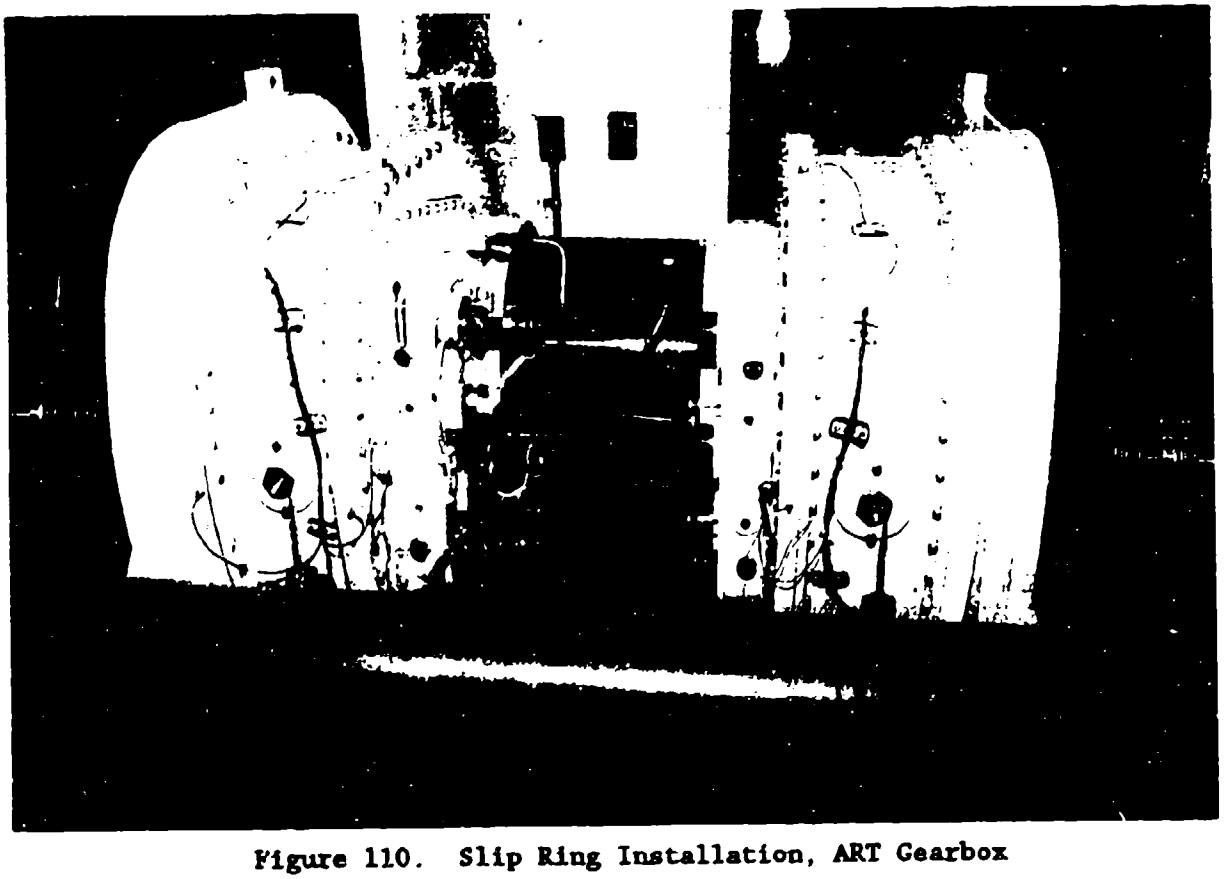

Figure 110. Slip Ring Installation, ART Gearbox

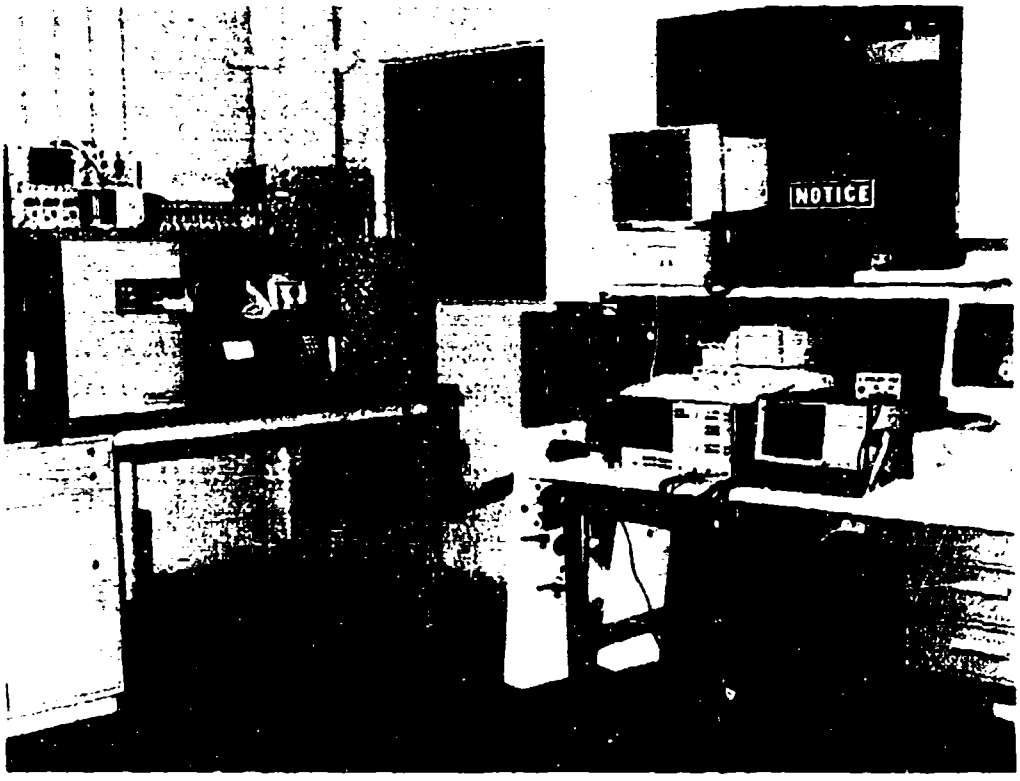

Figure 111. ART Instrumentation Console

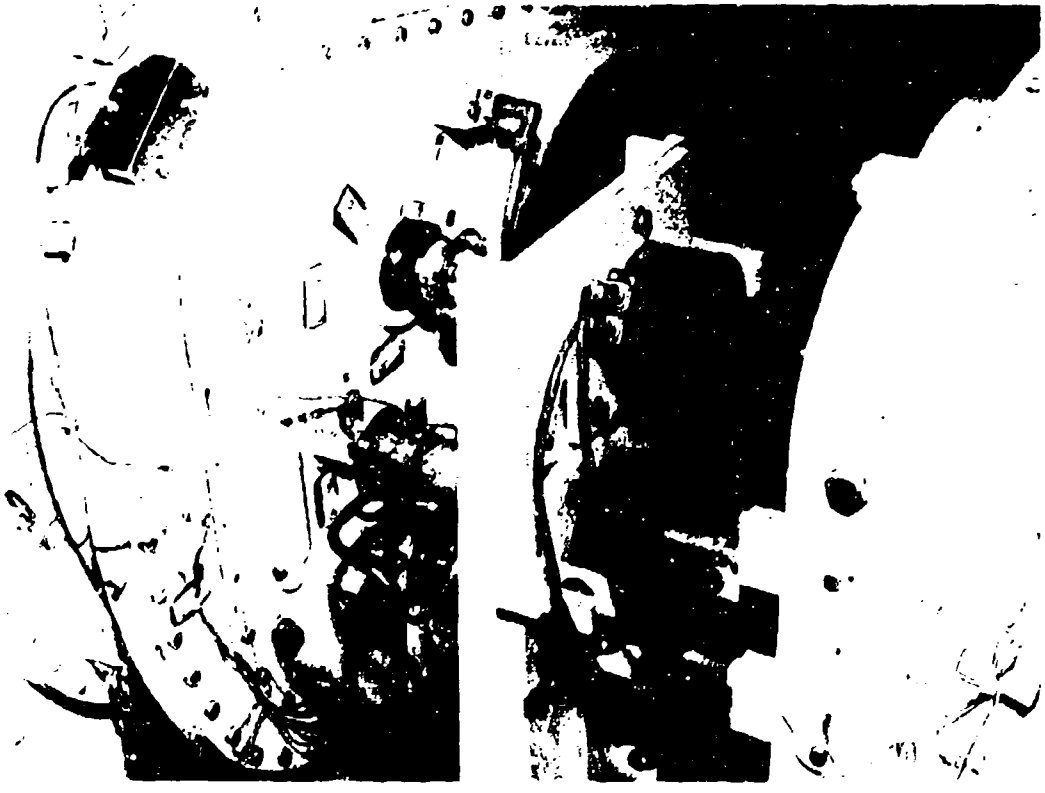

Figure 112. Transmission Error Encoder Installation

Bearing Test Facility/Instrumentation

A test machine was designed to conduct testing of the angular contact spherical roller bearing. All design and test work was accomplished at McGill Manufacturing Company, Valparaiso, Indiana. The test machine has the capability of applying simultaneous thrust and radial load at speeds to the full operating speed of 14280 rpm. The test equipment consists of a high speed induction motor capable of 40 HP at 15,000 rpm, a special spindle for holding the test bearing, load application devices for the thrust and radial loads, and instrumentation. A schematic of the facility is shown in Figure 113. A cross section of the test spindle which holds the test bearing is shown in Figure 114.

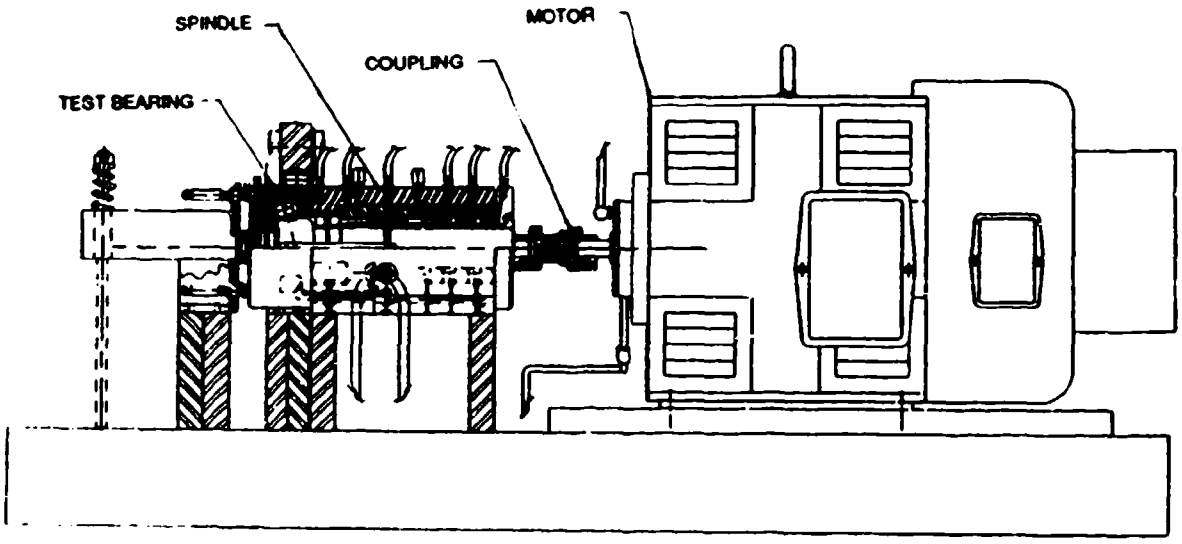

Figure 113. Schematic of Bearing Test Facility

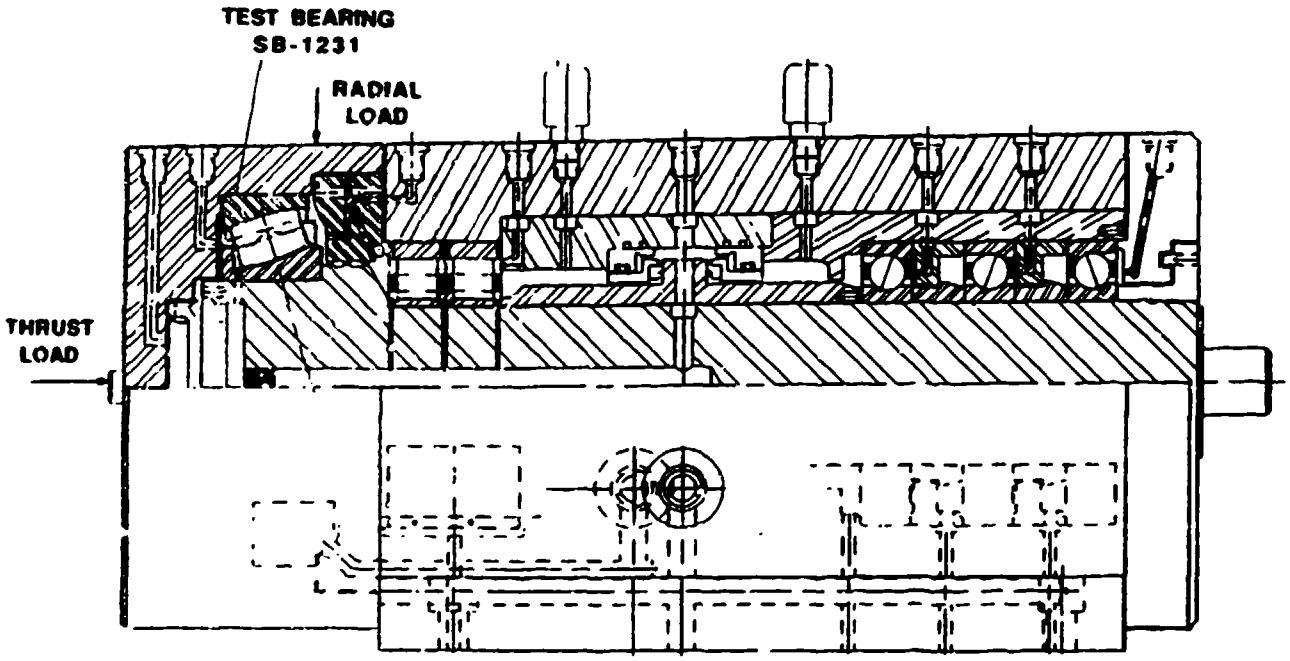

Figure 114. Bearing Test Facility Spindle

Automatic shutdown is provided for an overtorque or undertorque situation. The spindle and motor oil lubrication are separate systems. The coupling that joins the motor and spindle has internal shear pins to protect the spindle and motor from overtorque damage.

Radial load is applied vertically to the test bearing by a load arm system. The mechanical advantage of the radial arm is 3:1. Radial load is measured by strain gages mounted on the load arm and applied by a compressed, calibrated spring, which also serves to dampen any load fluctuations in the system. The load is applied through a hardened cylindrical roller to the test bearing housing which centers the load vertically, and provides an anti-friction method allowing the housing to rotate freely for torque measurements.

Thrust load is applied axially to the test bearing through a load arm with a 5:1 mechanical advantage located at the face of the housing. Load is applied through a thrust ball bearing to the housing, on the shaft and test bearing centerline. This serves to center the thrust load and offers a means of free rotation for torque measurements. Thrust is measured by strain gages on the load arm and a calibrated spring that applies load to the system.

Three load cells, positioned 120° apart, measure any moment loads from the test bearing. Each load cell is attached to a micrometer head for precise setting of a minimal preload. The three cells also stabilize the test bearing housing from any gimbaling movements. The load cells in conjunction with the load arm strain gages are designed to measure the decoupling forces during the test program.

The test bearing housing is restricted from rotation by a torque arm attached to the test housing. Calibrated strain gages attached to the torque arm and the rod connected to the test bed measure torque, and provide a means for determination of the coefficient of friction for this type of bearing.

Instrumentation for the facility and test bearing is listed in Table 44.

Table 44. Facility and Test Bearing Instrumentation

Measurement	Locations	Qty
Temperature	Test Bearing Outer Race	2
	Spindle Bearings	5
	Oil Inlet	1
	Oil Outlet	1
	Oil Sump	1
	Ambient Air	1
Pressure	Lube System Supply, Motor & Spindle	2
Flow Rate	Lube System Supply, Motor & Spindle	2
RPM	Spindle	1
Torque	Spindle Test Bearing	1
Axial Load	Load Arm Strain Gages	2
Radial Load	Load Arm Strain Gages	2
Vibration	Spindle Housing	2
Chip Detection	Spindle Oil Drain	1

Test Procedure

Material Test Procedure

A total of 20 fatigue fretting tests were conducted in accordance with the general procedures of ESM-K3-7016, Rev. 1, "Sikorsky Engineering Standard Method For Conducting Room Temperature Material Fatigue Tests on Sonntag SF-1-U Fatigue Machines" and also ASTM E466-82, "Constant Amplitude Axial Fatigue Tests of metallic Materials, Recommended Practice For". Prior to application of coupon fatigue loads, fretting pins were clamped against the coupon. Fretting pin contact stress was held constant at 15,000 psi for all tests. Fatigue loads were applied axially and were fully reversed (maximum/minimum stress ratio, R = -1). Loads of sinusoidal waveform and 30 Hz cycle frequency were employed for all tests. Peak loads were controlled to within 1 percent. Coupon fatigue loads and fretting pin loads were monitored at least twice daily to verify accuracy. Tests were run until fretting fatigue failure or 10 million cycle run out was achieved. Stroke limits were set to stop a

test prior to complete separation of a cracked coupon, so that fretting pins could be removed and minimize damage to the fretting scar. After pin removal, cracked coupons were broken statically to facilitate analysis of the fracture surfaces.

A total of five non-fretting fatigue tests, without fretting pins, were also conducted using the above procedures to develop additional fatigue baseline data.

Conventional metallurgical examinations were conducted on selected specimens to verify that the fatigue fracture was originated by the fretting. Fretting crack morphology was documented using standard techniques as well as with the scanning electron microscope.

1/2 Size Gearbox Test Procedure, No Load Lube

A no load lubrication survey was performed to evaluate lubrication characteristics of the test and dummy gearboxes at the conditions identified in Table 45. The initial series of test conditions (1-4) were performed with the test gearbox oil supplied at ambient temperature. The second series of test conditions (5-8) were performed with the test gearbox oil preheated to 185°F to simulate conditions representative of a state-of-the-art gearbox operating at rated power. No load lube surveys were conducted with the test and dummy gearboxes assembled in accordance with configuration #1 as shown previously in Table 40.

Table 45. No Load Lube Test Conditions

Test Condition	Input Speed rpm	Input Speed %Nr	Oil Inlet Temperature Test Gearbox	Oil Inlet Temperature Dummy Gear
1	1233	25%	70°F	70°F
2	2467	50%	70°F	70°F
3	3700	75%	70°F	70°F
4	4933	100%	70°F	70°F
5	1233	25%	185°F	70°F
6	2467	50%	185°F	70°F
7	3700	75%	185°F	70°F
8	4933	100%	185°F	70°F

The test stand was operated at each condition until gearbox bearing temperatures stabilized within ±2°F without exceeding a maximum allowable of 250°F. A Fluke data logger was used to monitor and record lubrication and bearing temperatures. Test and dummy gearbox housing vibration was recorded on magnetic tape. Tape speed was set at 30 in/sec providing a frequency response of 20 KHz.

1/2 Size Gearbox Test Procedure, Gear Pattern Development

A pattern development survey was performed to evaluate gear tooth contact patterns at each of the test conditions identified in Table 46. At the end of each incremental power condition, contact patterns were visually inspected through ports in the main housing and upper cover. In addition, gear strain distributions, recorded for the spur pinion and output double helical gear, were used to assist the evaluation of the observed patterns. The strain distribution of the spur gears and double helical pinions which were not strain gaged was assumed to be equal and opposite. All pattern surveys were conducted with the test and dummy gearboxes assembled in accordance with configuration #1 as shown previously in Table 40.

Table 46. Gear Pattern Development Test Conditions

Test Condition	Input Torque in-lbs	Input Torque %Torque	Test Duration Minutes	Input Speed rpm	Input Speed %Nr
1	0	0%	N/A(1)	4933	100%
2	2070	25%	10	4933	100%
3	4140	50%	10	4933	100%
4	6210	75%	10	4933	100%
5	8280	100%	10	4933	100%

Notes:

(1) A visual inspection of the gear patterns was performed following completion of all no load lubrication surveys, prior to application of any load.

To aid visual evaluation, several types of plating (0.0002 inch thick) were applied to consecutive teeth on the double helical pinions and spur gears of the test and dummy gearboxes. Plating types included silver, gold, copper, as well as black oxide coating. In addition, blueing was applied over several teeth of each type of plating.

If required, topological corrections of tooth geometry were to be applied upper/lower spur gear and the upper/lower double helical pinions. These gears were chosen for correction since each meshes with only one other gear and can therefore be modified without affecting the patterns generated at other mesh locations.

Pattern development surveys were performed with the test gearbox oil preheated to 185°F. Bearing temperatures were required to stay below a maximum allowable of 250°F. The Fluke data logger was used to monitor and record the parameters previously listed. Dynamic data was recorded on magnetic tape using two fourteen channel tape decks. Tape speed was set at 30 in/sec, providing a frequency response of 20 KHz. Parameters recorded on tape included:

Torque
Idler Shaft Torque, Upper (38072-35005-041)
Idler Shaft Torque, Lower (38072-35005-042)

Strain
Spur Pinion, 5 gages
Double Helical Gear, 10 gages

Acceleration
Upper Plate, 3 locations, Test Gearbox
Lower Plate, 3 locations, Test Gearbox
Upper Plate, 3 locations, Dummy Gearbox

1/2 Size Gearbox Test Procedure, Dynamic Surveys

Strain surveys were conducted at each of the conditions listed in Table 47 to evaluate:

a. Dynamic effects on gear tooth strain
b. Stress distribution across each gear tooth
c. Load sharing characteristics

The test and dummy gearboxes were assembled in accordance with configuration #1 as previously described in Table 40.

All dynamic surveys were performed with the test gearbox oil preheated to 185°F. Bearing temperatures were required to stay below a maximum of 250°F. The Fluke data logger was used to monitor lube and bearing temperatures. Data was recorded on magnetic tape using two, fourteen channel tape decks. Tape speed was set at 30 in/sec providing a frequency response of 20 KHz.

Parameters recorded on tape included:

Torque
Idler Shaft Torque, Upper (38072-35005-041)
Idler Shaft Torque, Lower (38072-35005-042)

Strain
Spur Pinion, 5 gages
Spur Gear 041, 5 gages
Spur Gear 042, 5 gages
Double Helical Pinion 041, 10 gages
Double Helical Pinion 042, 10 gages
Double Helical Gear, 10 gages

Strain gage output was recorded using slip rings installed on each shaft, however, the capacity of the slip rings was limited and not all gages were recorded concurrently.

Table 47. Strain Survey Test Conditions

Test Condition	Input Speed %	Input Speed rpm	Input Torque %	Input Torque in-lbs
1	~10%	500	0%	0
2	~10%	500	25%	2070
3	~10%	500	50%	4140
4	~10%	500	75%	6210
5	~10%	500	100%	8280
6	25%	1233	0%	0
7	25%	1233	25%	2070
8	25%	1233	50%	4140
9	25%	1233	75%	6210
10	25%	1233	100%	8280
11	50%	2467	0%	0
12	50%	2467	25%	2070
13	50%	2467	50%	4140
14	50%	2467	75%	6210
15	50%	2467	100%	8280
16	75%	3700	0%	0
17	75%	3700	25%	2070
18	75%	3700	50%	4140
19	75%	3700	75%	6210
20	75%	3700	100%	8280
21	100%	4933	0%	0
22	100%	4933	25%	2070
23	100%	4933	50%	4140
24	100%	4933	75%	6210
25	100%	4933	100%	8280
26	120%	5920	0%	0
27	120%	5920	25%	2070
28	120%	5920	50%	4140
29	120%	5920	75%	6210
30	120%	5920	100%	8280

Dynamic load sharing surveys were also conducted with the elastomeric load sharing devices replaced with steel members. The gearboxes conformed to configuration #2 as shown previously in Table 40. Load sharing was evaluated by direct comparison of the torque bridge outputs for each of the conditions outlined in Table 48.

Table 48. Load Sharing Survey Test Conditions - Steel

Test Condition	Input Torque in-lbs	Input Torque %Torque	Test Duration Minutes	Input Speed rpm	Input Speed %Nr
1	0	0%	N/A	4933	100%
2	2070	25%	10	4933	100%
3	4140	50%	10	4933	100%
4	6210	75%	10	4933	100%
5	8280	100%	10	4933	100%

Transmission error measurements were obtained under dynamic conditions for the spur pinion and each mating gear (041 and 042) as well as for the double helical gear and each of its mating pinions (041 and 042). Testing was initially performed with the steel load sharing devices installed in the gearbox (configuration #2) and then repeated with the elastomeric load sharing devices installed (configuration #3). Each mesh survey included speed sweeps (rpm order tracking) at a variety of steady torques as shown in Table 49.

Table 49. Transmission Error Survey Test Conditions

	Sweep Range 100%=4933 rpm	Torque 100%=8280 in-lbs
Spur Mesh		
a. Elastomeric	25 - 40% Nr	25, 50, 75, & 100%
b. Steel	30 - 50% Nr	25, 50, 75, & 100%
Double Helical Mesh		
a. Elastomeric	50 - 100% Nr	25, 50, 75, & 90%
b. Steel	50 - 100% Nr	25, 50, 75, & 90%

The speed and torque ranges used were determined by the operating limitations of the Ono Sokki equipment used and the location of resonant frequencies found in the encoder installations of the ART gearbox. T.E. data was not acquired at 0% torque for any mesh because the T.E. signals were unstable in the unloaded condition.

In addition to the speed sweeps performed, a limited amount of steady state data was also recorded at several locations and conditions including (a) the lower spur gear mesh (spur pinion mating with the 042 spur gear) in the elastomeric configuration at 1300 and 2000 rpm for 25, 50, 75, and 100% torque, (b) the upper spur mesh (spur pinion mating with 041 spur gear) in the steel configuration at 1300, 1500, and 2000 rpm for 25, 50, 75, and 100% torque, and (c) both the upper and lower double helical mesh in the elastomeric configuration at 2400 and 4933 rpm for 25, 50, 75, 90, and 100% torque.

During speed sweeps, vibration data was simultaneously acquired with TE data using the accelerometers mounted on the ART test box. The rotary encoders were mounted on specially designed support fixtures as shown in the facilities section of the report (See Figure 112). One encoder was mounted to the shaft of the pinion and one to the shaft of the gear of the mesh which was being

measured. The support fixtures facilitated alignment by providing vertical, lateral, and angular adjustment at each position. Shafts were installed between each encoder and the gearbox and connected at each end using a single laminate of a Thomas coupling. The single laminate coupling provided low bending stiffness but high torsional stiffness to reduce shaft bending and runout at high speeds. This approach reduced the radial vibration and misalignment loads transmitted to the encoders helping to ensure reliable TE measurements. Precise shaft speed measurements were obtained by mounting a photoelectric detector at the input shaft on the dummy gearbox.

The majority of the TE measurements were obtained using Ono Sokki Method A, shown schematically in Figure 115. For Method A, the square wave encoder output signals are input to the TE-700D, digitally adjusted in the real time by a ratio multiplier, and normalized by dividing each signal by the number of teeth on the contrary gear (i.e., signal Z1 is divided by the number of teeth on gear 2 and visa versa). The normalized encoder signals are then input to the transient torsional angle converter (PD-860) to determine the relative phase difference between the two signals and thus obtain an analog output signal proportional to the gear mesh transmission error. This analog output signal can then be displayed and analyzed on the CF-880 8 channel tracking Fast Fourier Transform (FFT) analyzer.

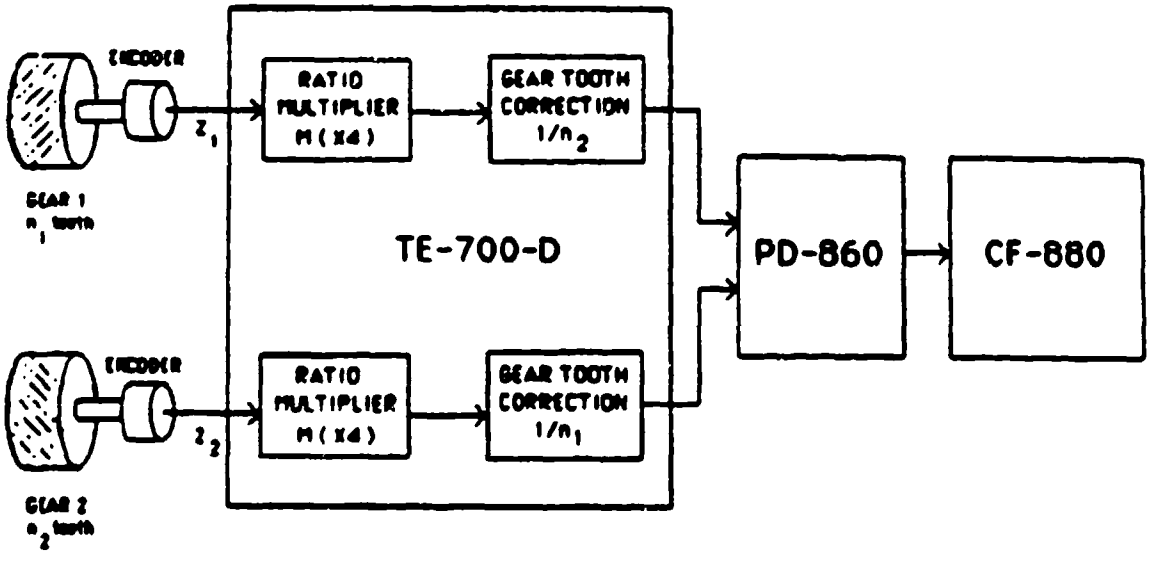

Figure 115. Transmission Error, Method A

The trade off between rpm range and resolution/sampling rate can pose a problem for high speed gear meshes with large numbers of gear teeth such as the input spur meshes on the ART gearbox where N1=26 and N2=101. Hence, although Method A TE measurements could be obtained up to a full rated speed for the double helical gear meshing the ART test gearbox, TE measurements for the spur meshes were limited to just over 50% (2600 rpm) of full rated speed and a sampling rate of only 4.5 samples per tooth mesh with a multiplier ratio of 2. The ratio multiplier was limited to 2 for the spur gear mesh TE measurements on the steel configuration because of the shaft vibration levels encountered with the ART test box installation. However, a ratio multiplier of 4 was achieved for the spur gear meshes in the elastomeric configuration.

The Ono Sokki TE measurements system has two other measurement systems designed to address the limitations of Method A. Both of these methods improve resolution and sampling rate but sacrifice rpm range and induce other problems. These methods were tried but proved unsuitable for the rpm order tracking data acquisition mode employed for TE testing on the ART gearbox.

A housing strain survey was conducted at each condition identified in Table 50 to determine the magnitude and direction of the principle strain. The locations were chosen based on the maximum strain calculated in the finite element modeling conducted during the detail design phase. The strain survey was performed with the test and dummy gearboxes assembled in accordance with configuration #4 previously described in Table 40. Strain data was recorded on magnetic tape. Tape speed was set at 30 in/sec providing a frequency response of 20 KHz.

Table 50. Housing Strain Survey Test Conditions

Test	Input Sped		Input Torque	
Condition	%	rpm	%	in-lbs
1	100%	4933	25%	2070
2	100%	4933	50%	4140
3	100%	4933	75%	6210
4	100%	4933	100%	8280

1/2 Size Gearbox Test Procedure, 200 Hour Endurance

A 200 hour endurance test was performed to evaluate the long term performance capability of the transmission. The endurance test included 40 cycles of the 5 hour spectrum presented in Table 51. The test and dummy gearboxes were assembled in accordance with configuration #4 as described previously in Table 40.

Table 51. Endurance Test Spectrum

Test	%	Torque	HP	Time		Input Speed
Cond	Torque	(ft-lb)	(ref)	(%)	(min)	(rpm)
1	55%	379	356	19%	57	4,933
2	75%	518	486	21%	63	4,933
3	100%	690	648	5%	15	4,933
4	65%	448	421	30%	90	4,933
5	95%	656	616	4%	12	4,933
6	75%	518	486	21%	63	4,933
		Totals		100%	300 Minutes	

Endurance testing was performed with the lube oil preheated to maintain an oil temperature of 185 ± 10°F on the test gearbox. Although the inlet oil on the dummy gearbox was not heated during this test, the reservoir temperature did increase when the gearboxes were operated over a long durations. Typical inlet temperatures of the dummy gearbox remained between 105 and 115°F.

The Fluke data logger was used to monitor rpm, torque, oil temperature,in and out, pressure, flow, and bearing race temperatures. Additional parameters listed below were recorded on magnetic tape. Tape data consisted of one minute records during conditions 1, 3, and 6 of each cycle of the endurance test. Monitored parameters included:

Torque
Spur Gear/D.H Pinion Shaft Torque (Upper, 041)
Spur Gear/D.H Pinion Shaft Torque (Lower, 042)

Vibration
Test Gearbox, Upper Plate, Vertical, Lateral, and Longitudinal
Test Gearbox, Lower Plate, Vertical, Lateral, and Longitudinal
Dummy Gearbox, Upper Plate, Vertical, Lateral, and Longitudinal

Strain
Spur Pinion, 5 gages
Spur Gear, 2 gages (041), 3 gages (042)
Double Helical Pinion, 2 gages (041), 2 gages (042)
Double Helical Gear, 2 gages

Strain gage outputs were recorded using slip rings installed on each shaft, however, because of the limited capacity of the slip rings, not all strain gages were recorded.

Gearbox inspections were performed after the first cycle (5 hours), 10th cycle (50 hours), 20th cycle (100 hours), and the 30th cycle (150 hours). These inspections included the following:

(a) Removal and inspection of the chip detector

(b) Visual inspection of the condition of each gear

Following completion of the endurance test, each gearbox was disassembled to allow inspection of all internal components for signs of wear, damage, cracks, etc. Bearing races and rolling elements were checked for evidence of "skidding", spalling, overheating, etc. The observed condition of all major components which showed evidence of deterioration were documented with sketches and/or photographs. Major components were subjected to a magnaflux crack inspection.

1/2 Size Gearbox Test Procedure, 200 Hour Overtorque

A 200 hour overtorque development test was performed to address the problems experienced during the endurance test and to continue to evaluate the long term performance capability of the transmission. The development test consisted of 40 cycles of the 5 hour spectrum presented in Table 52. The test and dummy gearboxes were assembled in accordance with configuration #5 described previously in Table 40.

Table 52. Overtorque Development Test Spectrum

Test Cond	% Torque	Torque (ft-lb)	HP (ref)	Time (%)	Time (min)	Input Speed (rpm)
1	60%	4,970	389	20%	60	4,933
2	85%	7,040	551	40%	120	4,933
3	100%	8,280	648	10%	30	4,933
4	75%	6,210	486	20%	60	4,933
5	120%	9,940	778	10%	30	4,933
		Totals 100%	300 Minutes			

Development testing was performed with Mobil SHC-629 oil. This lubricant provided increased viscosity over the DOD-L-85734 oil used during the endurance testing. The oil was preheated to maintain an oil inlet temperature of 185 ± 10°F on the test gearbox. Although the inlet oil on the dummy gearbox was not heated during this test, the reservoir temperature increased when the gearboxes were operated over long durations. Typical oil inlet temperatures of the dummy gearbox remained between 105 - 115°F.

The Fluke data logger was used to monitor rpm, torque, oil temperature in and out, pressure, flow, bearing race temperatures, temperature across the face of the double helical pinions, and oil fling off temperature on the upper double helical mesh. Additional parameters listed below were recorded on magnetic tape. Tape data consisted of one minute records during conditions 1, 3, and 5 of each cycle of the endurance test. Monitored parameters included:

Torque
Spur Gear/D.H Pinion Shaft Torque (Upper, 041)
Spur Gear/D.H Pinion Shaft Torque (Lower, 042)

Vibration
Test Gearbox, Upper Plate, Vertical, Lateral, and Longitudinal
Test Gearbox, Lower Plate, Vertical, Lateral, and Longitudinal
Dummy Gearbox, Upper Plate, Vertical, Lateral, and Longitudinal

Gearbox inspections were performed after the first cycle (5 hours), 10th cycle (50 hours), 20th cycle (100 hours), and the 30th cycle (150 hours). These inspections included the following:

(a) Removal and inspection of the chip detector

(b) Visual inspection of the condition of each gear

Following completion of the overtorque development test, each gearbox was disassembled to allow inspection of all internal components for signs of wear, damage, cracks, etc. Bearing races and rolling elements were checked for evidence of "skidding", spalling, overheating, etc. The observed condition of all major components which showed evidence of deterioration were documented with sketches and/or photographs. Major components were subjected to a magnaflux crack inspection.

Bearing Test Procedure

A series of preliminary tests were performed to obtain initial operating data for the angular contact spherical roller bearing at varying loads and speeds. The Bearing with steel rollers was assembled into the test stand in the condition for set-up #1 as specified in Table 53.

Table 53. Bearing Test Set-Up Conditions

Set-up #	Set-up Condition	Type of Load
1	5-10 lb preload	Radial & Thrust
2	.002/.004 in endplay	Radial
3	.008/.010 in endplay	Radial
4	.014/.016 in endplay	Radial
5	5-10 lb preload	Thrust

Tests were then conducted using the bearing with steel rollers for each set up condition listed in Table 53 at each of the loads and speeds shown in Table 54. The entire survey test was then repeated using the angular contact spherical roller bearing with ceramic rollers.

To set the oil flow conditions for the bearing, the flow was initially set at 0.5 gpm through the rotating shaft and at 0.125 gpm from each oil jet directing oil into the roller retainer area on both sides of the bearing. Oil pressure at the manifold was 60 psi. At the 100% load and speed condition, the flow rate was adjusted to achieve the lowest bearing operating temperature. The remainder of testing was then conducted at the established flow rate.

For each condition, the following data was recorded:

Bearing temperature, 2 locations
Oil inlet temperature
Oil outlet temperature
Oil flow rate, 3 locations
Axial force on load arm
Radial force on load arm
Torque on load arm
rpm

Table 54. Test Survey Loads and Speeds

Sequence	Test Load %	Radial	Thrust	Speed %	rpm
1	0%	0	0	25%	3,600
	0%	0	0	50%	7,200
	0%	0	0	75%	10,800
	0%	0	0	100%	14,400
2	25%	1,150	725	25%	3,600
	25%	1,150	725	50%	7,200
	25%	1,150	725	75%	10,800
	25%	1,150	725	100%	14,400
3	50%	2,300	1,450	25%	3,600
	50%	2,300	1,450	50%	7,200
	50%	2,300	1,450	75%	10,800
	50%	2,300	1,450	100%	14,400
4	75%	3,450	2,175	25%	3,600
	75%	3,450	2,175	50%	7,200
	75%	3,450	2,175	75%	10,800
	75%	3,450	2,175	100%	14,400
5	100%	4,600	2,900	25%	3,600
	100%	4,600	2,900	50%	7,200
	100%	4,600	2,900	75%	10,800
	100%	4,600	2,900	100%	14,400

A new bearing with steel rollers was mounted in the test spindle housing with a 5-10 pound preload applied by the load cells. The oil sump was preheated to 150°F. The loads and speeds were gradually increased to the 100% condition at 14,400 rpm with 4,600 pound radial load and 2,900 pound thrust load. Testing was then conducted for 250 hours at the 100% load and speed condition. The same data was monitored throughout the 250 hour test as was monitored in the survey testing shown above.

A new angular contact spherical roller bearing with ceramic rollers was then assembled into the test stand and the 250 hour test as described above was repeated for the ceramic bearing.

The angular contact spherical roller bearing with steel rollers from the initial survey testing was then reinstalled in the test spindle housing for purposes of conducting no oil survivability tests. The bearing was operated at 100% load and speed as in the 250 hour proof test. After the bearing temperature had stabilized, the oil was shut off to the test bearing at all three oil inlet locations. Simultaneously, the valve was closed in the outlet line from the test bearing to the scavenging pump and a drain was provided. The loads were reduced to 2,415 pounds radial and 1,525 pounds axial (52.5%) to represent the minimum power required to sustain level flight in a helicopter. Bearing temperature and torque were continuously monitored. The test

was stopped when the drag torque increased to a level sufficient to stop the motor. Other planned test stoppages that were not reached were 850°F bearing temperature and 60 minutes of operation.

The angular contact spherical roller bearing with ceramic rollers used in the preliminary survey tests was then mounted in the test spindle housing and the no oil survivability test repeated.

Test Results

Material Test Results

A summary of fretting fatigue test results is presented in Table 55. Fretting fatigue curves for polished and thin dense chrome (TDC) plated conditions are shown in Figure 116.

Table 55. Fretting Fatigue Test Summary

Test No.	Spec S/N	Specimen Condition	Vibratory Stress (KSI)	Test Cycles (Millions)	Comments
1	1	Polished	20	10.000	Runout
2	1	Polished	30	0.854	Prior Test #1, See Note (1)
3	2	Polished	30	0.594	
4	4	Polished	30	1.182	
5	6	Polished	25	0.390	
6	8	Polished	25	8.740	
7	5	TDC Plated	40	0.282	
8	21	TDC Plated	30	1.010	
9	19	TDC Plated	25	3.834	
10	11	TDC Plated	20	10.000	Runout
11*	11	TDC Plated	60	0.534	*Non fret. test (from #10)
12	10	Polished	60	0.118	Obser. Slip 70-105 Microns
13	3	TDC Plated	60	0.067	Obser. Slip 70-105 Microns
14	15	TDC Plated	30	1.730	No Slip Observed
15	7	TDC Plated	40	0.370	No Slip Observed
16	9	TDC Plated	25	8.974	No Slip Observed
17*	14	Polished	60	10.000	*Non Fret. Test, Runout
18*	14	Polished	90	0.214	*Non Fret. Test, (From #17)
19*	12	TDC Plated	70	3.176	*Non Fret. Test, (Grip Fail.
20	13	TDC Plated	25	9.467	No Slip Observed
21	18	Polished	40	0.401	No Slip Observed
22	20	Polished	40	0.294	No Slip Observed
23	22	Polished	25	8.428	No Slip Observed
24	17	TDC Plated	30	0.611	No Slip Observed
25*	16	Polished	75	0.490	*Non Fret. Test

Notes:

(1) Test #1 and #2 combined to give an equivalent point of 21.574 KSI and 10.854 million cycles.

All curves and curve shapes are derived using standard Sikorsky fatigue methodology for steel with fretting. The fretting fatigue data points at the 60 KSI level were not included in the mean curve calculations since they were below the 0.2 million minimum cycles recommended for application of standard curve shapes. Polished Coupon #1 test points were combined into an equivalent fracture point at the total number of cycles by finding an equivalent vibratory stress. The equivalent stress is calculated by finding the endurance limit for each test point individually using the standard curve shape for steel with fretting, finding the average, and then calculating the stress at the total combined number of cycles for the average curve.

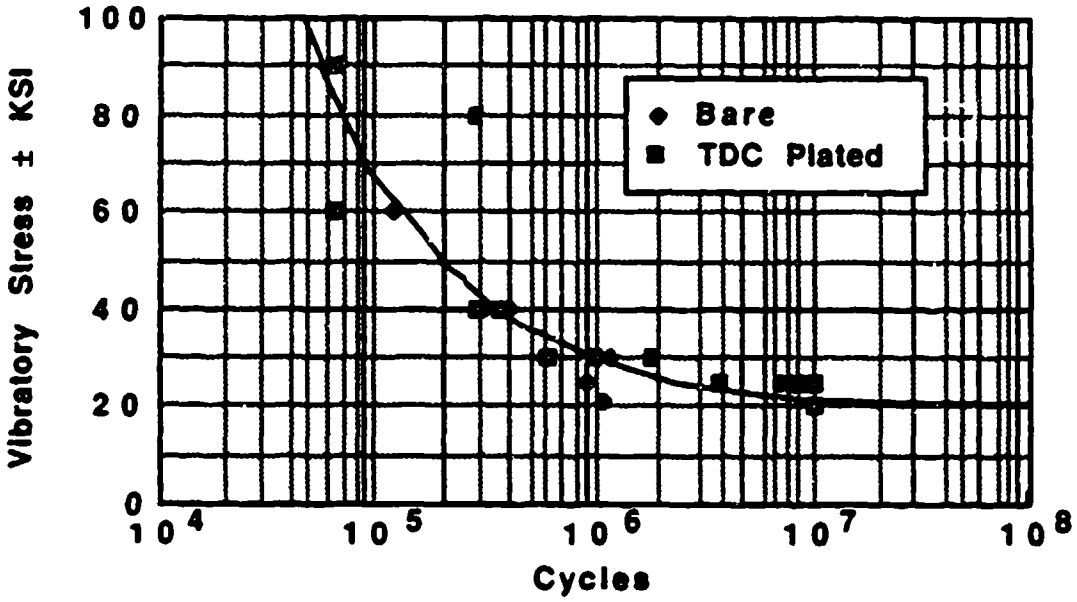

Figure 116. Fretting Fatigue S-N Curve for TDC Plated Pyrowear

No measurable slip was observed during fretting fatigue tests except at the 60 KSI stress level where approximately 70-105 microns peak-to-peak slip amplitude was observed for both polished and TDC plated conditions. Also, rust colored fretting debris was observed to be expelled from beneath the pin during testing, particularly for the polished coupons.

Metallurgical examination of fractured specimens confirmed that fatigue origins were at the fretting interface.

In Figure 116, one curve shape has been drawn through both sets of data. This is because the curves for polished and TDC specimens are essentially on top of each other. Thus no discernible difference was found between polished and TDC plated conditions. Data scatter is equivalent for both curves. The overall scatter (coefficient of variation) in the fatigue data indicates a reasonable fit of the standard curve shape parameters for the polished and for the TDC specimens.

The fretting fatigue strength for Pyrowear 53 for both conditions is comparable to Sikorsky data for 150 KSI steel. The Pyrowear 53 data in fact falls slightly above the 150 KSI data which is likely related to the slightly higher tensile strength of the Pyrowear 53 coupons (approximately 175 KSI). Comparison with high cycle fatigue strength shows an approximate 74% reduction in mean fatigue strength of polished Pyrowear 53 coupons due to fretting. This is comparable to Sikorsky fretting results for carburized AISI 9310 steel.

1/2 Size Gearbox Test Results, No Load Lube

The no load lubrication survey was completed in accordance with the procedure discussed above. Initial surveys, performed with the lube oil supply at ambient temperature, were completed without difficulty. Bearing temperature stabilized to within ±2°F at the completion of each test condition at temperatures well below the allowable maximum of 250°F. A summary of stabilized lube oil and bearing temperatures is presented below in Table 56.

Table 56. No Load Lube Test Results, Ambient Temperature (°F)

Test Gearbox Thermocouple Locations	Input Speed (%Nr) 25%	50%	75%	100%
Lube Oil Inlet	67.2	91.4	97.0	102.5
Lube Oil Outlet	87.2	91.4	97.0	103.8
Input Shaft, Upper Cover Roller Brg	87.9	94.1	101.9	109.1
Input Shaft, Lower Cover Ball Brg	86.2	91.3	97.2	103.2
041 Idler Shaft, Upr Cvr Roller Brg	86.0	91.4	97.8	104.0
041 Idler Shaft, Lwr Cvr Roller Brg	85.2	98.8	95.6	101.0
042 Idler Shaft, Upr Cvr Roller Brg	87.8	92.9	99.5	105.9
042 Idler Shaft, Lwr Cvr Roller Brg	87.7	94.0	100.5	107.9
Output Gear, Upper Timken Brg	86.9	92.2	99.4	106.5
Output Gear, Lower Timken Brg	85.9	91.1	98.1	105.5
Output Gear, Instr. Ball Brg	76.2	80.8	85.9	89.8

Dummy Gearbox Thermocouple Locations	Input Speed (%Nr) 25%	50%	75%	100%
Lube Oil Inlet	79.9	86.2	93.0	99.6
Lube Oil Outlet	80.2	87.1	94.6	101.9
Input Shaft, Upper Cover Roller Brg	80.1	87.1	94.7	101.9
Input Shaft, Lower Cover Ball Brg	80.5	88.7	96.3	103.7
041 Idler Shaft, Upr Cvr Roller Brg	80.4	87.5	95.2	103.2
041 Idler Shaft, Lwr Cvr Roller Brg	79.9	86.6	93.7	100.4
042 Idler Shaft, Upr Cvr Roller Brg	80.7	87.8	94.9	102.3
042 Idler Shaft, Lwr Cvr Roller Brg	79.8	86.3	92.9	99.6
Output Gear, Upper Timken Brg	80.4	90.2	100.2	109.8
Output Gear, Lower Timken Brg	79.6	89.2	98.7	108.6

Following the ambient temperature survey, an additional survey was performed with the test gearbox oil supply preheated to 185°F. Bearing temperatures were stabilized within ±2°F at the completion of each ten minute test condition. All bearings stabilized well below the maximum allowable of 250°F. Successful completion of this survey indicated that the gearbox would operate satisfactorily at higher power conditions. A summary of the stabilized lube oil and bearing temperatures observed is presented in Table 57.

Table 57. No Load Lube Test Results, Elevated Temperature (°F)

Test Gearbox Thermocouple Locations	Input Speed (%Nr) 25%	50%	75%	100%
Lube Oil Inlet	169.0	170.4	171.2	172.3
Lube Oil Outlet	165.1	165.5	166.3	167.8
Input Shaft, Upper Cover Roller Brg	167.6	169.9	172.0	174.4
Input Shaft, Lower Cover Ball Brg	163.5	164.0	162.7	162.0
041 Idler Shaft, Upr Cvr Roller Brg	161.0	164.9	167.9	169.8
041 Idler Shaft, Lwr Cvr Roller Brg	159.6	158.9	158.5	159.3
042 Idler Shaft, Upr Cvr Roller Brg	167.6	169.5	171.0	172.9
042 Idler Shaft, Lwr Cvr Roller Brg	166.6	168.3	169.0	170.4
Output Gear, Upper Timken Brg	166.4	166.8	168.3	169.8
Output Gear, Lower Timken Brg	162.6	164.1	166.6	167.6
Output Gear, Instr Ball Brg	113.0	113.5	114.1	115.4

Dummy Gearbox Thermocouple Locations	Input Speed (%Nr) 25%	50%	75%	100%
Lube Oil Inlet	84.1	87.8	90.9	95.4
Lube Oil Outlet	85.0	89.9	93.9	99.5
Input Shaft, Upper Cover Roller Brg	84.1	89.1	92.9	99.0
Input Shaft, Lower Cover Ball Brg	83.8	89.8	95.5	101.8
041 Idler Shaft, Upr Cvr Roller Brg	84.6	89.4	93.4	101.1
041 Idler Shaft, Lwr Cvr Roller Brg	83.7	88.3	92.1	97.1
042 Idler Shaft, Upr Cvr Roller Brg	85.2	89.8	93.0	99.0
042 Idler Shaft, Lwr Cvr Roller Brg	83.4	87.7	91.4	96.7
Output Gear, Upper Timken Brg	87.6	98.1	103.7	110.8
Output Gear, Lower Timken Brg	85.2	94.1	99.8	107.3

Under no load conditions, the amount of heat generated within the test gearbox was extremely small. At elevated temperatures, the gearbox acted as a heat sink, evidenced by the fact that the oil inlet temperature was higher than the oil outlet temperature. The gearbox rejected more heat, radiated into the test cell, than the facility lube oil preheater was capable of generating. As a result, the oil inlet temperature fell approximately 15°F below the desired set point of 185°F at the completion of each survey.

Vibration levels increased slightly with increasing speed, however, all levels were considered low during no load surveys. A typical power spectrum of the vibration experienced on the upper cover of the test gearbox, in the vertical and lateral direction, at 100% Nr is presented in Figure 117 as an example.

1/2 Size Gearbox Test Results, Gear Pattern Development

Gear pattern development began after successful completion of the no-load lube tests. Patterns were generated by operating the gearbox at increasing power levels in accordance with the procedure outlined above. Pattern inspections were conducted at the end of each incremental power condition but were difficult to perform even with the assistance of a boroscope. As a result, the gearboxes, both test and dummy, were disassembled for detail pattern inspection prior to committing to the 100% power condition. Load sharing observed during these initial tests was within 2% as documented in Figure 118. Vibration levels increased slightly with increasing power, however, all levels were considered low. A typical power spectrum of the vibration experienced on the upper cover of the test gearbox in the vertical and lateral direction at 100% Nr, and 75% torque is presented in Figure 119 as an example.

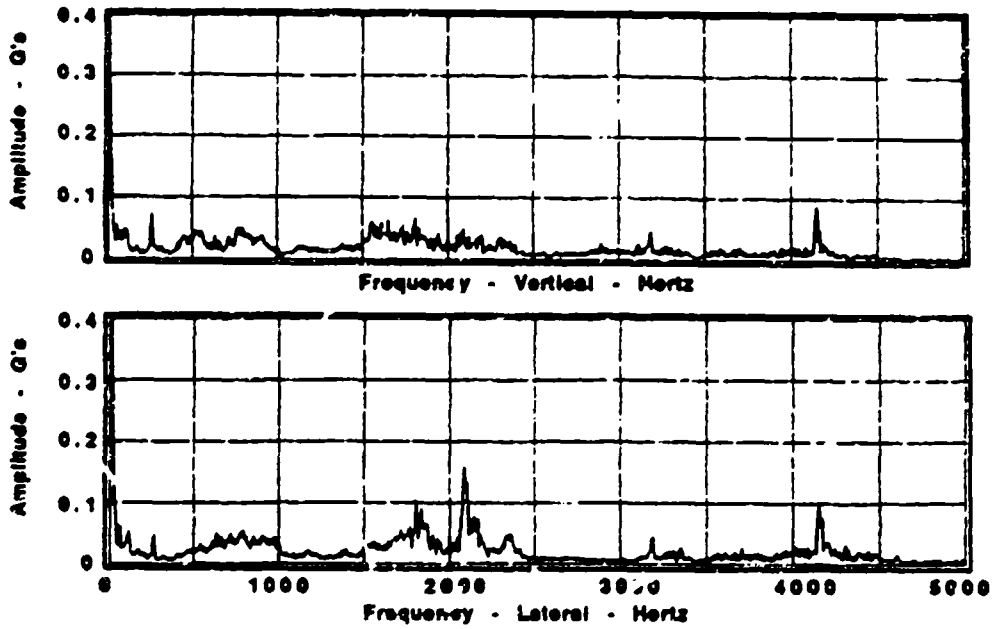

Figure 117. Typical Vibration Signature, No Load

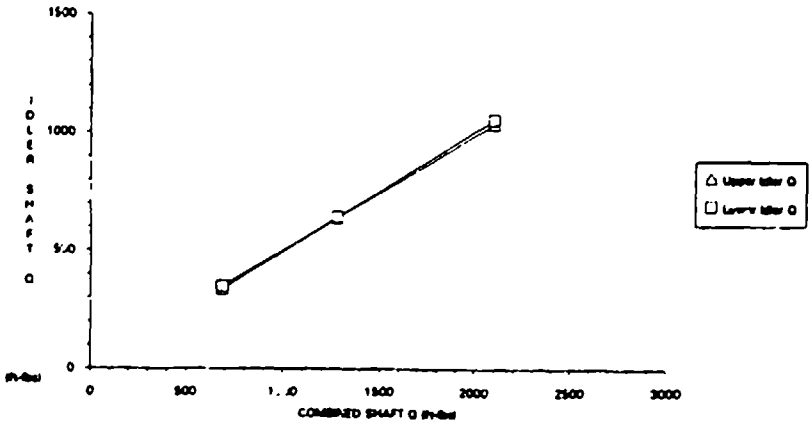

Figure 118. Load Sharing, Initial Pattern Development Survey

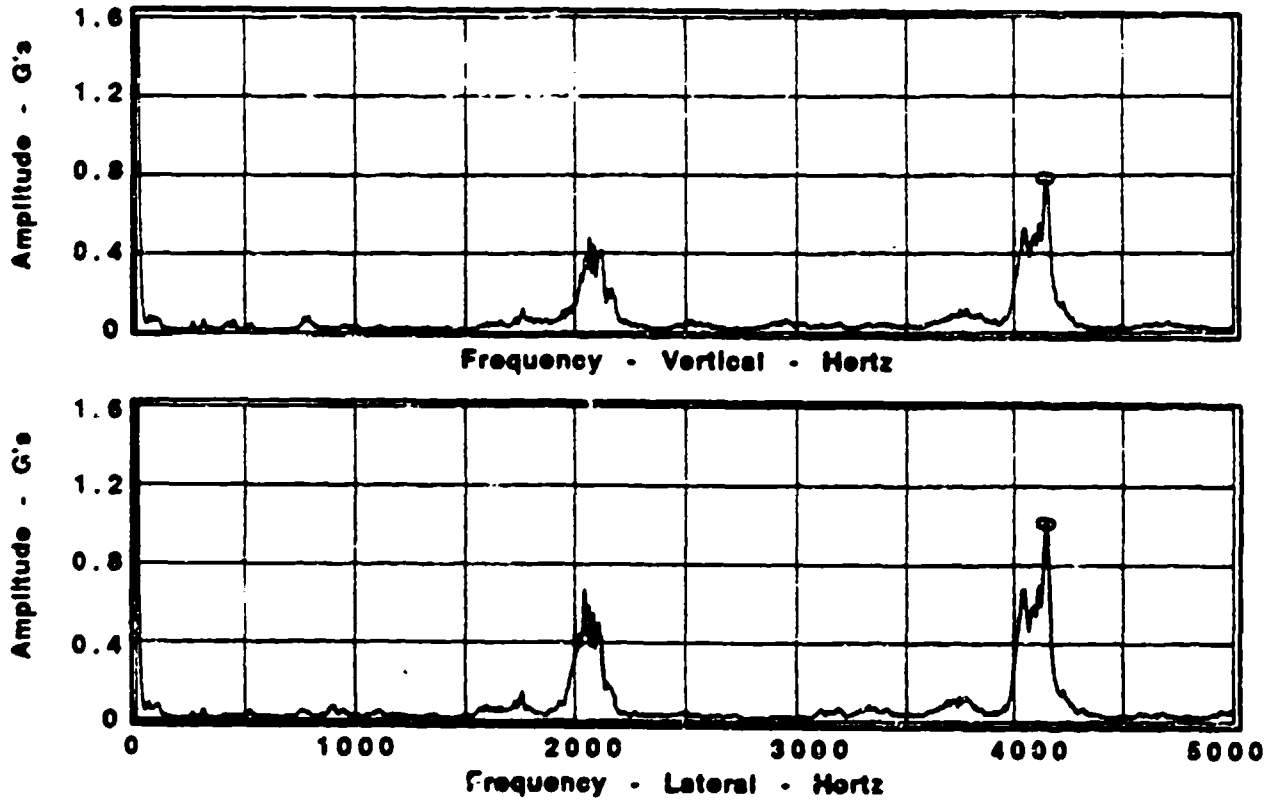

Figure 119. Typical Vibration Signatures, Pattern Development

Disassembly revealed that contact patterns had spread across the full width of the tooth on each gear at the 75% condition with no signs of surface distress. Both the test and dummy gearbox gears were similar. In addition to the visual inspections, strain data was also examined to assist in evaluating the contact patterns observed. The silver and copper plating, added to aid the visual examination were effective in helping to evaluate the contact patterns. The silver and copper plate was more effective than gold plate or black oxide. Blueing also worked well at low temperature, providing the best overall indication, but washed away when the gearbox temperature was increased.

Based on visual examination and analysis of the strain data, the patterns were judged to be acceptable to continue to the 100% condition. The gearboxes were then reassembled and the 100% power condition was run. Load sharing during the subsequent power sweep is presented in Figure 120. As seen, load sharing was excellent at 100% torque but showed a slight difference at 25% torque. The cause of this torque difference and why the reading changed from the start of the pattern development test was not known at this time.

At the conclusion of the 100% pattern development test, the gearboxes were disassembled and inspected. Based on the visual patterns seen and on the examination of the strain survey data, the patterns were judged to be acceptable and further topological corrections of tooth geometry were not required. The testing showed that the topological corrections manufactured into the initial test parts, and calculated by finite element analysis, worked well in establishing uniform loading across the tooth at full load.

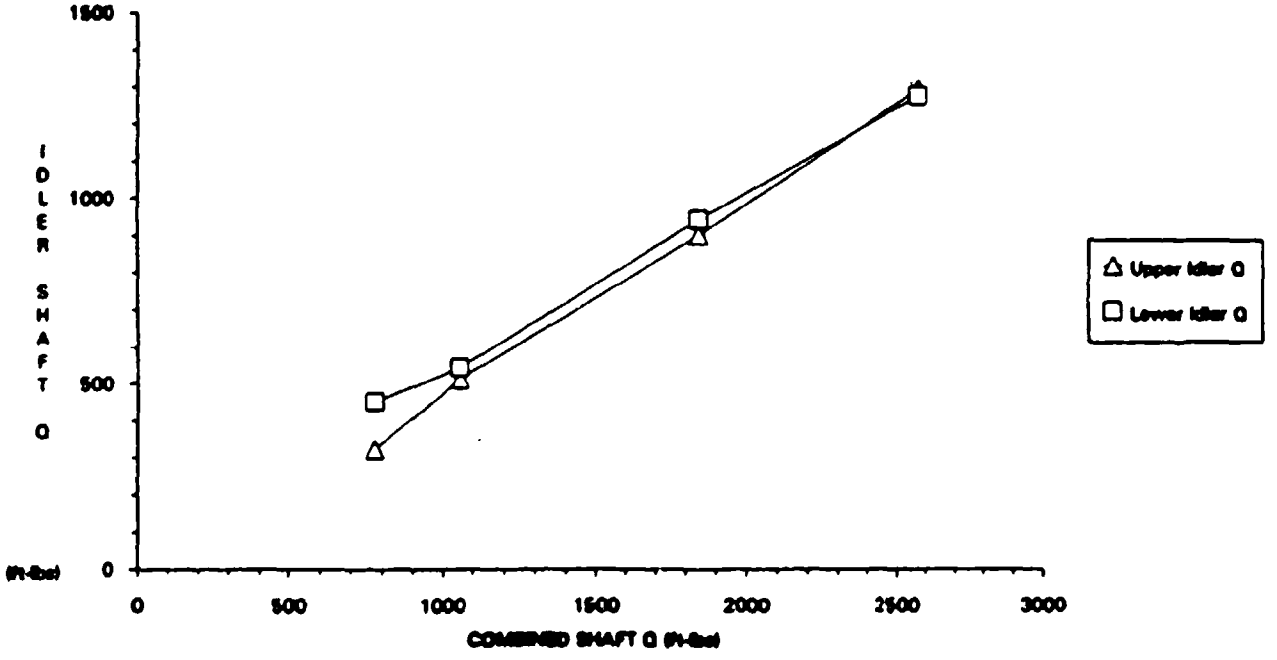

Figure 120. Load Sharing, Final Pattern Development Survey

1/2 Size Gearbox Test Results, Dynamic Surveys

Strain surveys were performed in accordance with the test procedure presented previously. All strain data was converted to stress by using Hook's law: stress = (strain) (modulus of elasticity). Examples of the time history of strain (converted to stress) measured on each gear are presented in Figures 121 through 126. Vibratory Stress (peak-to-peak divided by 2) measured for each strain gage location are presented in Figures 127 through 134 as a function of load. These figures illustrate the effect of increased load on the stress distribution across the face of each tooth. Surveys were also taken at varying speeds with constant torque. These tests showed that the ART gearbox dynamic load factor is approximately 1.00 since no changes of strain with speed were noted.

All strain gages remained functional throughout testing with the exception of HERGR39 which appears to have disbonded since it is functional but the output is extremely low. Spur pinion slip ring data was noisy because of higher operating speeds on the spur mesh and the data is of poor quality.

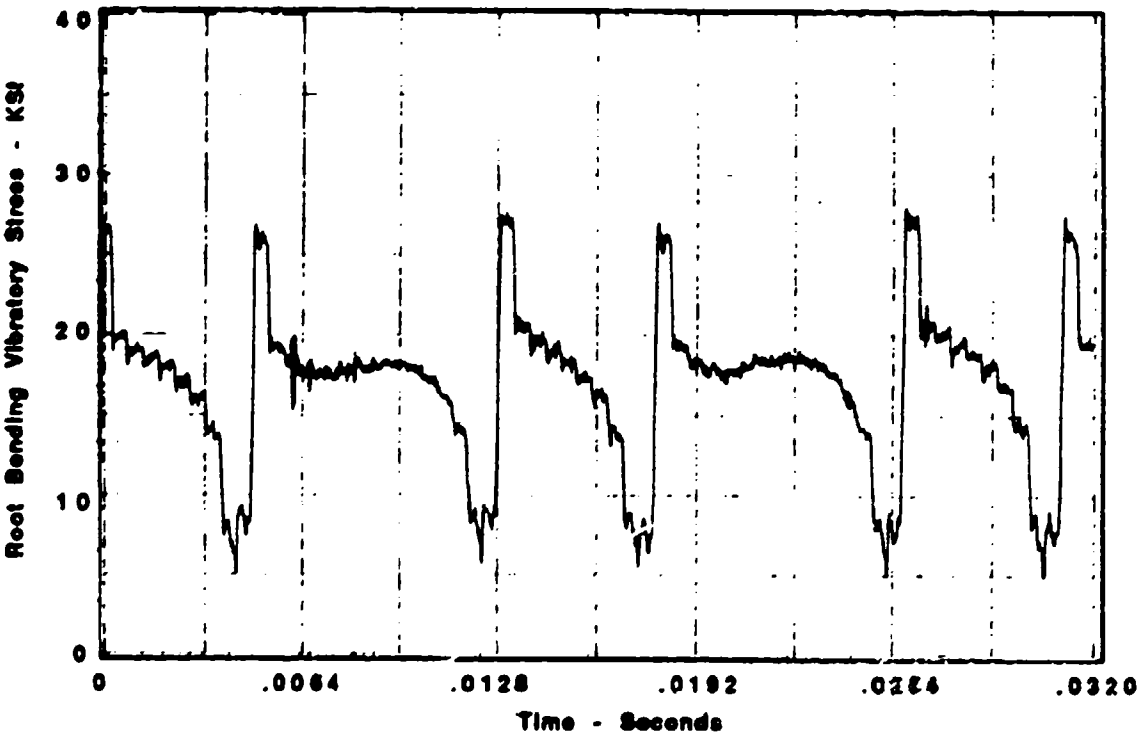

Figure 121. Stress vs Time, Spur Pinion, Gage #3

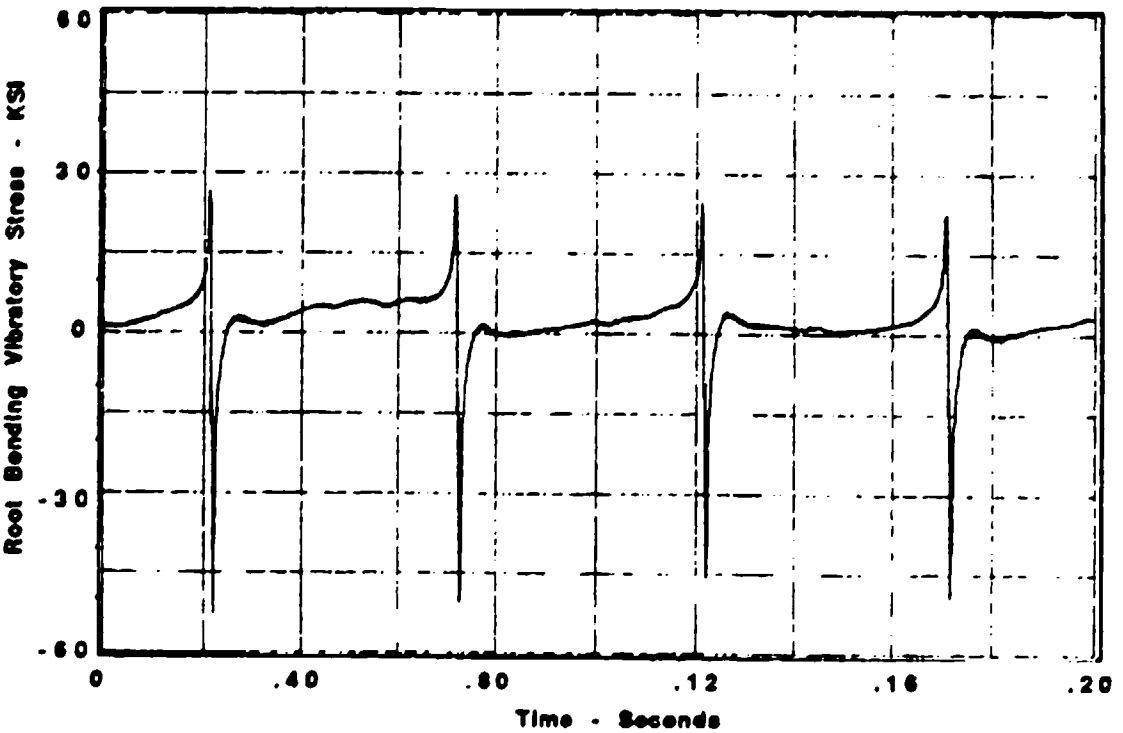

Figure 122. Stress vs Time, Upper Spur Gear, Gage #10

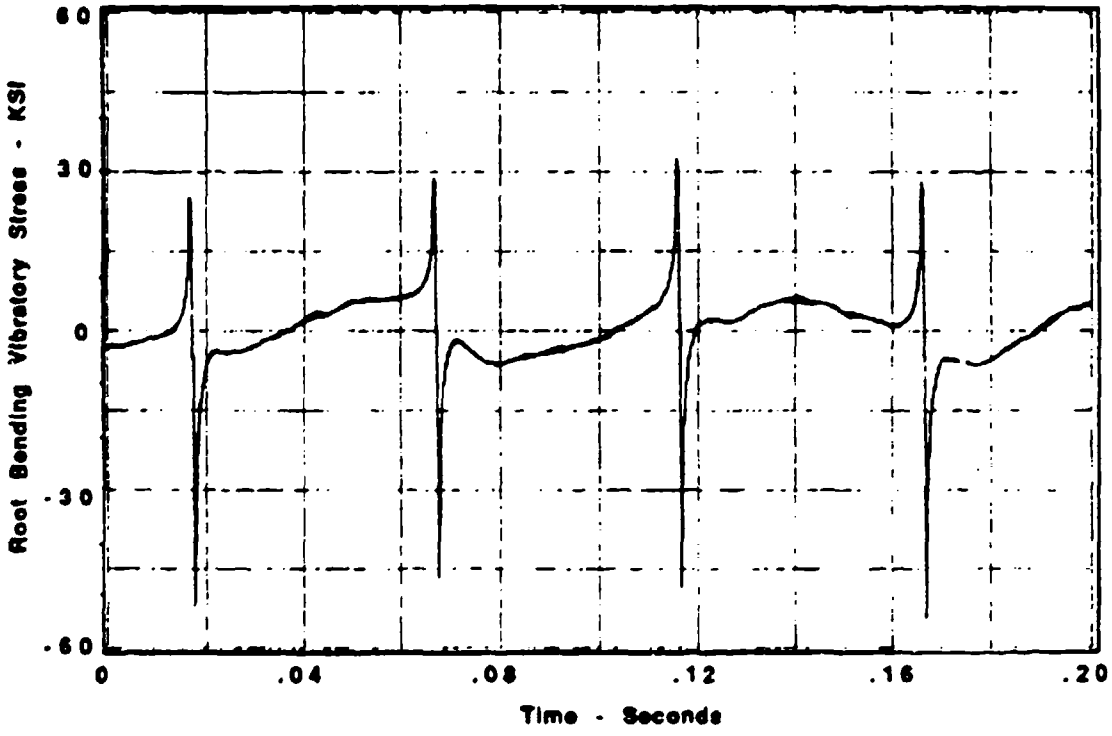

Figure 123. Stress vs Time, Lower Spur Gear, Gage #15

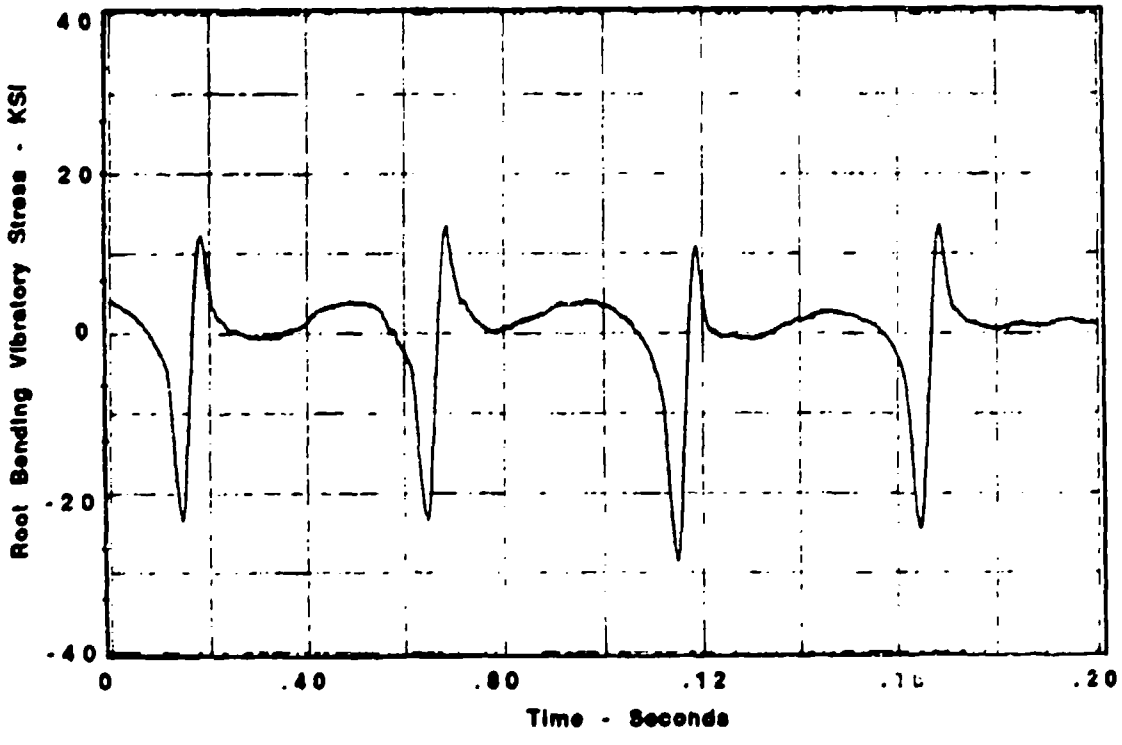

Figure 124. Stress vs Time, Upper Double Helical Pinion, Gage #19

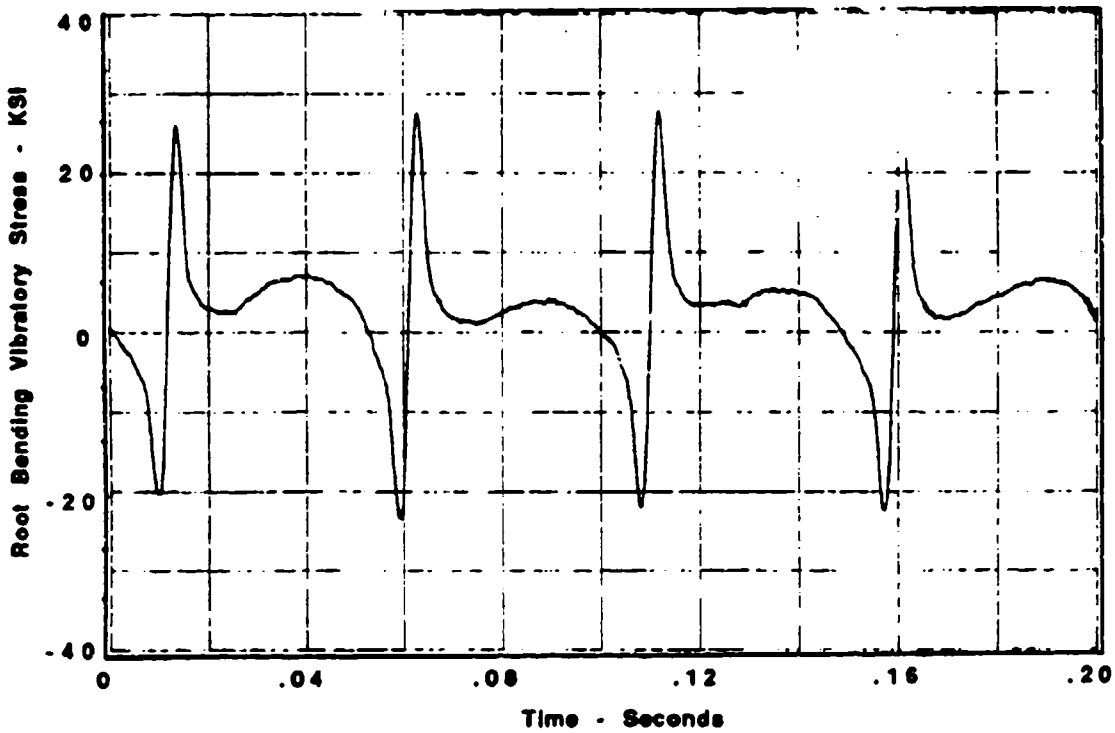

Figure 125. Stress vs Time, Lower Double Helical Pinion, Gage #32

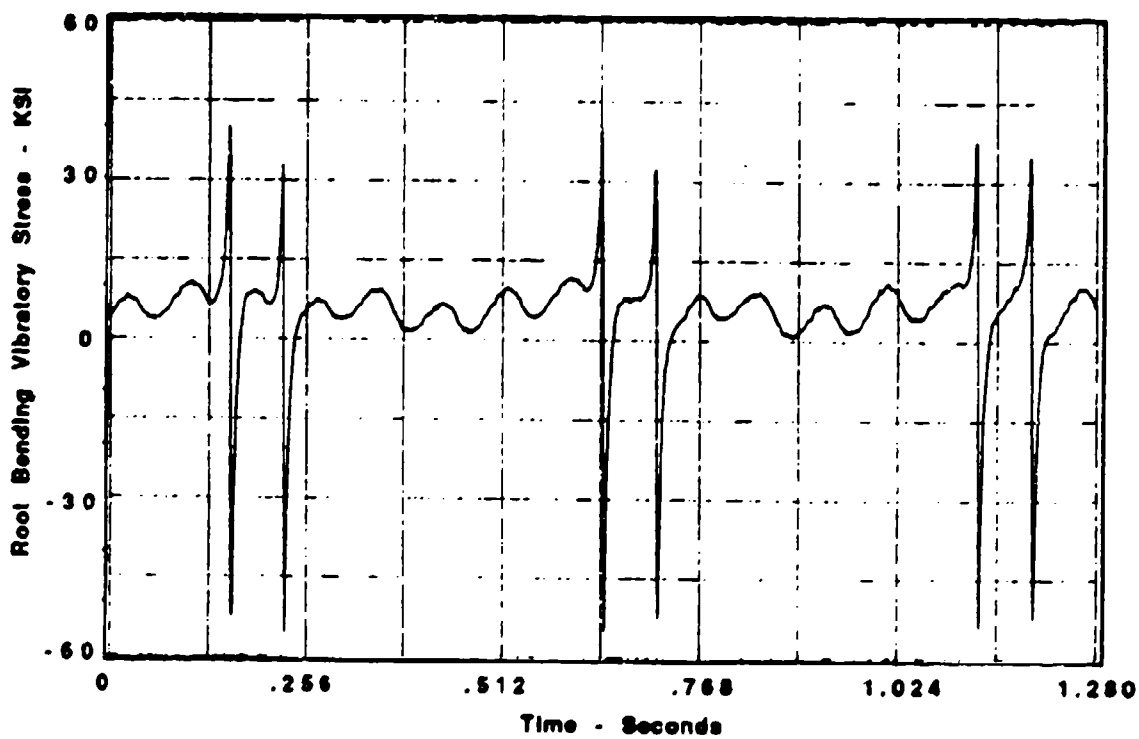

Figure 126. Stress vs Time, Double Helical Gear, Gage #38

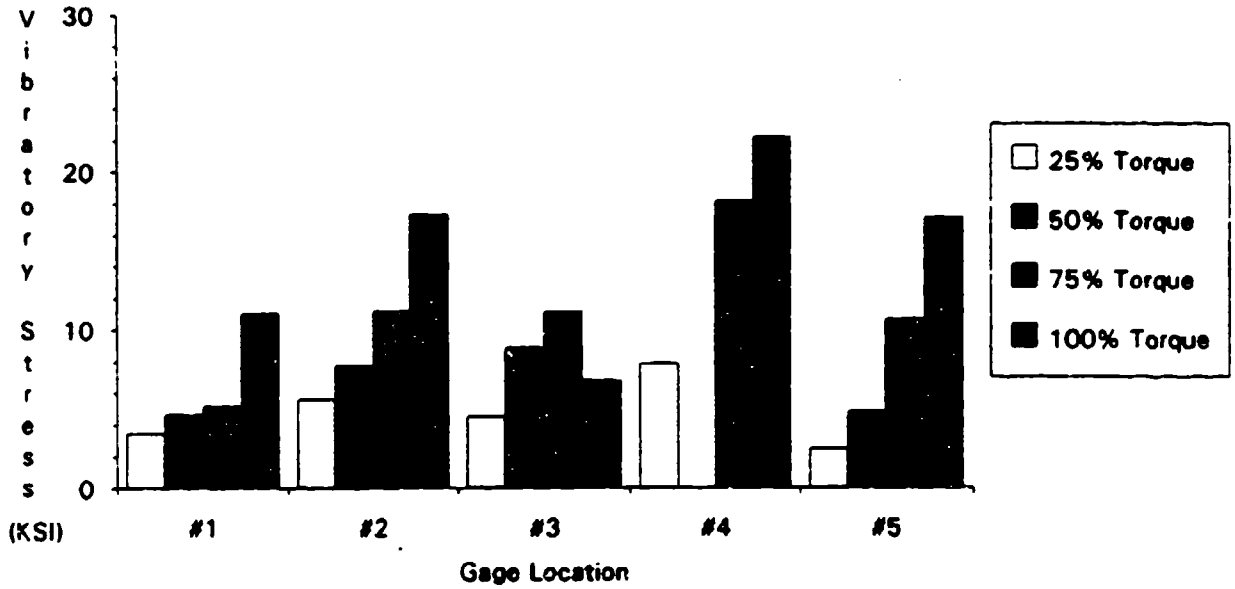

Figure 127. Vibratory Stress, Spur Pinion Meshing w/Upper Spur Gear

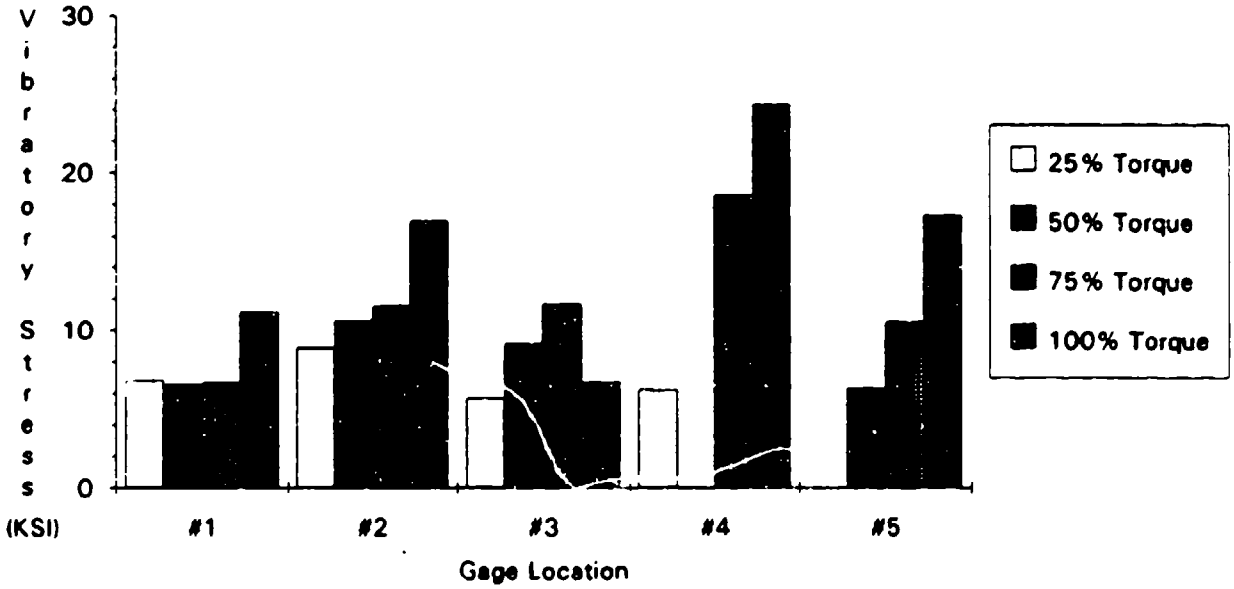

Figure 128. Vibratory Stress, Spur Pinion Mesh w/Lower Spur Gear

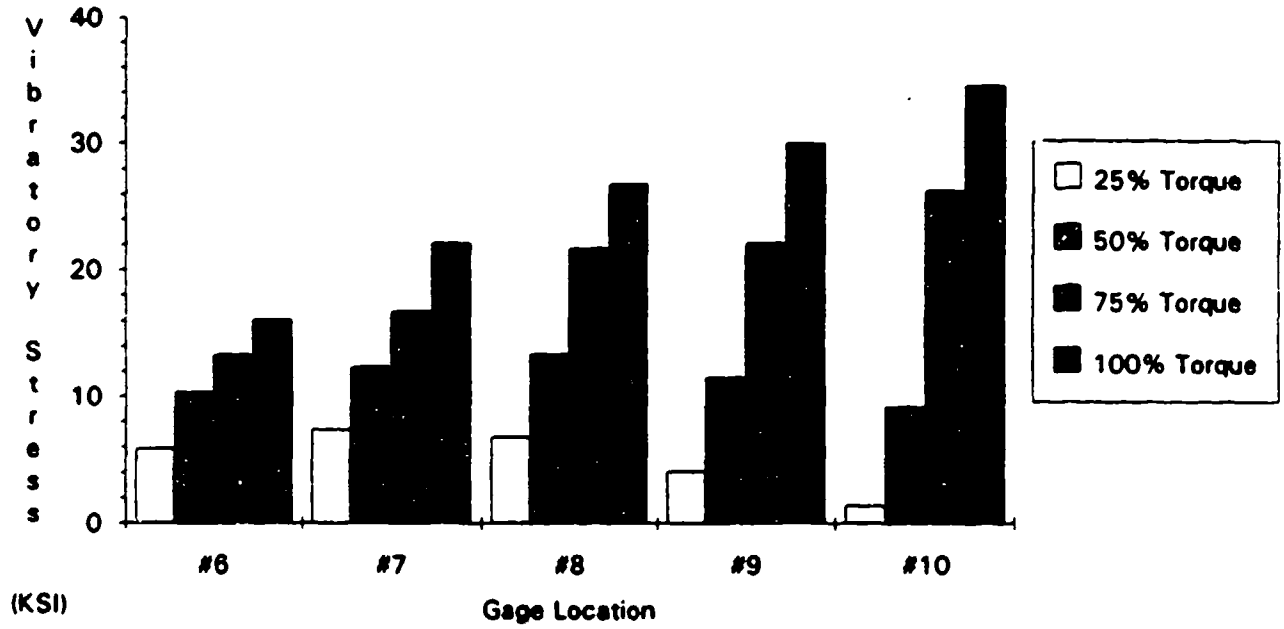

Figure 129. Vibratory Stress, Upper Spur Gear

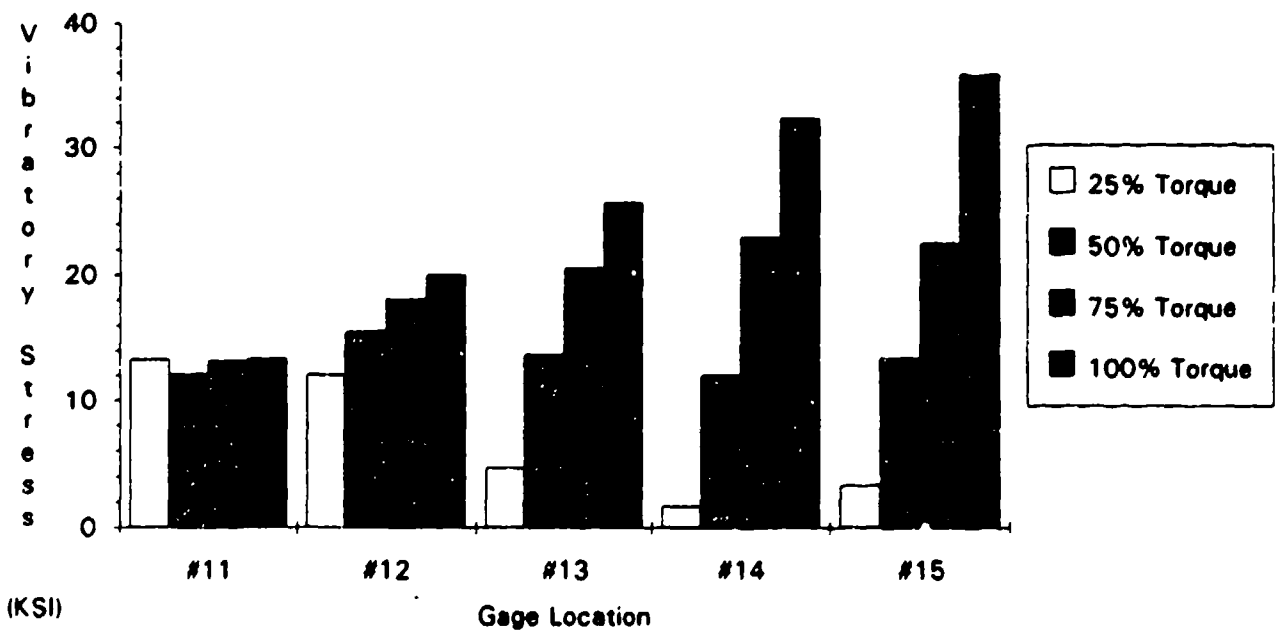

Figure 130. Stress vs Time, Lower Spur Gear

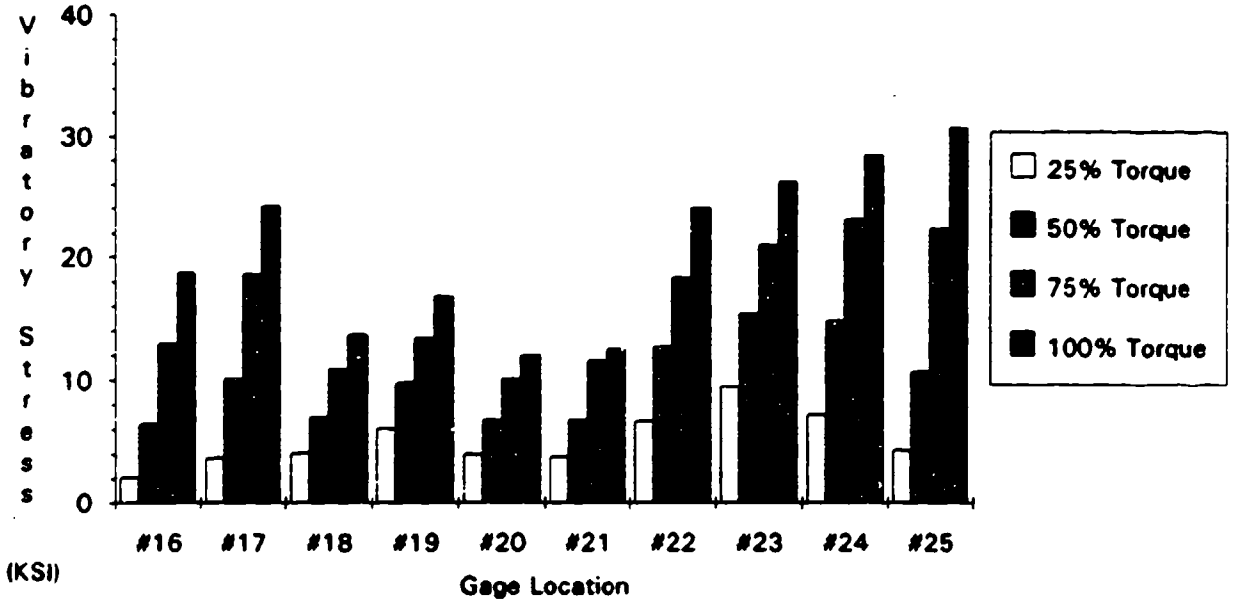

Figure 131. Vibratory Stress, Upper Double Helical Pinion

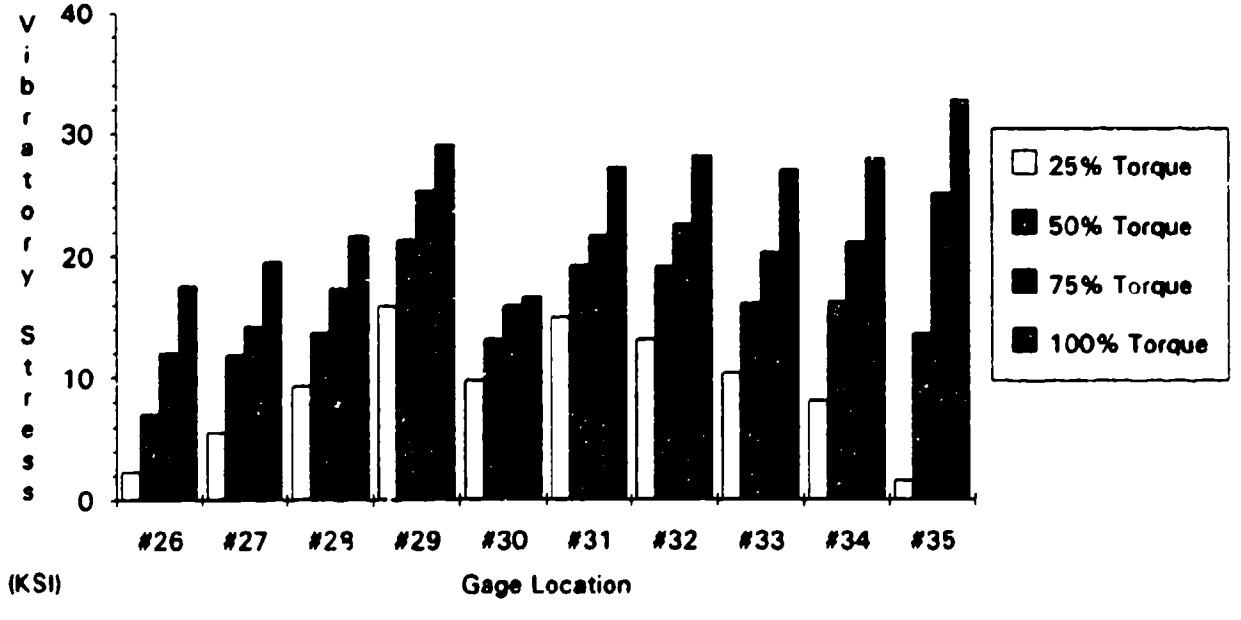

Figure 132. Stress vs Time, Lower Double Helical Pinion

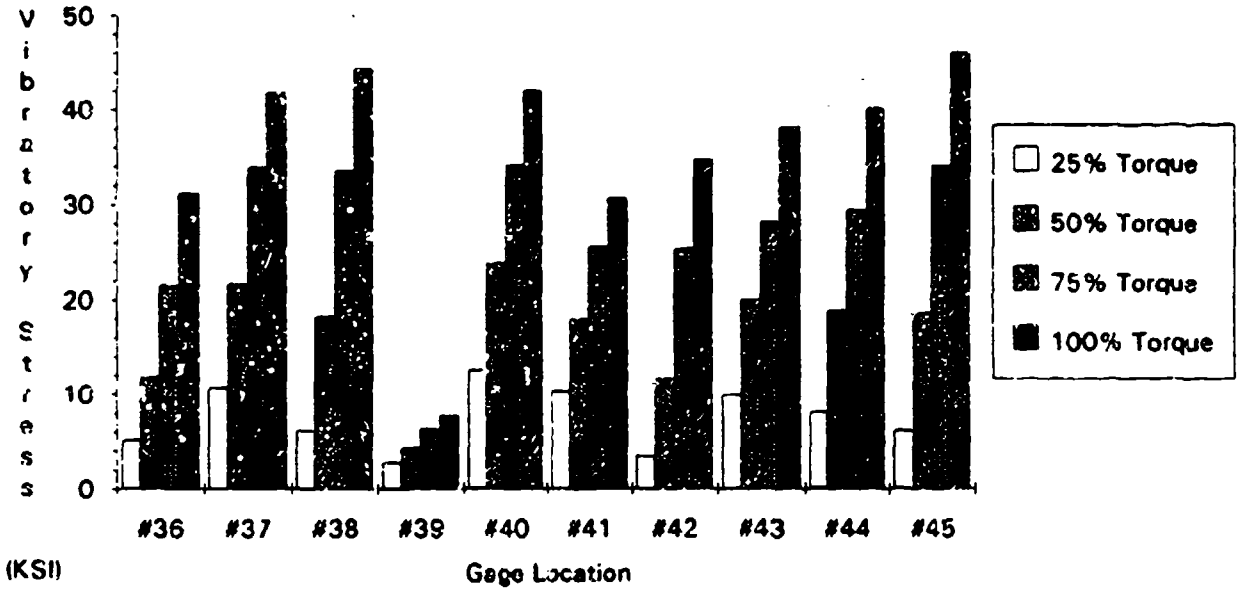

Figure 133. Vibratory Stress, DH Gear Meshing w/Upper DH Pinion

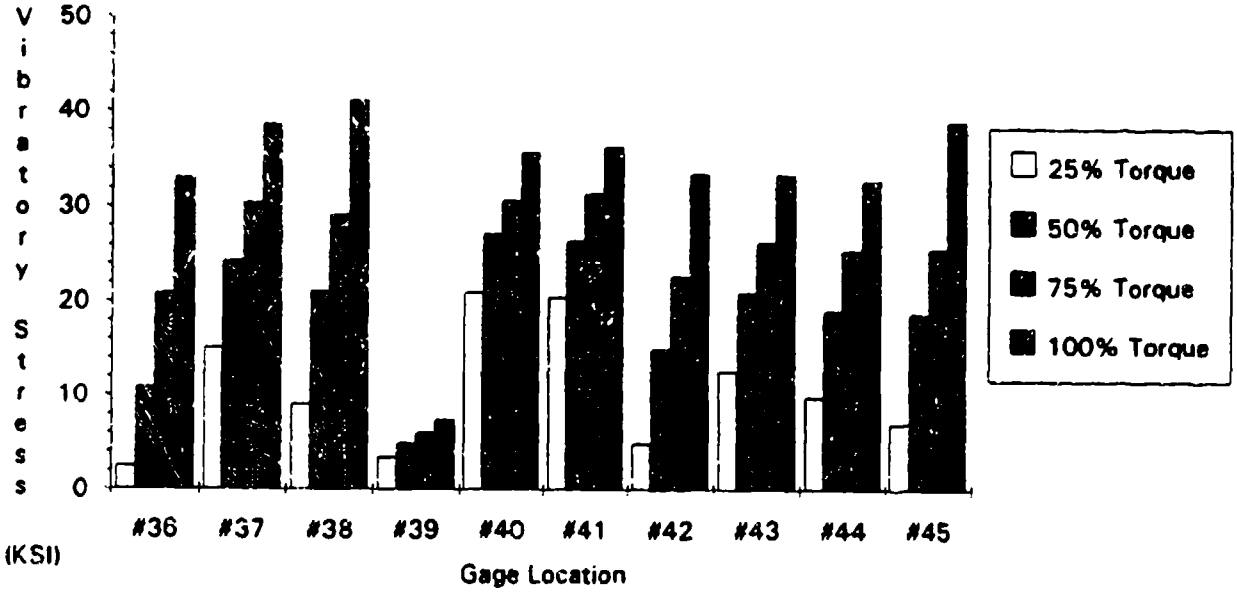

Figure 134. Vibratory Stress, DH Gear Meshing w Lower DH Pinion

In addition to the strain measurements, upper (041) and lower (042) idler shaft torque was monitored and recorded during the dynamic surveys. At the end of the gear pattern development, the torque split was within 2%. However, as the dynamic surveys began, load sharing deteriorated. The torque split during the first and second half of the dynamic surveys are shown in Figures 135 and 136. Data for each plot (or data set) was taken during one day of operation. load sharing remained consistent during each day/data set but changed when the test stand was shut down and allowed to cool. At the completion of the dynamic surveys, load sharing had deteriorated to a torque split of approximately 7% at 100% load. Although torque splits of up to 20% are considered acceptable, the cause of the deterioration was unknown at this time.

Following the dynamic surveys with the elastomeric load sharing devices installed, the test gearbox was disassembled so that the elastomeric load sharing devices could be replaced with steel members. During this disassembly, the following observations were made:

- Spline backlash measurements taken before and after test showed that rotational movement had occurred in each double helical pinion/spur gear assembly. Total movement (closure) on the upper and lower assemblies was 0.0482 inch and 0.0369 inch respectively. Initial gaps were 0.0812 inch and 0.0819 inch for configuration #1.

- Axial shimming measurements taken before and after test showed that the elastomer had taken a "set" in the axial direction of 0.005 inch and 0.003 inch on the upper and lower assemblies respectively.

- There was no loss of preload on the bolts that clamp the elastomer side plates to the web of the spur gear.

- There was no wear or fretting on the bolted connection.

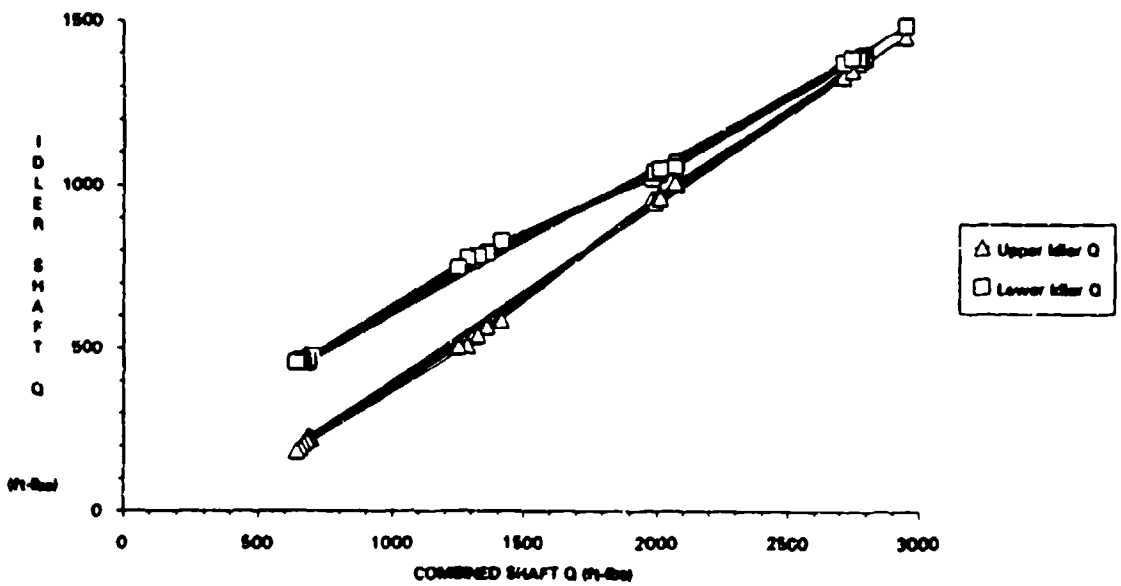

Figure 135. Load Sharing, 1st Half of Dynamic Surveys

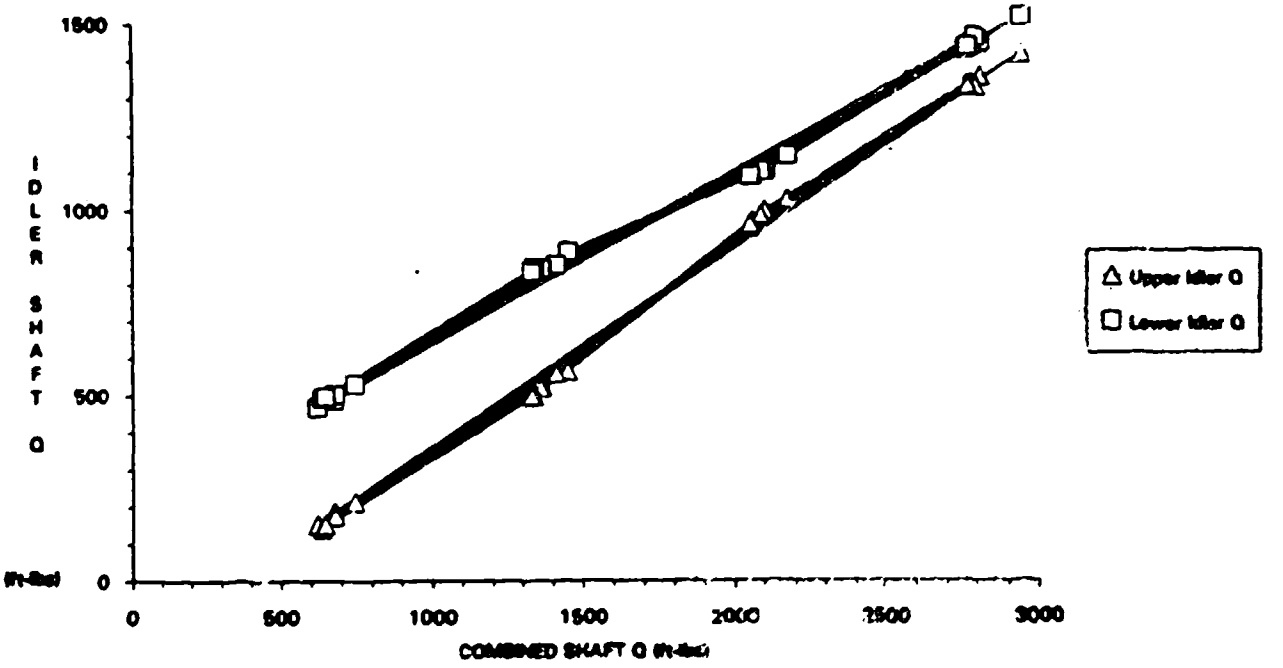

Figure 136. Load Sharing, 2nd Half of Dynamic Surveys

- There was no wear of fretting on the cone section of the spur gear or the elastomeric load sharing device.

- The back up spline showed evidence of contact during operation.

The observations listed above indicate that a shift in the timing of the index teeth of the double helical pinion and the spur gear had taken place. Subsequent static testing using the fixture shown previously in Figure 96, showed that slippage was taking place at the interface between the outer cone surface of the elastomeric load sharing device and the inner cone surface of the spur gear. This slippage occurred because the elastomer lost some of its preload during operation, a condition which was further aggravated by the presence of lubricating oil which reduced the coefficient of friction on the mating surfaces. The solution to this problem was determined to be an increase in the applied preload during assembly. The initial preload value of 0.010 inch pre side was insufficient and was increased to 0.033 inch per side to account for these variables in subsequent assemblies. The 0.033 inch was chosen as the maximum value for a zero margin of safety in yield of the elastomeric load sharing device side plate at the highest operating temperature.

Load sharing surveys were performed with the steel load sharing devices installed in accordance with the procedure as previously outlined. The steel load sharing devices had the same external dimensions as the elastomeric load sharing devices but were manufactured of solid steel. Thus, installation of the steel load sharing devices effectively negated the function of the elastomer while retaining the same gear hardware. The measured torque per side is shown in Figure 137.

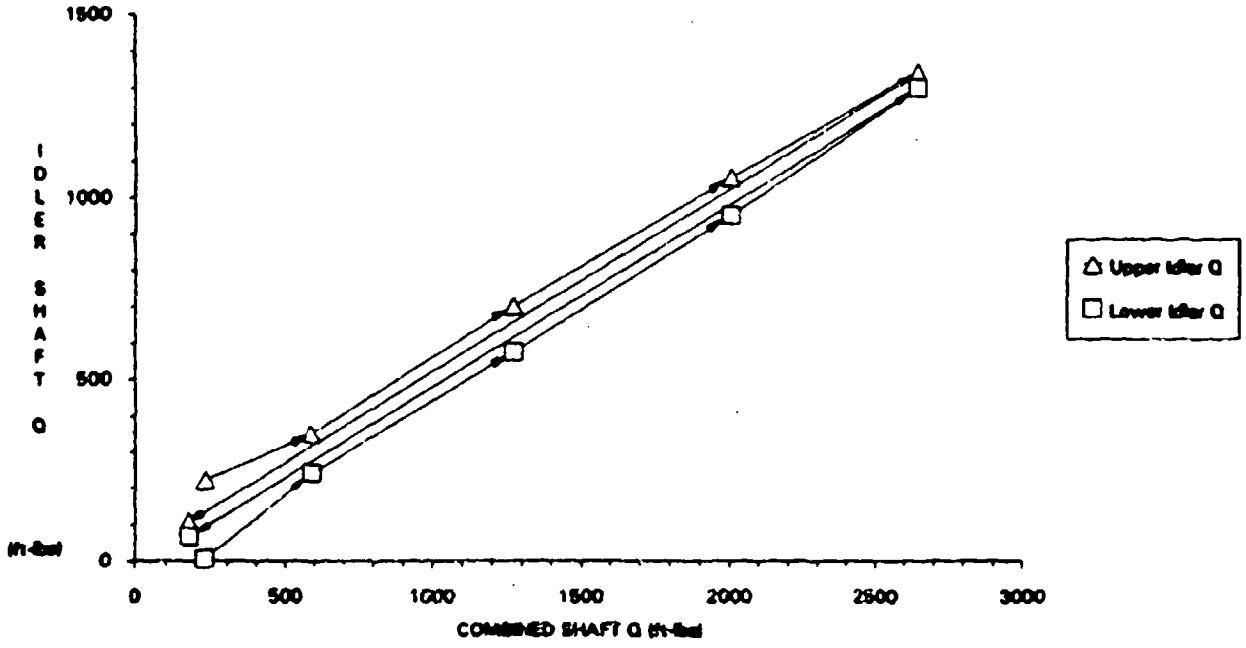

Figure 137. Load Sharing, Steel Survey

Note that when testing was initiated, load sharing at 10% torque was poor. However, as the applied torque was increased toward 25%, a shift in the torque split occurred, as shown in Figure 138. This shift improved the torque split significantly and was confirmed by reducing the applied torque back to 10% after the 100% torque condition. A comparison between the initial data at 10% torque and the final data at 10% torque demonstrates the improvement observed.

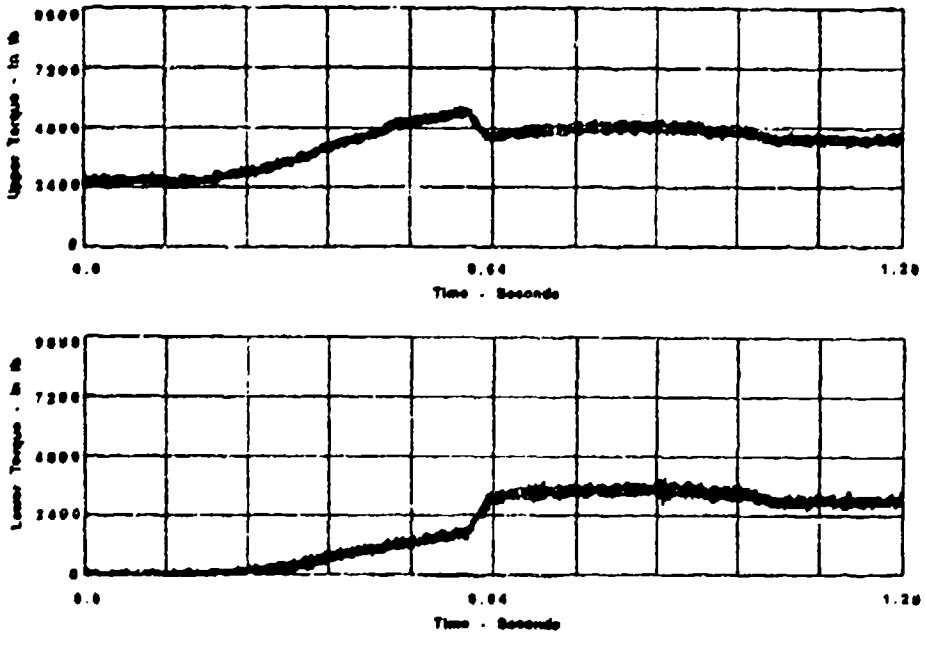

Figure 138. Idler Shaft Torque vs Time, Steel Survey

Based on the lessons learned during the disassembly and static testing of the elastomeric load sharing devices, insufficient clamp up was also suspected to be the root cause of the observed problems. If the clamp up is insufficient to transmit the applied torque without slipping between the outer cone of the load sharing device and the inner cone of the spur gear, then the shifts in the torque split would be the logical result.

This hypotheses was confirmed during the disassembly of the gearbox following completion of the surveys. Spline backlash measurements taken before and after test showed that rotational movement had occurred in each double helical pinion/spur gear assembly. Total movement (closure) on the upper (041) and lower (042) assemblies was measured to be 0.0815 inch and 0.0806 inch respectively and the internal backup splines were in direct contact. In addition, there was evidence of circumferential movement on the mating surfaces of the cone seat joint on the spur gear and load sharing device. There was minor fretting of the spline teeth indicating that they had been in contact during operation for some time. Although this movement is undesirable, observed results confirmed that if the proper orientation of the index teeth on the double helical pinion and spur gear can be maintained, the steel load sharing devices will also provide satisfactory load sharing.

During the survey with steel load sharing devices, vibration levels were observed to increase slightly with increasing power, however all levels were considered low. A typical power spectrum of the vibration experienced on the upper cover on the test gearbox in the vertical and lateral direction at 100% Nr and 75% torque is presented in Figure 139 as an example.

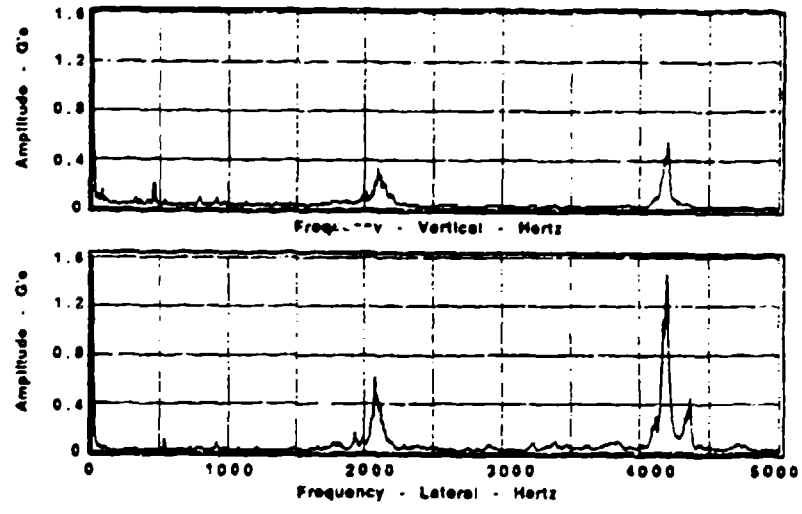

Figure 139. Typical Vibration Signatures, Steel Survey

Transmission error (TE) measurements were performed on each double helical and spur gear mesh in the ART test gearbox for both the elastomeric and steel load sharing devices. The primary method of data acquisition was simultaneous rpm order tracking of both the TE and vibration data on an 8 channel FFT analyzer. Use of rpm order tracking permitted the acquisition of data at a steady state torque which could then be compared as a function of rpm to other torque conditions or configurations. For each double helical gear mesh, the meshing frequency corresponds to 3.3465 times, or 3.3465 orders of the input shaft

frequency while the meshing frequency for each spur gear mesh is defined by 26 orders of the input shaft frequency.

Simultaneous order tracking of TE and vibration data on the 8 channel FFT analyzer provided direct comparisons between TE and housing vibration levels. Plots of measured TE levels in arc seconds (") versus vibration levels (g's) measured with the upper cover lateral accelerometer are shown in Figures 140 through 143 for the upper and lower spur mesh and for the upper and lower double helical mesh at 100% torque, with elastomeric load sharing devices installed. Vibration tracking is shown for the steel load sharing device in Figures 144 and 145 for the lower spur mesh and for the lower double helical mesh. These figures illustrate how the transmission error plotted vs frequency tracks the housing acceleration vs frequency and closely follows the same relative magnitudes (same shape curves). This is strong proof of the known fact that TE is the root cause of vibration and noise in transmission systems.

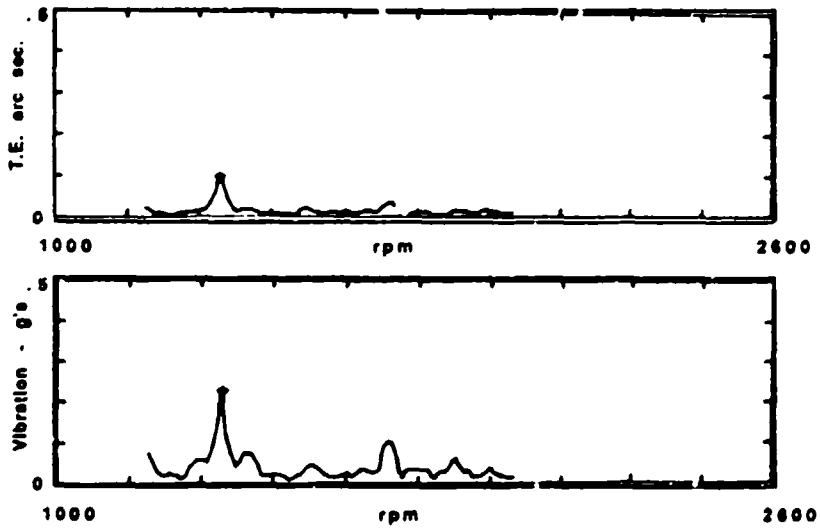

Figure 140. Upper Spur TE vs Upper Lat Vib, Elastomer @ 100% Torque

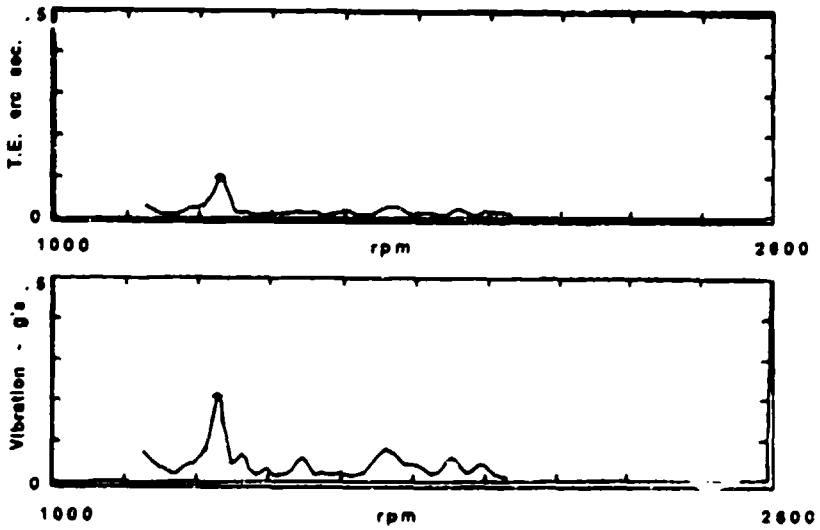

Figure 141. Lower Spur TE vs Upper Lat Vib, Elastomer @ 100% Torque

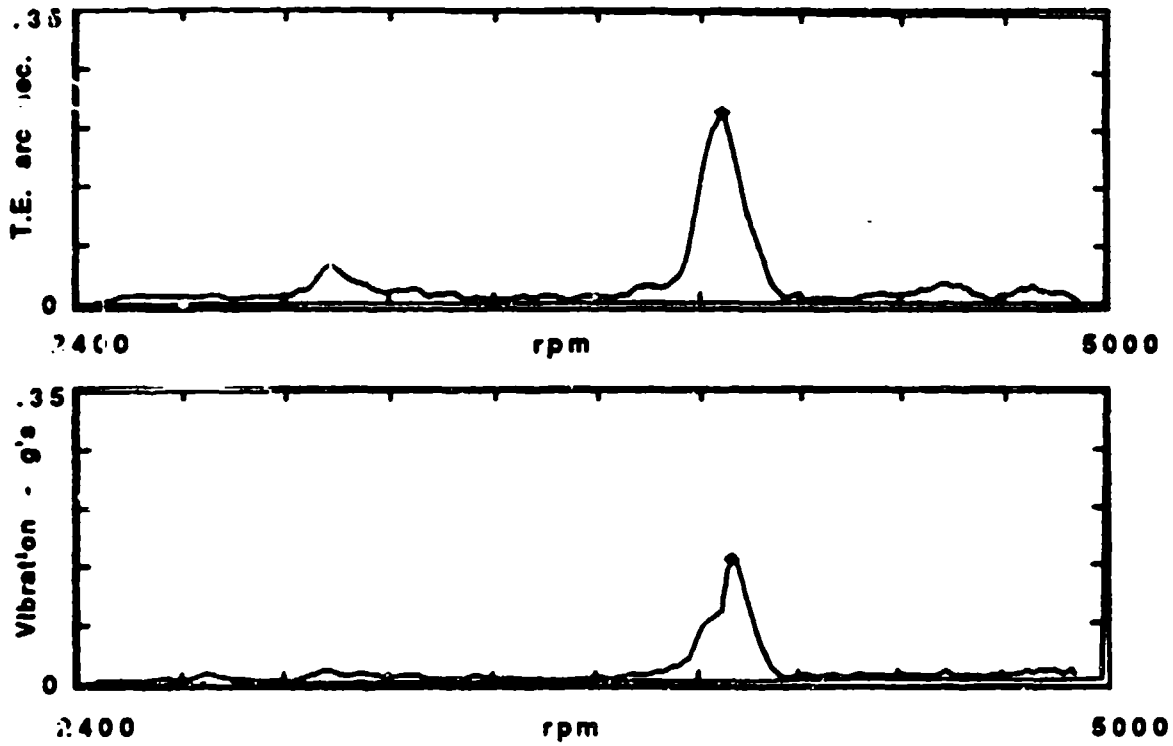

Figure 142. Upper D Hel TE vs Upper Lat Vib, Elastomer @ 100% Torque

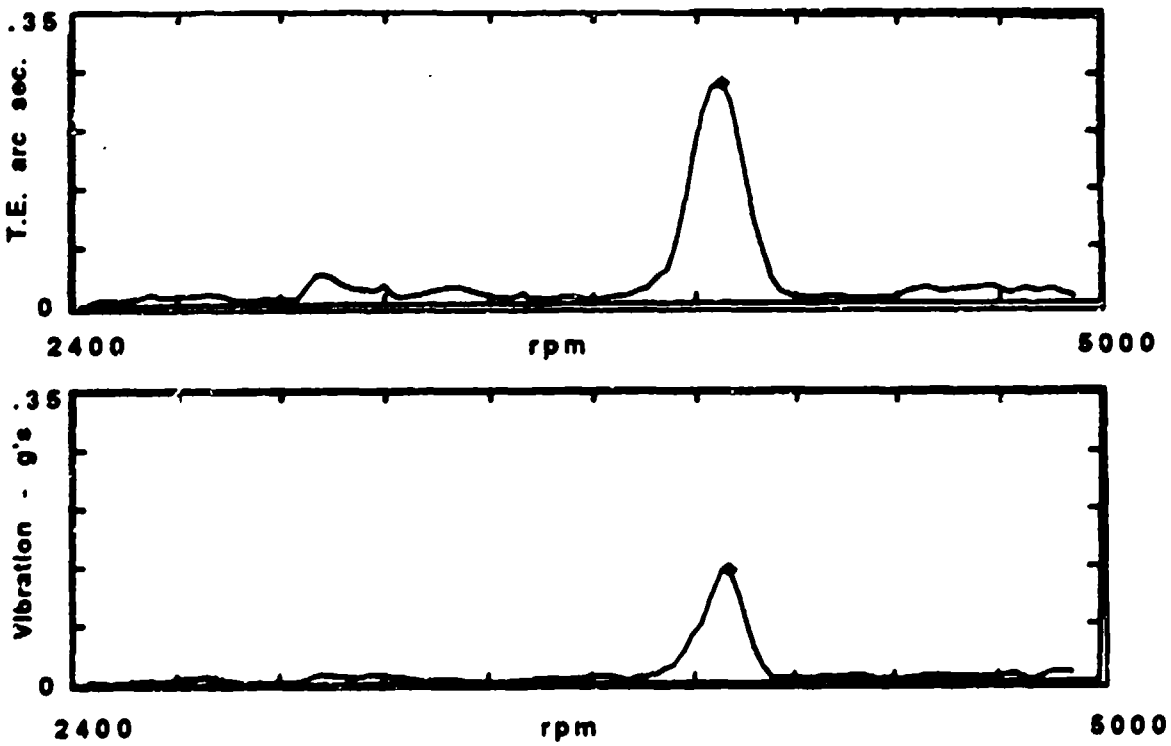

Figure 143. Lower D Hel TE vs Upper Lat Vib, Elastomer @ 100% Torque

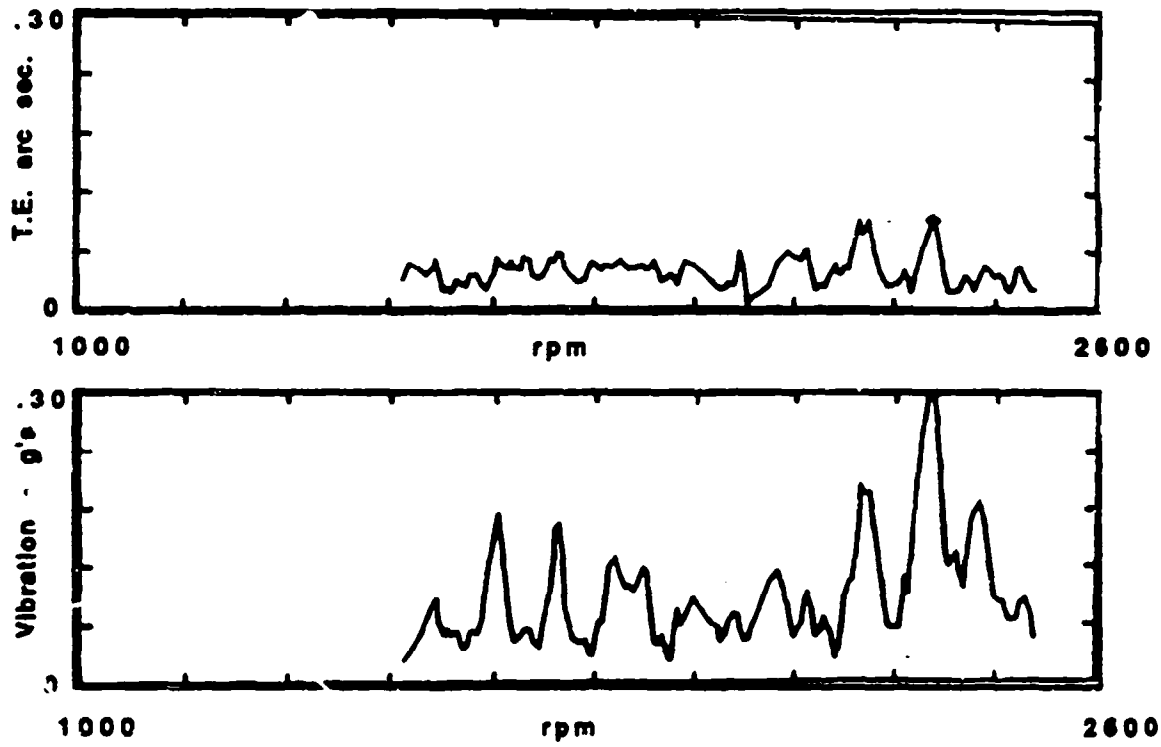

Figure 144. Lower Spur TE vs Upper Lat Vib, Steel @ 100% Torque

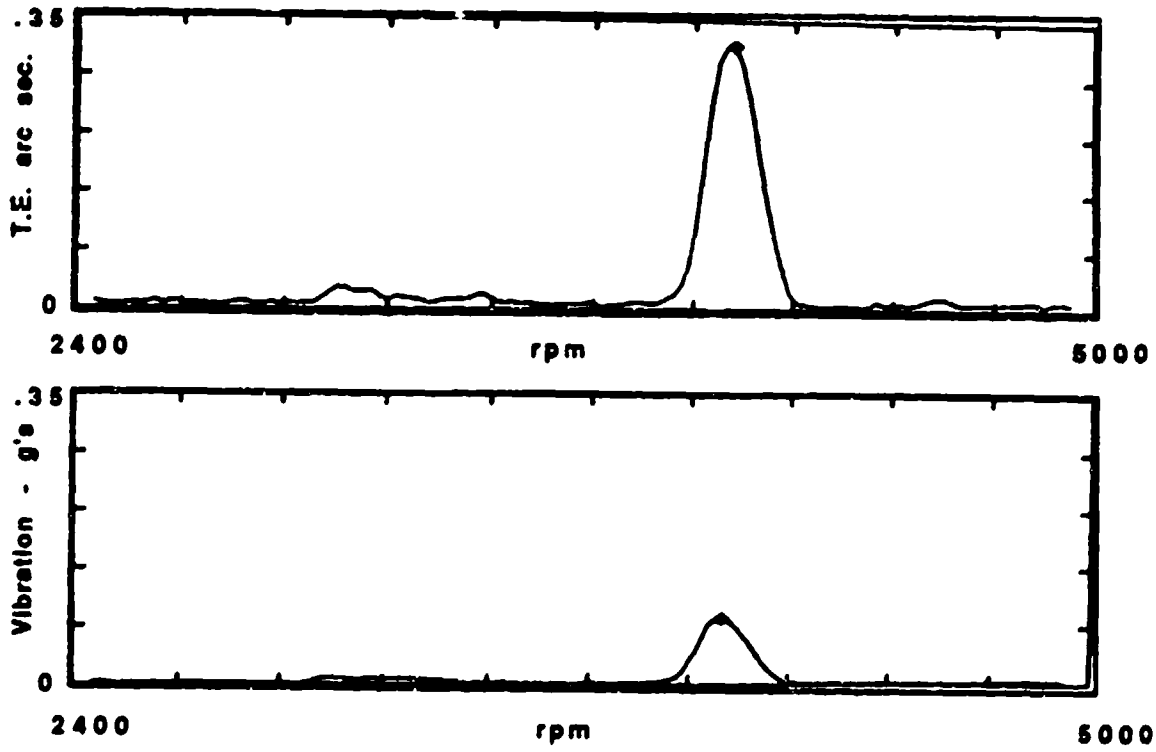

Figure 145. Lower D Hel TE vs Upper Lat Vib, Steel @ 100% Torque

Comparisons of TE measurements were also made between the elastomeric and steel load sharing device configurations. Figures 146 and 147 compare elastomer and steel configuration TE for the upper and lower spur gear meshes at 50% and 100% torque. Figures 148 and 149 compare TE for the upper and lower double helical gear meshes for elastomeric and steel load sharing device installations at 25% and 90% torque. The conclusions reached from examination of these data are that there is no significant effect on TE between steel and elastomer configurations for the double helical gear mesh whereas the opposite is true for the spur gear mesh. Significant reductions were achieved in spur gear mesh TE when the elastomer was installed. It is noteworthy to also mention that the reduction in TE is higher at lower torques and was easily distinguishable by ear during the testing when it was noted that the steel configuration appeared much noisier than the elastomeric configuration.

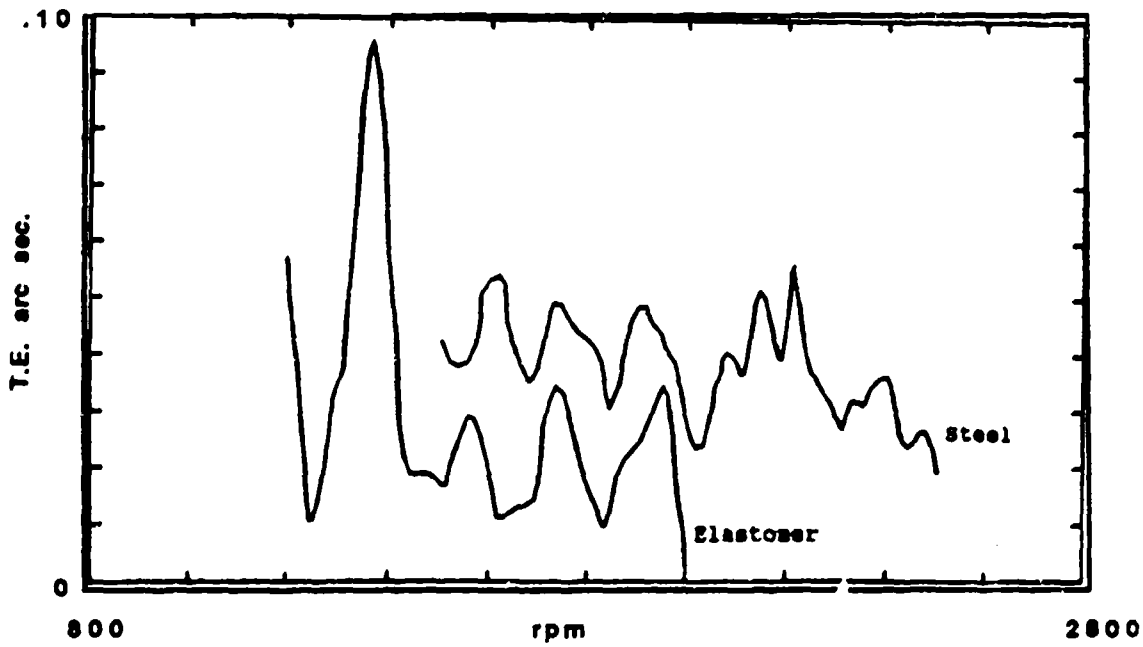

Figure 146. Lower Spur TE, Elastomer vs Steel @ 50% Torque

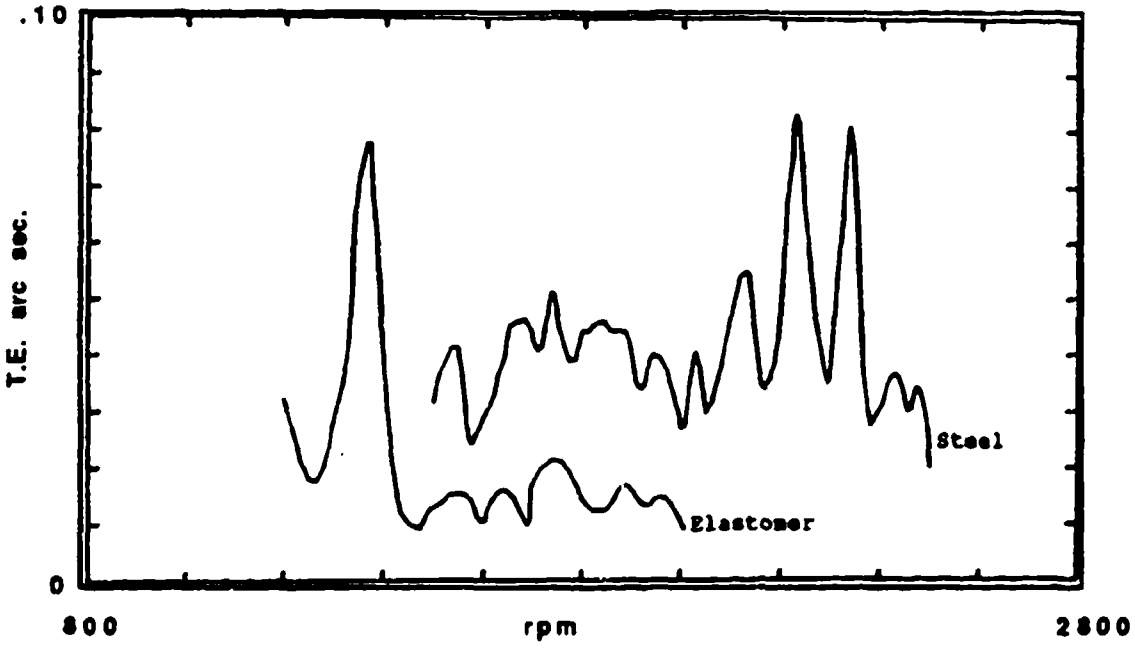

Figure 147. Lower Spur TE, Elastomer vs Steel @ 100% Torque

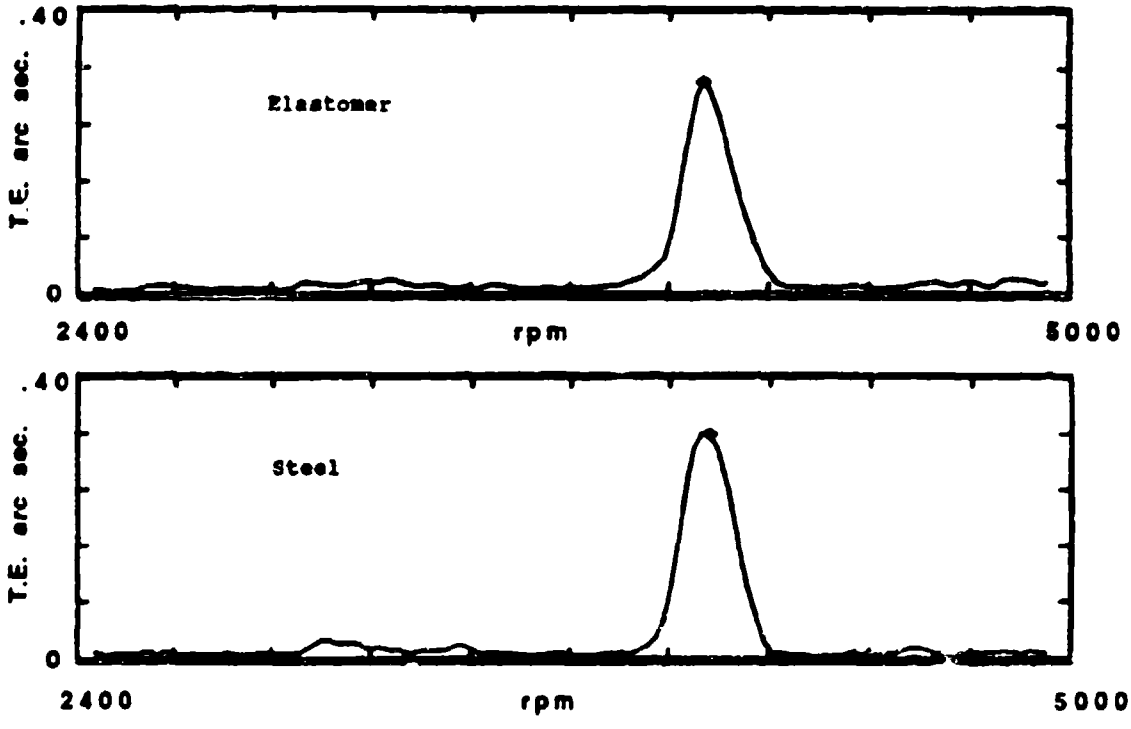

Figure 148. Lower D Hel TE, Elastomer vs Steel @ 25% Torque

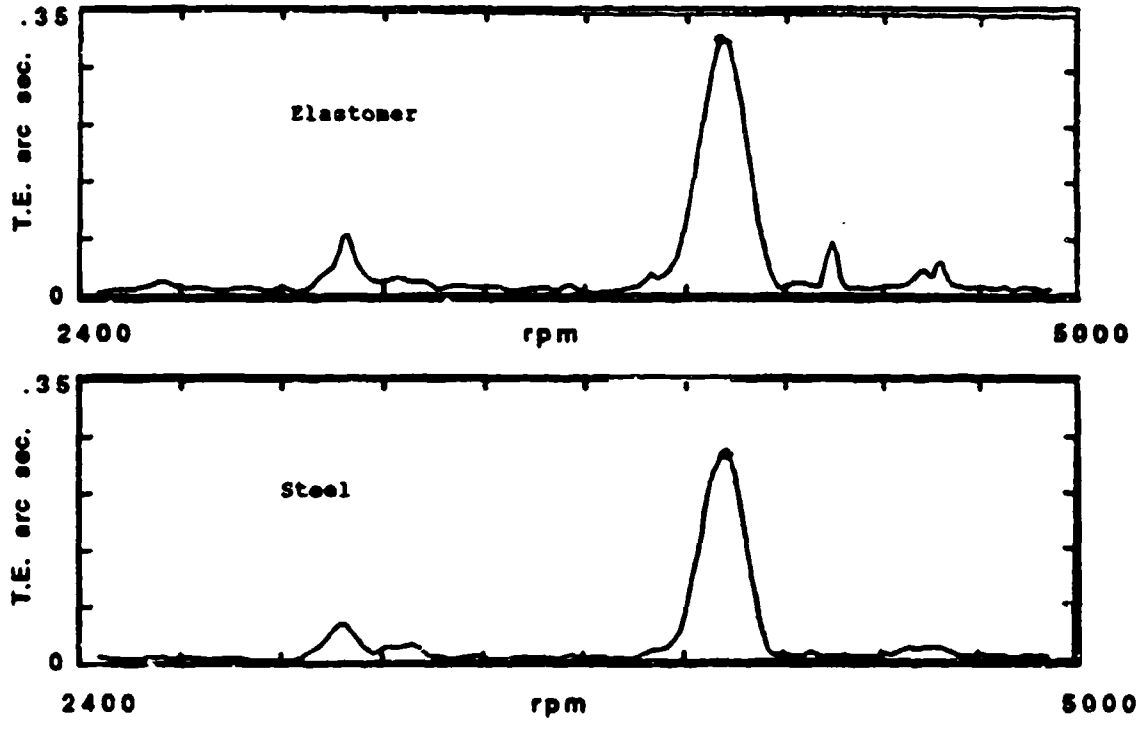

Figure 149. Lower D Hel TE, Elastomer vs Steel @ 90% Torque

Another interesting phenomenon was observed during the conduct of the ART 1/2 size gearbox testing and that can best be described as double helical gear "growl" at no load. The ART back-to-back test stand was run at zero load for periods of time during the initial testing. A non-constant growling noise was heard from within the gearbox. This noise was later traced to axial motion of each double helical pinion. The double helical pinion/spur gear shaft is free to float axially on its roller bearings mounted at each end of the double helical pinion. In its attempt to seek a position of balanced axial loading when the tangential tooth load is zero (or very low) contacts on the face of one side of the helical mesh can create an impact force which sends the shaft axially to the other helical mesh causing impact on the opposite mesh. If the rotation of the double helical pinion/spur gear shaft is not tracking exactly with the tooth ratio, i.e., if the shaft lags slightly behind because there is no load, impacts can also occur on the coast sides of the teeth. Displacement probes were placed on the end of each double helical pinion/spur gear shaft to measure the axial motion as a function of time. At no load, the result is seen in Figure 150.

As seen in the figure, axial motion is quite high and there was also evidence seen at disassembly that the double helical pinions had been in contact on the drive and coast sides of the teeth. As soon as even the smallest torque was applied (anything over 5%), the "growl" stopped, and the axial motion was greatly reduced as shown in Figure 151. In a helicopter installation, the transmission can never run without load since even in flat pitch, the rotor drag torque is considerable. Thus the growling sensation is unique to the test stand environment. The plot in Figure 151 is at 100% torque. At lower values of torque the plot is essentially the same except at zero torque when the plot of Figure 150 is obtained during the "growl". At no load, the growl is intermittent occurring on the order of 10% of the time.

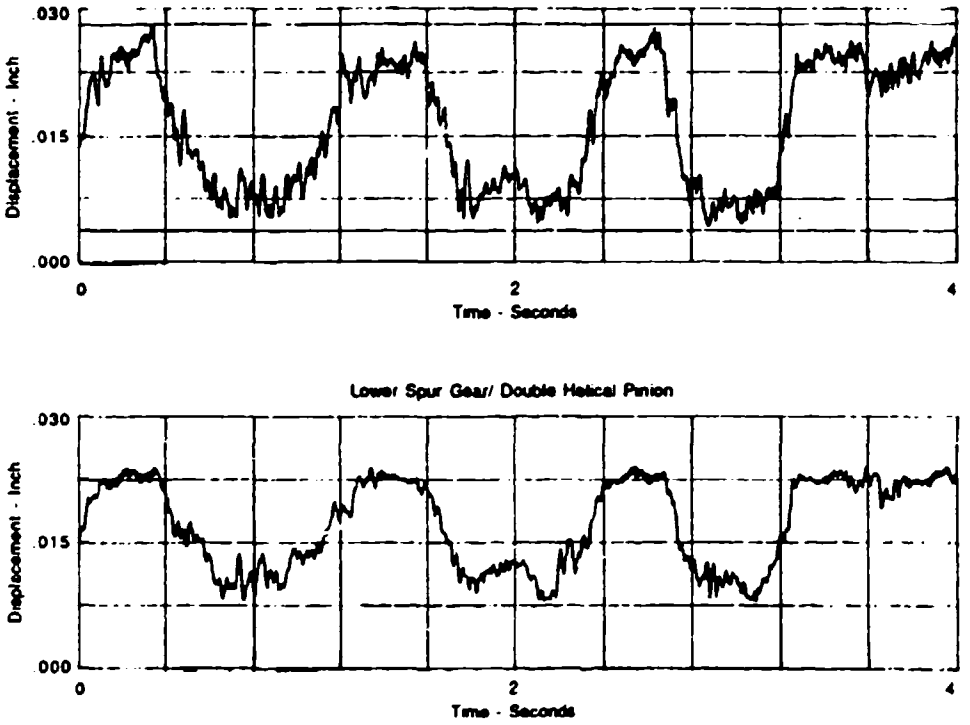

Figure 150. Axial Motion vs Time @ No Load

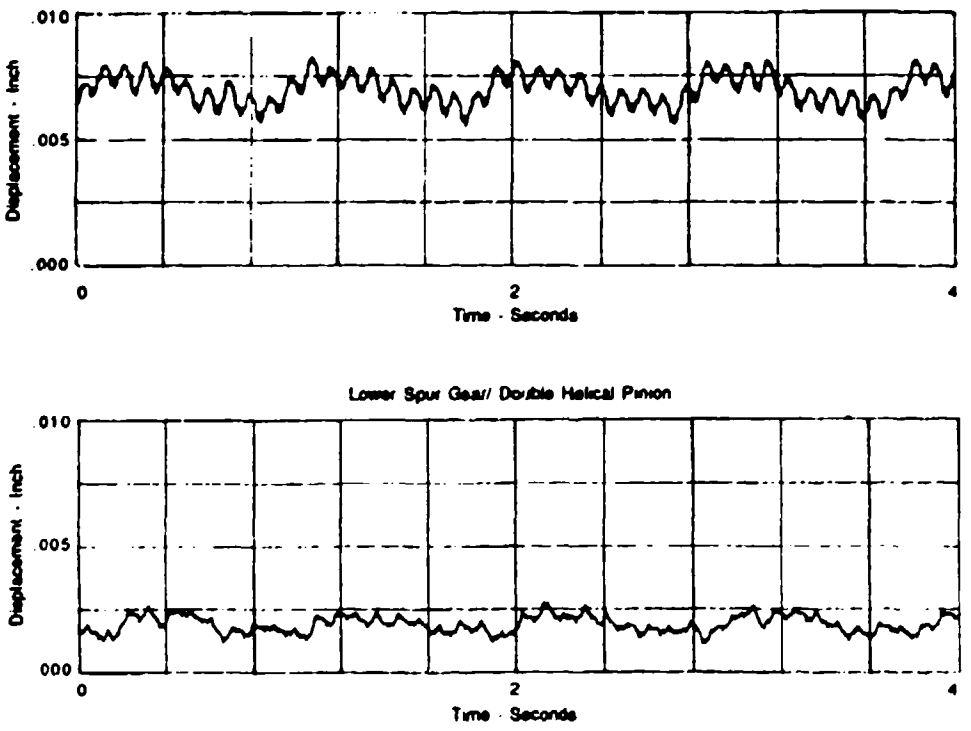

Figure 151. Axial Motion vs Time @ 100% Load

During the 1/2 size gearbox survey tests, strain surveys were taken on the test gearbox housings in accordance with the procedure previously outlined. Strain was monitored using strain gage rosettes so that principal strain could be determined. Each strain rosette was mounted at the maximum strain position as determined by finite element analysis. One rosette was mounted on the upper cover, one on the lower cover, and one on the center housing. A summary of the principal strain is presented in Table 58.

Table 58. Steel Housing, Strain Survey Results

Location	Test Condition Torque %	Principal Strain Maximum m in	Principal Strain Minimum m in	Principal Strain Axis
Gage #1	25%	11.1	-3.1	-40.9°
	50%	27.2	2.8	-40.3°
	75%	42.1	8.9	-42.4°
	100%	55.0	18.0	44.2°
Gage #2	25%	4.2	-14.2	-24.7°
	50%	7.3	-32.3	-23.5°
	75%	12.6	-51.6	-26.3°
	100%	17.0	-73.0	-26.6°
Gage #3	25%	41.5	-26.5	-24.3°
	50%	47.0	-38.0	-23.9°
	75%	55.6	-50.6	-23.3°
	100%	65.6	-64.6	-22.2°

1/2 Size Gearbox Test Results, 200 Hour Endurance

A 200 hour endurance test was conducted in accordance with the procedure presented previously. A summary of the cumulative time spent at each test condition is presented in Table 59.

Table 59. Endurance Test, Cumulative Test Time

% Torque	Hours	% Time
55%	38	19%
65%	60	30%
75%	84	42%
95%	8	4%
100%	10	5%
Total	200	100%

Load sharing, determined by comparison of individual idler shaft torques, was consistent and predictable during the initial part of the testing. However, during start up of cycle #20, Condition #3, load sharing was inconsistent with the largest torque split observed to be approximately ±10.3%. After load cycle #20, load sharing remained inconsistent throughout the remainder of

testing. Figure 152 presents the history of load sharing recorded at the 100% torque condition. In general, changes in the torque split occurred during start up or power changes. Once a particular condition was attained, the torque split remained relatively constant. These characteristics were symptomatic of slippage at the cone seat at the interface between the elastomeric load sharing device outer cone surface and the spur gear inner cone surface.

This problem was originally observed during dynamic surveys and the installed preload at the elastomeric/spur gear joint had been increased prior to the endurance test to address this problem. The increased preload was not successful in preventing slippage at the interface. Spline backlash measurements, taken during disassembly, confirmed that rotational movement had occurred in each double helical pinion/spur gear assembly. Total movement in the 041 and 042 assemblies was 0.1149 and 0.0799 inch respectively. Although rotation had occurred, blueing applied to the spline teeth of the spur gear and double helical pinion web prior to the start of test indicated that the spline teeth on either the 041 or 042 assembly, had not come into contact during this test.

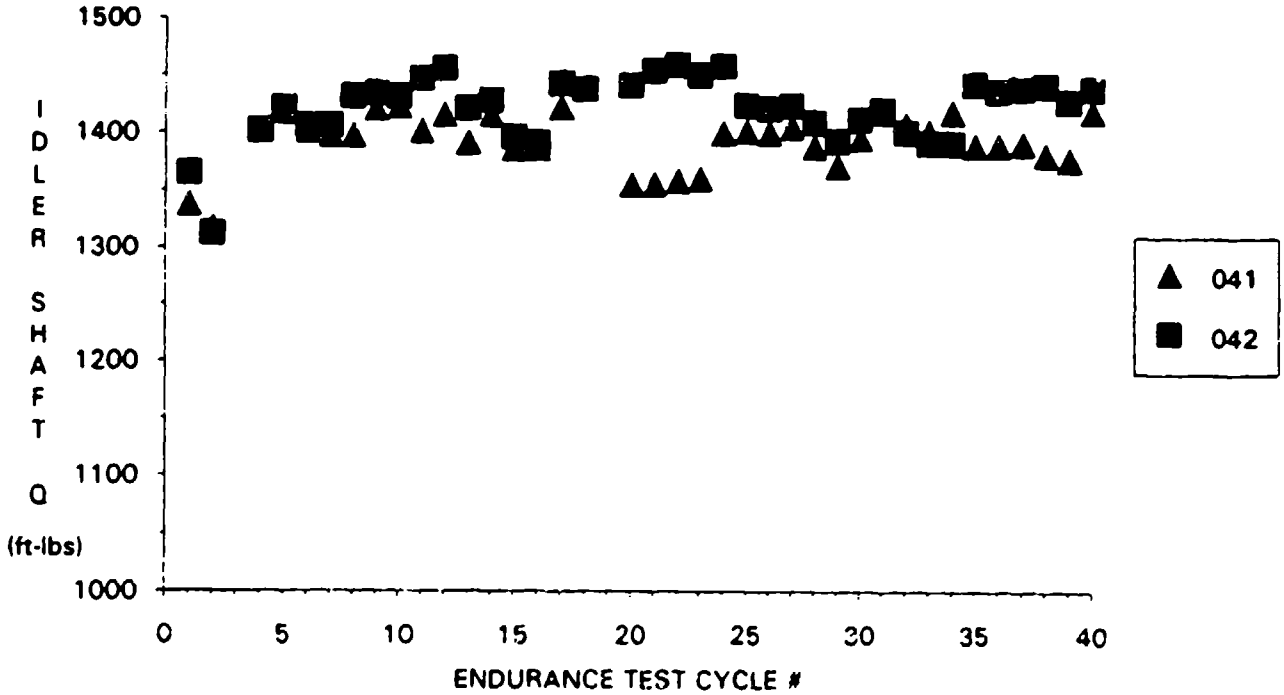

Figure 152. Torque Split History @ 100% Torque

The underlying cause of the loss of preload was the inability of the elastomeric material to endure thermal cycling without experiencing a reduction in the compressive forces created when the elastomer was put into preload compression at assembly. The material takes a set resulting in loss of clamping. It has also been observed that the "set" is not permanent but takes a matter of days to return to the original position. The phenomenon of preload loss with thermal cycling was verified by bench testing conducted at Lord Corp, Erie, Pa., the supplier of the elastomeric material. The results of a thermal cycling test conducted on the elastomeric material are presented in Figure 153. The test was conducted by subjecting one elastomeric load sharing device (1/2 of the assembly) to a constant axial deflection of 0.033 inch. This corresponded to the preload used during the endurance testing. The temperature was raised from room temperature to 250°F and held for a period of approximately 16 hours, then allowed to cool for 8 hours. This cycle was repeated three times while recording force and holding the 0.033 inch deflection. The results show that during constant temperature application, preload force was reduced. This is an indication of gradual material yielding. After cooling, the force generated by the initial preload was found to be below the magnitude at the start of heating. The reduction continued to occur after each cycle of heat/cool was applied and although the indication is that the rate of loss of preload was slowing, it had reached a point where there was insufficient preload to drive the torque in friction. Note that the initial preload value of 30,000 pounds at room temperature was reduced to 8,000 pounds after only one cycle. After the third cycle, the preload was reduced to 3,000 pounds at room temperature. When the elastomer was at elevated temperature, preload was increased which explains why the load sharing did not change once the test had started and the temperature was stabilized.

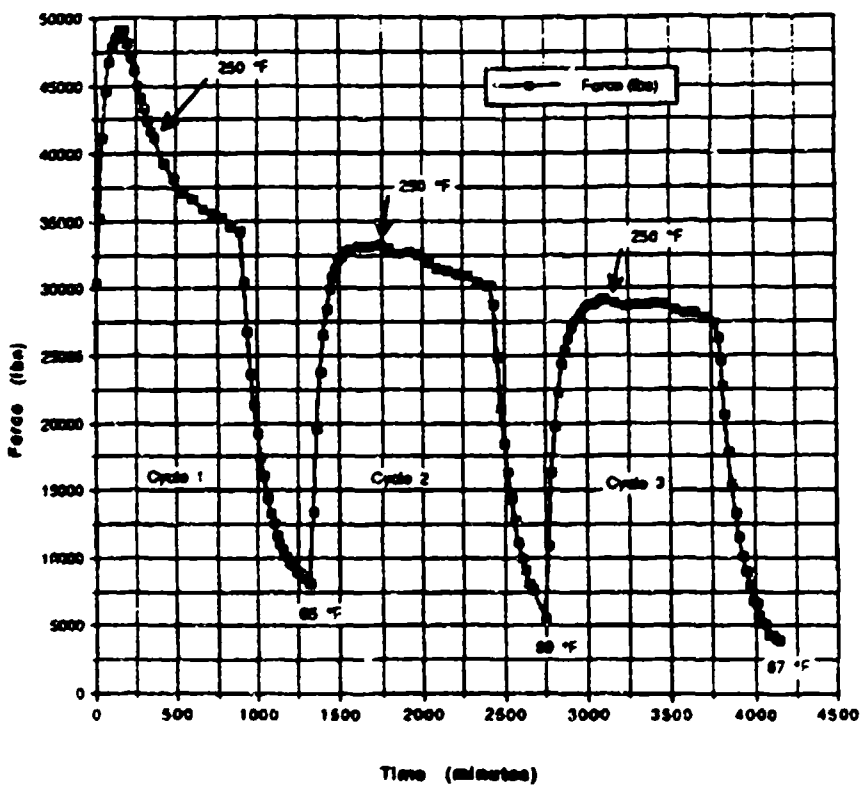

Figure 153. Thermal Cycling of Elastomeric Load Sharing Device

In addition to the performance of the elastomeric load sharing devices, the condition of the gear teeth was also an area of interest during the test. The first 150 hours of testing were performed without encountering any difficulties. However, during the 150 hour visual inspection, a spall was observed on the left hand helix of the upper double helical pinion of the test gearbox. The affected area was considered small and testing was continued. This points out an advantage of the double helical design in that the high overall contact ratio permits operation even with a spalled tooth since adjacent teeth will carry the load with no visible change in performance. At 183 hours, a chip light was produced on the test gearbox. Inspection of the chip detector showed that the chips were from the spalled area. Testing was continued to the 200 hour mark.

Post test inspection revealed two relatively shallow spalled areas on the left hand helix of the upper double helical pinion of the test gearbox (shown in Figures 154 and 155). Pitch line micro-pitting was present on this gear and was also evident to some degree on each double helical pinion. In addition, there was high polishing in the contact area of each double helical pinion. Although this was not considered a problem by itself, it was an indication of surface wear. The polishing was more pronounced on the test gearbox than on the dummy gearbox. The spur pinion and mating gears of both the test and dummy boxes were in excellent condition. Visual inspections of the gears and internal components for additional signs of wear, damage, or cracks did not reveal any discrepancies. Components were magnafluxed to identify cracks. None were found. No evidence of skidding, spalling, or overheating was evident on either the bearing races or the rolling elements.

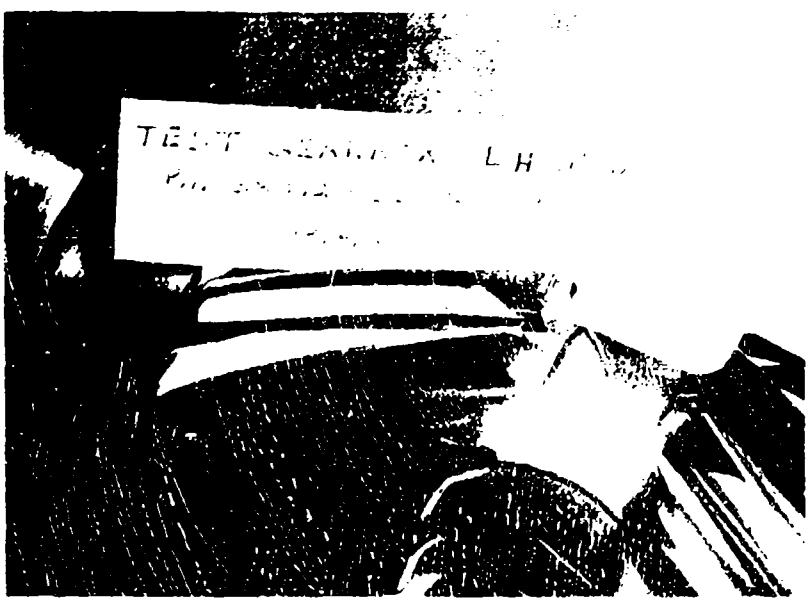

Figure 154. Test Gearbox, Initial Spalled Tooth, Double Helical Pinion

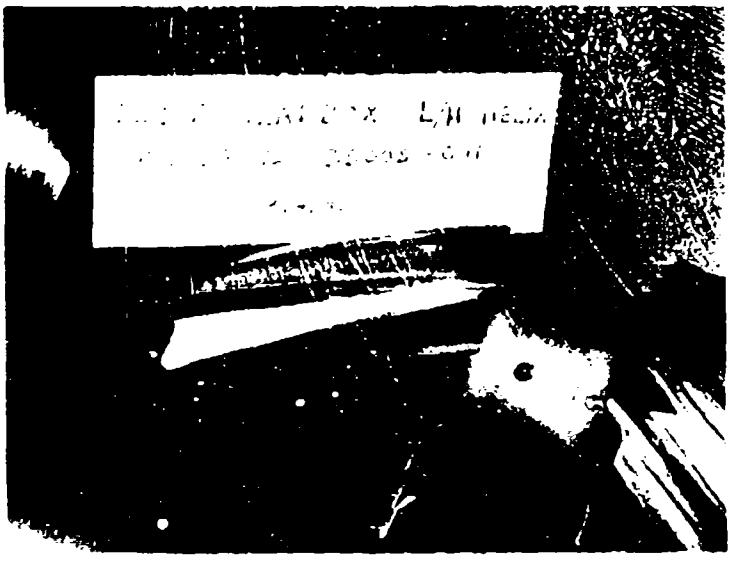

Figure 155. Test Gearbox, Spalled Tooth, Double Helical Pinion

The inspection of the test and dummy gearbox double helical pinions after testing showed that the test gearbox pinions had a higher degree of polish than the dummy gearbox. Since all loading conditions are the same, the test conditions were examined to determine the differences between the test and dummy gearboxes. Two factors are different in the test and dummy gearboxes. First, the test gearbox acts as a conventional pinion in that it has recess action whereas the dummy gearbox has approach action because it has reverse rotation direction and reverse torque direction. This makes the magnitude and direction of load identical in the test and dummy boxes but makes the dummy box pinions contact initially on the tip and slide towards the TIF of the teeth inducing approach action. This is known to be the worst case for surface distress but is not quantified. Second, and most importantly, the temperature of the dummy gearbox was lower than the test gearbox because the dummy gearbox oil system did not have a heater as did the test gearbox oil. The dummy gearbox operated at approximately 120°F vs 180°F for the test gearbox. The temperature difference causes the oil viscosity to be lower in the test gearbox than in the dummy gearbox. Viscosity is a major factor in determination of elasto-hydrodynamic or EHD film thickness. EHD lubrication is a regime which describes the generation of a load carrying film of oil which separates the surfaces of gears where high contact stresses are occurring. An analysis was conducted to determine the theoretical film thickness in the test and dummy gearboxes at the double helical mesh. A conventional way to examine EHD film thickness is to compare the film thickness to the surface roughness ratio, or λ ratio. When $\lambda = 1$, the film thickness is equal to the surface finish and the lubrication is said to be adequate. As the λ ratio drops, there are more "mountains" sticking out of the "valleys". Figure 156 is a plot of λ as a function of temperature which reflects the effect that viscosity has on EHD. The EHD thickness is calculated by the Dowson-Higginson method which is the popular method of calculation. As a note of interest, the investigation into the low EHD phenomenon pointed out the short comings in the current state-of-the-art methodology. Most production helicopters operate successfully without spalling of the output reduction stages of the main gearbox in the range of $\lambda = 0.4$. The current methodology will predict a high probability of distress with this ratio. The enigma lies in the fact that the

allowables are based on data derived from through hardened gears and carburized gears can operate at much lower film thickness successfully. This may explain why helicopter gear designers usually do not use the λ ratio published allowables.

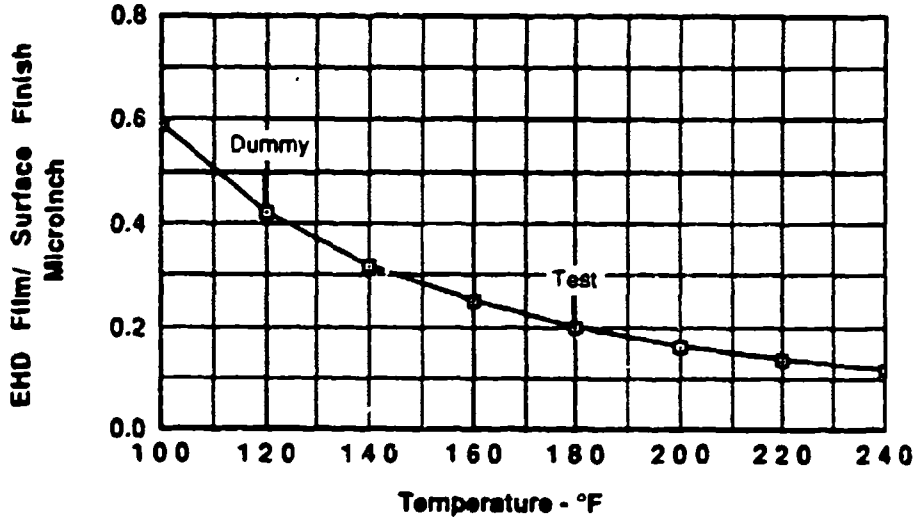

Figure 156. EHD Film/Surface Roughness vs Temperature

Note that the dummy gearbox λ ratio is approximately twice that of the test gearbox because of the temperature difference. The EHD film is greatly influenced by the viscosity of the oil used, and is also influenced by the pitch line velocity of the gears. Load has less of an effect on EHD thickness. The 1/2 scale gearbox modeled bending stress, Hertz stress, and deflection accurately, however it did not duplicate pitch line velocity. The pitch line velocity of the 1/2 size gearbox was exactly 1/2 of the full size gearbox. Since pitch line velocity has a large influence on EHD film thickness, with a higher velocity producing a higher film thickness, the EHD film of the test box was not representative of a full size ACA aircraft and in fact was about 1/2 of what it would be in a full size gearbox. Therefore the spalls generated as a result of the low EHD film thickness in the 1/2 size test gearbox are not representative of the full size ACA gearbox and resulted from unrepresentatively low pitch line velocity.

To address this problem, Mobil SHC 629 lube oil was substituted for the DOD-L-85374 lube oil prior to the start of the overtorque test. Mobil SHC 629 was chosen because it provides an increase in viscosity at the gearbox operating temperature. The increased viscosity provides the test gearbox with the same EHD film thickness at 1/2 the pitch line velocity as the full size ACA transmission.

During the 200 hour endurance test, bearing temperatures stabilized well below the established maximum of 250°F at all endurance test conditions. Table 60 presents typical stabilized bearing and oil temperatures for both the test and dummy gearbox operating at 100% torque.

Table 60. Typical Stabilized Temperatures @ 100% Torque

Thermocouple Locations	Stabilized Temperature °F Test Gearbox	Dummy Gearbox
Lube Oil - Inlet	184.7	96.3
Lube Oil - Outlet	192.4	113.7
Input Shaft - Upper Cover Roller Brg	204.4	131.1
Input Shaft - Lower Cover Ball Brg	179.8	113.8
-041 Shaft - Upper Cover Roller Brg	197.0	126.4
-041 Shaft - Lower Cover Roller Brg	177.3	108.6
-042 Shaft - Upper Cover Roller Brg	199.8	119.5
-042 Shaft - Lower Cover Roller Brg	188.1	118.0
Output Gear - Upper Timken Brg	186.2	111.2
Output Gear - Lower Timken Brg	183.5	109.7
Output Gear - Instrumentation Ball Brg	126.1	N/A

Vibration levels were relatively low with no detectable increase observed over the course of the endurance test. Typical frequency analysis of the vibration experienced on the upper plate of the test gearbox, assembled with the steel housing and elastomeric load sharing devices are shown in Figure 157 while Figure 158 shows the dummy gearbox, assembled with composite housing and elastomeric load sharing devices. The locations of the accelerometers on the test and dummy gearboxes was identical. Comparison of the vibration levels at these locations indicates that for the same operating conditions, the vibration levels on the composite housing are four to five times higher than on the steel housing.

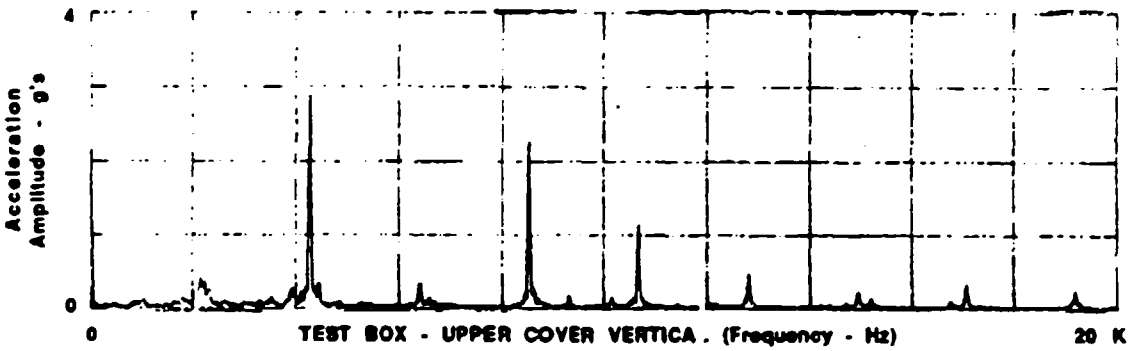

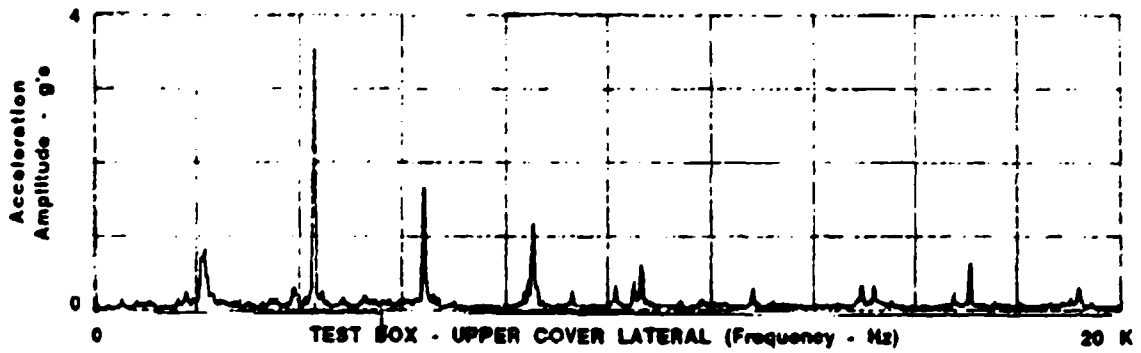

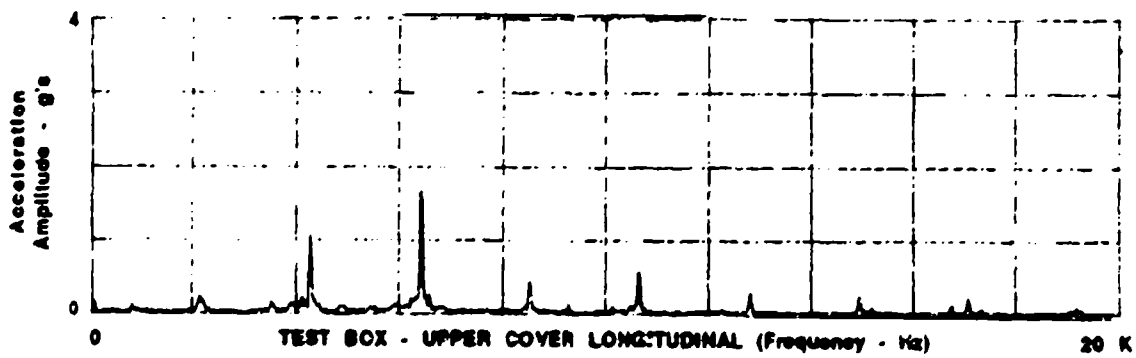

Figure 157. Upper Cover Vibration Frequency Analysis, Test Gearbox

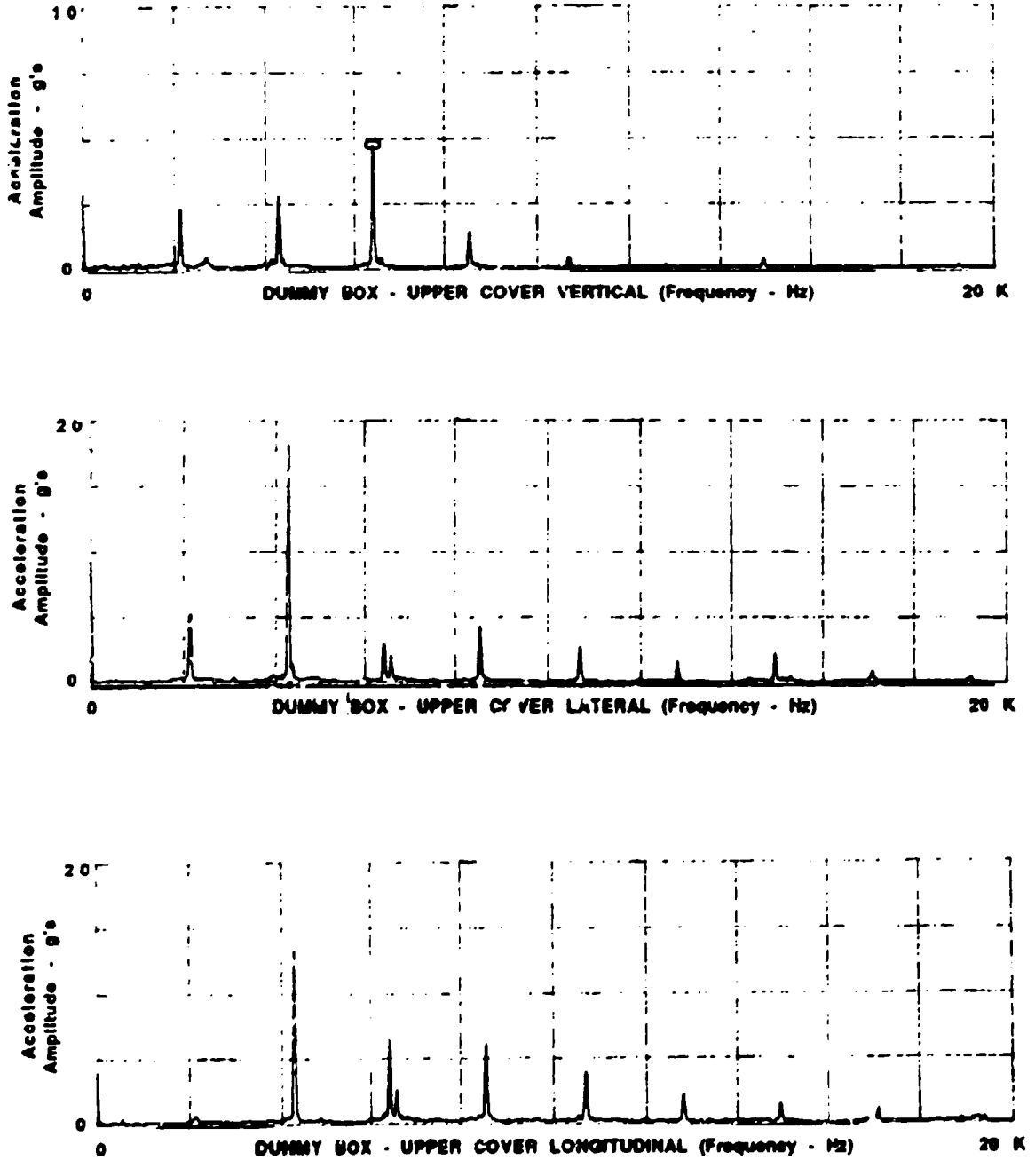

Figure 158. Upper Cover Vibration Frequency Analysis, Dummy Gearbox

1/2 Size Gearbox Test Results, 200 Hour Overtorque

Overtorque testing was conducted in accordance with the procedure presented previously. The configuration of the test box was the steel housing, steel isolators, and Mobil SHC 629 oil. The dummy gearbox had composite housings, steel isolators, and DOD-L-85374 oil. The test gearbox oil was heated to 180°F inlet temperature while the dummy gearbox was permitted to stabilize naturally without heating. Initial testing consisted of 5 hours of operation at 60% torque and an oil outlet temperature of 135°F. This was followed by an additional 5 hours of operation at 60% torque with an oil outlet temperature of 185°F. These low power conditions were intended to break-in the new double helical pinion installed as a replacement for the spalled pinion of the 200 hour endurance test. Once the break-in runs were complete, testing proceeded to the original test spectrum. The overtorque test was suspended after a total of 36.5 hours because of the poor load sharing experienced. During the first hour of break-in running, the load sharing varied considerably. By the end of the first hour of operation, the load sharing was stable at a fixed split of ±22%. Applied loads were limited to 120% on the highest loaded member and did not correspond to 120% total input because of the poor load sharing seen. When the torque on the highest loaded member was 120%, the input torque was at 100%. A summary of the cumulative time spent at each test condition is presented in Table 61.

Table 61. Overtorque Test #1, Cumulative Test Time

% Input Torque	Oil Outlet Temperature	Cumulative Test Time
60	135°F	5.0 Hours
60	185°F	8.5 Hours
75	185°F	6.0 Hours
85	185°F	14.0 Hours
100	185°F	3.0 Hours
120	185°F	0.0 Hours
TOTALS		36.5 Hours

The observed characteristics were symptomatic of "slippage" at the cone seat of the interface between the steel load sharing device and the spur gear. Post test disassembly confirmed that the poor load sharing was caused by slippage at the steel/spur gear interface. Spline backlash measurements indicated that the internal back up splines were in direct contact on both the -041 and -042 idler shaft assemblies. A similar situation was found on the dummy gearbox. This problem was originally observed during dynamic surveys conducted with the steel load sharing devices installed. The installed preload at the joint was increased prior to the overtorque test to address this issue but the increased preload was not successful in preventing slippage at the interface. Since the spline teeth were not intended as the primary drive mechanism, the angular orientation of the spline teeth with respect to the index teeth was not closely controlled. When the spline teeth came into contact from the slippage at the interface, the timing between the left and right members was inadequate and resulted in the poor load sharing seen.

To overcome this problem, the spline teeth of each double helical pinion were ground to correct the angular orientations so that the test and dummy assemblies were matched sets. The double helical pinions, spur gears, and steel load sharing devices were then reassembled with the splines in contact and overtorque testing was restarted. This approach no longer depended on the clamp-up at the cone seat to maintain the relative positions of the gear teeth.

The modifications to the spline teeth improved the load sharing to about ±7%. Although this was within acceptable limits, permitting operation at 120% input torque, it was not as good as expected. Pre-test measurements indicated that the load sharing would be nearly identical. These results indicate that additional factors, such as shaft and/or gear tooth deflections, contribute to the load sharing characteristics when using the solid steel isolators. It is important to note that when the test gearbox was assembled with the elastomeric load sharing devices using the same approach, excellent load sharing was observed prior to any slippage. This result indicates that the elastomeric load sharing devices have an advantage in that they are tolerant of any installation or assembly differences and/or combinations of shaft and tooth deflections because of the lower torsional spring rate.

The second overtorque test was interrupted at 11.5 hours when a chip light was produced on the dummy gearbox. Inspection revealed significant debris on the chip detector. A visual inspection of the dummy gearbox revealed scoring/scuffing was present on the right hand helix of both the upper and lower double helical pinions. The corresponding areas of the bull gear also showed signs of distress but to a lesser degree. The condition is shown in Figures 159, 160, and 161. Based on the degree of surface distress observed, further testing was suspended. A summary of the cumulative time spent at each condition is shown in Table 62.

Table 62. Overtorque Test #2, Cumulative Test Time

% Input Torque	Oil Outlet Temperature	Cumulative Test Time
60	185°F	3.0 Hours
75	185°F	2.0 Hours
85	185°F	4.5 Hours
100	185°F	1.0 Hours
120	185°F	1.0 Hours
TOTALS		11.5 Hours

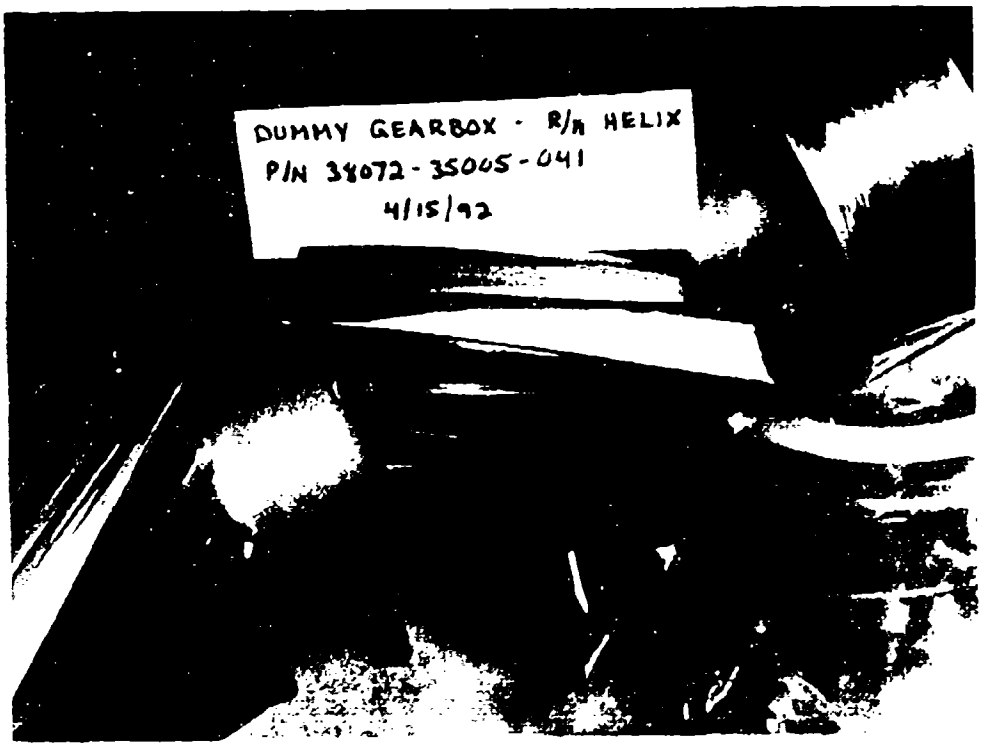

Figure 159. Scuffing on -041 DH Pinion, Overtorque Test

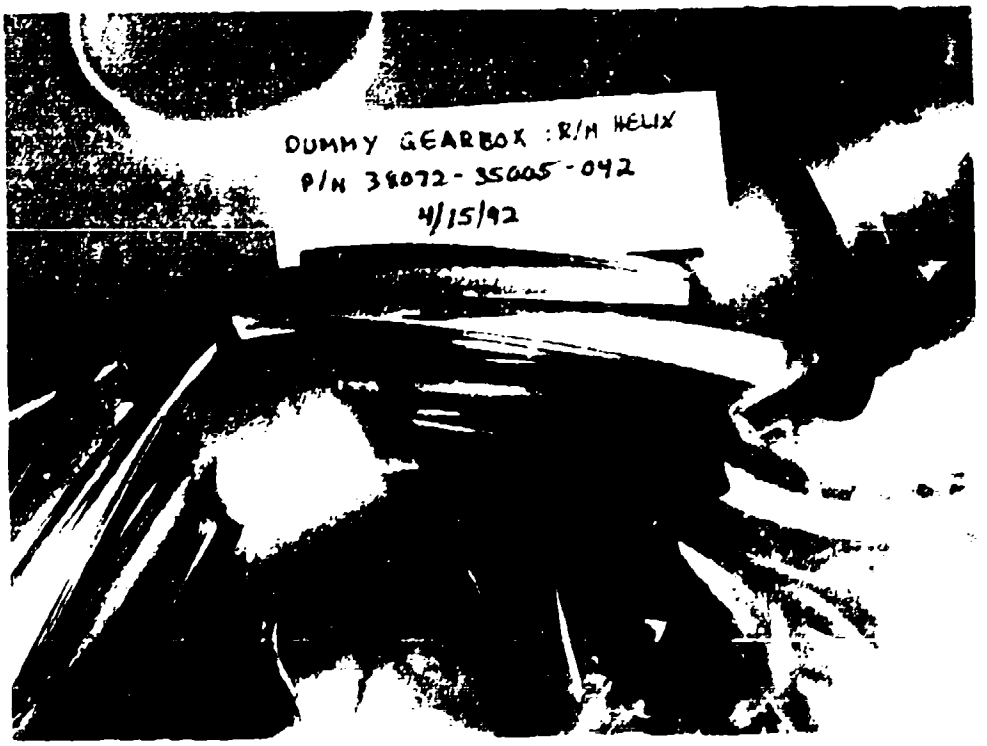

Figure 160. Scuffing on -042 DH Pinion, Overtorque Test

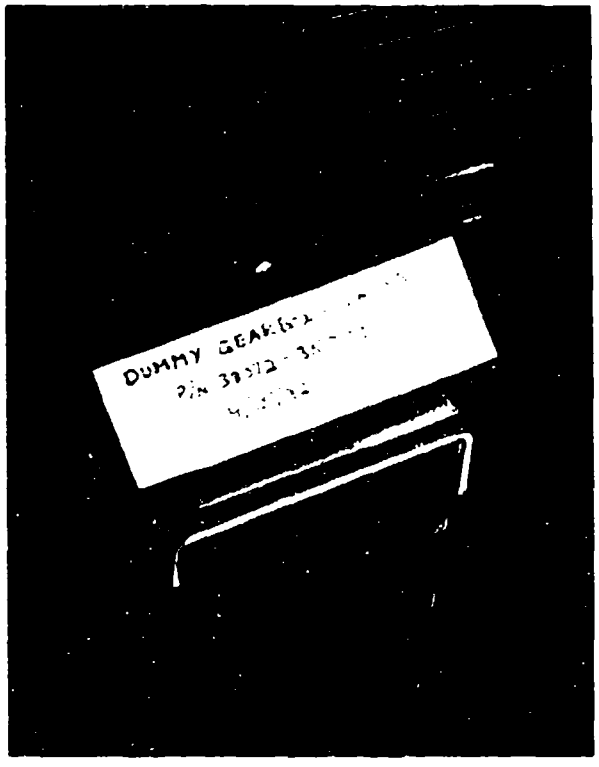

Figure 161. Scuffing on Bull Gear, Overtorque Test

Prior to the scuffing in the dummy gearbox, visual observations made during the scheduled 5 hour inspection found a high degree of polishing on the right hand helix of the -101 double helical pinion in the same area which eventually showed the surface distress. This characteristic was not present on the -102 double helical pinion. Since there was no surface distress in the polished area, testing continued. Post test inspection of the test gearbox showed no signs of distress on any components. The new double helical pinions did not show signs of polishing indicating that the heavier Mobil SHC 629 oil used kept the contacting surfaces apart. The spur pinion and mating gears of both the test and dummy gearboxes were in excellent condition. Magnaflux as well as visual inspection of the gears and other major internal components of the test and dummy gearboxes for additional signs of wear, damage, or cracks did not reveal any discrepancies. There was no evidence of skidding, spalling, or overheating on either the bearing races or rolling elements.

Post test inspection and analysis centered around identifying the cause of the scuffing experienced on the dummy gearbox. As part of this effort, the composite housing was inspected on a coordinate measuring machine. Results showed that the -041 idler shaft bearing bores were misaligned by 0.0064 inch at the upper bearing and 0.0021 inch at the lower bearing resulting in a cumulative error of 0.0085 inch. Since these bearings are located 8.58 inches apart, the -041 idler shaft was operating with a misalignment angle of approximately 0.001 inch/inch. This misalignment, illustrated in Figure 162, tended to shift the load toward the lower end of the right hand helix in the area where the surface distress occurred. Based on the inspection results and the visual polishing of the right hand helix of the dummy gearbox -101 double helical pinion prior to the scuffing, it is deduced that the scuffing first occurred on the -101 double helical pinion because of the shift in load from the misalignment combined with the 120% load condition. The scuffing then

transferred to the double helical gear and then to the -102 double helical pinion. The poor load distribution combined with the 120% load condition in combination with the approach action experienced from reverse tooth engagement of the dummy gearbox is suspected to have caused the surface distress seen.

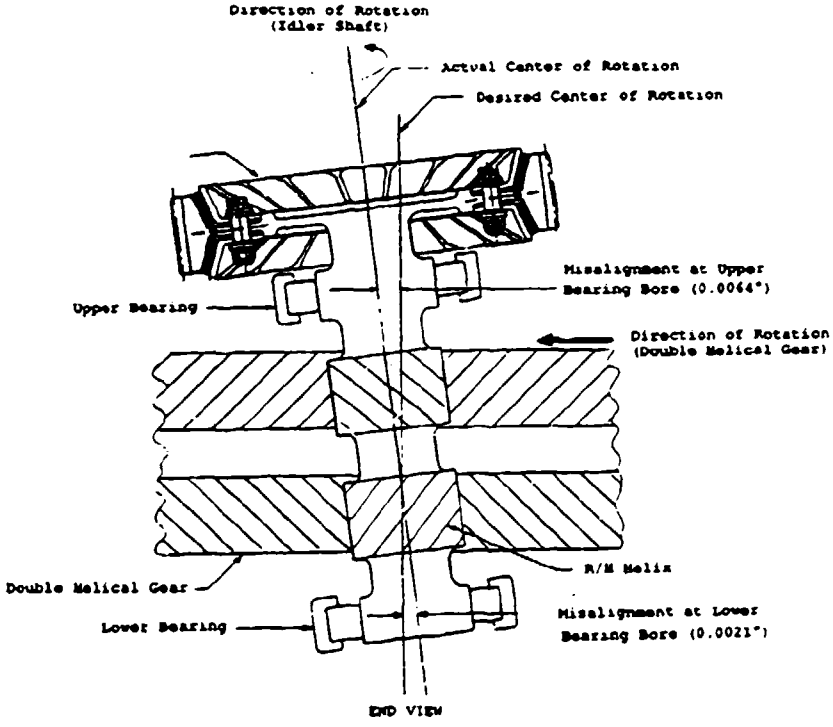

Figure 162. Illustration of Shaft Misalignment

Throughout the overtorque test, bearing temperatures stabilized below the established 250°F for all overtorque test conditions. Table 63 presents typical stabilized bearing and oil temperatures for both the test and dummy gearbox operating at 120% torque.

Table 63. Typical Stabilized Temperatures @ 120% Torque

Thermocouple Locations	Stabilized Temperature °F Test Gearbox	Dummy Gearbox
Lube Oil - Inlet	181.1	96.8
Lube Oil - Outlet	195.4	116.3
Input Shaft - Upper Cover Roller Brg	212.8	117.6
Input Shaft - Lower Cover Ball Brg	180.3	133.7
-041 Shaft - Upper Cover Roller Brg	201.1	125.1
-041 Shaft - Lower Cover Roller Brg	181.1	107.1
-042 Shaft - Upper Cover Roller Brg	209.5	123.2
-042 Shaft - Lower Cover Roller Brg	191.0	121.1
Output Gear - Upper Timken Brg	186.6	106.4
Output Gear - Lower Timken Brg	182.4	107.4
Output Gear - Instrumentation Ball Brg	120.8	N/A

In addition to bearing and lube oil temperatures, gear blank temperatures were also measured using thermocouples installed in the tooth roots of the upper and lower double helical pinions of the test gearbox. These measurements showed that the bulk temperature of the gear blank, calculated as the average of individual tooth root temperatures and corrected to an oil inlet temperature of 185°F was dependent on shaft load as shown in Figure 163. Note also that the bulk temperatures measured were significantly lower than the oil inlet and outlet temperatures. Typical gear blank temperatures were approximately 40 to 50°F below the oil temperatures.

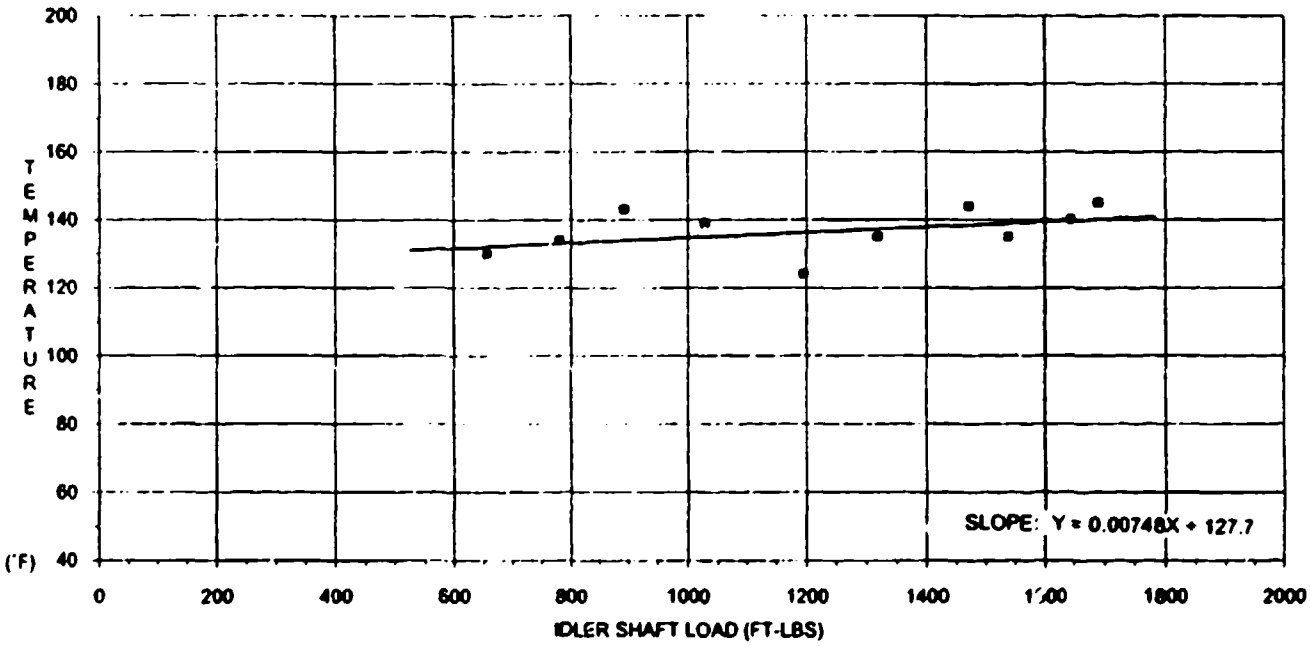

Figure 163. Gear Blank Temperature vs Idler Shaft Load.

Table 64 represents a typical distribution of gear blank temperature measured on the double helical pinion during the second overtorque test. Results have been tabulated as a function of shaft torque and have been corrected to an oil inlet temperature of 185°F. The temperatures represented for each power condition are the average of the cumulative data which was collected at that power. Note that the temperatures across the teeth were not constant. The variations between the upper and lower idler shafts illustrate the effect of shaft load on tooth root temperature since the lower shaft carried 14% more load than the upper shaft from the ±7% torque split.

Table 64. Tooth Root Temperature Distributions

Location	% Input Power		
	60%	100%	120%
Upper LH Helix, Gear End	145.3	148.9	151.8
Upper LH Helix, Center	135.7	134.3	139.4
Upper LH Helix, Input End	143.5	149.0	155.5
Upper RH Helix, Gear End	143.5	146.5	152.4
Upper RH Helix, Center	139.6	141.0	147.3
Upper RH Helix, Input End	no data	no data	no data
Lower LH Helix, Center	149.5	153.7	155.6
Lower RH Helix, Center	152.6	157.5	162.2

In addition to the tooth root temperature measurements, an additional thermocouple was installed directly in the path of the oil being ejected from the LH helix of the upper double helical pinion which measured the "fling-off" oil temperature. The intent of this measurement was to quantify the film temperature of the lubricant in the area where the spalling had occurred during the endurance test. Results indicated that this temperature was also dependent on shaft load as shown in Figure 164. The results have been corrected to an oil inlet temperature of 185°F. The fling-off temperature was generally found to be from 1 to 5°F higher than the oil outlet temperature.

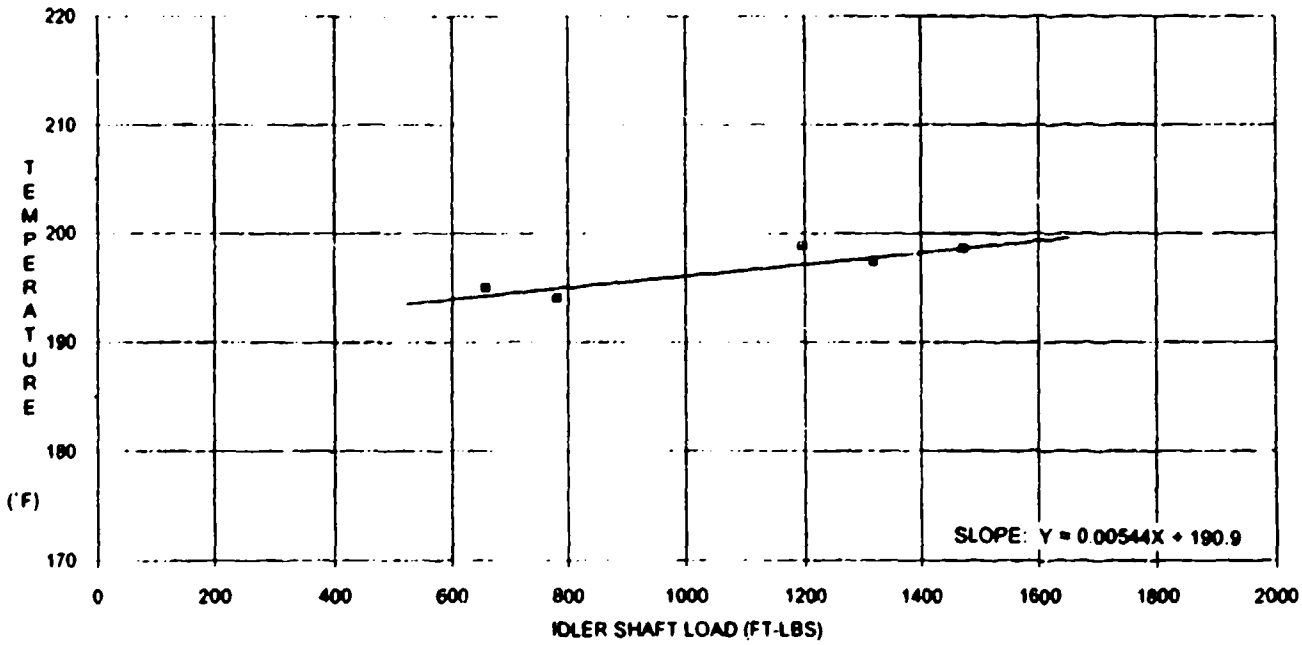

Figure 164. Fling-off Oil Temperature vs Idler Shaft load

Vibration levels experienced during the overtorque test were consistent with levels experienced during previous testing. Direct comparison of the vibration levels experienced with each type of housing (composite and steel) and each type of load sharing device (elastomeric and steel) are shown in Figure 165. Table 65 summarizes the vibration levels at the first and second harmonic of the spur gear clash frequency. The conclusions drawn from this data are as follows:

- The elastomeric load sharing device reduced the energy transmitted to the housings at the spur gear clash frequencies and the associated harmonics.
- The composite housing experienced higher vibration levels than the steel housing.
- The vibration energy associated with the spur gear mesh was much higher than the vibration levels associated with the double helical mesh.

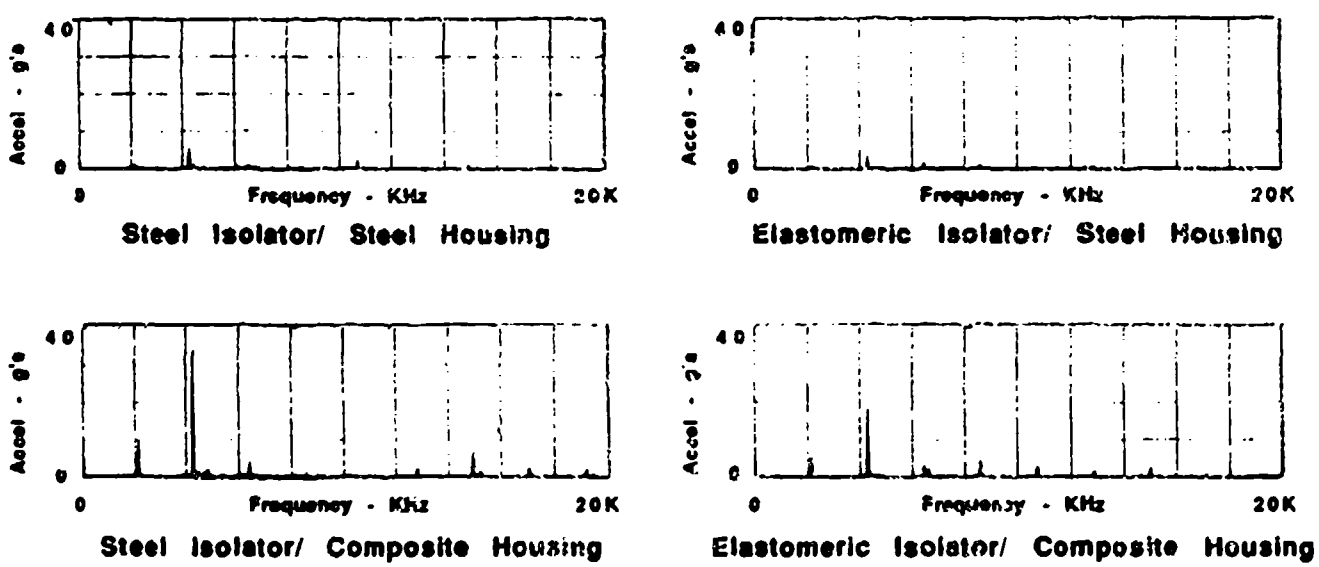

Figure 165. Comparison of Typical Vibration Levels

Table 65. Comparison of Typical Vibration Levels

Location	Elastomeric		Steel	
	Test	Dummy	Test	Dummy
2138 Hz Gear Clash, Up Cov Vertical	0.4	2.4	0.7	3.8
2138 Hz Gear Clash, Up Cov Lateral	0.8	5.2	1.1	10.1
2138 Hz Gear Clash, Up Cov Longitudinal	0.2	0.6	0.2	0.8
4276 Hz 2nd Harmonic, Up Cov Vertical	2.9	2.8	6.2	1.5
4276 Hz 2nd Harmonic, Up Cov Lateral	3.5	18.2	5.4	33.8
4276 Hz 2nd Harmonic, Up Cov Longitudinal	1.0	13.4	1.7	25.3

Bearing Test Results

Bearing testing was conducted at McGill Manufacturing Co., Valparaiso, Indiana. Two types of bearings were tested. Both bearings had identical inner and outer races fabricated from Pyrowear 53 carburizing material. The retainers were fabricated from SAE 8620 steel per AMS-6274 and were identical in each bearing. The difference between the two bearings was in the roller material which was Pyrowear 53 for the bearing termed "steel" and silicon nitride for the bearing termed "ceramic".

Testing of the angular contact spherical roller bearings consisted of a preliminary survey, a 250 hour proof test, and a lost lubricant survivability test for both the steel and ceramic bearings. The object of the tests was to show that the angular contact spherical roller bearing could replace the combination of a cylindrical roller and split angular contact ball bearing in a high speed application with improved reliability, service life, and survivability. The lost lubricant tests were conducted to demonstrate the improved survivability and compare performance of the steel and ceramic rolling elements.

Preliminary survey tests were conducted on both the steel and ceramic bearings. In these tests oil flow, end play from 0.002 to 0.016 inch, speed, thrust load, and radial load were varied and operating temperatures measured. The ceramic bearing had lower induced temperatures than the steel bearing for most load cases and also ran with lower vibration magnitudes. As an example, comparison of measured and calculated induced axial thrust for the steel bearing is shown in Figure 166 and for the ceramic bearing in Figure 167.

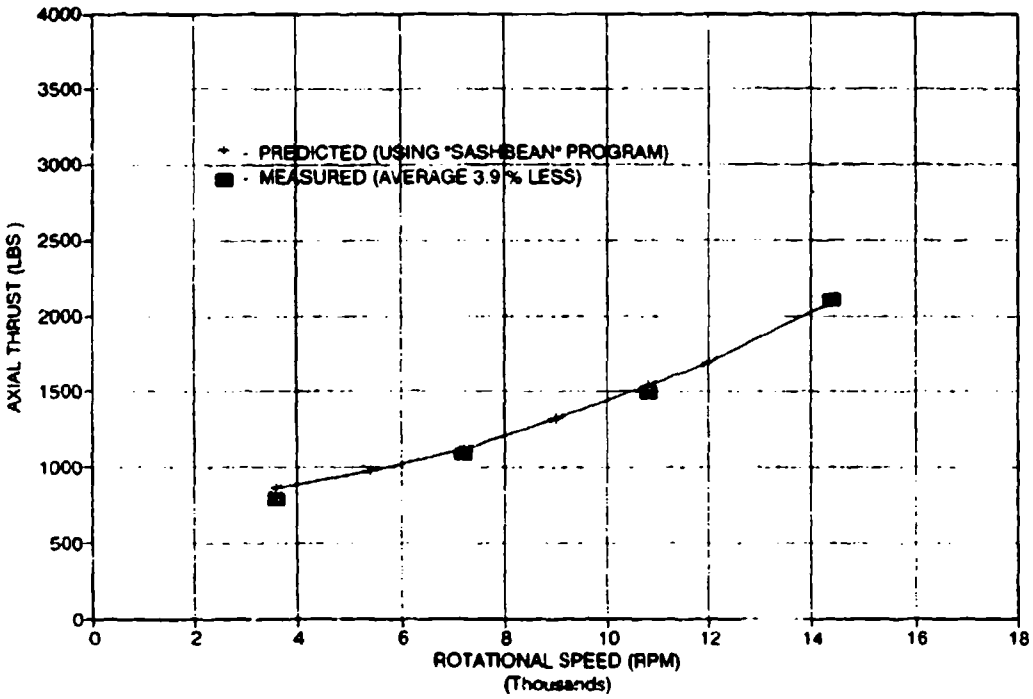

Figure 166. Measured and Predicted Induced Thrust, Steel Bearing

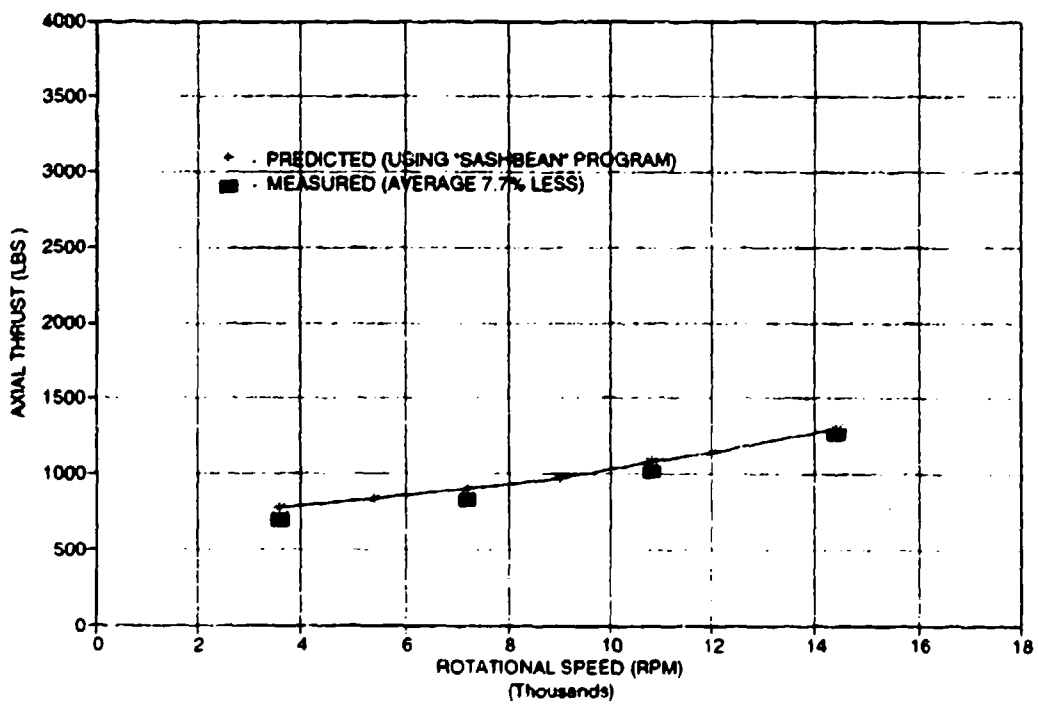

Figure 167. Measured and Predicted Induced Thrust, Ceramic Bearing

The predicted values are calculated by the computer program "SASHBEAN" which was developed during the ART program by McGill for conducting analysis of angular contact spherical roller bearings. The predicted thrust is based on 2400 pound radial load (50%).

After completion of the survey testing, the ceramic bearing was in excellent condition but the steel bearing had signs of discoloring and staining from oxidized oil and heat generated during the tests. A line of extremely small pits or micro spalling had developed at the juncture of the outer raceway and the retainer guiding land. Normally, the roller would not contact in this area and a change in design parameters will remedy the problem in future designs.

Proof tests of 250 hour duration were conducted on the steel bearing and ceramic bearing at 100% load. The 100% load condition was 14,400 rpm, 4,600 pound radial load, and 3,100 pound axial load. Table 66 compares average temperature readings taken on the steel and ceramic bearings during these tests.

Table 66. Steel vs Ceramic Bearings, 250 Hour Proof Tests

	Steel	Ceramic
Average Load Zone Temp (°F)	277	274
Average Manifold Temp (°F)	157	158
Average Ambient Temp (°F)	95	97

After the 250 hour proof tests, the bearings were visually examined. The steel bearing components showed that discoloration had developed on half of the inner race path, with a heavy buildup of oxidized oil on the surface not contacting the roller or the retainer bore. Oxidized oil buildup was also found on retainer faces and roller ends. The juncture of the spherical race and inner OD had developed a fine line of spalling from the rollers operating over the edge similar to that found in preliminary testing but to a lesser extent. The outer race and rollers also exhibited the discoloration in corresponding areas to that of the inner race but to a lesser degree.

Microscopic examination of the race load zone surfaces of the steel bearing revealed that minute metal particles were removed from the contact surfaces in the form of microspalls, which is an indication of lubrication related distress.

Visually, the ceramic bearing was in good condition after the 250 hour proof test. The inner and outer races were stained from the oxidized oil although not to the extent found on the steel bearing races. Again, a heavy buildup of oxidized oil was found on the roller ends, retainer faces, and the inner race OD where no contact was made. Along the roller length, in the contact area, the ceramic roller OD was lightly stained; however it could be easily removed.

Lost lubrication testing was also accomplished on the steel and ceramic bearings. The test was conducted by stabilizing bearing temperature at full load, shutting off the oil supply, and reducing the radial and axial load to 53% of maximum. Load zone temperature was then monitored. The steel bearing survived for 1 minute and 28 seconds while the ceramic bearing survived for 22 minutes. Figure 168 is a plot of load zone temperature vs time.

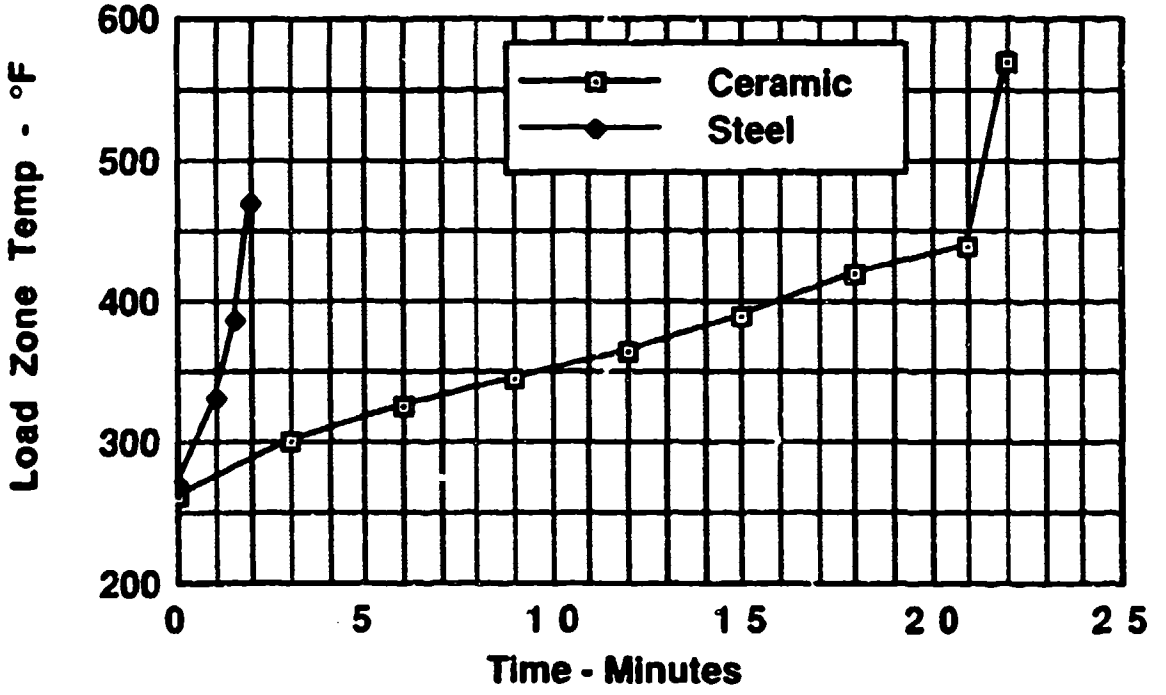

Figure 168. No Oil Survivability Test Results

Post test examination of the ceramic bearing showed that the cage had fractured on the outboard flange side, separating in one location. The rollers had skewed excessively in the pockets as a result of crossbar wear at the contact areas, causing the rollers to try to roll under the crossbar. This resulted in a bulge developing circumferentially over three or four rollers, which eventually failed in tension, rupturing the retainer end rail. The outer race load zone contained micro pits in the contact area from minute particles of metal that were pulled from the surface. Adjacent to the contact area, the oil that had remained in the bearing had oxidized, discoloring the surface or leaving a hard residue. The inner race was also pitted, stained, and oxidized similar to the outer. At no time did the bearing seize or lock up during the test, as no smearing or skidding was observed. The ceramic rollers were stained and oxidized, but did not show evidence of distress.

Examination of the steel bearing after the lost oil test showed that the cage had not failed, although the crossbars were heavily worn from contact with the rollers during the short test duration. The bore of the retainer was worn nearly 0.006 inch on one side while the opposite side exhibited minor wear. This could be attributed to the difference in area of contact between the two sides with the larger area having the smaller wear. The inner raceway was dented and pitted, with oxidized remnants of the lubricant present out of the

contact area. The outer and inner races were damaged from metal and silver debris from the retainer wear. The rollers exhibited the same condition as the inner and outer races, with pitting, denting, and metal adherence to the surfaces.

Both the steel and ceramic angular contact spherical roller bearings performed well during the above tests. The ceramic bearing could run with end plays up to 0.016 inch at full load while the steel could run at 0.008 inch. The validity of the designs was demonstrated by the 250 hour proof tests even under marginal lubrication conditions. Lost lubrication testing was partially successful and pointed out the problems with existing designs. Cage wear can be reduced by designing for greater contact area. It is perceived that the ceramic bearing can be made to last for one hour after loss of lubricant if cage wear can be reduced.

CONCLUSIONS

1. A split path gearbox with a high ratio double helical gear output stage is 23% lighter, greater than 10 dB quieter, and nearly 4 times more reliable than the current state-of-the-art transmission in an Army Cargo Aircraft.

2. A split torque gearbox characterized by a torque splitting planetary and a high reduction ratio double helical mesh on the output is lighter and more reliable than a state-of-the-art gearbox with planetary output stage but not as light or reliable as a split path gearbox.

3. An overrunning clutch located on the input of the transmission is significantly lighter than an overrunning clutch located at some other point in the transmission drive train because the torque is lower at the input. A spring type overrunning clutch is proposed for reduced dynamic high speed effects.

4. A derivative of weight with respect to output stage reduction ratio was found to be 270 pounds for each additional integer of reduction ratio. This equates to 3.3% weight for each additional integer of ratio or a 10% weight reduction for an increase in reduction ratio of 3 to 1 at the output stage.

5. Composites used in transmission systems in areas such as housings, main rotor shafts, quill shafts, support structures, and drive shafts result in significant weight savings.

6. Weight savings in the transmission system has an affect on other systems if the aircraft is resized such that a 23% reduction in transmission system weight saves 34% if all other aircraft weight savings are included in transmission weight savings.

7. ACA Transmission operating cost is reduced by more than $300 per flight hour from reduced depot maintenance associated with the MTBR improvement from 997 hours to 3890 hours.

8. Aircraft fleet life cycle costs are reduced by $1.7 billion as a result of the weight and reliability improvements.

9. As a result of the configuration of split path designs, accessories can be driven directly by available gearing without the need for additional drives.

10. Grinding of double helical gears with cubic boron nitride grinding wheels permits small wheel diameters to be used without sacrifice in grinding time compared to larger, conventional aluminum oxide wheels, and therefore results in designs with smaller shaft lengths between the left and right hand double helical gears. This leads to direct weight savings.

Fatigue fretting tests were conducted with Pyrowear 53 specimens with and without thin dense chrome plating. Based on the results obtained, the following conclusions are drawn:

11. There is no improvement or reduction in fretting fatigue allowables between Pyrowear 53 and 9310 gear materials.

12. There is no improvement or reduction in fretting fatigue allowables between bare Pyrowear 53 and thin dense chrome plated Pyrowear 53 gear materials.

Angular contact spherical roller bearings were tested with steel and ceramic rolling elements. Based on the results obtained, the following conclusions are drawn:

13. A single angular contact spherical roller bearing can be designed to carry combined radial and thrust loads and replace the current state-of-the-art ball/roller bearing combination typically used on the spiral bevel input section of helicopter gearboxes.

14. Ceramic rolling elements with steel races worked better than steel rolling elements with steel races in terms of prevention of surface distress in high speed applications.

15. No oil survivability testing showed that ceramic rolling element bearings generated less heat and survived longer than steel bearings (22 minutes for ceramic vs. 1.5 minutes for steel). With development work on the bearing cage for the ceramic configuration, survivability can be increased.

The ART 1/2 size gearbox accumulated approximately 323 hours of operation during the no-load lubrication, gear pattern development, dynamic surveys, endurance, and overtorque testing. Based on operational experience gained from these tests, the following conclusions are drawn:

16. Split path gearbox operating temperatures stabilized well within acceptable limits during all testing. The oil temperature rise was small throughout the gearbox indicating that churning and windage losses are low and efficiency is high.

17. Gear teeth were topologically modified during the design phase using finite element analysis. The initial grinding corrections incorporated into the original gear manufacturing process produced acceptable gear tooth patterns evaluated by visual inspection and by analysis of tooth root strain gage readings. These results demonstrate that topological tooth profiling, with grinding corrections developed during the design stage, can lead to reduced development testing.

18. The addition of copper and silver plating on several gear teeth permitted load patterns to be discerned more readily by visual examination during pattern development.

19. The pressure produced at the interface between the elastomeric load sharing device and spur gear cone seat and between the steel load sharing device and spur gear cone seat was insufficient to drive the gear in friction because of a "creep" phenomenon that was produced. Future designs must have a positive drive.

20. The elastomeric load sharing device will not meet operational requirements in its present form. Although the elastomeric load sharing devices resulted in excellent load sharing after initial assembly, the properties of the elastomeric material were affected by temperature cycling eventually resulting in loss of clamp up and slipping. Some form of temperature compensation or more resistant material is required in future transmission applications to perform satisfactorily.

21. Gearbox operation using the steel load sharing devices demonstrated that acceptable load sharing could also be achieved without any load sharing device as long as manufacturing and installation tolerances are adequately controlled.

22. Gear tooth surface degradation (spalling) observed at the end of the 200 hour endurance test was caused by an inadequate EHD oil film thickness. The root cause of the poor film thickness was the reduced size of the test gearbox (1/2 size) and was not representative of a full size gearbox.

23. Gear tooth surface degradation (scuffing/scoring) experienced during the overtorque test was caused by a combination of unrepresentatively low EHD oil film thickness, a misalignment of the pinion shaft bearing bores, and the approach action associated with the dummy gearbox as opposed to the normal recess action.

24. A composite housing was installed on the dummy gearbox throughout the endurance and overtorque testing. The dummy gearbox oil was not heated during testing and temperatures stabilized at 120°F or less. The temperature rise in the dummy gearbox with composite housing was approximately the same as in the steel housing. Although the low temperatures indicated good thermal stability, the composite material was not subjected to typical helicopter gearbox operating temperatures.

25. The double helical split path configuration was dynamically stable. The vibration energy associated with the spur gear mesh was much higher than the vibration levels associated with the double helical gear mesh. The use of elastomeric components reduced the vibration transmitted to the housings. Gearbox operation was quieter with the elastomers installed that with the steel load sharing devices.

26. The composite gearbox housings experienced higher vibration levels than the steel gearbox housings.

27. Transmission error (TE) and housing vibration measurements produced good correlation for the double helical and spur gear meshes as functions of operating speed and torque. The results demonstrated that the elastomeric load sharing devices decreased the TE levels measured at the spur gear mesh, but did not effect TE at the double helical gear mesh. Additional analysis of the TE data are required to confirm that the measurement system provided sufficient resolution and sampling rates to accurately measure the ART gearbox TE levels reported herein.

28. Tooth stresses calculated from strain data, showed vibratory amplitudes to be within material allowables at 100% load. Changes in speed had little effect on the gear tooth stresses produced indicating that the ART gearbox has a dynamic factor of approximately 1.

29. Housing strain levels were extremely low on both the steel and composite housings and well below allowable limits for each of these materials.

Appendix A, Results of Related IR&D Efforts

As separate programs, several IR&D efforts were undertaken that were related to work conducted during the ART program but not specified in the ART program statement of work. The components discussed below were developed under IR&D funds and tested in conjunction with the ART 1/2 size gearbox test.

Composite Housing

A composite gearbox housing was designed and fabricated for testing as the dummy gearbox of the 1/2 size gearbox test facility. The interface between the internal gearing and bearings of the ART 1/2 size test gearbox, which was fabricated from steel, was identical in the composite and steel gearbox housings. During the design phase of the ART program, the 1/2 size gearbox housing design was conducted as if were made of composite material, since the full size gearbox was also composite, and then steel was substituted for the test program. The majority of the tooth deflections in both the spur gear mesh and the double helical gear mesh were induced by deflections of the shafts, gear rims, and webs of the internal components rather than by the housing deflections themselves. This was true for the composite as well as the steel gearbox.

The composite housing was incorporated into the build-up of the dummy gearbox prior to the start of the 200 hour endurance test. The composite housing assembly consisted of two parts. The upper cover was essentially a 1 inch thick flat plate. This plate was fabricated from prepreg material and cured in an autoclave. The plate was then machined flat with the assembly holes completed and the bearing bores semi-finished. The lower housing was fabricated as a resin transfer molded (RTM) part. The RTM dies were made by first fabricating a wooden mock up of the housing. Fiberglass splashes were made of the interior and exterior surfaces of the wooden mock up. The fiberglass splashes were then used as molds for low melting point Kirksite alloys to make the RTM dies. Drapeable graphite was then assembled in a quasi-isotropic lay-up at orientations 0°, 90°, and ±45° to achieve the required thickness. The resin, which was an epoxy compounded with latex rubber, was then injected into the mold at a controlled temperature and pressure. The latex rubber with epoxy was used to improve the fracture toughness but results were not encouraging. The housing was first partly cured in the mold, then removed and finish cured. The test article was completed by the addition of steel liners. Finally, the upper and lower housing were assembled and finish machined as a matched set. The assembly of the 1/2 size gearbox with composite housing is shown in Figure 169 with a photograph of the unassembled housing matched set shown in Figure 170.

The 1/2 size composite housing was designed to withstand the loads by a single engine input path of a full sized gearbox. It is important to note that an actual ACA aircraft installation would not impose the unbalanced loads associated with a single engine input. Loads on the bull gear bearings from the engines would be balanced for equal powers on each engine since the three engine inputs are equally spaced in three groups of two pinions each about the bull gear. In actual applications, some percent of rotor loads would also be imposed redundantly on the housing with most of the loads being carried by the truss arrangement. The 1/2 size gearbox represents the worst case in terms of the resultant bull gear bearing load, and therefore housing strain, since it has only one unbalanced input even though the rotor loads are absent. Analysis has shown that less than 5% of rotor loads are reacted by the housing. In the 1/2 size gearbox, the resultant bearing load on the bull gear is in excess of 10,000 pounds at 100% load.

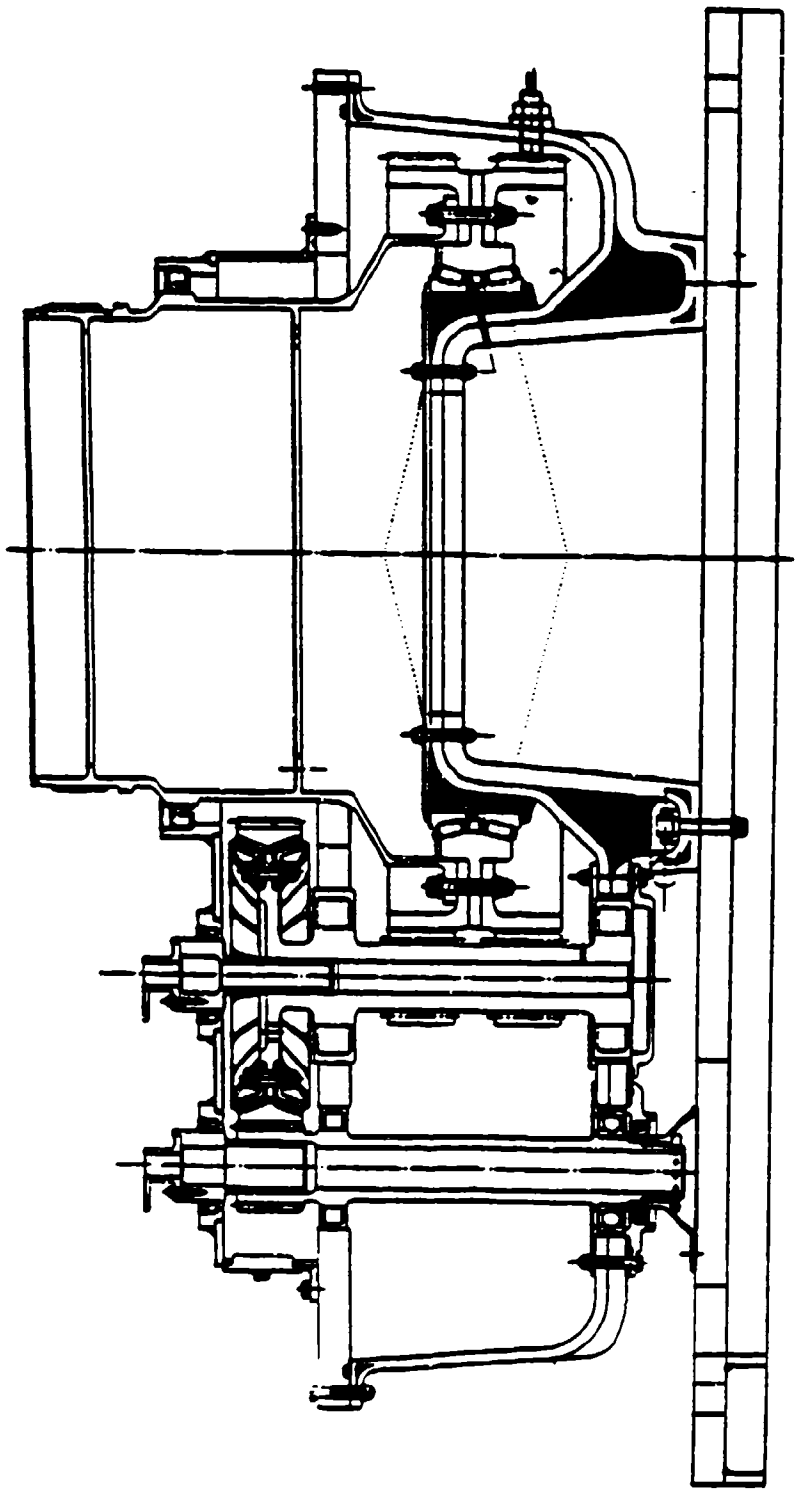

Figure 169. 1/2 Size Gearbox With Composite Housing

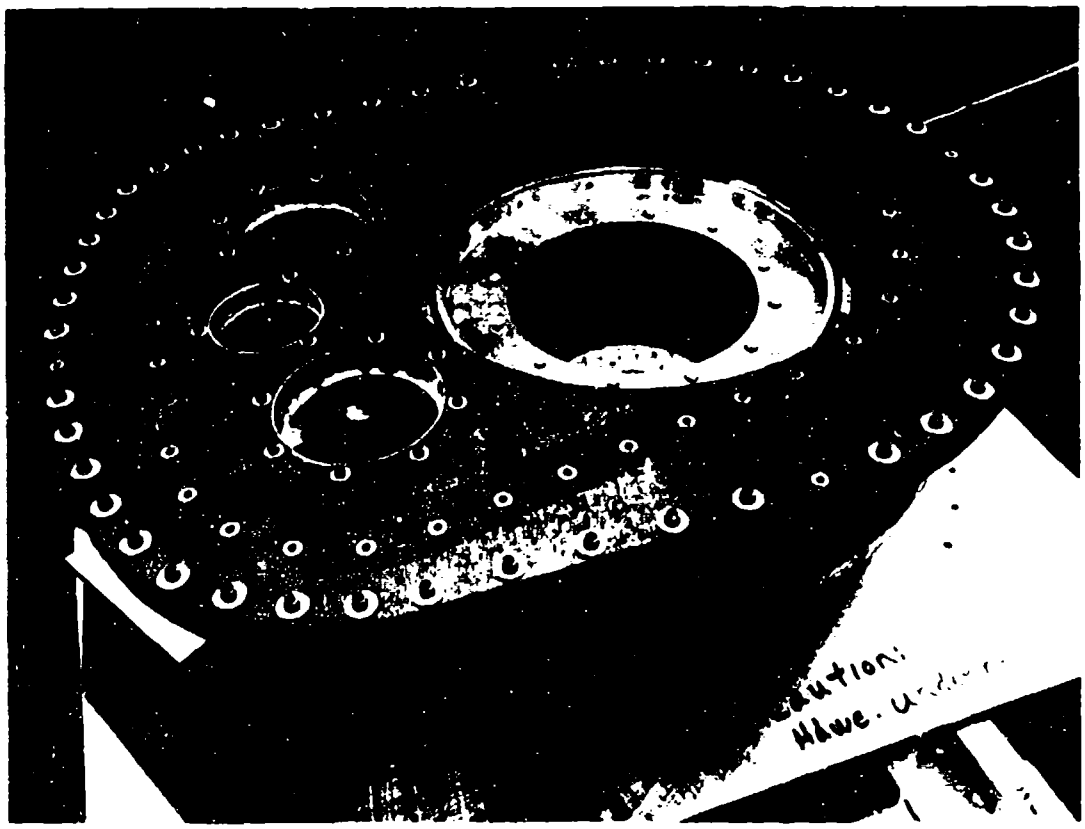

Figure 170. Unassembled Composite Housing Matched Set

The composite housing was instrumented to determine the magnitude and direction of the principle strain at key locations. Allowable housing strain was 4000 microinches per inch at the 100% power condition. A total of 10 strain rosettes (rectangular type) were applied to the housing with three rosettes located on the upper plate as shown in Figure 171 and seven rosettes located on the lower housing as shown in Figure 172. Gage locations were selected using a finite element analysis which predicted where peak strain points were expected. Strain rosettes were of the following type:

Make	Micro-Measurements
Model	CEA-03-250UR-350
Grid Length	0.250 inch
Range	0-2,000 microinch/inch
Accuracy	±5% Full Scale

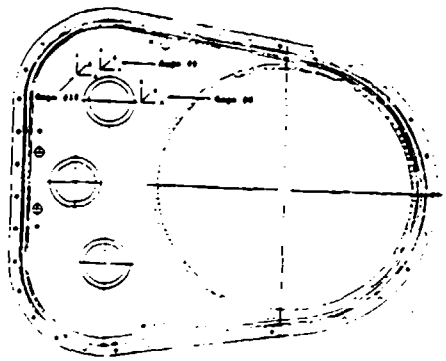

Figure 171. Composite Housing Strain Gage Locations, Upper Plate

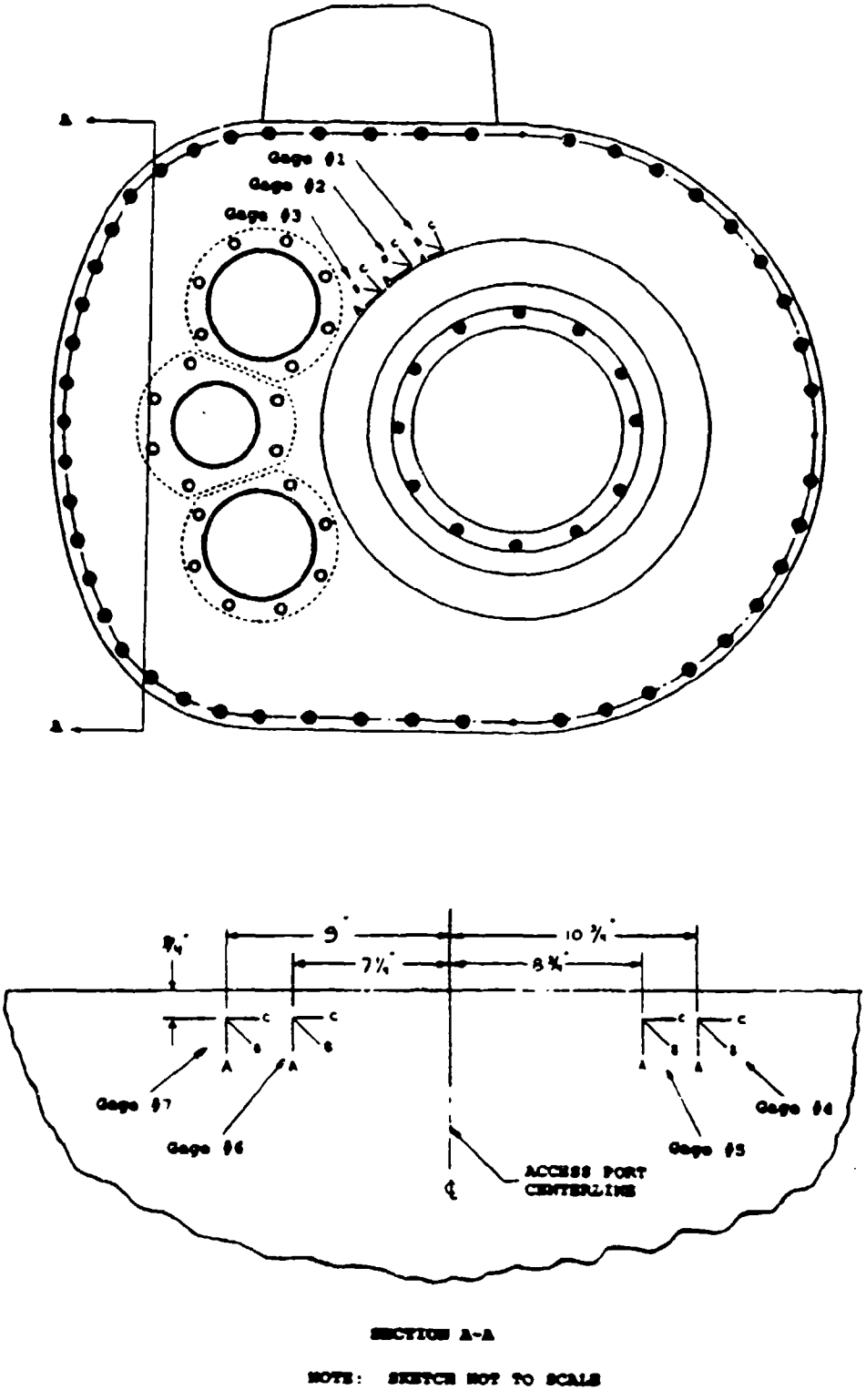

Figure 172. Composite Housing Strain Gage Locations, Lower Housing

A strain survey was conducted at each condition identified in Table 67. Strain data was recorded on magnetic tape using a fourteen channel SABRE 80 tape deck. Tape speed was set at 30 inches per second to provide a frequency response of 20 KHz.

Table 67. Housing Strain Survey Test Conditions

Test Condition	Input Speed %	Input Speed rpm	Input Torque %	Input Torque in-lbs
1	100%	4933	25%	2070
2	100%	4933	50%	4140
3	100%	4933	75%	6210
4	100%	4933	100%	8280

Data reduction was performed using the equations for rectangular rosettes. The rosette is shown in Figure 173 for reference.

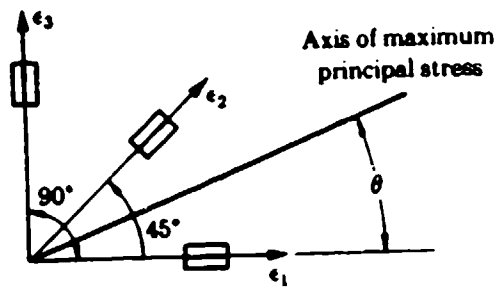

Figure 173. Rectangular Strain Gage Rosette

A summary of the principle strains for the composite housing is presented in Table 68. Strain levels were low on the composite housing and were below the allowable limit for this material.

Table 68. Composite Housing Strain Survey Results

Location	Test Torque %	Principle Strain Microinch/in Maximum	Minimum	Principle Strain Axis
Rosette #1	25%	106.4	4.6	17.7°
	50%	198.8	5.2	16.6°
	75%	295.5	5.5	16.2°
	100%	392.7	25.3	15.0°
Rosette #2	25%	95.2	-30.2	7.6°
	50%	187.4	-71.4	10.4°
	75%	295.6	-119.6	11.2°
	100%	414.8	-156.8	13.0°
Rosette #3	25%	224.5	-1.5	-12.4°
	50%	252.5	-4.5	2.5°
	75%	368.2	-19.2	6.6°
	100%	502.5	-41.5	7.2°
Rosette #4	25%	14.7	-3.7	-22.5°
	50%	38.3	-18.3	-16.0°
	75%	57.5	-30.5	-20.2
	100%	81.0	-52.0	-21.6°
Rosette #5	25%	7.4	-13.4	-36.7°
	50%	26.0	-17.0	-27.2°
	75%	47.8	-13.8	-27.1°
	100%	71.8	-23.8	-26.3°
Rosette #6	25%	24.7	-5.7	-8.6°
	50%	57.0	-11.0	-12.2°
	75%	92.0	-15.0	-18.7°
	100%	126.6	-27.6	-18.5°
Rosette #7	25%	24.5	-30.5	-39.8°
	50%	36.8	-55.8	-39.7°
	75%	56.1	-90.1	-36.7°
	100%	71.6	-140.6	-37.5°
Rosette #8	25%	20.0	-51.0	-19.6°
	50%	23.5	-92.5	-22.2°
	75%	20.6	-149.6	-24.6°
	100%	28.5	-210.5	-28.0°
Rosette #9	25%	47.2	-56.2	-14.2°
	50%	62.7	-109.7	-7.2°
	75%	87.4	-163.4	-4.4°
	100%	119.5	-225.5	-2.2°
Rosette #10	25%	11.2	-72.2	27.9°
	50%	33.9	-153.9	32.4°
	75%	53.6	-201.6	34.4°
	100%	71.9	-263.9	36.2°

Inductive Debris Monitor (IDM)

The inductive debris monitor (IDM) is an improved chip detector. Current magnetic chip detectors would benefit from improvement in capture efficiency, metallic but non-magnetic particle sensing (i.e. brass, aluminum, magnesium, and stainless steel), particle size discrimination, and particle rate. The IDM addresses all of these limitations.

The IDM probe consists of a hollow cylinder of conductive material through the center of which passes all gearbox oil to the pump. In most cases, the IDM can be used as a direct replacement for the existing magnetic chip detector probe. Construction of the probe sensor is simple, in that the sensor is a conductive tube. The ends of the tube are overlapped and separated by a material having a high dielectric constant to form an elongated, single turn coil whose separated, but overlapping edges form a capacitor. Electric leads are attached to either side of the capacitor in order to supply an alternating current to the two planes of the capacitor. When an alternating current is passed through the probe, it acts as a capacitor in a parallel tank circuit. The two major advantages of this approach are that the resonator has a very high Q (quality) factor implying that the effective electrical impedance of the resonator is greatly affected by small perturbations in the characteristic properties of the fluid flowing through the center of the probe. For a 0.75 inch diameter probe, this high sensitivity provides reliable detection of metallic particles with volumes equivalent to that of a 0.010 inch diameter sphere. Actual particles may be rod or flake shaped. The behavior of the resonator, however, is only slightly affected by changes in the dielectric constant such as would be caused by bubbles or entrapped air. For a 0.75 inch diameter probe, the noise signal produced by completely filling and emptying the probe with gearbox oil is approximately 1/9 that of a 0.010 inch diameter magnetic sphere.

Since all magnetic particles are electrically conductive, they influence the time varying electromagnetic field generated by the probe and thus the electric current flowing in the sensor tank circuit. Non-magnetic and magnetic particles affect the electromagnetic field differently resulting in different phase shifts in the electric current in the tank circuit. By observing the behavior of the sensor circuit, both the size and material characteristic may be determined.

The sensor circuit output is monitored by a computerized data acquisition system. Two sensor characteristics, referred to as "R" and "I" are monitored. The "R" channel is used to detect the size of the particles and the "I" channel is used to determine if the particle detected is magnetic or non-magnetic. When the "R" channel exceeds a user set value (corresponding to particle size), a one second data sample of both channels is saved by the data acquisition system. The one second record starts before the threshold is exceeded. Post processing software allows the user to interrogate the file and determine the number of particles, size of the particles, and weather or not each is magnetic.

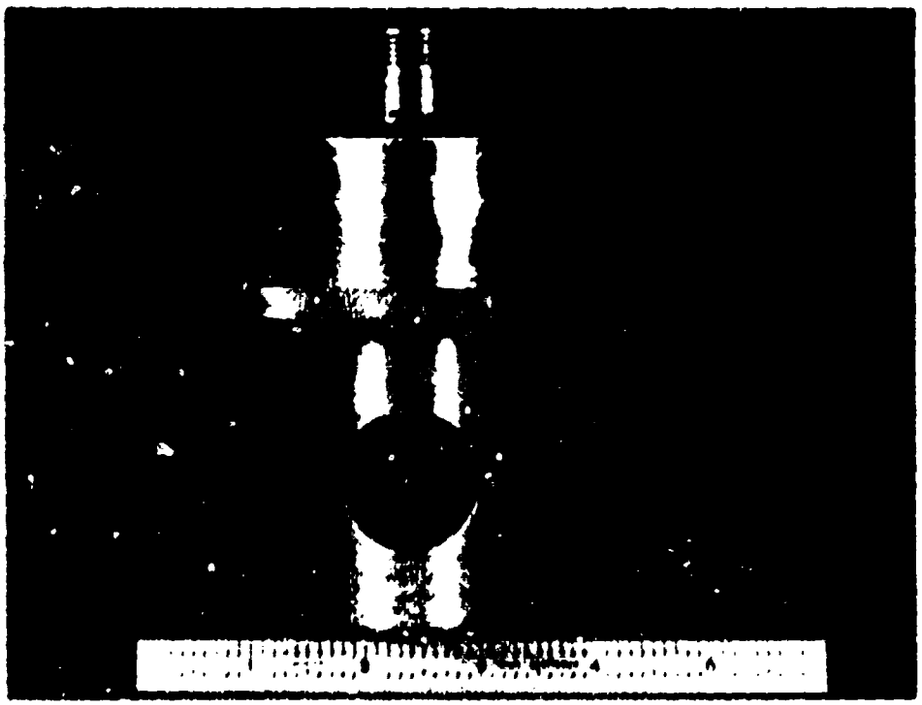

Figure 174. IDM Sensor Body

Figure 175. IDM Installed on Composite Housing

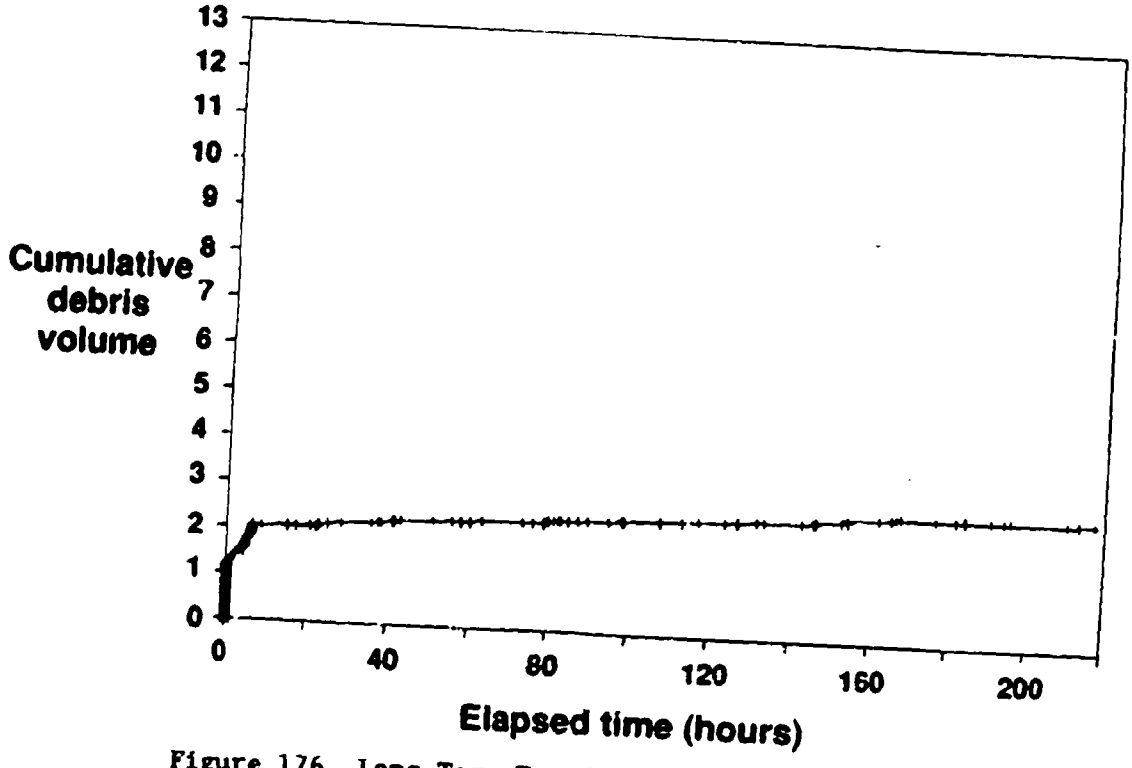

Figure 176. Long Term Trend of Particles Accumulated

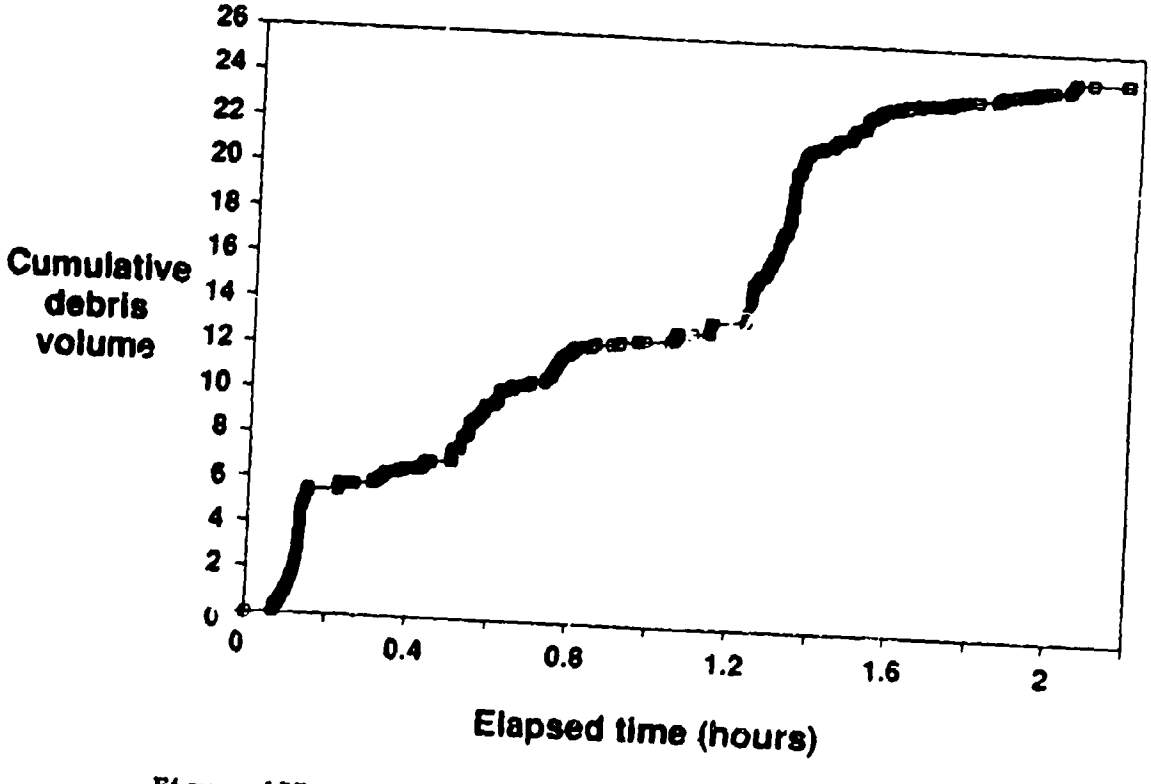

Figure 177. IDM Demo on Aircraft Gearbox With Chip Lights

During the ART testing, the IDM system was installed on either the test or dummy gearboxes. These tests were used to adjust and improve the software. A method of determining the probe characteristics was evaluated for proper operation along with probe durability. The ART testing demonstrated that operation of the IDM system was unaffected by entrained air. The lube system could be independently operated with 9 gpm oil supplied and 25 gpm oil/air scavenged, and air bubbles and "slugs" of oil were continuously generated without having an effect on the IDM. The IDM sensor body is shown in Figure 174 while Figure 175 shows the IDM installed on the composite dummy gearbox. Figure 176 shows the long term trend of the particles accumulated on the dummy gearbox during the 200 hour endurance test. The dummy gearbox did not experience any problems during this test. As a comparison, Figure 177 is an example of the particles accumulated during an engineering evaluation of an aircraft transmission which was rejected for the presence of metallic particles on the chip detector.

Acoustic Emission (AE) Accelerometers

Acoustic emission (AE) monitoring as a bearing diagnostic tool, has been successfully demonstrated on a wide range of mechanical systems that have included motors, compressors, helicopter drive shafts, and rocket engine turbopumps. The sensitivity of AE monitoring to bearing health has been used to provide an earlier warning of bearing degradation compared to traditional vibration techniques. The objective of using AE monitoring techniques on the ART program was to determine if AE could be equally successful in monitoring gear degradation in the high noise environment of a transmission gearbox.

The technique for AE data acquisition, processing, and analysis, is built around two pieces of hardware; (1) a patented acoustic emission point contact transducer (PCT), and (2) a digital acoustic acoustic emission system (DAES). The PCT a broadband, conical element, piezoelectric transducer that has a frequency response, flat to within 5 dB, from DC to approximately 1.5 MHz. The sensors conical shape prevents build-up of standing waves in the tip which broadens its bandwidth response in the higher frequency range. A dedicated DAES system was used to record the AE signal during gearbox operations. The DAES system analog filtered the AE sensor signal in the 100 KHz to 1 MHz band range. This frequency range prevented the recording of a continuous record of the AE signal by either digital or analog methods as is done with conventional sensors used on gearboxes. The AE test data was, therefore, collected as a series of snapshots or small time segments of the AE signal by high speed analog-to-digital (A/D) digitizers. The AE digitizers sampled the analog signal at 1.25 million times per second, for each of four channels, and placed the readings in a memory buffer. The cycle was then automatically repeated to take another snapshot of the signal. The time between snapshot collection of the AE data depended on the operating state of the gearboxes and the test program and ranged from a few seconds to 20 minutes.

The analog speed signal, from an optical trigger, the RMS of the AE signal, gearbox temperatures, and strain gage outputs were recorded on a second data acquisition system to provide continuous monitoring and visual quick-look capacity. The RMS capability of the DAES system integrated the high frequency AE signal to provide a slower time varying measure of the signal energy. In this manner, a continuous record of the AE signal energy could be monitored and recorded for the entire test run. The AE data acquired during these tests was compared to traditional monitoring, such as outputs from thermocouples, strain gages, and accelerometers that were also mounted on the gearboxes. The methodology is still in development.

REPORT DOCUMENTATION PAGE

Form Approved
OMB No. 0704-0188

Public reporting burden for this collection of information is estimated to average 1 hour per response, including the time for reviewing instructions, searching existing data sources, gathering and maintaining the data needed, and completing and reviewing the collection of information. Send comments regarding this burden estimate or any other aspect of this collection of information, including suggestions for reducing this burden, to Washington Headquarters Services, Directorate for Information Operations and Reports, 1215 Jefferson Davis Highway, Suite 1204, Arlington, VA 22202-4302, and to the Office of Management and Budget, Paperwork Reduction Project (0704-0188), Washington, DC 20503.

1. AGENCY USE ONLY (*Leave blank*)

2. REPORT DATE
March 1993

3. REPORT TYPE AND DATES COVERED
Final Contractor Report

4. TITLE AND SUBTITLE
Sikorsky Aircraft Advanced Rotorcraft Transmission (ART) Program – Final Report

5. FUNDING NUMBERS
WU-505-62-10
NAS3-25423
1L162211A47A

6. AUTHOR(S)
Jules G. Kish

7. PERFORMING ORGANIZATION NAME(S) AND ADDRESS(ES)
United Technologies Corporation
Sikorsky Aircraft Division
Main Street
Stratford, Connecticut 06601-1381

8. PERFORMING ORGANIZATION REPORT NUMBER

9. SPONSORING/MONITORING AGENCY NAMES(S) AND ADDRESS(ES)
Vehicle Propulsion Directorate
U.S. Army Research Laboratory
Cleveland, Ohio 44135-3191
and
NASA Lewis Research Center
Cleveland, Ohio 44135-3191

10. SPONSORING/MONITORING AGENCY REPORT NUMBER
NASA CR-191079

11. SUPPLEMENTARY NOTES
Project Manager, Timothy L. Krantz, Vehicle Propulsion Directorate, U.S. Army Research Laboratory, (216) 433-3580.

12a. DISTRIBUTION/AVAILABILITY STATEMENT
Unclassified - Unlimited
Subject Category 37

12b. DISTRIBUTION CODE

13. ABSTRACT (*Maximum 200 words*)

The objectives of the Advanced Rotorcraft Transmission program were to achieve a 25% weight reduction, a 10 dB noise reduction, and a 5,000 hour mean time between removals (MTBR). A three engine Army Cargo Aircraft (ACA) of 85,000 pound gross weight was used as the baseline. Preliminary designs were conducted of split path and split torque transmissions to evaluate weight, reliability, and noise. A split path gearbox was determined to be 23% lighter, greater than 10 dB quieter, and almost four times more reliable than the baseline two stage planetary design. Detail design studies were conducted of the chosen split path configuration and drawings were produced of a 1/2 size gearbox consisting of a single engine path of the split path section. Fabrication and testing was then conducted on the 1/2 size gearbox.

The 1/2 size gearbox testing proved that the concept of the split path gearbox with high reduction ratio double helical output gear was sound. The improvements were attributed to extensive use of composites, spring clutches, advanced high hot hardness gear steels, the split path configuration itself, high reduction ratio, double helical gearing on the output stage, elastomeric load sharing devices, and elimination of accessory drives.

14. SUBJECT TERMS
Transmissions; Gears; Bearings; Helicopters

15. NUMBER OF PAGES

16. PRICE CODE

17. SECURITY CLASSIFICATION OF REPORT
Unclassified

18. SECURITY CLASSIFICATION OF THIS PAGE
Unclassified

19. SECURITY CLASSIFICATION OF ABSTRACT

20. LIMITATION OF ABSTRACT